# UNIVERSITY OF SOUTHAMPTON

FACULTY OF NATURAL & ENVIRONMENTAL SCIENCE

Centre for Biological Sciences

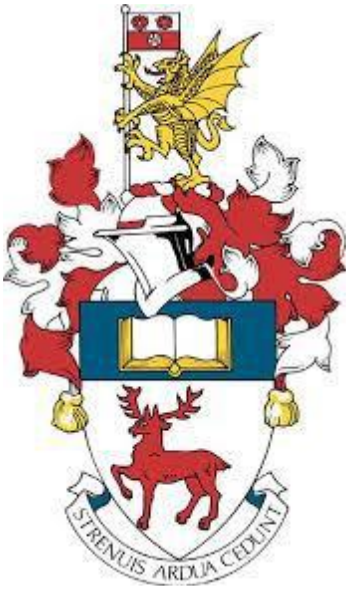


**Biochemical and biophysical characterization of conformationally distinct tau protein species and their relationship with dysfunction in two models of tauopathy**

Eva Daniela Ruiz Ortega

Thesis for the degree of Doctor of Philosophy

March 2021

# University of Southampton

## Abstract

FACULTY OF NATURAL AND ENVIRONMENTAL SCIENCES

School of Biological Sciences

Thesis for the degree of Doctor of Philosophy

**BIOCHEMICAL AND BIOPHYSICAL CHARACTERIZATION OF CONFORMATIONALLY DISTINCT TAU PROTEIN SPECIES AND THEIR RELATIONSHIP WITH DYSFUNCTION IN TWO MODELS OF TAUOPATHY**

Eva Daniela Ruiz Ortega

Abnormal aggregation of protein tau and subsequent neuronal dysfunction seems to be key pathological features in Alzheimer's disease and other related disorders, collectively referred to as tauopathies. It has been suggested that tau oligomers are important players in a process that precedes degeneration. However, the nature of tau aggregates and their relationship with toxicity is not well understood. The data described in this work have contributed to this research by exploring the tau species that might contribute to dysfunction at the onset of the disease and the tau species that might contribute to degeneration at the advanced stage of the disease.

To initially investigate the tau-mediated phenotypes and characterize their onset and progression, the shortest htau isoform with the P301S mutation was expressed in mouse and two different htau isoforms were expressed in *Drosophila.* In both models, the expression of tau causes a phenotype and this is manifested in the early and advanced stages of the disease. In *Drosophila*, tau expression caused reduced lifespan and deficits in climbing ability. These are two established tau phenotypes in this model and have been used as a readout to assess dysfunction due to the expression of tau in the nervous system. In the rodent model, tau expression caused locomotor impairment.

To investigate which tau species might be present and related to the appearance and progression of the observed phenotype, tau species were characterized using a number of biochemical and biophysical techniques. In both models, the earliest pathological feature was observed to be accompanied by species that resemble oligomers with altered conformation. Larger tau species (pre-NFT) with high β-structure are formed at late stages and might be potentially involved in degeneration.

In a *Drosophila* model expressing htau$^{2N4R}$, treatment with tau aggregation inhibitor (RI-AG03) partially rescues the phenotype and reduces tau aggregation. This further confirms that aggregation is critical for the onset and progression of the disease. Further research of the pathogenic tau species responsible for the onset of disease has the potential to lead to early diagnostic markers and therapeutic targets for tauopathies.

# Table of Contents

**Table of Contents**

# List of Figures

**List of Figures**

**List of Figures**

**List of Figures**

# List of Tables

# Research Thesis: Declaration of Authorship

Print name: Eva Daniela Ruiz Ortega

Title of thesis: Biochemical and biophysical characterization of conformationally distinct tau protein species and their relationship with dysfunction in two models of tauopathy

I declare that this thesis and the work presented in it are my own and has been generated by me as the result of my own original research.

I confirm that:

1. This work was done wholly or mainly while in candidature for a research degree at this University;
2. Where any part of this thesis has previously been submitted for a degree or any other qualification at this University or any other institution, this has been clearly stated;
3. Where I have consulted the published work of others, this is always clearly attributed;
4. Where I have quoted from the work of others, the source is always given. With the exception of such quotations, this thesis is entirely my own work;
5. I have acknowledged all main sources of help;
6. Where the thesis is based on work done by myself jointly with others, I have made clear exactly what was done by others and what I have contributed myself;
7. None of this work has been published before submission

Signature: .....Date:

# Acknowledgements

I would like to begin by thanking my lead supervisor, Professor Amrit Mudher. Thank you for your support and guidance during this process. For your mentoring and patience, I will always be grateful to you. I would also like to thank my second supervisor, Professor Sumeet Mahajan, for his support and guidance with the project. Thank you both for sharing with me, and all the members of your respective groups, your enormous passion for the field of research.

I would also like to thank the National Council of Science and Technology (CONACyT) for funding throughout this process. Without this support, it would not have been possible for me to continue my studies abroad. Also, I would like to give special thanks to John and Elizabeth Bouldin, who financially supported this project to make it possible. Thank you for your kindness and unrivaled interest in research.

A very special thanks to the people who provided me with mentoring and even direct support in the development of the data presented here. This includes Dr. Mariana Vargas-Caballero, Dr. Katrin Deinhardt, Dr. Renzo Mancuso and Dr. Anthony Aggidis.

My special thanks to Amrit Mudher lab current and previous members, including Dr. George Devitt, Dr. Shreyasi Chatterjee, Dr. Anna Crisford, Preeti Prasannan, Ben Batchelor, Bradley Richardson. Especially to Dr. Megan Sealey, for training me at the beginning of my Ph.D. Thank you all for your support and for making this experience invaluable.

I would like to end by thanking my family and friends, who despite the distance have been there for me at all times. Special thanks always to my parents, Irma and Leo, and my brothers, Héctor and Ibor for their unconditional support. Without you, none of this would have been possible. Finally, I would like to thank Łukasz Droździewicz for being my biggest support during my Ph.D. I will be forever grateful for all the unforgettable moments. Thank you for always being there.

# Definitions and Abbreviations

3R: 3-repeat

4R: 4-repeat

0N4R (tau-383): Tau protein containing 0 N-terminal domains and 4 repeat domain regions

0N3R (tau-352): Tau protein containing 0 N-terminal domains and 3 repeat domain regions

1N4R (tau-412): Full length tau protein containing 1 N-terminal domains and 4 repeat domain regions

2N4R (tau-441): Full length tau protein containing 2 N-terminal domains and 4 repeat domain regions

AD: Alzheimer's disease

AFM: Atomic Force Microscopy

ALS: Amyotrophic lateral sclerosis

ANOVA: Analysis of variance

APOE: Apoliproprotein APP Amyloid precursor protein

DLS: Dynamic Light Scattering

EDTA: Ethyenediamineetetracacetic acid

Elav: Pan-neuronal driver

EM: Electron Microscopy

FTDP-17: Frontotemporal dementia with Parkinsonism linked to chromosome 17 GAL4 Yeast transcription activator protein

GSK3β: Glycogen Synthase Kinase 3 β

GTO: insoluble granular tau oligomers

HCl: Hydrogen chloride

HD: High dose

HMW: High molecular weight

Htau0N3R: Human tau 0N3R isoform

Htau0N4R: Human tau 0N4R isoform

KDa: Kilodalton

LD: Low dose

LMW: Low molecular weight

MAP: Microtubule Associated Protein

MB: Mushroom bodies

MT: Microtubule

NaCl: Sodium Choride

NFT: Neurofibrillary tangles

NMJ: Neuromuscular junctions

NS: larger/ fibrillar insoluble tau

NS1: Aqueous soluble larger fraction

NS2: Detergent SDS- larger fraction

P2: Pellet insoluble oligomers

NP1: Pellet insoluble larger species

P301L: Proline to Leucine mutation at amino acid 301 in tau

P301S: Proline to Serine mutation at amino acid 301 in tau

PAGE: Polyacrylamide gel electrophoresis

PBS: Phosphate-Buffered Saline

pH: Power of Hydrogen

PHF: Paired helical filaments

PiD: Pick's Disease

Rpm: Revolutions per minute

S1: Aqueous soluble fraction

S2: Detergent SDS- soluble fraction

S3: Detergent-insoluble fractions

SDS: Sodium Dodecyl Sulphate

SDS-PAGE: SDS-Polyacrylamide Gel Electrophoresis

Ser: Serine

Sgg: Shaggy

SF: Straight filaments

TBS: Tris-buffer saline

Thr: Threonine

TEM: Transmission Electron Microscopy

ThT: Thioflavin T

UAS: Upstream activating sequence

WB: Western Blot

WT: Wild-typ

# Chapter 1 Introduction

## 1.1 Neurodegenerative diseases

Diseases that cause neurodegeneration are characterized as disorders that lead to selective and progressive loss of neurons (Dugger and Dickson, 2017). Neurodegenerative disorders can develop due to the combination of causes related to age (Brookmeyer et al., 1998; Hou et al., 2019) and in some cases due to genetic mutations which can increase the risk. Some of the most common neurodegenerative disorders are amyloidosis and tauopathies. In these, the main characteristic is the abnormal aggregation of misfolded proteins into filamentous protein aggregates (as reviewed in Dugger and Dickson, 2017). For example, the combined presence of 2 types of abnormal structures composed of amyloid-β (Aβ) protein and neurofibrillary tangle, consisting of paired helical filaments (PHFs) made up of protein tau. These two abnormal structures are the hallmarks of Alzheimer's disease. Understanding this abnormal protein aggregation is vital to understanding the underlying mechanisms of the disease and is the focus of the research presented in this thesis, with particular interest in tau protein and its role in tauopathies.

## 1.2 Alzheimer’s disease (AD)

Alzheimer’s disease (AD), first described by Alois Alzheimer in 1907 (Stelzmann et al., 1995), is a progressive neurodegenerative disease associated with memory deficits and cognitive decline (DeTure and DIsckson, 2019). AD is the most common form of brain disorder and contributes to around 60-80% of dementia cases (Alzheimer’s Association, 2020).

The main pathological characteristic of AD is the abnormal deposition of amyloid protein (Aβ) in the cortex and hippocampus. The hypothesis regarding the pathogenic mechanism of Aβ is that the metabolism of the amyloid precursor protein (APP) and the subsequent accumulation of peptide Aβ are the main events that drive AD (Li et al 2021). Genetic forms produce 1 to 5% of all AD cases and some of these genetic forms are caused by mutations in the amyloid precursor protein (APP) gene (Levy et al., 1990), from which Aβ is cleaved (Haass et al., 1992). Furthermore, mutations in genes that affect APP processing, such as presenilin 1 and 2, have also been found to cause genetic forms of AD (Scheuner et al., 1996).

Excluding these rare mutations, the disease is believed to develop due to multiple factors rather than a single cause (Alzheimer's Association, 2020). Different established risk factors that include, among others, an increase in the average age of humans, vascular disease, family history of dementia, and genetic factors (Li et al., 2015).

AD is more common in people over 65 years of age (late-onset Alzheimer's) and as the average age of humans increases, AD disease has become one of the disorders with the highest incidence worldwide. It is currently estimated that 50 million people have dementia worldwide and this number is predicted to triple by 2050 as the population ages (Alzheimer's Association, 2020). These statistics and their estimated impact, at the individual and societal level, are alarming. This is why improvements in our understanding of the disease, treatments, and patient care are desperately needed to overcome dementia.

As reported in the literature, it is believed that the pathogenic processes that lead to Alzheimer's disease begin at least 20 years before symptoms appear (reviewed in Alzheimer's Association, 2020). AD is clinically characterized by memory loss coupled with deficits in other cognitive functions including orientation, language, judgment, and decision-making (Yiannopoulou and Papageorgiou, 2013), eventually affecting the entire brain progressively disabling parts of the brain until it stops working.

Currently, there is no cure for AD. Available treatments accepted by the Food and Drug Administration (FDA) produce a modest improvement in symptoms (as revised in Hou et al., 2019 and Alzheimer's Association, 2020) and are used to improve cognitive symptoms temporarily (Alzheimer's Association, 2020). One type of treatment consists of cholinesterase inhibitors that target loss of the neurotransmitter acetylcholine. This strategy has its origins in the cholinergic hypothesis of AD, which concludes that cholinergic neurons located throughout the lower and upper areas of the brain involved in memory are selectively lost early during AD progression. The cholinergic hypothesis considers the crucial role of acetylcholine in human cognitive function. In this theory, the activity of choline acetyltransferase and the pyruvate dehydrogenase complex decrease and, as they are responsible for the synthesis of acetylcholine, it translates into a decrease in cholinergic transmission (Kuca et al., 2016). The loss of acetylcholine neurons, loss of enzymatic function for acetylcholine synthesis, and degradation results in memory loss and deterioration of other cognitive and noncognitive functions (Yiannopoulou and Papageorgiou, 2013).

Cholinesterase inhibitors are approved for the treatment of mild to moderate AD (Birks, 2006). These counteract the neurotransmitter alteration of the disease (Yiannopoulou and Papageorgiou,

2013). By inhibiting acetylcholinesterase (an enzyme that breaks down the neurotransmitter acetylcholine) they increase acetylcholine levels in the synaptic cleft.

Commercially available drugs of this type are rivastigmine (Novartis), donepezil (Pfizer), galantamine (Birks, 2006). Memantine, is a drug approved for treatment for moderate to severe AD (McShane et al., 2006). Memantine is an antagonist of N-methyl-D-aspartate (NMDA) and is believed to have the ability to prevent excitotoxicity-induced cell death, by preventing excessive extra-synaptic NMDAR disease activation (Yiannopoulou and Papageorgiou, 2013; Folch et al., 2018). Although these drugs have proven to be beneficial in treating patients with mild to moderate forms of AD, they are not beneficial to patients in severe stages of AD. These drugs do not modify the disease, therefore, they do not slow the progression of the disease. For this reason, greater efforts are needed in understanding the pathogenesis of the disease in order to develop new therapeutic interventions.

A disease modifying therapy can be described as treatment that affect mechanisms of the pathophysiology of the disease resulting in benefiting the patient (Cummings, 2009), either by delaying or blocking the characteristic process of the disease, such as the formation of the two main pathologies in the brain. These two pathological hallmarks are extracellular deposits of amyloid plaques made up of amyloid beta (Aβ) protein and intra-neuronal accumulation of neurofibrillary tangles (NFTs) made up of abnormal tau protein (**Figure 1**). The consequences of these pathological processes include neurodegeneration with synaptic and neuronal loss leading to macroscopic atrophy (Lane et al., 2018). Understanding how these pathologies are formed during the disease is an important subjet of this thesis.

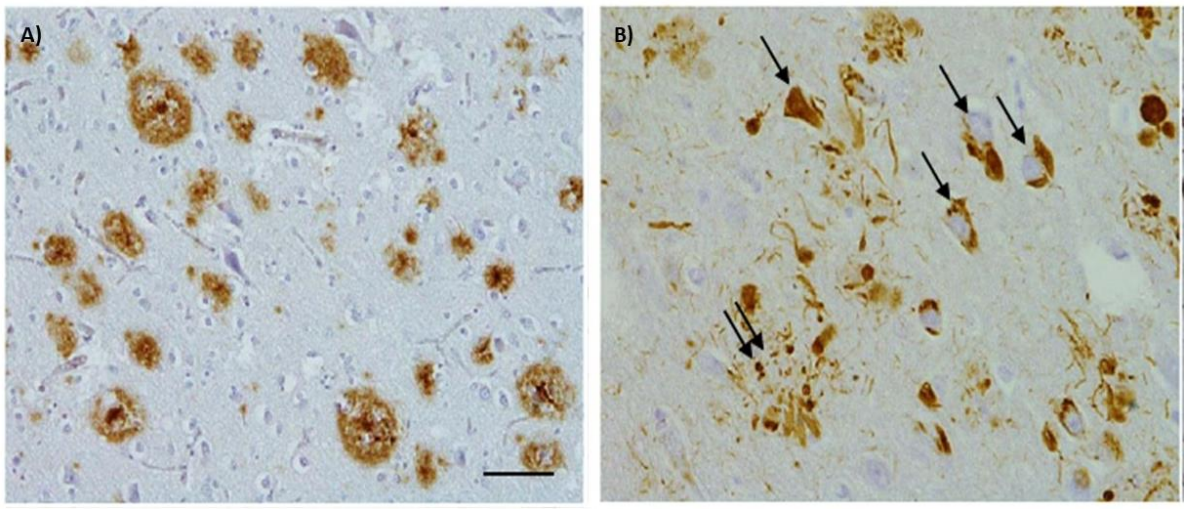


**Figure 1. Pathology of Alzheimer's disease**

A) Aβ immunohistochemistry highlights the plaques in the frontal cortex. B) Tau immunohistochemistry demonstrates both neurofibrillary tangles (arrows) and neuritic plaques (double arrow). The bar represents 50 µm in (A) and 25 µm in (B). Figure taken from publication in (Lane et al., 2018).

## 1.3 Tauopathies

Tauopathies are a class of neurodegenerative disorders that affect millions of people and are associated with the development of pathological tau. Tauopathies comprise a heterogeneous group of more than 20 different neurodegenerative disorders (Williams, 2006) characterized by, for the most part, the deposition of insoluble tau protein as abnormal filamentous deposits in nerve cells (as reviewed in Goedert, 2004).

The most common of the tauopathies is Alzheimer's disease (AD) (Goedert, 2004). In tauopathies, tau deposits have different morphology and distribution patterns that define each of them in this heterogeneous group as described in **Table 1** and **Figure 2** (showing some examples of tau pathology across different tauopathies). For example, in AD the pathology propagates across the brain in a characteristic pattern as AD progresses (Braak and Braak, 1991). The deposits of tau pathology are morphologically presented as paired helical (PHF) and straight (SFs) filaments (Kidd 1963; Crowther and Wischik, 1985) that comprise the NFTs (**Figure 2-A**). The density of NFTs corresponds to the areas of neuronal loss (Braak and Braak, 1991). The progression across the brain is called as Braak staging that involves 6 different stages. In stages I-II, NFTs begin to appear in the transentorhinal regions of the brain and symptoms in patients are not apparent. In stages III-IV,

NFTs are found in the limbic regions of the brain and the symptoms begin to manifest. In stages V-VI, the disease symptoms are developed and NFTs are found to have spread to the neocortical structures of the brain (Braak and Braak, 1995).

In progressive supranuclear palsy (PSP) a different tauopathy, tau is morphological, ultrastructural, and biochemically distinct to that found in AD (Williams et al., 2006). Tau pathology is present as neurofibrillary tangles, globose tangles, coiled bodies, and star-shaped astrocytic tufts (Williams et al., 2006; Alyenbaawi et al., 2020). In this tauopathy, tau affects basal ganglia first, then the pathology progresses to affect areas of the frontal and parietal lobes (Alyenbaawi et al., 2020) (as described in **Table 1**).

Tau is also characterized by the accumulation in inclusion bodies (Arai et al., 2001). For instance, in Pick's disease (PiD), tau is found in characteristic inclusions called Pick bodies with a different distribution than NFTs in AD and PSP. In PiD, the tau pathology distribution is found in neocortical and limbic areas in the frontotemporal regions. This spreads to the subcortical structure and the brainstem, followed by the motor cortex (Irwin, et al., 2016). The filaments are narrow filaments and straight filaments (SFs) (**Figure 2-A**).

In the case of corticobasal neurodegeneration (CBD), tau pathology is distributed anterior to the frontal cortex, amygdala, and the basal ganglia. This pathology progresses to more prominently affect the frontal and parietal cortices, amygdala, caudate, subthalamic nucleus (Ling, et al., 2016). The filaments found are narrow single-stranded filaments and wide double-stranded filaments (**Figure 2-D**). Since the main characteristic of these various diseases are the appearance of insoluble tau inclusions and neuronal loss, it is believed that these diseases share similar neurodegenerative mechanisms involving pathological tau (Williams, 2006). In section **1.8**, characteristic aspects, such as morphological and structural, of the filaments of tau will be discussed.

In addition to different morphological characteristics and differential ability to affect certain brain regions, the deposits of tau aggregates also vary in their isoform composition (3 and / or 4-repeat tau isoforms) (As described in **Table 1**). These differences suggest the existence of different aggregate tau conformers (Fitzpatrick et al 2017). Tau isoforms and their relationship to tauopathies will be described later in section **1.4** when explaining the structure of tau. Before that, it is important to consider the normal biology of tau.

**Table 1. Examples of tau aggregates across the tauopathies**

| Disease | Affected Brain region | Tau pathology | Filaments | Reference |
|---|---|---|---|---|
| Alzheimer's Disease (AD) | Enthorhinal cortex, hippocampus, cortex | Neurofibrillary tangles, neuropil threads, neuritic plaques | PHFs and SFs. Contain all 6 tau isoforms | Fitzpatrick et al., 2017 |
| Frontal temporal dementia with Parkinsonism linked to chromosome 17 | Frontal and temporal cortices, hippocampus | Neurofibrillary tangles and glial pathology, resembling sporadic tauopathies | The tau filaments can be Twisted ribbon-like filaments containing only 4R tau isoforms with a small amount of the most abundant 3R isoform. SFs and PHFs (if contain the 3R and 4R isoforms like AD). | Goedert and Spillantini, 2000 |
| Progressive supranuclear palsy (PSP) | Basal ganglia, thalamic fasciculus | Neurofibrillary tangles, globose tangles, coiled bodies, and star-like or tufted astrocytes | Filaments consist of 4R tau isoforms. Tau filaments formed are SF with rare twisted filaments. | Alyenbaawi et al., 2020 |
| Pick's Disease (PiD) | Neocortical and limpic areas in frototemporal areas. | Round cytoplasmic tau aggregates (known as Pick bodies), ramified astrocytic filaments, and neuropil threads | Filaments are narrow filaments with slight helical twists, SFs, and small portions as wide filaments. structures that are primarily composed of 3R tau, with a variable amount of 4R tau | Falcon et al., 2018 |
| Corticobasal degeneration (CBD) | Frontal and parietal cortices | Filaments in the shape of comma or coil-like (coiled bodies), astrocytic plaques and neuritic threads, globose tangles | The filaments are heterogeneous, containing narrow single-stranded filaments and wide double-stranded filaments. Glial tauopathy with astrocytic plaques | Zhan et al., 2020 |
| Paired helical filaments (PHFs); Straight filaments (SFs); 3-repeat tau isoforms (3R); 4-repeat tau isoforms (4R) | | | | |

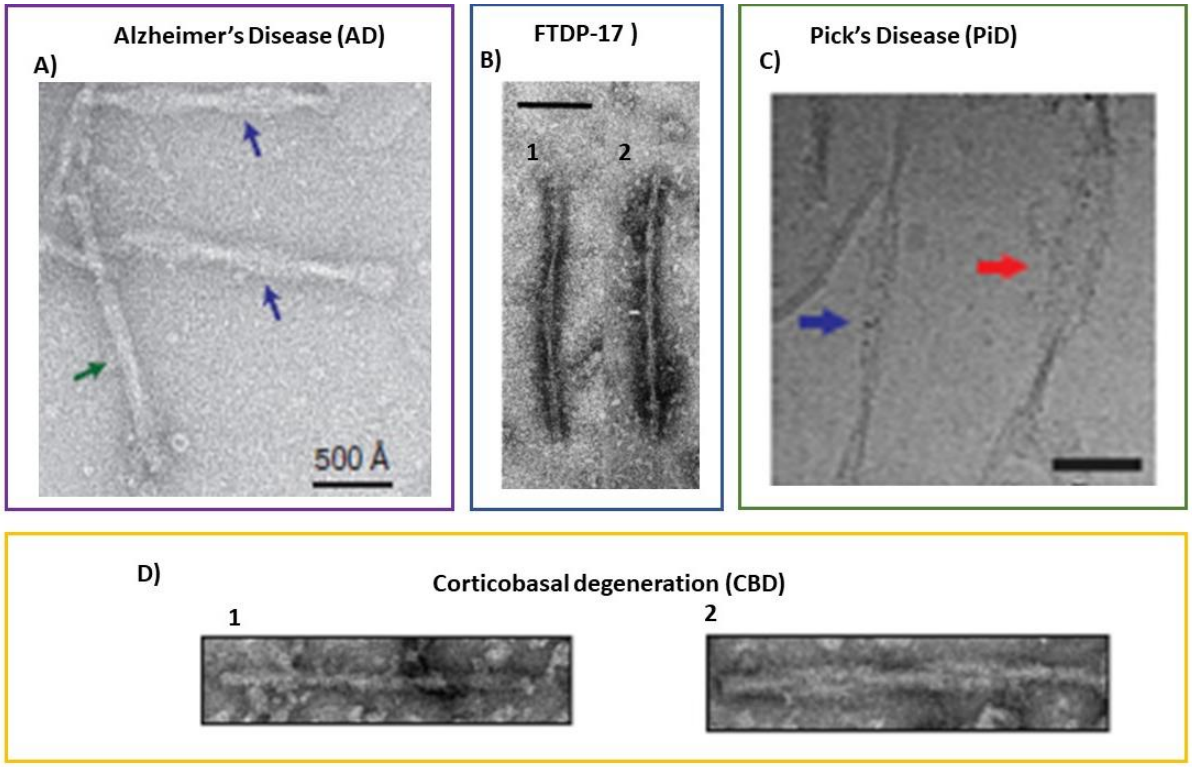


**Figure 2. Examples of tau filaments across tauopathies**

**A)** Negatively stained electron micrograph of purified tau filaments from AD brains. Blue arrows show PHF and green arrows show SF. Taken from (Fitzpatrick et al., 2017). **B)** Tau filaments in FTDP-17 narrow twisted ribbons (1) an occasional rope-like filaments (2) Scale bar: 100 nm. Taken from (Goedert and Spillantini, 2000. **C)** Cryo-electron micrograph of tau filaments extracted from the grey matter of the frontotemporal cortex of a PiD patient. The image shows narrow Pick's filaments in blue arrow while the red arrow shows wide filaments. Scale bar, 500 Å. Taken from (Falcon et al., 2018). **D)** Negative staining electron micrographs of tau filaments extracted from the frontal cortex of a CBD patient. The image shows both narrow type (1) and wide type (2) filaments. Scale bar, 50 nm. Taken from (Zhan et al., 2020).

## 1.4 Tau protein

Tau protein is a natively unfolded soluble protein primarily located mainly in the axons (Weingarten et al., 1975). Tau belongs to a group of proteins called microtubule-associated proteins (MAPTs), is abundant in the central nervous system (CNS) and its expression is predominantly in neurons (Lee et al., 2001). The expression of tau is similar in neurites and in the cell body of immature neurons (Dotti et al., 1987). Whereas in mature neurons, tau is mainly found in axons (Kubo et al., 2019; Kempf et al., 1996; Dotti et al., 1987) and can be secreted from cells and found in extracellular fluids, such as cerebral interstitial fluid (ISF) (Yamada et al., 2014). Tau is a multifunctional protein but one of its most important functions is in stabilizing microtubules (MTs) in neurons and other

cells (Weingarten et a., 1975). The interaction of tau with microtubules (MTs) is based on the tau repeat domain and flanking regions (Gustke et al., 1994; Mukrasch et al., 2005).

## 1.5 Tau structure

Tau protein is mainly composed of two domains which are defined based on their interactions with microtubules and their amino acid characteristics (Alyenbaawi et al., 2020). There are isoforms produced by alternative mRNA splicing of exon 2, 3, and 10 of the MAPT gene (Goedert et al., 1989; Sergeant et al., 2005; Goedert 2016). The tau isoforms expression is developmentally regulated (Cassimeris and Spittle 2001). In adult human brain, six isoforms are found, ranging in size from 352 to 441 amino acids long and are between 45 kDa- 65 kDa in size (Buée et al., 2000). The different isoforms are usually classified into several domains (Gustke et al., 1994). First an N-terminal domain; a microtubule binding domain, and C-terminal tail (as can be seen in **Figure 3**).

The N-terminal domain contains two inserts of 29 amino acids each termed N1 and N2 which correspond to the alternatively spliced exon2 and 3. The alternative splicing determines the expression of the N-terminal repeats with different isoforms containing 0, 1 or 2 repeats (Himmler et al., 1989). Next to the N-terminal domain is the region that contains numerous prolines, mainly in the form of SP (Ser-Pro) or TP (Thr-Pro) motifs. These regions can be phosphorylated by proline-directed kinases (such as MAP kinase, GSK3β, cdk5). This region also contains seven PXXP motifs that can form binding sites for proteins with SH3 domains (Mandelkow and Mandelkow, 2012,).

The C-terminal half contains three or four semi-conserved repeated sequences of 31 or 32 amino acids. Most of the C-terminal half contribute to the interaction with the microtubules (MTs), and hence it is called ¨microtubule binding-domain¨. The repeat region encoding exon 10 leads to the expression of tau with 4 repeats (4R) of tau binding to MTs (0N4R, 1N4R, 2N4R); alternatively, elimination of exon 10 leads to expression of 3 repeats (3R) of tau binding to MTs (0N3R, 1N3R, 2N3R) (Goedert et al., 1989).

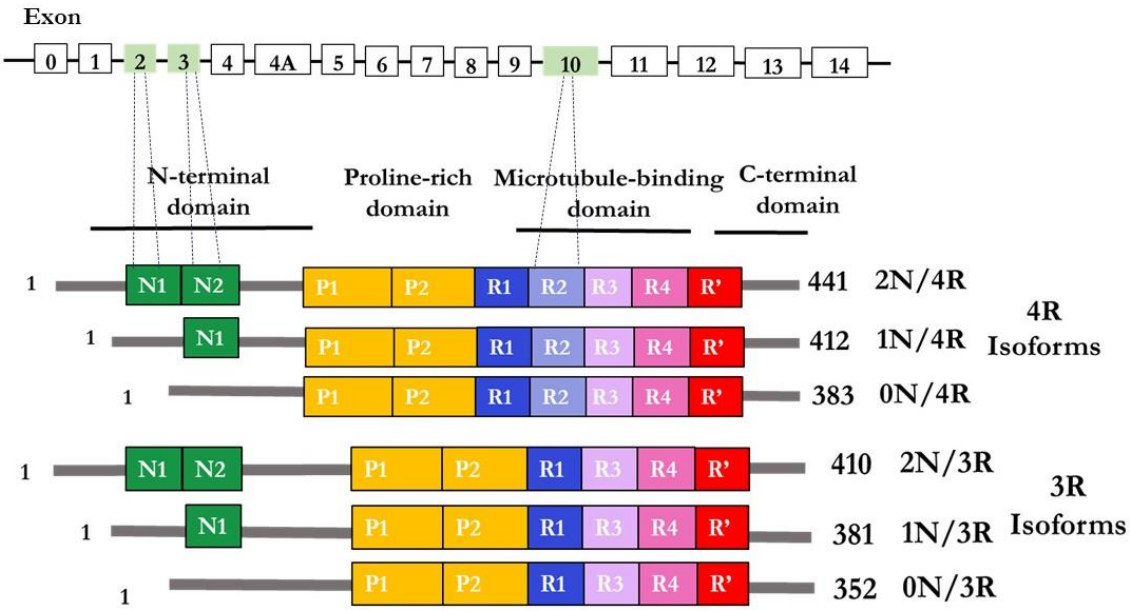


**Figure 3. Schematic representation of the human tau gene and the six tau isoforms**

A) Representation of human tau gene located at chromosome 17q21. B) There are 6 different isoforms of Tau with different chain lengths. Alternative splicing of exon 2 (N1), 3(N2) and 10 (R2) determines the length of the various isoforms. P1 and P2 = Proline rich region. Figure adapted from (Zeng et al., 2021).

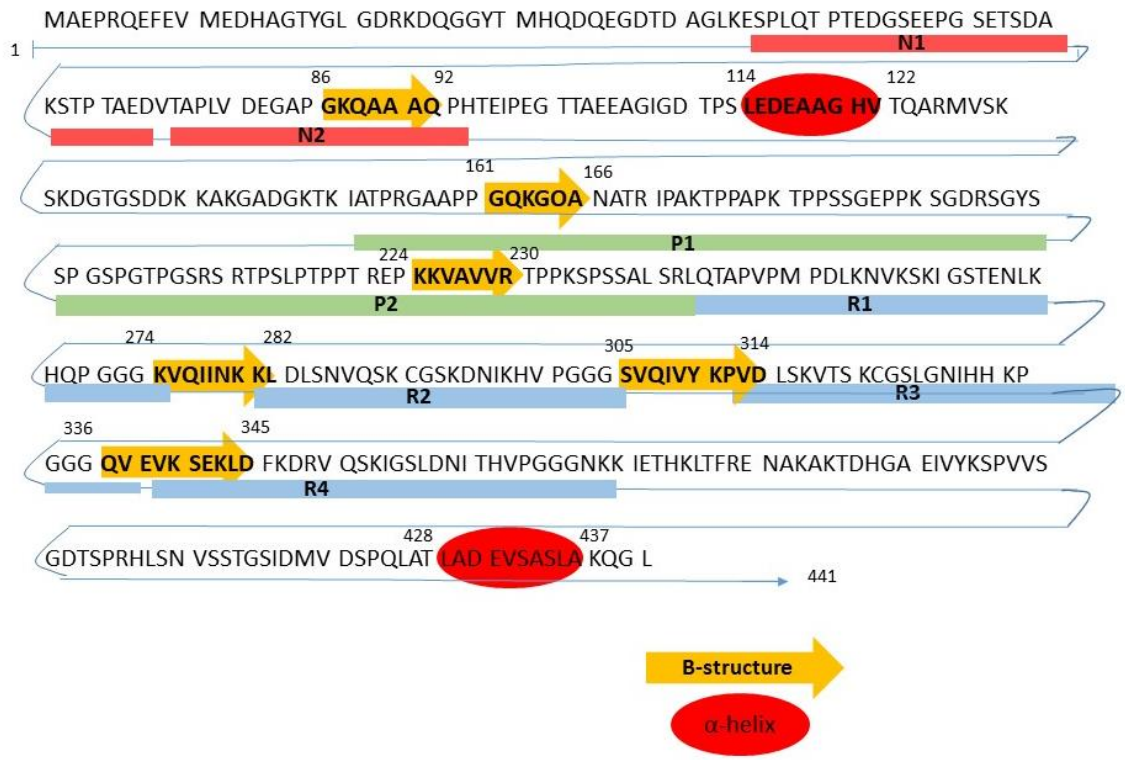


**Figure 4. Tau primary sequence**

The image shows the primary amino acid sequence and probable secondary structures of the longest tau isoform in the central nervous system. N1 indicates sequences encoded by exon 2 and N2 by exon 3. R1 to R4 are microtubule-binding domains encoded by exons 9-12, respectively. Also shown are domains with β-sheet structure (yellow) and α-helix content (red). Figure adapted from (Šimi´c et al., 2016).

The different isoforms are believed to have different physiological roles. For instance, the shortest isoform of tau (0N3R) is the only isoform of tau expressed in the fetal brain, while all six isoforms are expressed in adulthood (Kosik et al., 1989). There is also some evidence to suggest that different isoforms of tau are differentially expressed in different subsets of neurons. For example, only 3R isoforms are found in granule cells of the dentate gyrus (Goedert et al., 1989). In the adult brain, the ratio of 3R and 4R isoform expression is approximately equal (Hong et al., 1998).

The alternative expression of the N- and C-terminal repeats potentially underlies the differences in the functions of the different isoforms. For example, 4R isoforms have been shown to bind and stabilize microtubules more strongly than 3R isoforms (Panda et al., 2003).

It has been suggested that poor regulation of MAPT alternative splicing may play an important role in tau dysfunction (Alyenbaawi et al., 2020). This poor regulation can result in an imbalance between the 3R and the 4R isoforms.

The imbalance between the 3R and the 4R isoforms may be involved in the development of different tauopathies. This relationship has become evident after the identification of mutations, such as a dominantly inherited form of frontotemporal dementia and Parkinsonism linked to chromosome 17q21–22 (FTDP-17). MAPT mutations account for approximately 5% of familial FTLD cases. These are located in exons and intron mainly in regions within the repeat domain region (Ghetti et al., 2015) and can affect tau by, for example, leading to an imbalance in the ratio of tau isoforms. For example, that increase alternative splicing of mRNA in exon 10 of MAPT results in overproduction of 4R tau and consequent formation of tau deposits (Goedert, 2016). Mutations can also have a negative effect on the ability of tau to bind to microtubules, increasing its propensity to aggregate or phosphorylate, leading to the dysfunction and neurodegeneration characteristic of tauopathies.

Different isoforms of tau have been implicated in various tauopathies, as shown in **Table 2**. For instance, in AD disease, all 6 isoforms (both the 3R isoform and the 4R isoform) are present in pathology. Other tauopathies are characterized by the predominant aggregation of the 3R or 4R tau isoform (Iqbal, et al., 2005). For example, in Pick's disease (PiD) the 3R isoform is the one that aggregates predominantly. Whereas progressive supranuclear palsy (PSP), frontotemporal dementia, Parkinsonism linked to chromosome 17 (FTDP-17) and corticobasal degeneration (CBD) are associated with the 4R isoforms (Sergeant et al., 2005). These observations suggest that different isoforms of tau have different pathological roles.

Currently, the role of isoforms in the different tauopathies is not entirely clear. However, evidence has been reported to suggest that the 4R isoform has a greater propensity to aggregate than the 3R isoform (Adams et al., 2010). It has been previously shown in a mouse model of tauopathy, in which the 4R vs 3R tau ratios are manipulated, that increasing the ratio of the 4R tau isoform leads to increased aggregation (Schoch et al., 2016). It is believed that differential aggregation propensities of tau isoforms could be explained by structural differences. The 4R isoform contains the two hexapeptides that are believed to be necessary to form the structures in β sheets. These are found at the beginning of the third repeat domain, R3 ($^{306}$ VQIVYK $^{311}$) and in the second repeat domain, R2, ($^{275}$ VGIINK $^{280}$) (as shown in **Figure 4**) and have been reported as for the aggregation of tau (Li and Lee, 2006, von Bergen et al., 2000). However, to establish a clear association between the structural differences between the isoforms and the pathology of tau, many studies are still necessary.

**Table 2. Examples of form of tauopathies and isoform**

| Disease | Isoform of tau |
|---|---|
| Alzheimer's Disease (AD) | 3R and 4R isoforms |
| Dementia pugilistica | 3R and 4R isoforms |
| Down's Syndrome | 3R and 4R isoforms |
| Familial British dementia | 3R and 4R isoforms |
| Frontotemporal dementia with parkinsonism linked to chromosome 17 (FTDP-17) | 3R and 4R isoforms |
| Hippocampal tauopathy in cerebral ageing | 3R and 4R isoforms |
| Neurofibrillary tangle-only dementia (NFT-dementia) | 3R and 4R isoforms |
| Niemann-Pick disease type C | 3R and 4R isoforms |
| Parkinsonism with dementia of Guadeloupe | 3R and 4R isoforms |
| Postencephalitic parkinsonism | 3R and 4R isoforms |
| Amyotrophic lateral sclerosis/ parkinsonism-dementia complex of Guam (ALS) | 3R and 4R isoforms |
| Pick's Disease (PiD) | 3R isoforms |
| Argyrophilic grain disease (AGD) | 4R isoforms |
| Corticobasal degeneration (CBD) | 4R isoforms |
| Progressive supranuclear palsy (PSP) | 4R isoforms |

The biophysical characteristics of tau are relatively well known. Tau is a highly hydrophilic protein (von Bergen et al., 2005; Jeganathan et al., 2008; Schweers et al., 1994) with a limited secondary structure (α-helix and β-strand) detected by circular dichroism (CD) and Fourier transform infrared spectroscopy (FT-IR) (Schweers et al., 1994). Detailed studies using NMR confirm that the protein (the full-lenght tau) has a disordered structure (Mukrasch et al., 2009).

In solution, it is believed that tau adopts a paper clip conformation, where tau folds so that amino and carboxy terminals interact with the repeat domain (Jeganathan et al., 2008) as shown in the **Figure 5.** These characteristics give it flexibility in its structure to interact with other proteins, as well as enable it to interact with itself.

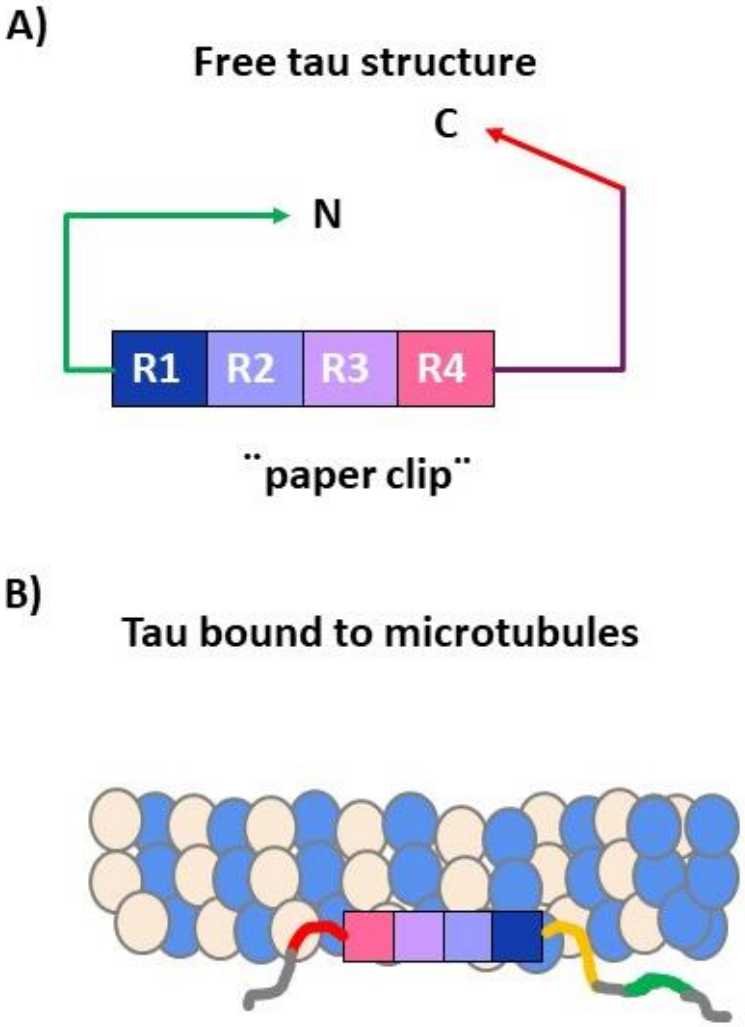


**Figure 5. Possible tau structures**

(A) The proposed "Paper-clip" structure of tau, in which both the N and C terminals are closely associated (Von Bergen et al., 2001). B) Representation of tau bound to microtubules, the two terminals are separated with the N-terminal projected away from the microtubules (Guo et al., 2017). Figure adapted from (Alyenbaawi et al., 2020).

## 1.6 Changes in tau related with pathology

As mentioned, the most important function of the tau protein is believed to be to promote the assembly and stability of MTs (Crowther, 1991). It has been shown that tau-mediated assembly of MTs can be modulated by post-translational modifications, such as phosphorylation, acetylation,

glycosylation, etc. (Wang and Mandelkow, 2016). Among the post-translational modifications, the most commonly studied is phosphorylation (Avila et al., 2004).

In 1975 the tau protein was identified as a protein present in association with microtubules (Wingarten et al., 1975). In this study, co-purification of tau associated with porcine brain tubulin was carried out through assembly and disassembly cycles, describing the ability of tau to induce tubule formation (Wingarten et al., 1975). Subsequently, the tau protein was described as a phosphoprotein (Baudier et al., 1987). Furthermore, dephosphorylated tau has been shown *in vitro* to promote extensive polymerization of MTs (Lindwall and cole, 1984). This has shown that phosphorylation participates in the regulation of the ability of tau to bind to MTs and suggests that phosphorylation of tau inhibits its ability to bind to MTs (Lindwall and Cole, 1984; as explained in Avila et al., 2004 and Stoothoff and Johnson, 2005). Phosphorylation modifies the form of tau and thus regulates its biological activity. Tau contains phosphorylation sites that are mostly found in the Ser-Pro and Thr-Pro motifs, and some other sites in other residues (Morishima-Kawashima et al., 1995).

In the tau protein, around 85 potential phosphorylation sites have been reported (Hanger et al., 2007; Mair et al., 2016; Iqba et al., 2016). These sites are distributed throughout the tau sequence (as seen in **Figure 6**). Interestingly, in AD human brain, tau has been found to be highly phosphorylated (Ksiezak-Reding et al., 1992) (also shown in **Figure 6**). More recently, 45 sites have been reported to be phosphorylated in AD (Noble et al., 2013).

Although phosphorylation may be related with tau pathology, the contribution of phosphorylation, and other post-translational modifications, to tau pathology, such as aggregation and toxicity is unclear, these changes in tau also occur in a normal physiological conditions (as shown in **Figure 6**).

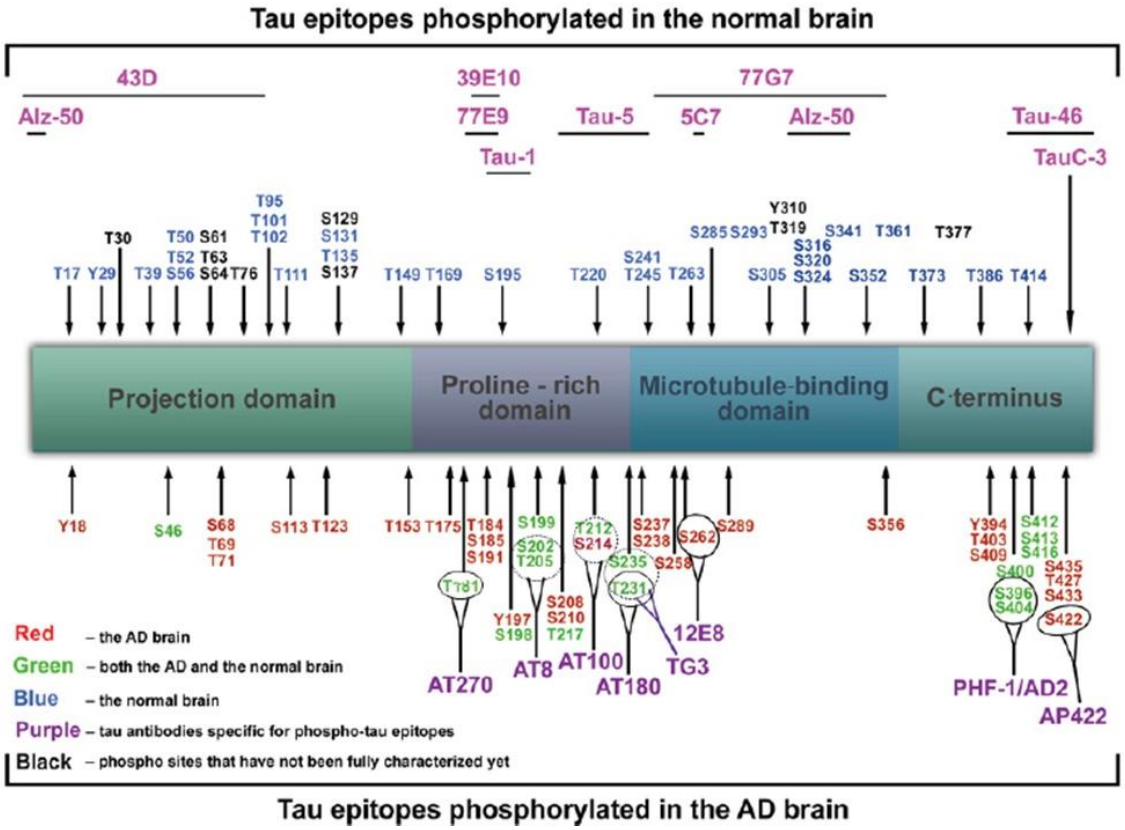


**Figure 6. Putative phosphorylation sites on tau protein and epitopes specific for major tau**

Red color denotes amino acids phosphorylated in AD brain; green color denotes both AD and normal brain, blue in normal brain and black color denotes phosphorylation sites that have not been characterized. Tau antibodies specific for phosphor-tau epitopes given in purple, pink color denotes antibodies specific for non-phosphorylated epitopes. Figure taken from (Šimi´c et al., 2016).

Although in this thesis one of the main objectives is to study the changes in the solubility properties and the conformational changes of tau, it is important to consider the role played by post-translational modification and its role in toxicity.

Tau undergoes post-translational modifications that can alter its normal functions and lead to pathology. Therefore, understanding the role of these tau modifications is important to understanding the mechanisms underlying the disease. Particular interest in the phosphorylation of tau was sparked by the discovery that paired helical filaments (PHF) from AD disease were phosphorylated (Grundke-Iqbal et al., 1986).

Due to the importance of phosphorylation, specific phosphorylation sites modulated by various kinases and phosphatases have been described. These sites are found primarily in the proline-rich domain in tau or flanking the microtubule-binding domains (as shown above in **Figure 3**).

Two distinct types of kinases can be phosphorylated. The first type, the proline directed kinases target the SP and TP amino acid motifs. Proline-targeted kinases include glycogen synthase kinase-3 (GSK-3) (Hanger et al., 1992), cyclin-dependent kinase 5 (cdk5) (Baumann et al., 1993), and adenosine monophase activated protein 5 'kinase (AMPK) (Thornton et al., 2011) (**Figure 7**)

The second type of kinases that phosphorylate tau are non-proline-directed kinases. These include casein kinase 1 (CK1) (Hanger et al., 2007), microtubule affinity regulatory kinases (MARK) (Drewes et al., 1995), and cyclic AMP-dependent protein kinase A (PKA) (Andorfer and Davies, 2000). On the other hand, tyrosine kinases such as Fyn (Lee et al., 2004) have also been implicated in the phosphorylation of tau. These examples show that the predominant way in which tau function is regulated is phosphorylation (as reviewed in Avila et al., 2004).

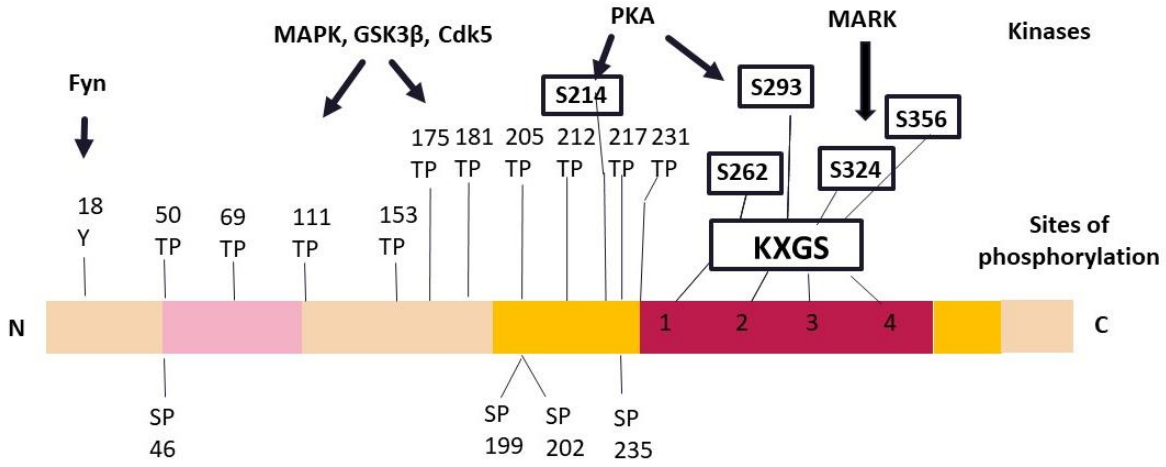


**Figure 7. Diagram of the longest tau isoform showin Kinases and Phosphorylation sites of Tau**.
It is show number of sites available for phosphorylation in tau protein. The proline directed kinases are targeting the SP and TP amino acid sequences. The KXGS motifs are targeted by kinases like MARK. Adapted from (Schneider and Mandelkow, 2008).

Dysregulation of kinases and phosphatases may be important in tauopathies including AD. For instance, it has been observed that in brains with AD 26 of the 45 identified phosphorylated sites are phosphorylated by GSK-3 (Noble et al., 2013). In particular, two isoforms of GSK-3 are known to be found in mammals, GSK-3α and GSK-3β (Doble and Woodgett, 2003). The active form of GSK-3β (phosphorylated at Tyr326) has been reported to increase in the frontal cortex of AD brains (Yamaguchi et al., 1996, Pei et al., 1997).

In line with this, in animal models, overexpression of GSK-3β has been shown to induce hyper-phosphorylation of tau and subsequent neurodegeneration (Lucas et al., 2001), suggesting a role for GSK-3β in mediating the tau toxicity.In contrast, it has been shown that inhibition of GSK-3β can reduce phosphorylation of tau and alleviate tau-mediated toxicity. For instance, the use of lithium as a GSK-3 inhibitor in reducing tau phosphorylation and improving the tau-mediated behavior and axonal transport deficit in a *Drosophila* model that overexpress the human tau isoform 3R, ($htau^{0N3R}$) (Mudher et al., 2004). Similar results have been reported in mutant tau mouse model in which the inhibition of the tau kinase GSK3β has been shown to reduce tau phosphorylation and neuronal loss (Noble et al., 2005). These studies indicate that dysregulation of GSK-3 activity increases in the disease. Furthermore, GSK-3β has been described to co-localize with NFT in AD brain (Pei et al., 1997). These studies demonstrate the implication between alteration in phosphorylation and tau pathology.

Phosphorylation has been implicated as one of the main causes of changes in the tau protein that can lead to the generation of forms of tau that are toxic (as reviewed in Avila et al., 2004). Phosphorylation has also been implicated in causing conformational changes and triggering the misfolding of tau. As mentioned in section **1.5**, protein tau contains little ordered structure when isolated in monomeric form and in solution, tau adopts a ¨paper-clip¨ conformation in which both the N and C terminals are closely associated (Von Bergen et al., 2001; Jeganathan et al., 2008).

It has previously been observed that phosphorylation prompts a compacted folding of tau confirmation. This tighter folding of tau, it is reactive to conformation-specific antibodies, for instance, Alz50 and MC1. Interestingly, this tighter and compacted folding is closely related to AD (Weaver et al., 2000; Jeganathan et al., 2008), as these conformational antibodies have more affinity for tau found in AD brains compared to control brains (Weaver et al., 2000). This observation suggests that misfolding is an important aspect of tau pathogenesis.

In a study conducted by Carmel et al., 1996, it was observed that the Alz50 antibody bind to a discontinuous sequences of tau, including both the N-terminus and the microtubule binding domain

(Carmel et al., 1996). In this study, it was suggested that tau adopts a distinct conformation when polymerized into filaments and that Alz50 recognizes this conformation selectively (Carmel et al 1996). In this study, it was shown that unphosphorylated tau also contains the sequences necessary for Alz50 binding, however, it also suggests that factors other than primary structure play a role in the high affinity interaction between filaments and Alz50 (Carmel et al 1996). This is in line with previous observations suggesting that although phosphorylation is not required for epitope recognition, it may contribute to high affinity binding of Alz50 by stabilizing certain conformations of tau (Uéda et al., 1990).

In a study carried out by Mondragón-Rodríguez and collaborators, which sought to determine the chronological sequence of tau changes that play a fundamental role in AD, a significantly higher number of phospho-tau-positive tau filaments was observed compared to Alz50. This observation suggests that the conformational changes of tau occur after phosphorylation. Furthermore, the authors observed that phosphorylation at the Ser396 site is co-labelled with Alz50 but some filaments display phosphorylation at Ser396 without Alz50 conformational change. This indicates that phosphorylation occurs before the conformational change detected by Alz50 (Mondragón-Rodríguez et al., 2008) and that phosphorylation at Ser396 is probably necessary for conformational changes in tau. In line with this, *in vitro* studies have demonstrated that phosphorylation at specific sites (Ser202/Thr205 and Ser396/Ser404) also induce conformational change in tau. This evidence indicates that phosphorylation of these sites induces a tighter folding of tau and makes tau reactive to the MC1 antibody (Jeganathan et al., 2008). Therefore, these studies show evidence that relates phosphorylation as a cause of conformational changes in tau.

*In vitro* studies provide strong evidence suggesting that phosphorylation of tau not only may reduce the ability of tau to polymerize MTs (Lindwall and Cole, 1984; Necula and Kuret, 2004; Sun and Gamblin. 2009) but may also promote aggregation (Necula and Kuret, 2004), even when phosphomimetic mutations are introduced in tau (Necula and Kuret, 2004). For instance, when 11 mutant proteins were prepared containing selected pseudophosphorylation mutations at 12 positions spanning proline-rich, microtubule-binding and C-terminal domains of tau, it has been described that this pseudo-phosphorylation is capable of reducing the affinity of tau for MTs and capable to induce formation of aggregates and fibrillation (Necula and Kuret, 2004). These findings may suggest that the loss of the ability of tau to bind to microtubules may expose motifs in the repeat domains, allowing interaction with other tau-free molecules leading to aggregation.

It is believed that phosphorylation induce an increase in the total negative charge of tau and this promotes aggregation (Alyenbaawi et al., 2020). However, the complex patterns of phosphorylation

*in vivo* and their causal effect on aggregation are not currently clear. Nonetheless, it has been suggested that phosphorylation plays a significant role in the early stage of pathogenesis (Noble et al., 2013), and it is considered that this alteration is closely related to the loss-of-function of the tau protein (as described in section **1.7**).

## 1.7 Loss of function

As mentioned before, in AD and tauopathies, alterations in tau lead to the development of pathology. During these, tau becomes increasingly phosphorylated, undergoes a conformational change, and becomes aggregated and insoluble (Goedert and Spillantini 2006). This suggests a relationship between the conformational changes of tau and the pathogenesis of AD and tauopathies. Although the mechanisms of AD and other tauopathies' pathogenesis are not completely clear, there are two theories in relation to the mechanisms that contribute to the manifestation of toxicity. One hypothesis is the loss of function of the tau protein. In this, the event that leads to toxicity occurs after dissociation of the pathological tau from the MTs. This dissociation produces the loss of cytoskeletal structure, which leads to the breakdown of axonal transport and dysfunction of neurons (**Figure 8**).

The decreased affinity of tau for MTs, as well as destabilization of the microtubule cytoskeleton, have been demonstrated in human brains with AD. For example, low levels of acetylated α-tubulin (Hempen and Brion, 1996) and reduced density of MTs (Cash et al., 2003) have been reported. The loss-of-function of tau hypothesis, from the point of view of both tau-MT interaction and MT destabilization, suggests that neuronal functions, such as axonal transport, will be disrupted as their function depends on intact MTs.

As discussed in section **1.6**, it has been hypothesized that abnormal tau phosphorylation -mediated reduced ability of hyperphosphorylated tau to bind and stabilize MTs, and that this might be the mechanism by which tau disrupts neuronal function (as reviewed in Cowan et al., 2011). In support of this, a reduction in stable MTs has been demonstrated in AD brain (Hempen & Brion, 1996). In addition, phosphorylation of tau at specific sites has been implicated in reducing the ability of tau to bind to MT (Sengupta et al., 1998, Schneider et al., 1999). These phosphorylation sites include Ser262, Thr231, Ser235, and Ser214 (Sengupta et al., 1998, Schneider et al., 1999). This evidence suggests that it is possible that high phosphorylation causes the MT cytoskeleton to be compromised, and disrupt the neural network (as reviewed in Cowan et al., 2011).

Although MT overstabilization can cause neuronal dysfunction due to the disruption of axonal transport (Ebneth et al., 1998), accumulating evidence showing that tau is highly phosphorylated in tauopathies indicates that loss of MT binding by hyperphosphorylated tau could be the mechanism involved in the disease (Ksiezak -Reding et al., 1992) by inducing the loss of tau function.

MT destabilization upon hyper-phosphorylation, has been demonstrated in a number of different tau models. For example, in *Drosophila* melanogaster, which overexpresses the 3R isoform of human tau, it has been reported that tau is highly phosphorylated at Serine 202 and Ser396/Ser404, and results in the breakdown of MTs. As a consequence, axonal transport is interrupted and behavioural deficits are observed (Cowan et al., 2010). In particular, this result suggests tau that is highly phosphorylated is functionally incompetent. Additional finding in this study is that hyperphosphorylated htau$^{0N3R}$ sequesters endogenous *Drosophila* tau (dtau) away from the MT by binding to dtau (Cowan et al 2010). This observation suggests that functionally incompetent tau is capable of causing the pathogenic conversion of normal endogenous tau (Cowan et al 2010).

As mentioned in section **1.6**, treatment with specific inhibitors of GSK-3β, such as lithium and AR-A014418, results in the reduction of tau phosphorylation and improves locomotor behavior and axonal transport deficit, as a result of the recovery of the integrity of the cytoskeleton (Mudher et al., 2004). In addition, it shows that drugs capable of preventing hyperphosphorylation or helping to stabilize MTs, such as treatment with NAP in the same *Drosophila* model (Quraishe et al., 2013) are capable of rescuing axonal transport and behavioral phenotypes. These findings provide additional evidence that supports the importance of the stability of MTs for neuronal function. Furthermore, it supports that loss of normal tau function plays a role in axonal dysfunction.

In line with the above, in a mouse model that expresses htau$^{0N3R}$, a reduction in intact MT and loss of axonal transport were reported (Ishihara et al., 1999). Together, these studies demonstrate that phosphorylation of tau can cause MT destabilization and subsequently a breakdown in axonal transport. This would inhibit the necessary transport of essential material along the axons (As reviewed in Cheng and Bai, 2018) thus affecting synaptic function and potentially triggering the initiation of neurodegeneration.

The impact of tau expression on synaptic dysfunction has been reported in mouse models. For example, in a rodent model in which human tau is expressed with the P301S mutation (FTDP-17 associated mutation), hippocampal synapse loss and impaired synaptic function have been reported (Yoshiyama et al., 2007). Similarly, it has been described that mice that express normal

human tau isoforms (6 isoforms of human tau) present a phenotype of the pathology as learning impairment caused by synaptic interruption (Polydoro et al., 2009).

Additional to the above, overexpression and hyper-phosphorylation of tau have been reported to have a negative effect on mitochondrial axonal transport (Eckert et al., 2014). This is in line with a considerable number of studies suggesting that mitochondria could be affected in terms of morphology, bioenergetics, and transport in AD (as reviewed in Cabezas-Opazo et al., 2015 and Wang et al., 2015). For instance, in studies carried out in cell and mouse models, it was indicated that overexpression and hyper-phosphorylation of tau have an effect on both the location and distribution of mitochondria, also causing loss of axonal transport and loss of synapses (Cabezas-Opazo et al., 2015; Wang et al., 2015).

Together, these and many other studies suggest a causal relationship between phosphorylation and neuronal dysfunction. However, the mechanisms involved in the pathology are not completely clear and the loss of unction is not the only way in which tau becomes toxic to neurons. Despite the evidence indicating that loss-of-function produces the disease-characteristic tau toxicity, it has been suggested that loss-of-function may be necessary to trigger the disease, however, it is not the cause of the extensive degeneration that is observed in human tauopathies (Goedert, 2016). This indicates that other factors could be involved in tau-mediated dysfunction and tau-mediated neurodegeneration.

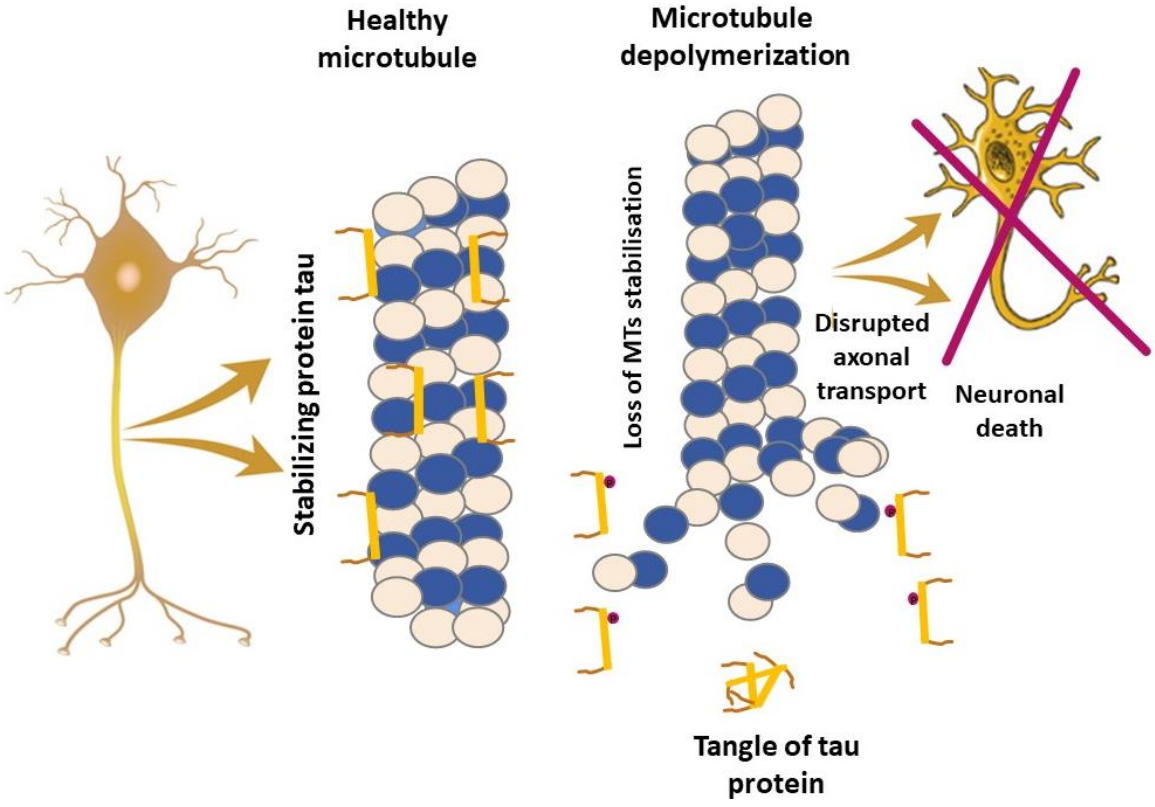

**Figure 8. Schematic representation of loss of function toxicity**

Post-translational modifications such as phosphorylation separate tau molecules from microtubules disrupting tau function; the free tau molecule aggregates and forms paired helical filaments.

When discussing tau and its loss of function, it is important to consider that the physiological function of tau remains largely unclear, making it difficult to understand the mechanisms that lead to toxicity in Alzheimer's disease.

As mentioned before, several animal models of tauopathy have been developed. However, the vast majority of model systems used, express human tau when already expressing endogenous tau. Therefore, interpretations of results should consider the expression of endogenous tau in these particular models (As reviewed in Lee et al., 2005). For example, in *Drosophila*, there is little information about how the htau expression compares to the expression of the endogenous dtau, for that reason the expression of htau gene is likely to be over-expressed. In addition, although some studies have examined how htau affects endogenous dtau and whether or not this contributes to the htau phenotype (Cowan et al. 2010) is not always clear, as there is limited knowledge in the field.

One way to extend our knowledge is to investigate the consequences of removing endogenous tau from the models commonly used to investigate tauopathies. It has been suggested that functionally, the reduction of tau protein may be equivalent to pathogenic mutations in the tau gene identified in familial FTD with parkinsonism linked to chromosome 17 (FTDP-17) (Zhukareva et al., 2001, 2003). In line with this, previous studies have shown that in humans, tau reduction is a characteristic of frontotemporal lobar degeneration variants with granulin (GRN) mutations (FTLD-TDP-GRN) (Zhukareva et al., 2001, 2003; Papegaey et al., 2016).

The physiological function of endogenous tau and its reduction has been investigated in the models used in this thesis, rodents and fruit flies. To do this, gene targeting to produce animals lacking the tau gene, knock-out (tauKO), has been developed. In a mouse model, the loss of tau produced subtle axonal defects, indicating that when tau is absent, other MAPs partially compensate for its activity (Harada et al., 1994; Bettencourt da Cruz et al., 2005; Barlan et al., 2013).

Few studies of this type have been carried out in the fly model. In one study, it was observed that the elimination of endogenous dtau does not impair the survival of flies. Likewise, it did not impair the ability to climb or neuronal function (Burnouf et al (2016). This is consistent with previous

studies in mouse models without mtau, where the mice do not have an obvious phenotype (Harada et al., 1994; Dawson et al., 2001; Fujio et al., 2007). Despite this, it is interesting that in KO mouse models, it has also been observed that with increasing age, mice develop motor deficits, and alteration in the locomotor ability (Ikegami et al., 2000; Lei et al., 20012).

In a more recent study conducted by Papanikolopoulou et al. 2019 using Drosophila tauKO and transposon insertion mutant Mi{MIC} tau, it was shown that the absence of dtau has an effect on the cytoskeletal dynamics in the adult brain. It was also found that loss of dTau has a dramatic effect on neuronal proteostasis and plasticity (Papanikolopoulou et al. 2019). Furthermore, it has been indicated that this lack of phenotype is not a consequence of the positive regulation of other proteins associated with MTs, as the loss of dtau does not affect the levels of the fly homologs of MAPs (in particular MAP1 and MAP7) that could compensate for the absence of dtau (Burnouf et al., 2016) (Papanikolopoulou et al. 2019), contrary to what has been reported in mouse models (Harada et al., 1994; Bettencourt da Cruz et al., 2005; Barlan et al., 2013).

Understanding the role of endogenous tau in animal models generated to investigate human tauopathies, improves the general knowledge as to whether the endogenous tau, normally expressed in these models, are real human tau orthologs. Additionally, the absence of endogenous tau provides insights suggesting that elimination of endogenous tau could help the brain resist toxic effects of Aβ in AD (Roberson et al., 2007).

Overall, in order to understand how endogenous tau can play a role in other characteristics that can trigger pathology, many studies are needed focusing on expanding knowledge of its physiological functions thatwould improve our understanding of the molecular and cellular mechanisms onfluencing its function and leading to tauopathies.

## 1.8 Toxic gain of function

In addition to loss of function and consequent role in synaptic dysfunction and degeneration, changes in tau such as phosphorylation, misfolding, and aggregation are believed to lead to a gain of toxic function. Toxic gain of function, as tau aggregation, is characteristic of all human tauopathies (Goedert, 2016). In this, tau enters an aggregation pathway that leads to the formation of filaments and paired helical filaments (PHF) that can cause dysfunction and degeneration. It is

believed that these aggregated forms of tau can cause toxicity by blocking, the axon, preventing the transfer of materials along the microtubules (Wolfe al., 2012). Therefore, it is possible that both loss of function and gain of function are involved in the pathogenesis of tau (Trojanowski and Lee, 2005).

It is important to understand how new toxic species are formed. As mentioned in **section 1.5**, an accepted theory is that phosphorylation is an early event in the formation of filamentous aggregates (Braak and Braak 1995). Due to this phosphorylation, the protein is detached from the microtubules, thus losing its normal function of stabilizing the microtubules, which leads to a breakdown in axonal transport (Cowan et al., 2010) (**Figure 9**). Therefore, free tau molecules can interact with each other until they finally form filamentous structures that culminate as intra-neuronal neurofibrillary tangles (NFTs) (Serrano-Pozo et al., 2011). However, it is unclear whether this event is sufficient to assemble tau aggregates into filaments and how these alterations lead to toxicity. Studies have yielded unclear evidence regarding the link between phosphorylation and the formation of aggregates. For example, while dephosphorylation of tau isolated from AD human brains has been shown to prevent the propensity for tau aggregation and PHF formation *in vitro* (Alonso et al., 2001), others have reported that high levels of tau phosphorylation are not sufficient to cause aggregation, which shows that other factors are necessary to promote tau assembly (Tepper et al., 2014).

Therefore, while phosphorylation is undoubtedly a key pathological alteration, aggregation can be considered as the most common modification suffered by tau, associated with the pathology.

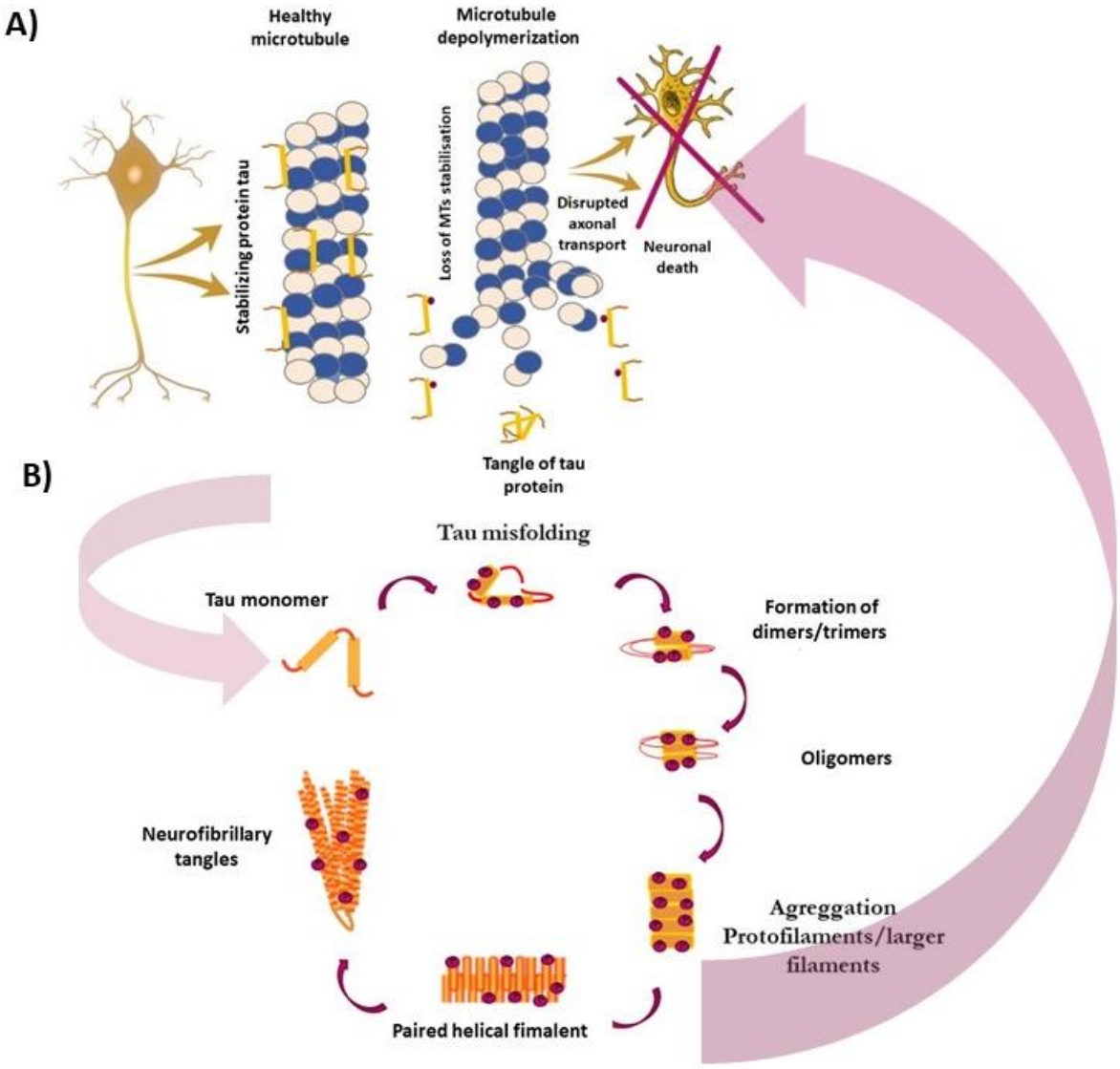


**Figure 9. The generation of different tau species; phosphorylation, misfolding and aggregation**

**A**) Phosphorylation separate tau molecules from microtubules disrupting tau function; the free tau molecule aggregates and forms paired helical filaments. **B**) Tau monomers become hyper-phosphorylated at specific phosphorylation sites, which induces misfolding of tau. Misfolding is hypothesised to preclude aggregation into dimers, trimers and larger aggregates termed oligomers. These are then thought to aggregate to form larger species termed paired helical filaments (PHFs) and neurofibrillary tangles (NFTs).

Tau aggregates, either in the form of filamentous neuronal or neuronal and glial tau inclusions, are associated with degeneration in affected brain regions. Therefore, they are the most common neuropathological feature that defines tauopathies (Lee et al., 2001). Although it is not clear how these filamentous inclusions form under physiological conditions (Cogdon et al., 2008), tau aggregation is reasonably well characterized *in vitro*. This has allowed us to understand some aspects that play an important role in the aggregation of tau and the formation of filaments.

For example, it is known that aggregation is achieved using polyanionic cofactors that compensate for the basic charge of tau, such as heparin or heparan sulfate (Goedert et al., 1996), and nucleic acids (Kampers et al., 1996) among others. These cofactors can initiate the nucleation of the aggregation, due formation of β-sheet conformation, which induces self-assembly with other tau molecules to form aggregates. Nevertheless, other factors might be involved in this process.

Another key factor for aggregation is the ability of two hexapeptide motifs, in the tau protein, to change conformationally from a native disordered structure to an abnormal β-sheet structure (Von Bergen et al., 2005; Murkrasch et al., 2005). These hexapeptide motifs are VQIVYK at the beginning of the third repeat domain R3, and VQIINK at the N-terminus of the second repeat domain R2 (von Bergen et al., 2000) (**Figure 10**). Thus, these hexapeptide motifs are known to be critical in driving the aggregation of tau protein (Von Bergen et al., 2000; von Bergen et al., 2001; Li and Lee, 2006; Bulic et al., 2010). In particular, it has been described that hexapeptide motif at the beginning of R3 $^{306}$VQIVYK$^{311}$ stimulates pathological aggregation, forming the nucleus of PHFs (Jeganathan et al., 2008; Von Bergen et al., 2006; Lee et al., 1989). On the other hand, the presence and interaction of $^{306}$VQIVYK$^{311}$ with $^{275}$VQIINK$^{280}$ is believed to produce twisted PHF-like filaments (Von Bergen et al., 2000). Description of these types of filaments are explaining later and examples of their morphology are shown in **Figure 10**.

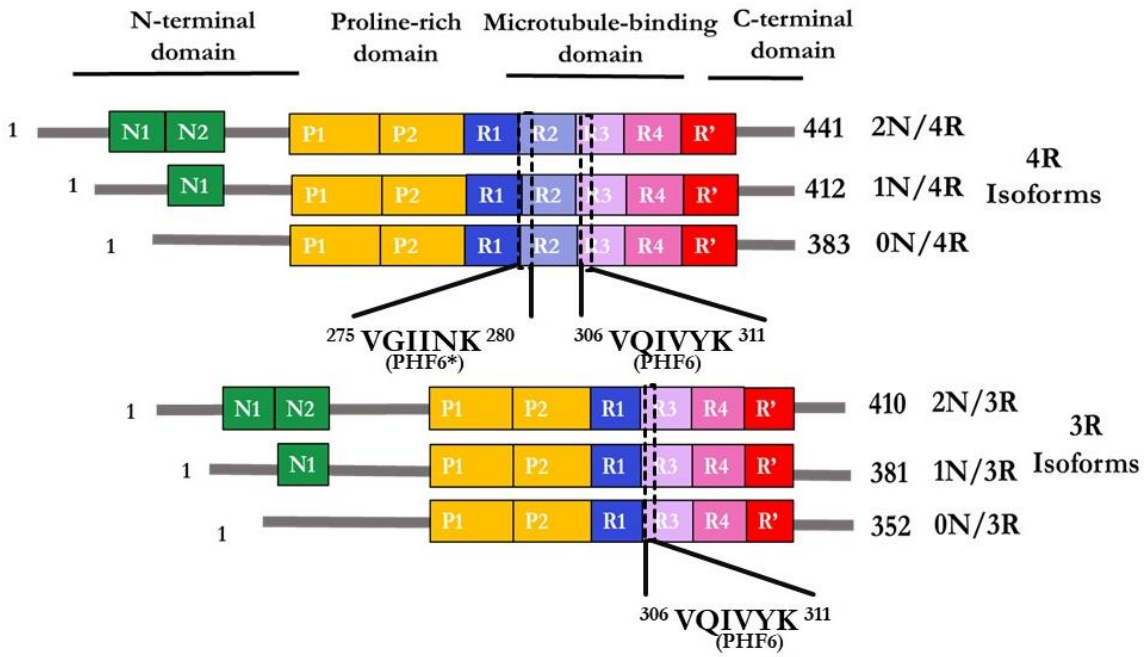


**Figure 10. Schematic representation of the six tau isoforms and hexapeptide motifs**

There are 6 different isoforms of Tau with different chain lengths. The two hexapeptide motifs necessary for formation of β-sheet ($^{275}$VQIINK$^{280}$ and $^{306}$VQIVYK$^{311}$) are present at the beginning of repeat region R2 and R3. Figure adapted from (Zeng et al., 2020)

Along with this, examples of mutations that can alter tau function and thus induce pathology have been identified (Hutton et al., 1998; Poorkaj et al., 1998; Spillantini et al., 1998). In AD and other tauopathies, genetic alterations cover 5% of cases. For example, the P301S mutation in exon 10 of tau has been shown to cause a reduction in the ability of mutant tau protein to promote microtubule assembly and a marked effect that stimulates the assembly of tau filaments (Goedert et al., 1999; Sperfeld et al., 1999; Morris et al., 2001). Furthermore, these mutations in the gene related to FTLD disorders are believed to increase the propensity for the β-structure of tau, thus inducing tau aggregation. For example, FTDP-17 mutations in the repeat domain, such as ΔK280 or P301L, have been reported to promote tau aggregation in PHF forms (Barghorn et al., 2000). Specifically, it has been shown that the ΔK280 mutation in repeat domain constructs (K18 construct) induces aggregation *in vitro*, even without the need to use aggregation inducers such as heparin (Barghorn et al., 2000, von Bergen et al., 2001, Kaniyappan et al., 2017). This shows that mutations accelerate tau aggregation due to the propensity to form β structure.

### 1.8.1 Tau aggregation: filaments and NFTs

The morphologies of tau fibrils isolated from brain tissue with AD and fibrils formed *in vitro* have been characterized. The dominant components of neurofibrillary lesions in AD have been characterized by optical microscopic techniques, as previously shown, and by techniques that allow confirmation of both their β-sheet structure and their twisted helical structure. Thus, these dominant components of the lesions have been reported as paired helical filaments (PHF) and straight filaments (Kidd 1963). The ultrastructural characteristics of tau filaments isolated from AD brain tissue and formed *in vitro* have been extensively studied.

For instance, the paired helical filaments (PHFs) appear to be composed of two filaments that twits around one another forming the typical periodic structures of approximately 65-80nm and a variable width of between 8 and 20nm in diameter (Crowther and Wischik, 1985) and average length of 530 nm (Moeozova et al., 2013). Straight tau filaments (SFs) have been reported with an average width from 10 to 15 nm (Crowther, 1991). It has been confirmed that both structures are composed predominantly of abnormally hyper-phosphorylated tau proteins (Wischik et al 1988, Lee et al 1991). In AD, it has been reported that all six tau isoforms are present in the PHF. In addition, it has been reported that the repeat domain forms the core of the PHF (Wischik et al., 1988).

On the other hand, both the N-terminal and C-terminal regions separate from the core structure and have been described as the diffuse layer of PHF (Crowther and Wischik, 1985). This diffuse layer has the characteristics of a "brush of soft polymer "that extends from the PHF core (Wegmann et al., 2013; Wegmann et al., 2010) and is mobile even upon aggregation (Sillen et al., 2005). Examples of these PHFs and SFs are shown in **Figure 11.** The filaments from AD and from recombinant proteins have similar features and dimensions when viewed under electron microscope. However, it has been reported that fibrils generated *in vitro* from full-length tau, present different lengths, and morphology (Wegmann et al., 2010). Likewise, it has been suggested that tau can assemble into structurally similar subunits that are arranged differently to form polymorphic fibril shapes (Wegmann et al., 2010).

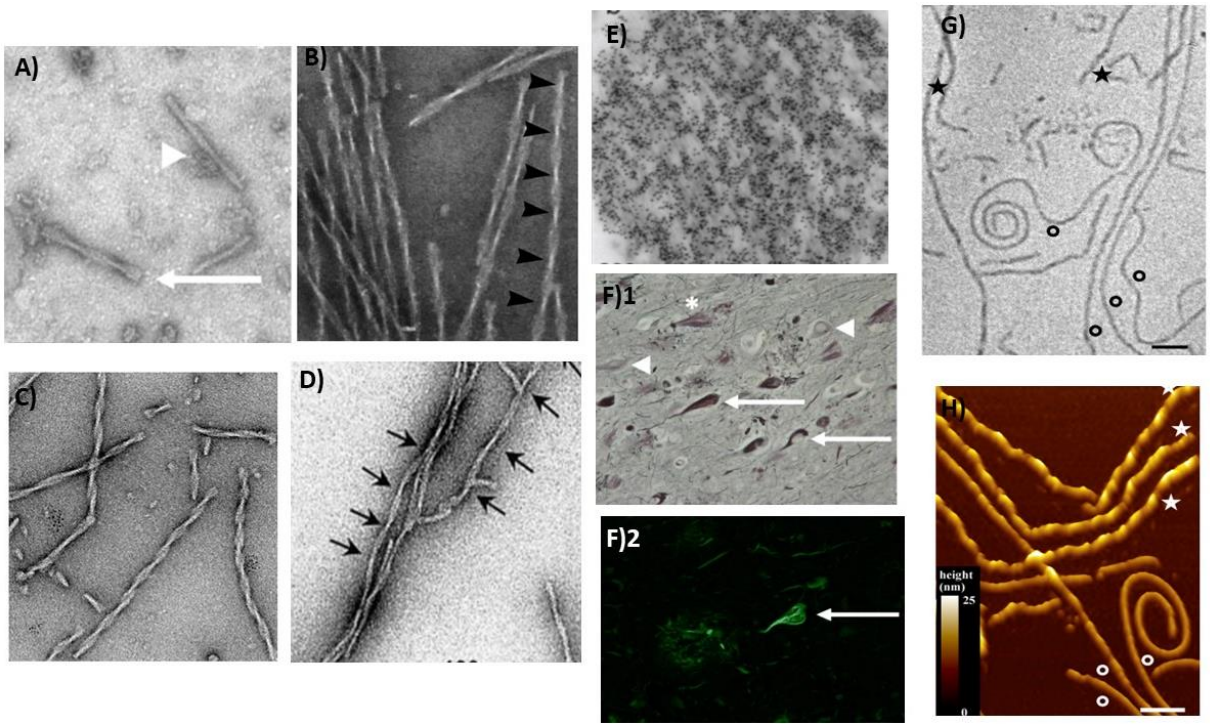


**Figure 11. Examples of filaments and NFTs morphology**

**A)** Electron Micrographs of PHF Twisted filaments (arrows) and Straight Filaments (arrows heads) isolated from Alzheimer's brain tissue. Taken from (DeTure and Dickson, 2019). **B)** Electron Micrographs of PHF Twisted filaments isolated from Alzheimer's brain tissue, arrowheads pointing the double-stranded twisted appearance with a cross-over repeat of 80 nm. **C)** Filaments generated in vitro from the pro-aggregant tau repeat domain (K18ΔK280). **D)** PHF generated in vitro Htau23 (the smallest, fetal isoform) assembled in the presence of cofactor heparin. Taken from (Mandelkow and Mandelkow, 2012). **E)** A neurofibrillary tangle, immunogold labeled with anti-tau antibody. Taken from (Bukar Maina et al., 2016). **F)** Neurofibrillary tangles formed from intracellular pre-tangles containing misfolded tau and small tau aggregates to mature NFTs containing bundles of cross-linked tau filaments before the neuron dies and an extracellular ghost tangle (asterisk) remains. Silver staining (1) and Thioflavin S (2) capture many mature tangles (arrows) and some pre-tangles (arrowheads). Taken from (DeTure and Dickson, 2019). **G)** EM images of hTau40 fibril, heterogeneous mixture of fibril shapes. **(H)**, AFM topography of the same fibril preparation confirms the heterogeneity of fibril structures. Taken from (Wegmann et al., 2010).

Filaments structures have been described by using Cryo-electron microscopy (Cry-EM) techniques with image reconstruction, allowing the confirmation of a prominent structure of β-structure in the repeat domain. In addition, when comparing the filaments from Pick's disease and those from Alzheimer's (Falcon et al, 2018) using these techniques, differences between folds have been

described in the repetitions of different types of diseases (**Figure 12**) (Falcon et al., 2018). This observation suggest that different pathologies can be explained by structural differences between different tau isoforms.

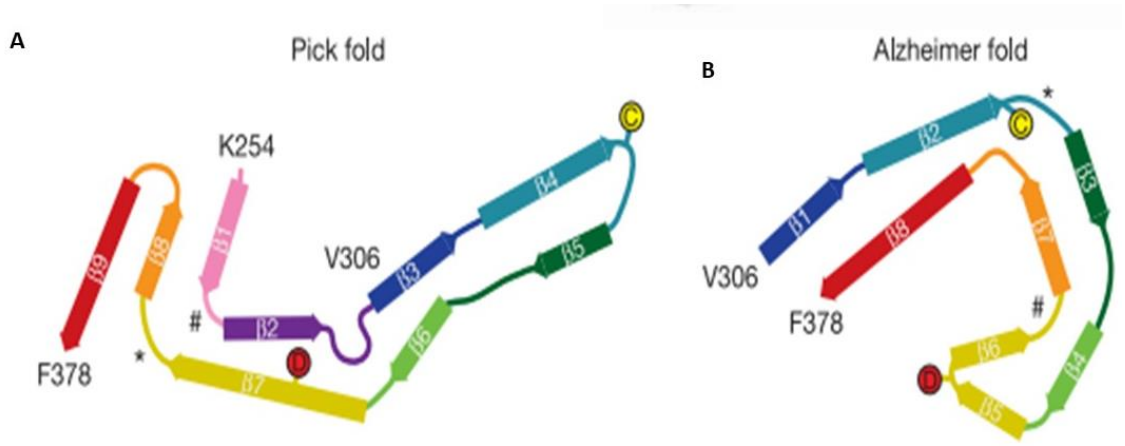


**Figure 12. Example of structural differences in filaments in AD and Pick disease**

A) Shows the secondary structure elements in the Pick and Alzheimer folds. It is shown the position of Cys322 (yellow 'C') and Asp348 (red 'D) in the two folds are highlighted. The asterisk and hash symbols mark conserved turns of homologous regions in the Pick and B) Alzheimer folds (taken from Falcon et al., 2018)

To understand these disorders, it is important to understand the role of the filamentous species of tau and neurofibrillary tangles in neuronal dysfunction and degeneration.

### 1.8.2 Filaments and NFTs in toxicity

The presence of NFTs and neuropil threads are key pathological hallmarks in AD and other tauopathies. Because of this, the classical view associates these conformational species with the pathology. One of the most important pieces of evidence to corroborate the causal role of NFTs in pathology is that their presence correlates with neuronal loss and their proliferation throughout the brain is related to the severity of symptoms (Braak and Braak, 1991; Arriagada et al., 1992, Dickson et al., 1995). The NFTs accumulate and propagate across the brain in a characteristic

pattern as AD progresses. The NTFs have been used as a histopathological characteristic of the disease by positive immunoreactions. Thus, its progression through stereotyped neuroanatomic stages allows its description and classification. The NFTs are believed to undergo morphological changes of maturation ranging from pre-tangles, which occur in early stages, detectable intracellular NFTs, to ghost tangles (extracellular tangles, which were formed from death neurons, previously housed in intracellular NFTs) at a late stage (Uematsu et al., 2018). For example, moderate pathology is assigned when immunoreactive structures are easily visible, and severe classification is assigned when NFTs and neuropil threads (NTs) are clearly visible.

In a recently published study, a new feature of early pathology called “diffuse pathology” has been described using a novel technique that allows the visualization of tau multimers both in vitro and in situ (Bengoa Vergniory et al., 2021). These authors reported the ability of a method, described as tau-proximity ligation assay (Tau-PLA), to detect multimerization of tau from pre-symptomatic Braak stages as shown in **Figure 13**. In this study, the authors, in addition to demonstrating maturity with a time of formation of NFTs, provide a method that allows studying and detecting pathology at an early stage (Bengoa Vergniory et al., 2021).

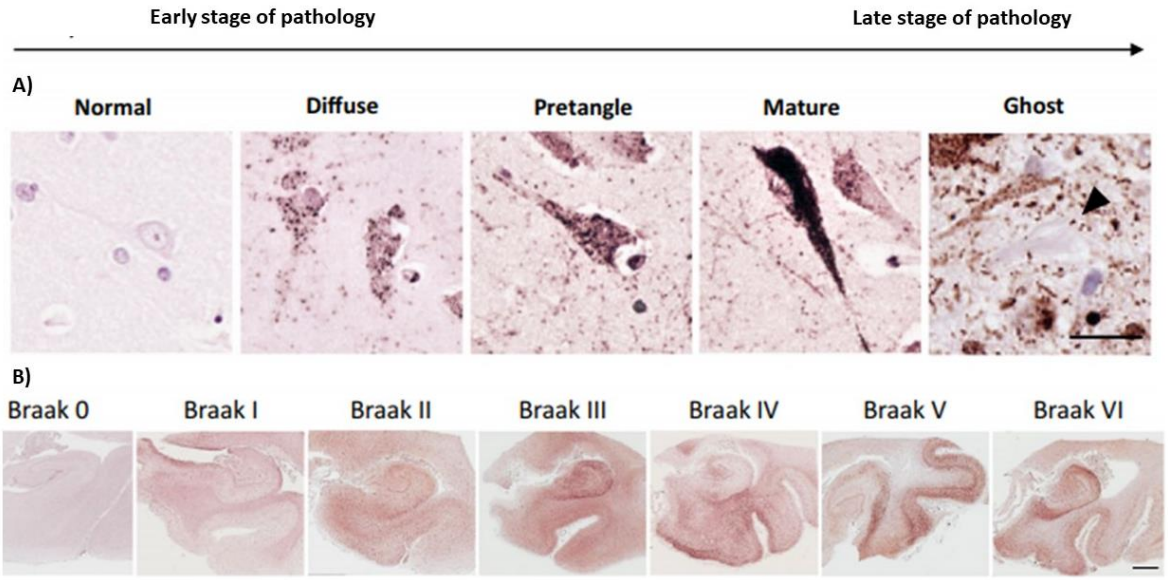


**Figure 13. Morphological changes of NFTs**

Characterization of Neurofbrillary tangle maturity using tau-proximity ligation assay (tau-PLA). A) Shows tau-PLA staining for normal, diffuse, pre-tangle, mature NFTs and ghost pathology. Scale bar 50 µm. B) Shows, tau-PLA distribution through the different Braak stages. Taken from (Bengoa-Vergniory et al., 2021)

One of the main questions to understand the pathology is to understand how NFTs are related to toxicity in neurons? The morphological changes that occur with NFTs and are associated with pathology indicate that one of the possible mechanisms of tau-mediated toxicity, which is the propensity to spread, thus affecting different regions of the brain. As in human tauopathies, in transgenic mouse models, tau filament formation correlates with the death of nerve cells (as reviewed in Lee et al., 2001). In particular, this has been observed in mouse models expressing human tau with mutations related to FTDP-17. For example, cell loss, specifically in the number of motor neurons, has been reported in these transgenic mice of both the human tau line P301L and P301S in the presence of filaments at 19.5 weeks and 21 weeks respectively (Lewis et al., 2000; Allen et al., 2002). These studies, suggest a causal role of filaments in dementia. Corroborating these findings, in studies carried out in a mouse model transgenic for wild-type human tau, the formation of tau filaments or loss of nerve cells has not been reported, suggesting that the presence of tau filaments such as NFT cause pathogenesis of tau (Ishihara et al., 1999; Spittaels et al., 1999; Probst et al., 2000).

Despite the early focus on the large insoluble tau filaments, such as NFTs, as causative of pathology, the evolving weight of evidence is reconsidering the role of NFTs as a primary cause of the disease (as reviewed by Frost et al., 2015). The large insoluble tau filaments and NFTs typically form after the onset of pathogenesis (Gómez-Isla et al., 1997; Barghorn and Mandelkow, 2002; Maeda et al., 2006; 2007) and this can suggest that NFTs may be a consequence of disease rather than a cause.

To support this notion, some studies have suggested that the formation of such deposits is not necessary for the appearance of pathological symptoms such as behavioural abnormalities. For instance, in studies conducted in mouse models expressing non mutant tau, NFTs are formed, however, cognitive deficits occur earlier than NFTs formation (Andorfer et al., 2005). In addition, in P301L tau transgenic mice model, behavioural changes have been related to initial aggregation of mutant tau. For instance, in a mouse line expressing human P301S tau, synapse loss and impaired synaptic function in 13 weeks-old mice was indicated when no noticeable tangle pathology was found in the mouse brains (Allen et al., 2002, Xu H et al., 2014).

Other studies demonstrated that, in mouse models of tauopathy where tau expression is switched off, memory deficits were found to improve but NFTs were still found to accumulate (SantaCruz et al., 2005, Spires et al., 2006), suggesting a different species is responsible for tau-mediated deficits in memory. Similarly, in case of inducible mouse models, upon suppression of tau full length tau-ΔK280 mutation (Eckermann et al., 2007) the memory function improved but the NFTs continued

to accumulate. Similar observations have been reported in other animal models. For instance, some studies using *Drosophila* demonstrate that human tau overexpression is sufficient to cause behavioral deficits as a result of neuronal dysfunction and subsequent age-dependent degeneration) without the formation of NFT (Wittmann et al., 2001; Mudher et al., 2004; Cowan et al., 2010; 2015; Ali et al., 2012; Sealey et al., 2017) . Collectively, these observations suggest that NFTs are not required for dysfunction and their role in degeneration is not clear.

It has been reported that the intermediate species, such as oligomers, induce synaptic and mitochondrial dysfunction after injection into wild type mice (Lasagna-Reeves et al., 2011). In this study, it was demonstrated that these aggregates could cause behavioural deficits and neurodegeneration. In a recent study, it was reported that oligomers generated *in vitro*, from the pro-aggregated tau repeat domain, induced synaptoxicity, however, they did not affect cell viability (Kaniyappan et al., 2017). Hill et al. reported that oligomers generated *in vitro* from full-length tau (2N4R) induced synaptic dysfunction when injected into the brain of mice (Hill et al., 2019). These studies indicate that oligomeric species are the tau species that potentially induce neuronal dysfunction in the disease.

How do these oligomers form? The aggregation pathway into PHFs and NFTs has been described as a process consisting of several steps involving the formation of various and heterogeneous aggregates, including aggregation of monomers and spherical small soluble oligomers (**Figure 14**). The conformational change of tau monomers may favour spontaneous association leading to the formation of dimers (Chirita et al., 2005). These dimers play a key role as intermediate in the formation of larger oligomers, and further aggregates (Sahara et al., 2007, Patterson et al., 2011; Kaniyappan et al., 2017). Therefore, tau dimers have been established as key intermediates in the assembly of PHF (Wille et al., 1992), acting as effective building blocks (Friedhoff et al., 1998). Covalently linked dimers can be formed by disulfide cross-linking (Friedhoff et al., 2000).

Oligomers can be defined as molecules ranging from small, as dimers, to prefibrillar and non-fibrillary forms (Kaniyappan et al., 2017). These species can be compatible with further polymerization and fibrillary formation or not compatible with fibrillary elongation (as indicated in **Figure 14**). Oligomers are defined by means of their solubility in aqueous solution or in detergents (Kaniyappan et al., 2017). Oligomers compatible with fibrillary formation adopt a β-sheet conformation, and eventually lead to the formation of insoluble aggregates (kenyappan et al., 2017) that culminate as NFTs (as shown in **Figure 14**).

It is believed that soluble oligomers can be formed by several dozen-protein molecules. For example, small soluble oligomers can consist of less than 10 protein molecules. These small oligomers can be detected on SDS gels and the morphology can be detected by AFM (Atomic Force Microscopy). Larger or granular tau oligomers, can consist of hundreds of subunits. Insoluble tau oligomers, obtained by pelleting assay, can be formed from up to 70 protein molecules. Understanding how these pathological species form in AD and other tauopathies is a key focus of research.

The NFTs share a common "cross-β sheet" structure commonly seen within the neurons of AD patients and serve as a histopathological marker and are a common feature of many amyloid-like deposits (Lansbury, 1999). In these, the β strands run perpendicular to the helix axis forming a “cross-β sheet" motif (Blake and Serpell, 1996). These structures can be stained with certain dyes, such as Congo red or thioflavin S, that interact with the repeating β strands (Glenner et al., 1972). Some of these dyes allow the monitoring of PHF assembly *in vitro*, yielding valuable information on how these structures are formed. For instance, in an *in vitro* study that relies on the use of Thioflavin S (ThS) dye, it has been reported that aggregation occurs after a lag period in which no increase in the fluorescence intensity is observed (Friedhoff et al., 1998). This suggests that aggregation requires the formation of β strands structures and this can be monitored following the fluorescence intensity of the ThS. Furthermore, using this same method, the authors have also reported that oligomers ranging from 8 to 14 protein molecules (monomers) act as nucleation seeds, which then elongate (due to polymerization and formation of β-sheet structure) into PHFs (Friedhoff et al., 1998). These observations demonstrated that the formation β-sheet structure is necessary to form NFTs. In line with this, it has been demonstrated that in the case of oligomers comprised of dimers and trimers generated from full length tau constructs with deletion of one hexapeptide sequence ($^{306}$VQIVYK$^{311}$) unable to form β-sheet structure, cannot form filament (showing aggregation compatible with filament formation) (Sahara et al., 2007).

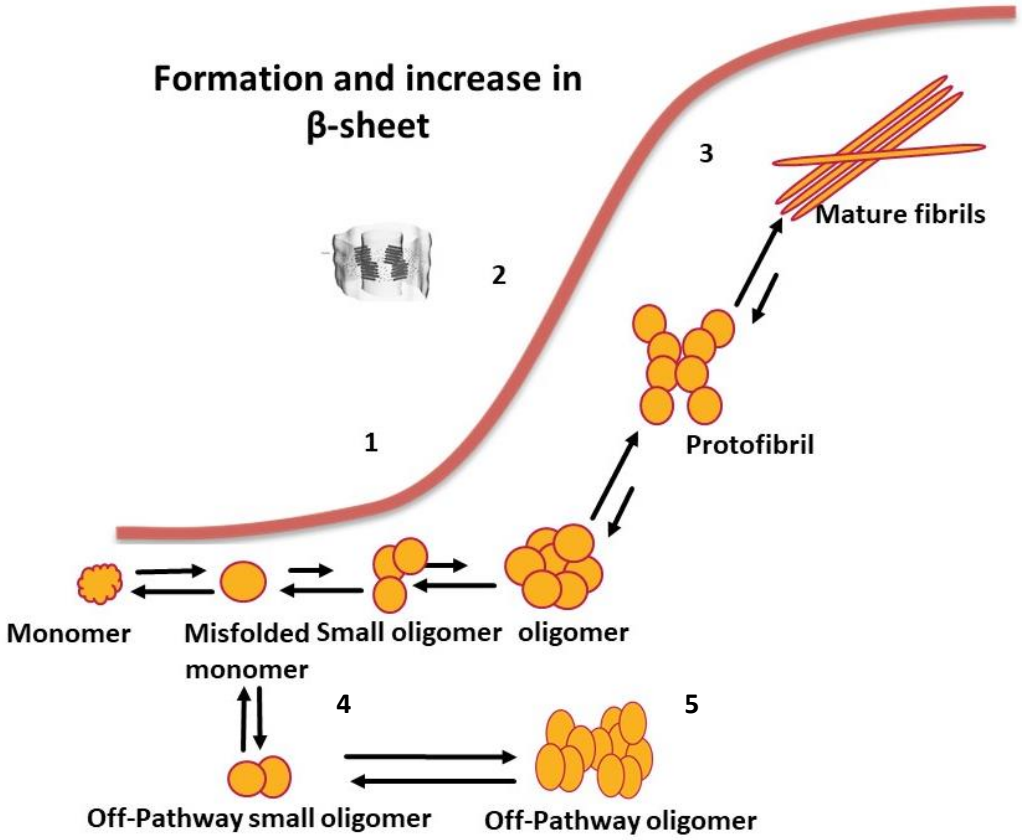


**Figure 14. Schematic representation of aggregation pathway**

The classical amyloid aggregate formation typically consists of three phases: **1**) a nucleation phase, in which the monomers undergo conformational change, misfolding and associate to form oligomeric nuclei, and **2**) A elongation phase, in which nuclei grow rapidly by sequestrating monomers and forming **3**) larger fibrils rich in β-sheet. On the other hand, **4-5**) other species are not compatible with β-sheet conformation, elongation and fibrillary formation.

Together, this evidence suggests that NFTs or PHFs are not the main cause of the disease and implies that distinct species play a role in the initiation and progression of the disease. In this thesis it is suggested that intermediate species such as oligomers are responsible for the dysfunction that arises at the beginning of the disease; NFTs or PHFs are responsible for toxicity in the form of degeneration and are formed during the advanced stage of the disease (as shown in **Figure 15**).

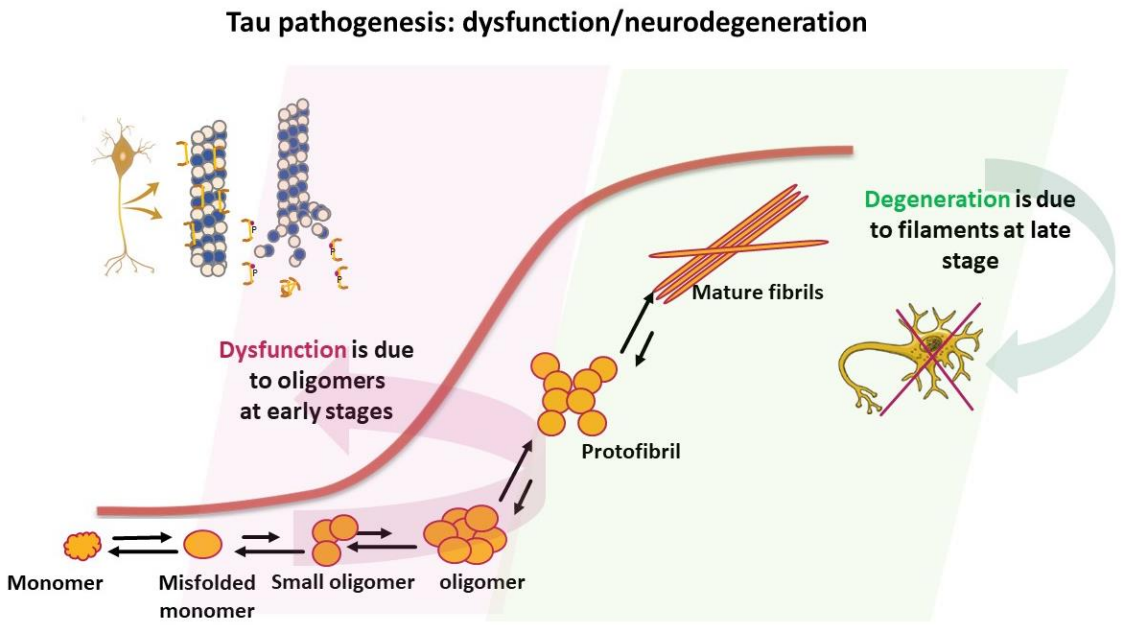


**Figure 15. Schematic representation of possible mechanisms of tau pathogenesis**

Intermediate tau oligomers are the pathogenic tau species that cause tau-mediated neuronal dysfunction in the early stages. Fibrillary tau are the tau species that cause degeneration and are formed during the advanced stage of the disease.

## 1.9 Seeding and propagation

Tau-mediated toxicity can occur through propagation mechanisms. In disease, the progression of pathology has been demonstrated. Progression has been shown to be based on the ability of pathological tau to transform naïve protein (healthy monomeric protein) into aberrant forms. This concept is known as seeding, and describes the ability of aggregate forms to act as "seeds" that template the aggregation of a healthy protein. This concept has been reported as a characteristic feature in the field of prion pathology (Prusiner, 1982).

In particular, the initial event that allows the transformation from physiological normal protein to the aberrant form is not completely understood (Mudher et al., 2017). However, this and the concept of seeding can be explained by the extensive observations reported in *in vitro* studies in which the mechanisms of protein self-assembly have been studied (these mechanisms have been described in detail in the review published by Goedert, 2016).

Among these mechanisms, it is important to consider the nucleation-dependent polymerization mechanism. In this, self-assembly depends on the formation of a nucleus in the reaction, this nucleus has a different conformation than the healthy monomeric protein (**Figure 16**). Once the nucleus is formed, the protein monomers aggregate to form aggregate species that can act as seeds. The formation of the nucleus is energetically unfavorable and therefore it is a slow process (Goedert, 2016). However, as the seeds form, self-assembly occurs rapidly (**Figure 16**). When performed seeds are added to the reaction, the self-assembly and further aggregation (forming larger aggregates and filaments) occur rapidly, since the slow nucleation process is not necessary (Goedert, 2016).

Another mechanism important to understand this concept is the nucleated conformational conversion. In this, oligomeric species form at the early stages of the reaction. However, at this stage, these oligomers do not have the ability to incorporate monomers. These oligomers become prone to aggregation until they change their conformation and become nuclei. In particular, it has been suggested that the latter mechanism could occur in the aggregation and seeding of the tau protein (Goedert, 2016).

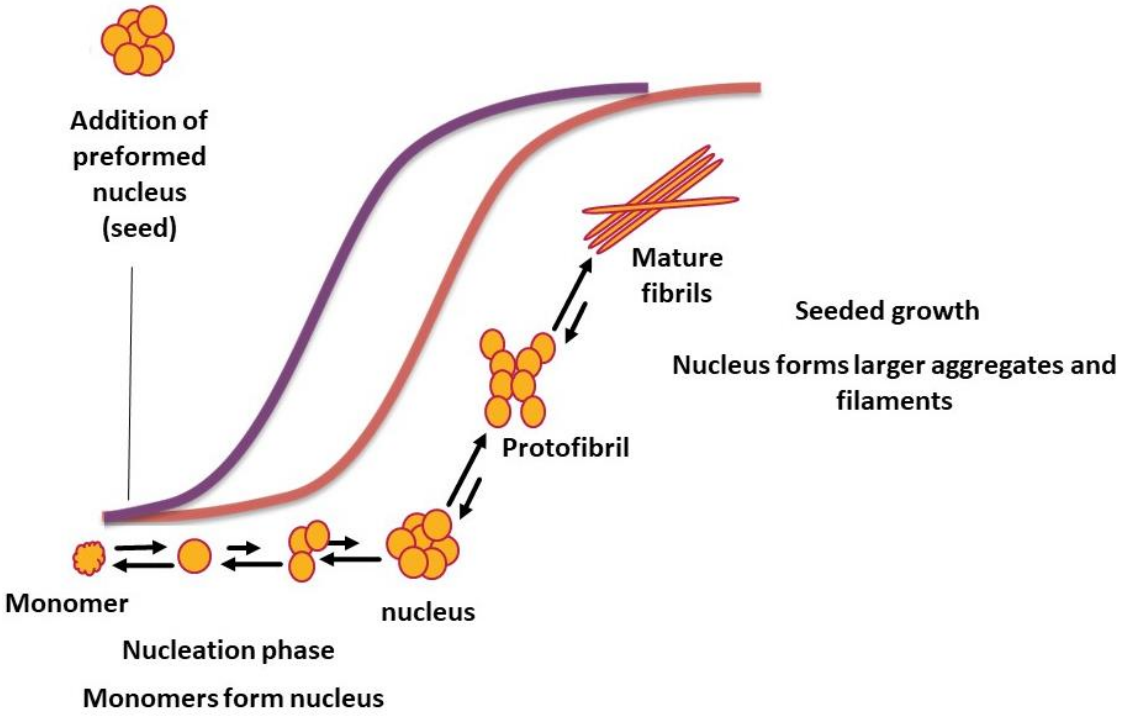


**Figure 16. Representation of nucleation-dependent polymerization mechanism**

During the nucleation phase, the monomeric protein misfolds adopt a conformational change, and form a nucleus. Then, the protein monomers aggregate self-assembly and form aggregate species that can act as seeds. This process occurs during the nucleation phase and is energetically unfavourable and therefore it is a slow process. As the seeds form, self-assembly occurs rapidly allowing seeded growth. As shown in purple, when preformed seeds are added to the reaction containing monomers, the self-assembly and further aggregation (forming larger aggregates and filaments) occurs rapidly, since the nucleation process is not necessary.

In the field of tauopathies, some previous studies have shown the addition of preformed tau protein seeds, inducing the aggregation and filament formation (Alonso et al., 1996; Frost et al., 2009) and this process can occur in an accelerated manner (Clavaguera et al., 2009; Frost et al., 2009). For example, in a study conducted by Alonso et al., it has been shown that hyper-phosphorylated tau isolated from AD brains induce self-assembly when added to the in vitro reaction with recombinant tau (Alonso et al., 1996). This study demonstrated for the first time that tau had the ability to act as a seed and template the aggregation of monomeric tau. In line with this, it was also shown that preformed seed aggregation (synthetic tau filaments) had the ability to accelerate tau aggregation and filament formation under *in vitro* conditions (Frost et al., 2009). Similarly, in studies carried out in both mouse models and in cell models, evidence has been reported indicating that when preformed aggregates of tau are added extracellularly, these aggregates act like seeds, seeding the

aggregation of tau and inducing subsequent propagation (Spillantini and Goedert, 2013; Goedert, 2016).

As in prion pathology, the formation of seeds with the ability to spread has been demonstrated (as reviewed in Alyenbaawi et al., 2020). The progression of tau aggregates through the connected brain regions has been extensively described in AD and other tauopathies (as reviewed in Mudher et al., 2017 and Alyenbaawi et al., 2020) (**Figure 17**). In this sense, the propagation of tau in a prion-like manner could be an explanation for this phenomenon, indicating similar characteristics of tau to prion pathology (Alyenbaawi et al., 2020). For example, this property has been described in a transgenic mouse model in which when brain extract from transgenic mouse expressing human tau (0N4R isoform) with the P301S mutation is injected into mice expressing wild-type human tau (2N4R), the injected mice developed filaments. In contrast, mice expressing only wild-type human tau did not develop filaments or signs of neurodegeneration. These results demonstrate the seeding capacity of the pathological tau protein. In addition, in this study, it was indicated that the spread of the tau aggregates towards regions distant from the injection site (Clavaguera et al., 2009).

Currently, the nature of the species of tau aggregates that have the capacity to seed the pathology is not very clear. Some evidence suggests that the oligomeric forms are the species capable of seeding the tau pathology. Small oligomers (trimers) isolated from both *in vitro* formed aggregates and isolated from AD brains have been reported to be capable of inducing seeding (Mirbaha et al., 2015). Similarly, in primary neurons and mice using tau species isolated from brain extracts, seeding through species of soluble tau oligomers but not monomers were detected (Takeda et al., 2015).

However, more studies are necessary to elucidate the species responsible for the seeding of aggregates and potential involvement in both transmission and toxicity.

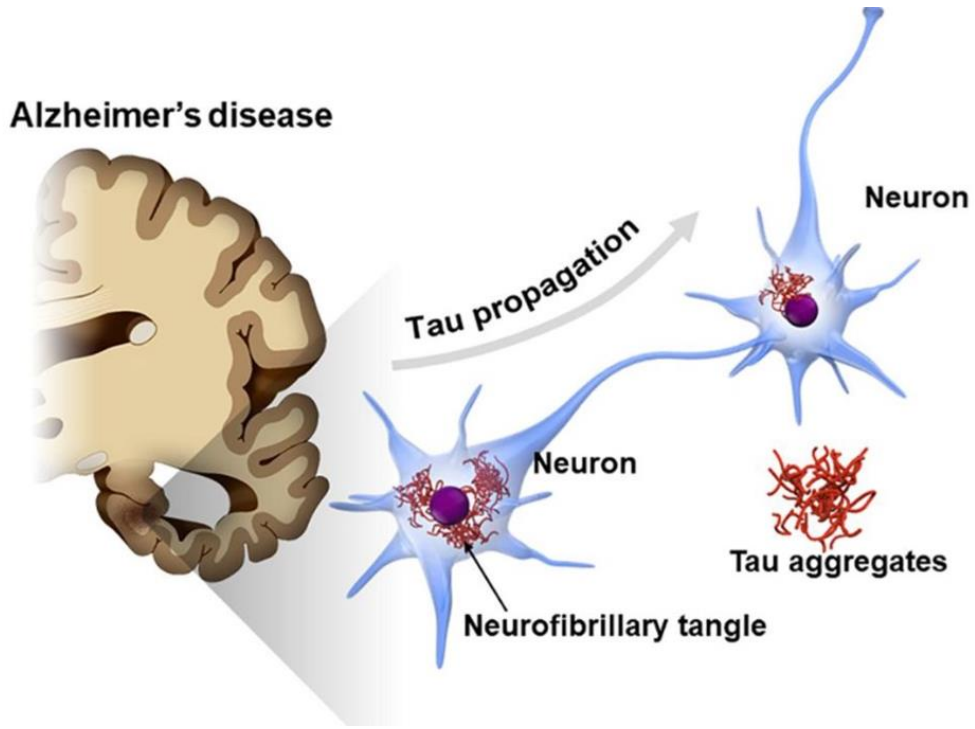


**Figure 17. Spreading of tau pathology in the Alzheimer's disease (AD)**

The image shows the spread of tau pathology in the Alzheimer's disease (AD) brain. Tau pathology in the AD brain (NFT) spreads in the neural network in a stereotyped manner. Interneuron transfer of the pathological form of tau may underlie the stereotyped progression of AD neuropathology (tau propagation hypothesis). (From Takeda, 2019).

In particular, when the template in a cell generates the seeding, it is possible that some of these seeds of cells that have been affected (donor cell) escape and are transferred to adjacent cells (recipient cells) or tissues. For this reason, it has been suggested that various factors such as cell uptake of aggregates, seeding, and secretion are necessary processes for aggregate propagation (Frost et al., 2009; Falcon et al., 2015). However, although there are different hypotheses about the mechanisms in which tau is released from the cell and transferred to another acceptor, these mechanisms and implications in tau pathology under physiological conditions are not completely clear (Mudher et al., 2017).

Another concept of prion pathology is the concept of strain. This concept refers to the existence of different strains of aggregates with different conformations. As mentioned in section **1.3**, there is evidence to suggest that there are different tau conformations with different morphological characteristics and different abilities to affect certain regions of the brain (Clavaguera et al., 2013; Sanders et al., 2014).

Evidence that demonstrates the existence of different strains has been established through studies in which homogenized human brains are injected into models of tauopathies. For example, in one study, homogenates from the brains of patients with various tauopathies (AD, TD, PiD, AGD, PSP, and CBD) were injected into mice expressing a single isoform of wild-type human tau. In this study, the injection of homogenates was carried out in the hippocampus and cerebral cortex of transgenic mice. What these authors report is the formation of the pathological structures that define the corresponding tauopathy of the injected homogenates, either AGD, PSP, or CBD (Clavaguera et al., 2013). More recently, ultrastructural studies using Cryo-EM have shown structural differences between tau filaments (Fitzpatrick et al., 2017; Falcon et al., 2018).

On the other hand, it has been shown that filaments isolated from the brains of AD patients or isolated from transgenic mice have better seeding capacity than recombinant tau (Morozova et al., 2013; Falcon et al., 2015). For instance, recombinant tau has been reported to be more resistant than transgenic mouse brain aggregates, when evaluated by guanidine hydrochloride disintegration and proteinase K digestion. This suggests that more stable aggregates possess less seeding activity (Falcon et al., 2015).

Despite the evidence that suggests the existence of different strains of tau with different capacities to induce different tauopathies, more research is needed to clarify their role in human tauopathies.

## 1.10 Transgenic animal models to investigate tau pathology *in vivo*

Transgenic animal models have been used extensively to study tau-mediated neurodegeneration AD and other tauopathies *in vivo*. To do this, a number of transgenic animal models expressing human tau and mutant tau have been generated. Such well established models exist in both rodents (Allen et al., 2002; Lewis et al., 2000; Tanemura et al., 2001; Tatebayashi et al., 2002) and *Drosophila melanogaster* (Mudher et al., 2004; Chatterjee et al., 2009; Folwell et al., 2010; Quraishe et al., 2013; Sealey et al., 2017). These models mimic the essential characteristics of human tauopathies, which makes them suitable for investigating important aspects in relation to the mechanisms of tau-mediated toxicity in tauopathies. For instance, some of these models have provided valuable information on the causal role of on the species associated with toxicity.

As mentioned in section **1.8.2**, NFTs are the most common neuropathological feature that defines AD and other tauopathies (Lee et al., 2001). The presence of these pathological species of tau is

correlated with neuronal loss and their proliferation throughout the brain is related to the severity of symptoms (Braak and Braak, 1991; Dickson et al., 1995). Because of this, the classical view associates these conformational species with pathology. However, some transgenic models have provided important evidence dissociating the causal role of these species in the disease.

Recapitulating AD, in transgenic mouse models expressing tau with mutations related to FTDP-17, the formation of NFT and the loss of neurons are observed in parallel in the same regions of the brains. For example, the expression of P301L mutant tau in mice under the Thy 1.2 promoter causes neuronal loss and NFT formation at the same location (Lewis et al., 2000; Gotz et al., 2001). These studies showed a strong association of causal role of NFTs in pathology. However, it was not until tools that allowed the regulation of human tau expression in these models were developed that the evidence began to look for another form of tau species responsible tau-mediated toxicity (SantaCruz et al., 2005; Spires et al., 2006). Similar models in which the full-length repeat domain is expressed with the ΔK280 tau mutation (Mocanu et al., 2008; Sydow et al., 2011) or with the full-length tau (Eckermann et al., 2007) were generated later supporting the notion that alternative species (pre-NFTs formation), such as oligomeric species, might be responsible for the disease. Moreover, it provides novel evidence suggesting that the pathology could be reversible by stopping the formation of new pre-NFTs species.

The first description of these models was reported by SantaCruz et al. These authors described a regulable model of tauopathy expressing human tau with the P301L (FTDP-17 related) mutation (rTg4510 mouse model). In this, the expression of tau was regulated by tetracycline (which is analogous to doxycycline). When characterizing this model after tau expression, the authors observed memory alterations (assessed by the Morris water maze) evident at around 11 weeks of age (SantaCruz et al., 2005). At 17 weeks of age, the tau pathology became evident as deposits and as the disease progressed towards 43 weeks of age, macroscopic cerebral atrophy was evidenced with the presence of abundant NFTs. The authors demonstrated that this model recapitulates the formation and progression of pathology and neuronal impairment. However, when the authors turned off the continuous expression by repressing the tetracycline promoter with doxycycline, improved memory and rescued from neuronal impairment were described, while the accumulation of neurofibrillary tangles continued. These results demonstrated evidence for the first time that filaments and NFTs by themselves are insufficient to alter the cognitive function observed in tauopathies (SantaCruz et al., 2005).

Subsequent studies using this model described that the expression of tau leads to PHF1-positive tau accumulation in neurons that closely resemble those from human tauopathy (Spires et al.,

2006). These inclusions appeared as early as 11 weeks of age and at 34 weeks of age show region-specific progress, mimicking the progression described in human disorders. The onset was evidenced at 11 weeks of age, in dentate gyrus. This loss progresses to hippocampal areas (CA1 and CA2 / 3) at 24 weeks of age. In addition, at 34 weeks of age, the loss was evident in the cortex (Spires et al., 2006). This demonstrated that all regions suffered severe age-dependent neuronal loss. In contrast, suppression of the transgene expression prevented further neuronal loss without preventing further accumulation of neurofibrillary pathology (Spires et al., 2006). Together, these studies have provided important evidence suggesting that NFTs or PHFs are not the primary species causing toxicity, but rather suggest that other types of tau species, such as oligomeric species, may be required for tau-related toxicity.

In addition to rodent models, *Drosophila* model for tauopathies has provided valuable information on the causes and mechanisms of tau-mediated toxicity and dysfunction in tauopathies. In this model, numerous evidence corroborates observations made in mouse models, suggesting that alternative species (pre-NFTs formation) could be responsible for the toxicity. To achieve these studies *Drosophila* models have been generated using the UAS/GAL4 binary expression system to achieve the expression of tau proteins targeted to either general cell-types (such as neurons or glia) or specific cell types (such neuronal populations, as motor or sensory neurons). For example, tau expression has been demonstrated in all neurons using elav-GAL4 (Wittman et al., 2001) and in glial neurons using Repo-GAL4 (Colodner and Feany, 2010). In addition, tau has been expressed in particular brain structures such as the eye using GMR-GAL4 (Jackson et al. 2002) and in subsets of neurons such as motor neurons (D42-GAL4) (Mudher et al., 2004) and the mushroom body neurons (Kosmidis et al., 2010). These and other *Drosophila* models of tauopathies have shown that human tau overexpression is sufficient to cause behavioral deficits as a result of neuronal dysfunction and subsequent age-dependent degeneration in the absence of filament formation. (Wittmann et al., 2001; Mudher et al., 2004; Cowan et al., 2010; 2015; Ali et al., 2012; Sealey et al., 2017; Pasarella and Goedert, 2018).

Collectively, the examples presented here demonstrated that transgenic animal models recapitulate some of the pathological features observed in human tauopathies. The evidence demonstrates that NFTs or PHFs are not the main cause of the disease and implies that distinct tau species play a role in the initiation and progression of the disease. However, it is still unclear the nature of the tau species that become pathogenic initially. To investigate this, it is important to first consider the need to characterize the models to be used to identify the onset and progression of the disease in these models of tauopathy. Only then, these models can be used to identify the tau species that form initially and are responsible for the onset of disease and the tau species

responsible for the progression of disease. For this, some published studies in these models have shown insight into phenotypes that can be correlated with different stages of the disease.

### 1.10.1 Emergence and progression of the disease in rodent and *Drosophila* models of tauopathy

The characterization of the tau-mediated phenotype at the beginning and end of the disease is necessary to identify the species responsible at each stage of the disease. Although this has been studied, the characterization of the responsible species and their direct association with the observed phenotype has not been done extensively. Therefore, it is necessary to complement these studies with a detailed characterization of the species that appear in different stages of the disease and their relationship with the phenotype they produce. Understanding the nature of the different species that appear during the onset and evolution of the disease could be beneficial to understanding the mechanisms of toxicity and for the development of disease-modifying therapies.

From the large number of studies published in rodent models, few of them have been correlated to the early and advanced stage of disease by characterizing the phenotype. Among these, the transgenic mouse model that expresses the human tau with the P301S mutation in neurons (using the neuron-specific promoter elements of the mouse Thy1 gene) is particularly relevant, and this model has been used for the development of this thesis.

Some studies in this model have explored the correlation between the emergence of the phenotype and tau-mediated pathology at different stages throughout adulthood providing some insight into the early and advanced stages of disease in this model. Some features of these studies are described in **Table 3** and are schematically represented in **Figure 18**.

When Allen and collaborators generate and characterized their model, they observed that the tau pathology leads to a dramatic loss of motor neurons in the spinal cord and is reflected in a progressive motor impairment that culminates in the paralysis of the lower limbs around 21 weeks to 26 weeks of age (Allen et al., 2002). The biochemical analysis showed species of tau that are strongly immunoreactive with phosphorylation-dependent anti-tau antibodies including AT270, AT8, pT212, AT180, 12E8, AD2, PG5, and AP422 (Allen et al., 2002). Further studies focus on the investigation of the onset of tau phenotype.

By doing this, it has been reported that the early stage is characterized by the onset of memory deficit from 11 weeks of age which progresses over time (Xu et al., 2014). When Scattoni and his colleagues studied the early behavioral markers of the disease, they found that hyperactivity and disinhibition manifested at 8.5 to 13 weeks of age. However, they did not observe a cognitive deficit at this stage (Scattoni et al., 2010). On the other hand, a decrease in the density and length of the spine has been reported from 11 weeks of age in the hippocampus (Xu et al., 2014). Further characterization of this model has shown the loss of superficial cortical neurons that manifest at 13 weeks of age and progress over time (Hampton et al., 2011). When investigating the tau species from brains biochemically, the presence of oligomers was found as early as 8.5 weeks of age (Delobel et al., 2008).

Additional studies show neuronal cell death at 21 and 26 weeks of age (Hampton et al., 2010; Xu et al., 2014). Biochemical analysis showed an increase in all the pathological species in the soluble fraction, as compared to the early stage, and the presence of pathological AT180 and CP13 that is apparent only in the insoluble fraction at 26 weeks of age (Delobel et al., 2008; Xu et al., 2014). The increase of these pathological species also correlated with the onset of motor deficits at this older age (Allen et al., 2002; Xu et al., 2014) and might be related to the dysfunction (Xu et al., 2014). When investigating the morphology of the Sarkosyl-insoluble fraction at this advanced stage, using electron microscopy, the presence of abundant filaments made of hyper-phosphorylated tau was reported (Allen et al., 2002). In detail, the majority of the filaments resembled the half-twisted ribbons described previously in cases of FTDP-17, with a minority of filaments resembling the paired helical filaments of Alzheimer's disease.

In humans, motor neuron disease (MND), also known as amyotrophic lateral sclerosis (ALS), has been described as a neurodegenerative disorder of the locomotor system, characterized by the degeneration and loss of upper and lower motor neurons. This loss leads to progressive weakness and atrophy of the extremities, bulbar muscles, and trunk. Furthermore, in this disease, death usually occurs within 2-3 years of the onset of symptoms (Al-Chalabi and Hardiman, 2013). It has been reported that in both sporadic cases, and the majority of familial cases (those associated with C9orf72, TARDBP, UBQLN1 or VAPB), the disease is characterized by the presence of neuronal cytoplasmic inclusions (NCI) within motor neurons in spinal and brainstem compounds composed of the 43KDa TAR DNA-binding protein, TDP-43, while cases associated with mutations in SOD-1 and FUS show NCI within these same cell types that contain these respective proteins (Al-Chalabi and Hardiman, 2013).

In particular, these mouse models, similarly as in humans, exhibit behavioural phenotypes and pathology characterized by the formation and deposition of abundant filaments made of hyper-phosphorylated tau protein and nerve cell degeneration. Collectively, these observations suggest that intermediate species that emerge before NFTs might be the important players in precede neurodegeneration. This demonstrates that the tau aggregation process is essential for the appearance and progression of the pathology but implies that different aggregates play a different role at a different stage of the disease. Details about the nature of these tau species are not entirely clear, nor is their direct relationship with the behavioural phenotype in models of tauopathy.

**Table 3. Examples of tau-induced phenotypes and pathology in P301S mice model of tauopathy**

| Tau isoform | Phenotype Onset | Phenotype Advance stage | Tau species identified when phenotype emerges | Tau species identified in advanced phenotype | Reference |
|---|---|---|---|---|---|
| 0N4R with the P301S mutation | n/a | Locomotion defects<br>Neurodegeneration in spinal cord.<br>Loss of motor neurons<br>Astrocytosis<br>Eye inflammation<br>Only 5-6 months old tested | n/a | Half-twisted ribbons; PHF filaments<br>By immuno-EM | Allen et al., 2002 |
| 0N4R with the P301S mutation | n/a | n/a | Posible pre-filaments (4 weeks of age) | Posible pre-filaments and Filamnets (21 weeks of age)<br>By immuno-EM | Delobel et al., 2008 |
| 0N4R with the P301S mutation | Abnormal emotional behaviour (7 to 8 weeks of age)<br>Decline in motor coordination (13 weeks of age) | Severe decline in motor coordination (17 weeks of age) | n/a | n/a | Scattoni et al., 2010) |
| 0N4R with the P301S mutation | Neuronal cell loss (13 weeks of age)<br>Cortical astrogliosis/ astrocytosis precede neuronal loss. | Neuronal cell loss (21 weeks of age) | Ring-like neurons containing tau deposits lesions (17 weeks of age) | Neurons containing tau abundant deposits lesions (21 weeks of age) | Hampton et al., 2010 |
| 1N4R With P301S mutation | Abnormal behaviour prepulse inhibition (PPI)<br>(13 weeks of age)<br>impaired sociability/object recognition memory<br>Impairments in spatial learning and memory<br>Reduction of axonal transport in optic nerve<br>(13 weeks of age) | n/a | n/a | n/a | Takeuchi et al., 2011 |
| 0N4R with the P301S mutation | Memory deficits (11 weeks of age)<br>Spinal pathology (11 weeks of age)<br>Atrophy and structural changes in hippocampus (11 weeks of age) | Severe memory deficits (26 weeks of age)<br>Locomotor deficits (21 weeks of age)<br>Neuronal cell loss (26 weeks of age) | n/a | n/a | Xu H et al., 2014 |

Low molecular weight (LMW); High molecular weight (HMW); Paired helical filaments (PHFs); Straight filaments (SFs); Electron microscopy (EM); Atomic force microscopy (AFM)

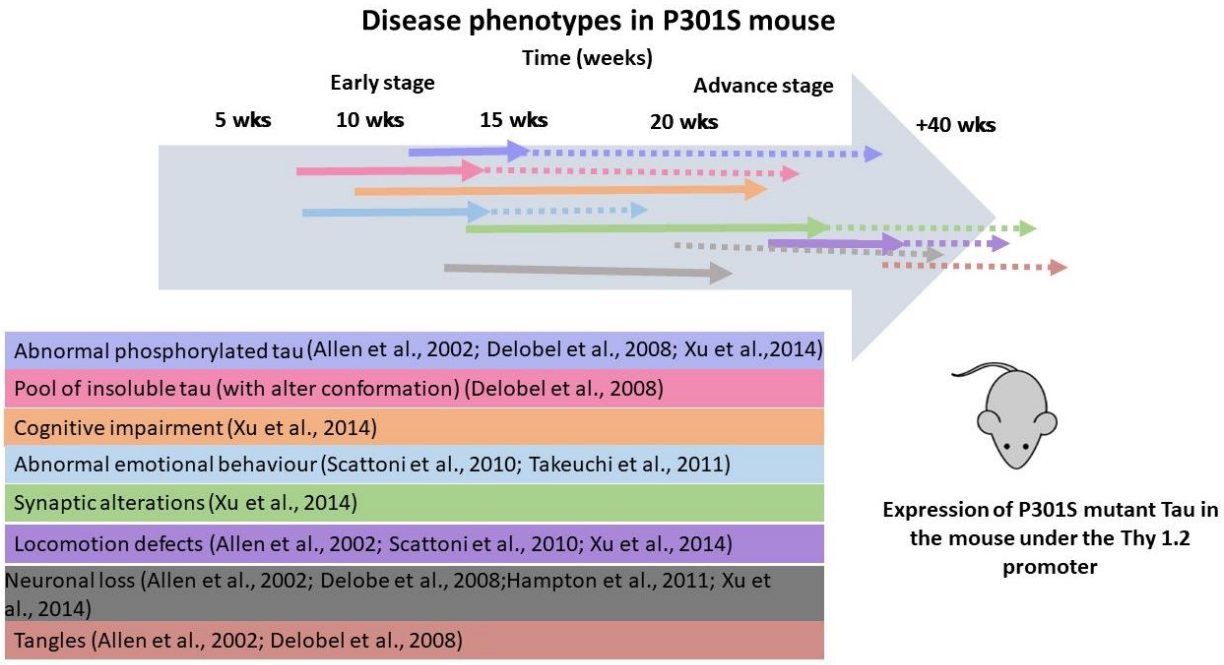


**Figure 18. Schematic representation of onset and progression of disease phenotypes in P301S model of tauopathy**

Mice expressing human tau mutation P301S in neurons (using the neuron-specific promoter elements of the mouse Thy1 gene) recapitulates pathology observed in human tauopathies

Behavioural phenotypes and pathogenicity mediated by tau have also been investigated in *Drosophila*. As described in **Table 4**, several studies have found that expression of human tau reduces lifespan (Wittmann et al., 2001; Folwell et al., 2010; Colodner and Feany 2010; Sealey et al., 20017; Passarella and Goedert 2018). Deficits in locomotion have also been found in *Drosophila* larvae (Mudher et al., 2004; Quraishe et al., 2013) and in adult flies (Folwell et al., 2010, Roy and Jackson 2014; Sealey et al., 20017; Passarella and Goedert 2018).

As in rodent models, some studies have also explored the correlation between the emergence of the phenotype and tau-mediated pathology at different stages providing some insight into the early and advanced stage of disease (as shown in the schematic representation in **Figure 19**. Additionally, unlike in mouse models where the use of transgenic lines expressing mutant tau is necessary to emulate human disease, in *Drosophila*, the over-expression of wild-type human tau is sufficient to reproduce some characteristics of AD and other tauopathies.

For instance, it has been shown that the expression of human tau (htau$^{0N4R}$) in neurons, using the pan-neuronal driver elav-GAL4, induced disease phenotypes that develop with increasing age. The disease phenotypes included reduced lifespan and age-dependent neurodegenerative phenotypes. In this model, the reduction of the lifespan begins at ∼2-weeks after eclosion and progresses with age. At 7 weeks a severe reduction of lifespan was reported accompanied with neurodegeneration Wittmann et al., 2001.

It was also reported that the phenotype was more severe after the expression of mutant tau (R406W). Its expression in the nervous system produces phenotypes with the onset around 1 week after eclosion and greater neurodegeneration at ∼3 weeks after eclosion (Wittmann et al., 2001). In this study, neurodegeneration was investigated by histological analysis of the fly brain following tau expression. This revealed increased numbers of vacuoles and degenerating cells compared to control brains. Although both pathological phosphorylation (12E8, AT100, and AT180) and positive staining of pathological confirmation (Alz50, MC1) have been reported with increasing age, no large filamentous aggregates were identified. However, in this study, the authors cannot exclude the possibility of the presence of small aggregates and pre-tangle species.

The expression of human tau (1N4R) in neurons, using elav-GAL4 and in motor neurons, using D42 GAL4 has been indicated to induce a locomotor dysfunction at the first week after eclosion and the phenotype worsens at 3 weeks after eclosion. As for the lifespan, the expression of tau in neurons produces premature death that begins at 2.5 weeks and worsens at 7 weeks after eclosion. When brain homogenates were investigated, the reactivity for AT8, AT180, and Tau-1 was found in young flies (1-day-old) (Folwell et al., 2010).

In subsequent studies in a similar model as the one reported by Wittmann et al, in which the htau$^{0N4R}$ isoform was expressed in neurons, the reduction in life expectancy began to be evident at 4 weeks and worsened at 13 weeks after eclosion. As for the locomotor dysfunction, this begins to become evident around 2 weeks and deteriorates at 6 weeks. In this model, deficits in learning and memory appear at early stage, however this was studied only at 2 weeks of age. When investigating the tau species potentially responsible for the phenotype using biochemical assays, a lack of abundant insoluble oligomeric was reported in both young and aged flies (Sealey et al., 2017). Further biochemicall analysis of the homogenates from the brain of young adult flies (1-3days-old) indicated that tau was immunoreactive with anti-tau antibodies dependent on phosphorylation including AT8, AT180, PHF-1, pS396, AT100, and abnormal conformation MC1 (Sealey et al., 2017). These results indicate that the species responsible for the phenotype are potentially small, soluble and with abnormal conformation.

The effect of the expression of the htau$^{0N3R}$ isoform in neurons was also studied, in the same study, indicating differences in the effect of toxicity compared to the expression of the htau$^{0N4R}$ isoform. In this model, the reduction in life span begins considerably earlier (2 weeks after eclosion) than the expression of 4R. Likewise, the reduction in life span worsens at 6 weeks. Similarly, the onset of locomotor dysfunction in 3R expressing flies began at 1 week after eclosion and becomes severe at 5 weeks. When these two isoforms were expressed in R7 sensory receptor neurons (pan-R7-GAL4), an apparent degeneration was established at 3 weeks, being more evident in htau$^{0N4R}$ – expressing flies. The degeneration worsened at 6 weeks. These results indicate that expression of 3R isoforms produces a more severe phenotype. However, when investigating learning and memory, the expression of 3R did not show any disruption as 4R did (Sealey et al., 2017). These observations suggest differences between the tau isoforms. After the expression of this isoform, similar results as in the 3R were reported regarding the limited presence of insoluble oligomers and immunoreactivity of brain homogenates from young flies. This indicates that possibly small aggregate is the cause of the initial phenotype and the possibility of pre-tangle species being formed and playing a role in disease at the different stages of disease in this study cannot be excluded.

In another published study, it was shown that overexpression of tau (0N3R) in larvae motor neurons (using D42-GAL4 driver) disrupts axonal transport *in vivo* causing vesicle aggregation associated with loss of locomotor function. The phenotype is observed in the absence of neuronal death or evidence of tau aggregation. In particular study, the assessment of the locomotor function was done using adult flies after the expression of tau in the motor neurons. Thus, an insight into the effect of tau and progression in age-depending manner was investigated. The onset of the locomotion deficit began at 2 weeks after eclosion and become more severe after 5 weeks after eclosion. Additionally, in this study, authors demonstrated that the co-expression of human tau and the *Drosophila* homolog of glycogen synthase kinase-3GSK-3β (GSK-3β) in larvae, enhances axonal transport and locomotor abnormalities (Mudher et al., 2004). When investigating vesicular aggregations using EM, no evidence of inclusion bodies or abnormal filaments was found. The authors suggest that disruption in axonal transport is an early symptom of dysfunction that appears when tau protein is overexpressed (prior to aggregation) and prior to degeneration without abundant formation of larger insoluble species (Mudher et al., 2004).

In line with the above, other studies from the same group have reported that the expression of human tau (0N3R) in neurons results in destabilization of the cytoskeleton, disruption of axonal transport and synaptic dysfunction *in vivo*, also in the absence of filament formation (Cowan et al.,

2010;2015; Quraishe et al., 2013). Collectively, these authors suggest that soluble and non-aggregated tau is the tau species capable of interrupting neuronal function at initial stages of tauopathy.

Interestingly, in a subsequent study of this group in the same model, when flies were treated with an inhibitor of glycogen synthase kinase-3beta tau kinase (GSK 3β) (using lithium or AR-A01448) an improvement in larval phenotypes was observed. When tau species were investigated using various techniques, the presence of oligomeric forms was demonstrated. For example, when investigating axonal sections by EM in treated larvae, electron dense granules (GTO) of around 20 to 50 nm in diameter were identified. This result was confirmed by investigating the GTOs isolated from these treated larvae. In this, insoluble granular oligomers between 20 and 50 nm were identified by immuno-gold EM (Cowan et al., 2015).

The size and morphology of these oligomers were also analyzed using AFM, showing that these structures resemble the oligomeric structures in AD. The structures were reported as having widths from 5–50 nm, with an average width and height of 20 nm (Cowan et al., 2015). Thus, it was demonstrated that this phenotype improvement is due to an accumulation of non-phosphorylated tau oligomers, without evidence of conformation associated with toxicity (β-structure) and non-toxicity (Cowan et al., 2015). These results demonstrate aggregation upon expression of tau and formation of oligomers potentially inert after treatment with the inhibitors of GSK 3β. This study highlights the complexity of aggregated tau species and their relationship with toxicity, underlining the need to investigate the nature of the different forms of tau aggregates and their role in the tau-mediated phenotype in order to develop disease-modifying drugs.

In a more recent study, evidence has been shown to suggest that tau aggregation occurs in *Drosophila*. It was also suggested that the propensity to form a β-sheet structure could play an important role in neurodegeneration (Passarella and Goedert 2018). In the study conducted by Passarella and Goedert, the expression of wild type tau ($hTau^{0N4R}$) in neurons, induces a shortened lifespan with the onset at the first 3week after eclosion that becomes severe at 6 weeks after eclosion. The locomotor dysfunction was tested only at 4 weeks of age showing defects. The expression of Δ306–311 0N4R tau (with the deletion of the hexapeptide motifs that reduce tau assembly and β-sheet formation) either in neurons or in the eye, the tau-mediated phenotypes and neurodegeneration were completely rescued (Passarella and Goedert 2018).

On the other hand, it has been indicated that the expression of wild-type tau 0N4R in the fly retina induces a degeneration that is apparent around 2 weeks of age (Passarella and Goedert 2018). This

phenotype becomes more severe when flies progress to 4 weeks of age. The authors investigated the tau insoluble species in Sarkosyl obtained from transgenic tau flies, however, no evidence of insoluble tau species was found. Aggregation was confirmed *in vitro*, using recombinant tau in the presence of heparin, by fluorescence spectroscopy using thioflavin T (Passarella and Goedert 2018).

Furthermore, the authors comfirmed the relationship between formation of β-sheet and neurodegeneration was confirmed. To do this, the authors indicated that when Δ306–311 0N4R tau (with the deletion of the hexapeptide motifs that reduces tau assembly and β-sheet formation) was expressed either in neurons or in the eye, the tau-mediated phenotypes and neurodegeneration were completely rescued. These findings also demonstrate that expression of tau generates aggregates and that the assembly of tau into β-sheets is necessary for neurodegeneration (Passarella and Goedert 2018).

In *Drosophila* models very few studies have reported oligomers and filaments that resemble early tangle formation (pre-NFT). For instance, Ali and colleagues also reported that neuronal expression of wild-type ($htau^{0N4R}$) or mutant (R406W) tau in a *Drosophila* model, affects learning, memory, locomotor functions, and neurodegeneration dependent on age. In this model, the learning and memory deficits begin at ∼3 weeks after eclosion and progress with age. Ali and colleagues also indicate reduction in locomotor performance with the onset at 1.5 weeks and progressing until ∼3 weeks of age. At this age, a decline in cognitive functions begins and multiple vacuolizations in the brain indicate severe neurodegeneration (Ali et al., 2012). When investigating the form of tau biochemically, they detected hyper-phosphorylated (AT8, pSer262) oligomeric species in *Drosophila* brains increasing after 3 weeks (Ali et al., 2012).

Similarly to the above, in another fly model in which $htau^{0N4R}$ was expressed in the retina, using GMR-GAL4 driver, the presence of high molecular weight and insoluble species of tau were reported. The presence of these species was characterized by age-dependent accumulation (Blard et al., 2006). As described in **Table 4,** the early stage was established upon eclosion (2-days-old) and the late stage was established after 1.5 weeks after eclosion. At this late stage, abnormal phosphorylation of tau was reported for AT8, AD2, and PHF1 when analyzing the homogenates of fly heads, in addition to being positive for MC-1. These results suggest that changes in tau, in abnormal phosphorylation and conformational change (potentially oligomeric forms) occur early in the disease in these flies (Blard et al., 2006). It is important to consider that as the eye surface is generated during the final stages of adult development the progression of degenerative phenotype mediated by tau expression (using the GMR-GAL4 driver) cannot be directed entirely by the progression with age. However, it is useful to study tau-induced degeneration.

Additionally to the potential oligomeric species, some studies have reported the presence of filament-like aggregates (as shown in **Figure 20**). In a study conducted by Colodner and Feany, it was shown that the expression of tau in glia cells, using Repo-GAL4 driver, induces a shortened lifespan beginning at 2 weeks of age to a maximum life span of 5 weeks of age. The authors identified age-dependent neuronal cell death starting at 3 weeks and progressing to 5 weeks. The expression of tau in glial cells could induce this accumulation of larger structures that become increasingly misfolded and insoluble over time as observed with rodents. An age dependent increase in insoluble tau species has been seen in 1 and 3 weeks-old glial tau transgenic flies. The presence of filaments was demonstrated using immunoelectron microscopy (Colodner and Feany 2010) from 3 weeks (**Figure 20 A-1**) and 3.5 weeks after eclosion (**Figure 20-A-3**). Some examples of published studies demonstrate that the expression of tau produces a phenotype characteristic of tauopathies in addition to the formation of filamentous structures.

Wu et al., 2013 indicated that the expression of human wild-type tau (2N4R) on dopaminergic neurons (DA) induced motor and learning deficits that coincided with progressive neurodegeneration. Furthermore, this effect was accompanied by the age-dependent formation of tau pathology (tangle-like). In this model, a severe deficit in locomotion began at 4 weeks after eclosion and progressed to 6 weeks (**Figure 20-B**). The authors indicated a modest learning deficit at 3-week-old. By immunohistochemical analysis, the morphology of DA neurons from tau expressing flies show morphological changes of the soma DA neurons at 2 weeks. At 3 weeks after eclosion, abnormal tangle-like morphology, resembling NFTs at the microscopic level in most DA neurons was observed. The few cells that survived until 6 weeks experienced soma shrinkage and β-sheet conformation stained by Congo red was found. When additional biochemical analyses was performed on whole brain extracts from aged flies expressing tau, a gradual reduction of monomeric tau, and an increase in high-molecular-weight species with increasing age and reactivity to AT8, AT100, and AT180 was observed. TEM examination on the insoluble tau species extracts from fly brains of 4 weeks after eclossion, revealed abundant filamentous aggregates composed by PHF or SF, with diameters of 15–40 nm (Wu et al., 2013) (**Figure 20-B1-2-3**).

Jackson and collaborators showed that co-expression of wild-type tau (2N4R) human tau in the retina and the pan-neural expression of the *Drosophila* homolog of glycogen synthase kinase-3 (GSK-3β) Shaggy, enhances neurodegeneration induced by tau overexpression alone, leading to neurofibrillary pathology in the fly. As described in **Table 4** the phenotype includes a reduced eye with complete loss of normal ommatidia and most bristles. The pathological phosphorylation and positive staining of pathological conformation have been reported. Here, neurofibrillary aggregates

showed AT100 immunoreactivity in dystrophic neurites and cell bodies. Moreover, the EM examination on the Sarkosyl-insoluble tau species extracts from fly brains revealed the presence of straight filaments and PHF, whereas these structures were not observed in flies overexpressing tau alone (Jackson et al., 2002) (as shown in **Figure 20-C1-C4**). These filaments are similar to the PHF characteristic in AD bran, for instance, PHF filaments from 410 nm long and 30nm wide with a periodicity of 45 nm were described. Moreover, straight filaments were also described here from 160 to 210nm long and 20nm wide (Jackson et al., 2002). In this study, the authors indicate that phosphorylation of human tau by the *Drosophila* GSK-3β homolog Shaggy resulted in the formation of neurofibrillary pathology.

**Table 4. Examples of tau-induced phenotypes and pathology in *Drosophila* models of tauopathy**

| Tau isoform Tissue and (GAL4 Drivers) | Phenotype Onset | Phenotype Advance stage | Tau species identified when phenotype emerges | Tau species identified in advanced phenotype | Reference |
|---|---|---|---|---|---|
| 0N4R<br>CNS:Pan-neural (Elav) | Reduce lifespan<br>(2 weeks-old) | Reduce lifespan<br>(7 weeks-old)<br>Vacuolization and degeneration of cells | n/a | n/a | Wittmann et al., 2001 |
| R406W mutant tau<br>CNS: Pan-neural Elav | Reduced lifespan<br>(1 weeks-old) | Severely reduced lifespan (3 weeks-old)<br>Vacuolization and degeneration of cells | n/a | n/a | Wittmann et al., 2001 |
| Co-expression of 2N4R tau in retina with pan-neural expression of shaggy<br>Eye model: GMR<br>CNS: Pan-neural Elav | (Larval and adults)<br>Early cell loss, and irregularities in differentiating neurons<br>(Larval eye disc) | Rough eye phenotype<br>Vacuolisation in medulla<br>Degeneration in photoreceptor neurons | PHFs and SFs)<br>By EM | PHFs and SFs)<br>By EM | Jackson et al., 2002 |
| 0N3R<br>Cell-type:motor neurons D42 | L3<br>locomotion defects<br>L3 axonal transport dysfunction<br>Locomotor defects in adults<br>(2 weeks-old) | Greater locomotor defects in adults (5 weeks-old) | n/a | n/a | Mudher et al., 2004 |
| 0N4R<br>Eye model: GMR | HMW and insoluble tau species<br>early stage<br>(2-d-old) | HMW and insoluble tau species<br>Late stage (10-d-old) | n/a | n/a | Blard et al., 2006 |
| 0N4R<br>Pan glial<br>Repo | Reduced lifespan<br>(2-weeks-post-eclosion) | Maximum lifespan (5 weeks post-eclosion) | Insoluble species (1-weeks-psot-eclossion) | SFs<br>By EM (4-weeks-old) | Colodner and Feany 2010 |

| | | | | | |
|---|---|---|---|---|---|
| 0N3R<br>CNS: Pan-neural Elav and Cell-type:motor neurons D42 | Disruption of MT.<br>Reduced binding ability of dtau to MTs (L3 and 1-day-old) | n/a | n/a | n/a | Cowan et al., 2010 |
| 1N4R,<br>CNS: Pan-neural And Cell-type: motor neurons D42 | L3 Axonal transport dysfunction<br>Morphology defects in NMJ<br>Reduce lifespan (2.5-weeks-old)<br>Locomotor dysfunction (1-week-old)<br>Vesicular aggregation | Severe adult locomotor defects (3-weeks-old)<br>Adult Reduced lifespan (7-weeks-old) | n/a | n/a | Folwell et al., 2010 |
| 2N4R<br>and<br>R406W-(2N4R) mutant<br>CNS:<br>Pan-neural Elav | Decline in memory performance (3-weeks-old)<br>Decrease in locomotion (1-week-old) | Greater decrease in locomotor activity (3- weeks-old)<br>vacuolisation (3- weeks-old and progress) | LMW Oligomers (2 days-old) | n/a | Ali et al., 2012 |
| 2N4R<br>Dopaminergic neurons<br>TH | Locomotor deficit (4-weeks-old)<br>Learning deficits (3-weeks-old)<br>Limited loss of neurons (2-weeks-old)<br>Rough eye phenotype | Severe locomotor deficits (6-weeks-post-eclossion)<br>Severe loss of neurons (4-weeks-post-eclosion) | HMW Oligomeric tau and tangle-like (began 3 weeks-old) | Filaments by TEM (4 weeks-post-eclossion) | Wu et al., 2013 |
| 0N3R<br>CNS:<br>Pan-neural Elav and Cell-type: motor neurons D42 | Young adults and L3 locomotor impairment and L3 disrupted axonal transport | n/a | GTO-like structures By EM and AFM (0-3-days-old and L3 larvae) | n/a | Cowan et al., 2015 |
| 0N3R<br>And<br>0N4R<br>CNS: Pan-neural Elav and Cell-type: motor neurons D42<br>R7 sensory receptor-neurons | L3 D42 locomotor defects<br>Larvae axonal transport defects<br>Adult locomotor alterations (2-weeks-old)<br>Reduce lifespan (2-weeks-old in 3R)<br>Reduced learning and memory (4R at tested at 2-weeks-old)<br>Degeneration of sensory neurons (3-weeks-old) | Severe adult locomotor alteration (6-weeks-old)<br><br>Reduce lifespan (maximum-6weeks-old in 3R;<br>13 weeks in 4R)<br><br>Severe degeneration of sensory neurons (6-weeks-old) | Insoluble oligomers | n/a | Sealey et al., 2017 |
| 0N4R | Reduced lifespan (3-weeks-old)<br>Reduced lifespan<br>Rough eye phenotype (2-weeks-old) | Reduced lifespan (max-6-weeks-old)<br>Reduced locomotion (only 4-weeks-old flies tested)<br>Severe rough eye phenotype (4-weeks-old) | n/a | n/a | Passarella and Goedert al., 2018 |

Third instar larvae (L3) Third instar larvae motor neurons D42 (L3D42); Neuromuscular junction (NMJ) ; Granular tau oligomers (GTO); Low molecular weight (LMW); High molecular weight (HMW); Paired helical filaments (PHFs); Straight filaments (SFs); Electron microscopy (EM); Atomic force microscopy (AFM); R406W and V337M- FTDP-17-linked mutants .

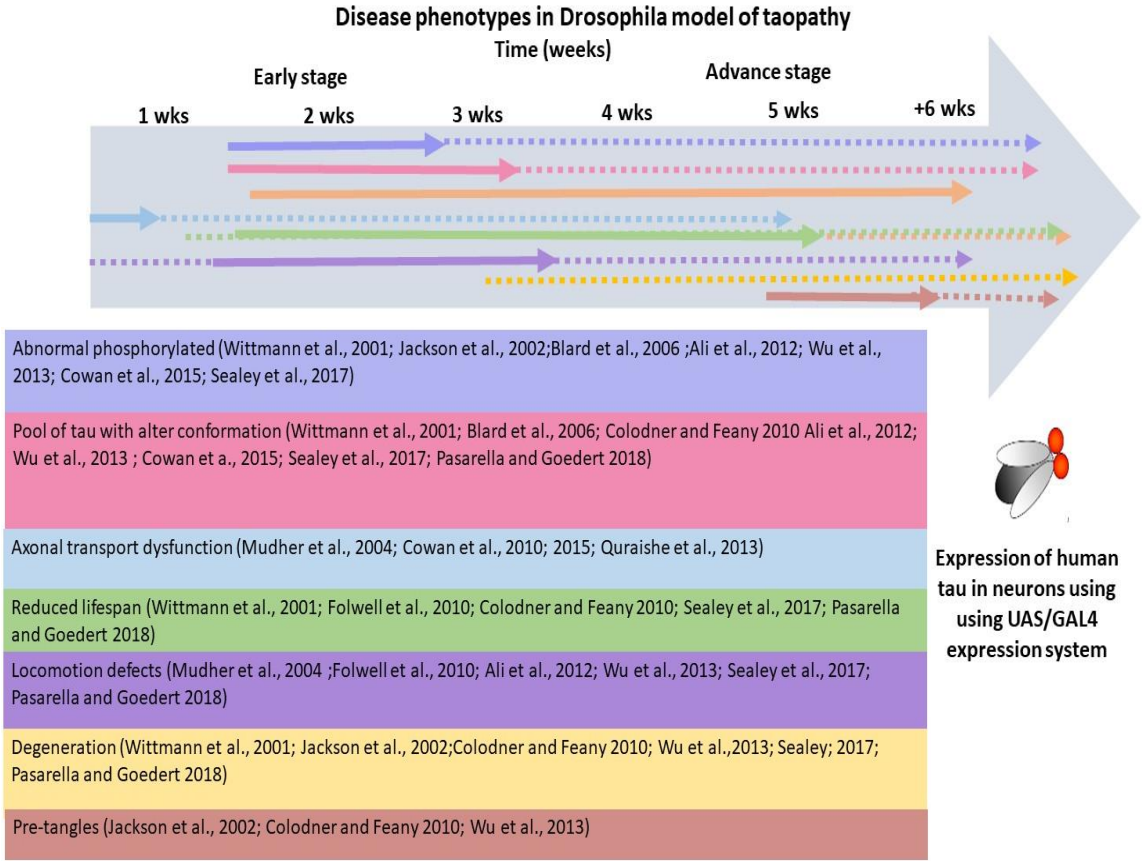


**Figure 19. Schematic representation of onset and progression of disease phenotypes in *Drosophila* model of tauopathy**

*Drosophila* models expressing human tau in neurons (using UAS/GAL4 system recapitulates some features observed in human tauopathies)

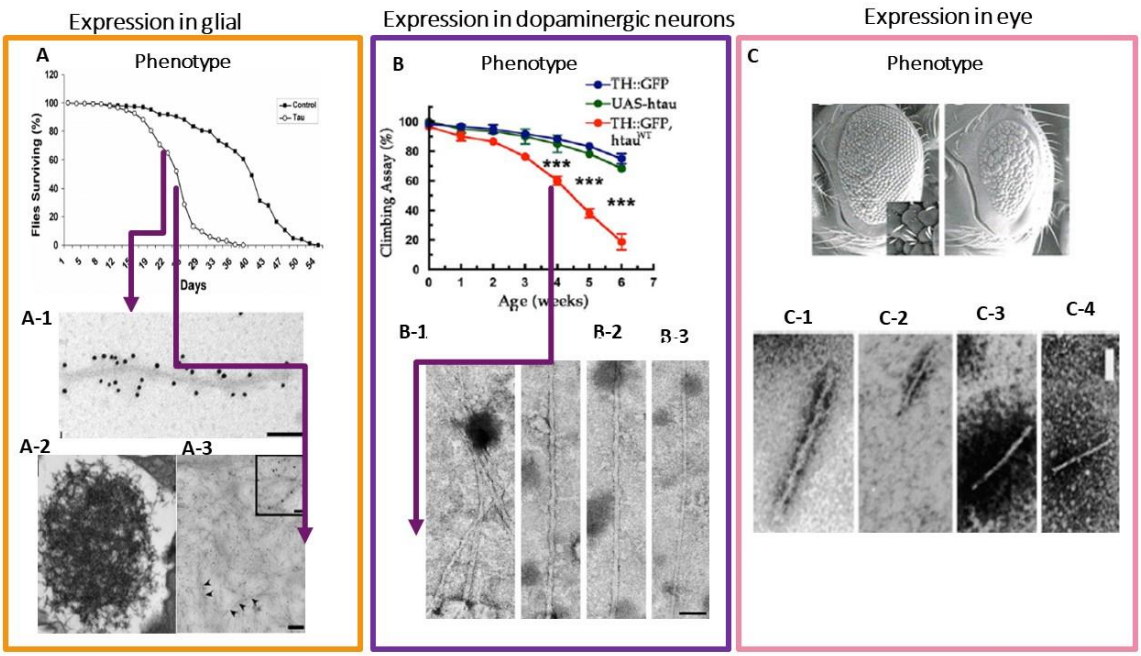


**Figure 20. Examples of published studies that demonstrate that the expression of tau produces a phenotype characteristic of tauopathies in addition to the formation of pre-NFTs structures**

**A)** Expression of human tau in adult *Drosophila* glia reduces lifespan compared with control flies (tau transgenic (open circles) and control (filled boxes). **A-1)** Immunoelectron microscopy of the Sarkosyl-insoluble fraction isolated from glial tau transgenic flies (3 weeks-old), using a phosphorylation-independent polyclonal antibody (Dako) showing filaments. Scale bar, 100 nm. **A-2)** Standard transmission electron microscopy of the glial tau transgenic flies reveals the presence of tau filaments (3.5 weeks after eclosion). **A-3)** Immunoelectron microscopy using the phospho-specific antibody AT8 labels tau fibrils in glial tau transgenic flies. Scale bar 200 nm. Taken from (Colodner and Feany 2010). **B)** Climbing assay of driver control (blue), transgene control (green), and human tau transgenic (red) flies. **B-1)** Electron micrographs of abnormal filaments (PHF) extracted sarkosyl-insoluble fraction of 4-week-old fly brains expressing human tau showing a single PHF; B-1-2-3) shown straight filaments from the tau expressing flies. Scale bar 100 nm. The filamentous have diameters of 15–40 nm. Taken from (Wu et al., 2013). **C)** Electron micrographs showing the rough eye phenotype from flies expressing tau and *Drosophila* homolog of (GSK-3β) Shaggy* in the eye; **C-1-4)** Shows electron micrograph of filaments extracted from fly brains. C-1) shows PHF from 410 nm long and 30nm wide with a periodicity of 45 nm. **C-2-3)** straight filaments of 160 to 210nm long and 20nm wide. **C-4)** Shows a filament isolated from AD brain, these straight filaments range from 290nm long and 20nm wide. Scale bar 200nm. Taken from (Jackson et al., 2002).

Collectively, these studies show that transgenic animal models such as *Drosophila* and rodent models recapitulate the essential characteristics of human tauopathy and AD. Demonstrating their potential as a tool to investigate the tau species responsible for the onset and late stage of disease.

## 1.11 *Drosophila* as a suitable model to study human tauopathies

In order to investigate the tau species responsible for the onset and late stage of disease, it is necessary to use a tauopathy model as it is not possible to investigate this in the human brain. As most neurodegenerative disorders such as tauopathies in humans are sporadic so that the disease can be modeled in animals. It is necessary to use transgenic lines that express mutations in the tau gene, which is found in FTDP-17, with the purpose of investigating pathological characteristics such as NFTs formation and neurodegeneration (Hutton et al., 1998; Goedert and Jakes. 2005). These mutations induce self-association of tau molecules leading to filament formation (Goedert et al., 1999; von Bergen et al., 2001). While mutations are key in mouse models of tauopathy, in *Drosophila*, it is not a limiting factor in inducing the disease-related phenotype. In *Drosophila* the overexpression of human tau is sufficient to induce some of the phenotypes of the disease. However, in this model, the process of tau aggregation and subsequent filament formation and ovillosagregation appears to be much slower compared to the rate of aggregation and filament formation in mouse models (as reviewed in Sivanantharajah and Mudher, 2019). Regarding this, it is believed that in *Drosophila*, this main aspect of disease requires long periods for aggregation, oligomerization, and filaments maturation. Even so, this is particularly important if one seeks to study initial aspects in the evolution of the pathology. In addition, it highlights the great potential of fly model as a tool to study AD and other tauopathies.

### 1.11.1 *Drosophila* tau

In *Drosophila*, 75% of the human genes known to be associated with neurological conditions have orthologs (Bier 2005). These include those that cause AD (APP and presenilin) and tauopathies such as FTDP-17 (tau) (Reiter et al., 2001). The conservation of human disease-related genes, such as AD, is the main characteristic that makes an animal model useful. An additional characteristic is the simplicity of the genome, in comparison with the human genome. This simplicity allows us to analyze the function of genes related to diseases and facilitate their understanding.

For studying neurological disorders related to the tau protein, *Drosophila* represents a good model. In *Drosophila*, the existence of the main isoform has been corroborated, in addition, a second, larger isoform has been evidenced at lower levels (Heidary and Fortini 2001; Burnouf et al. 2016). In humans and rodents, there are multiple protein isoforms associated with the neurological disorders related to tau protein. In particular, in the case of rodents, three isoforms have been found (Mavilia et al. 1993), while in humans, six isoforms expressed in the central nervous system (CNS) have been found (Ksiezak-Reding et al. 1988).

### 1.11.2 *Drosophila* as a model of tauopathy

As mentioned before, the importance of *Drosophila* as a model of tauopathy relies on the possibility of mimicking some of the essential features of human tauopathies. These models provided valuable insight into the mechanisms that contribute to neuronal dysfunction and neurodegeneration that gives rise to the disease. Neuronal dysfunction is one of the key pathological features in many neurodegenerative diseases as in AD and other tauopathies. In this regard, *Drosophila* models of tauopathy have been used to investigate how tau plays a role in neuronal dysfunction. In AD and other tauopathies, it is believed that tau becomes hyper-phosphorylated and this abnormal phosphorylation interrupts the binding to microtubules. Thus, the MT destabilized and break down (Alonso et al., 1994). This has been demonstrated in *Drosophila* models of tauopathy.

The effect of the expression of human tau (0N3R) in larvae mediating destabilization of microtubules and axonal transport deficits has been demonstrated (Mudher et al., 2004, Cowan et al., 2010). Similarly, other *Drosophila* models have been also demonstrated destabilization of microtubules (Cowan et al., 2010; Quraishe et al., 2013; Roy and Jackson et al., 2014) and axonal transport disruption (Folwell et al., 2010; Quraishe et al., 2013; Roy and Jackson 2014). Similarly, this particular model has been used to investigate the effect of tau expression at the synapse. Because of cytoskeleton breakdown, the expression of human tau (0N3R) in motor neurons results in the disruption of cell-to-cell communication. Here, disruption of the morphology and transmission at the neuromuscular junction (NMJ) was reported resulting in synapses dysfunction (Chee et al., 2005).

As in AD, one of the risk factors is age and the symptoms develop slowly and get worse over time. Therefore, as described before, age-related phenotypes, such as lifespan and locomotion can be used as a readout to study the effect of tau expression in the neuronal function of the effect of tau

expression in the nervous system (Mudher et al., 2004; Folwell et al., 2010; Quraishe et al., 2013; Sealey et al., 2017; Passarella and Goedert, 2018).

Neuronal death is another important feature of neurodegenerative disorders and for that, a number of *Drosophila* models has been generated to study degeneration (Wittmannet al., 2001; Jackson et al., 2002; Colodner and Feany, 2010; Ali et al., 2012; Wu et al., 2013; Sealey et al., 2017; Passarella and Goedert, 2018). These studies have been described when tau is expressed in the brain (Witmann et al., 2001; Ali et al., 2012; Pasarella and Goedert, 2018) as when tau is expressed in different populations cells. For instance, in the mushroom bodies (Kosmidis et al., 2010), in glial cells (Colodner and Feany 2010), dopaminergic neurons (Wu et al., 2013), as in the *Drosophila* eye (Jackson et al., 2002; Passarella and Goedert, 2018). When using the adult brain, the degeneration can be studied by characterizing the appearance of vacuoles. This indicates cell loss (Khurana et al., 2010). When using the eye, the tau phenotype results in disruption of the normal pattern of ommatidia, and these manifest in the rough eye phenotype.

In human tauopathies, different tau variants, such as different isoforms and mutants, have been implicated in different diseases. Thus, *Drosophila* model of tauopathy has been also useful to investigate how tau variants, such as different isoforms and mutants, play a different role in toxicity. For instance, it has been shown that the expression of mutant tau results in greater toxicity when compared to wild-type. It has been reported that the expression of human tau and mutant tau (R406W) in the nervous system resulted in premature death with the neurodegenerative phenotype (Wittman et al., 2001). In this model, the phenotype was more pronounced with the expression of disease mutant tau. In line with this, it has been shown that the expression of different isoforms results in different toxicity. For instance, the expression of human wild type htau$^{0N3R}$ and htau$^{0N4R}$ in *Drosophila* exert different phenotypes (Kosmidis et al., 2010; Sealey et al., 2017). It has also been found that the expression of htau$^{0N3R}$ is associated with dysfunction in the absence of neuronal death (Mudher et al., 2004; Cowan et al., 2010). Conversely, the expression of htau$^{0N4R}$ is associated with degeneration (Sealey et al., 2017). These studies demonstrate the suitability of the *Drosophila* model to investigate how this may underlie the different tauopathies.

To achieve all the possible advantages of the *Drosophila* model, genetic tools have been generated to express different tauopathy tau variants in a temporal and spatial dependant manner. In Drosophila models, the most widely used system to express transgenes in a restricted manner is the UAS / GAL4 system. GAL4 is a gene transcription regulator that will bind to an upstream activating sequence (UAS) to activate transcription. As shown in **Figure 21**, the use of this system is carried out through the crossing of two *Drosophila* lines, one containing a UAS and another

containing GAL4 element. A variety of different tissue specific GAL4 lines have been elaborated, allowing the targeted expression of a specific protein of interest in whole cells or tissues subset (Brand & Perrimon, 1993). In this thesis work, the Elav-GAL4 line is the main one used. Elav-Gal4 drives the expression of proteins in a pan-neuronal fashion (Brand and Perrimon 1993).

Collectively, these and other studies have been demonstrated that *Drosophila* models of tauopathy are a suitable model to study tau-mediated neurodegeneration AD and other tauopathies *in vivo.* Moreover, these studies provide evidence to suggest their potential advantage to investigate the tau species responsible for the onset and late stage of disease in this thesis.

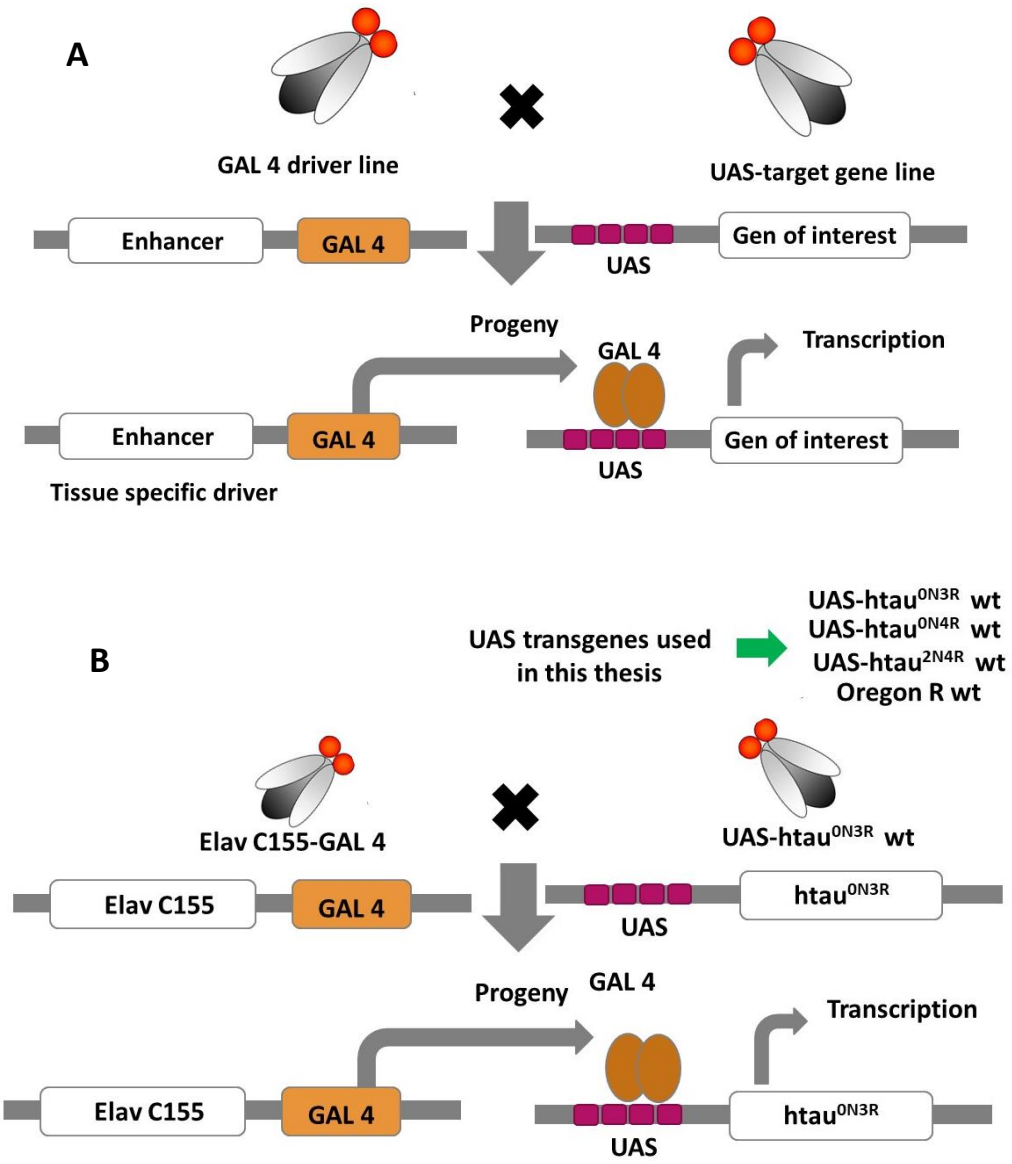


**Figure 21. Schematic representation of gene expression systems in *Drosophila***

**A**) In the UAS/GAL4 system, a tissue specific driver is put upstream of the GAL4 element. For crossing two *Drosophila* lines, one containing a UAS and another containing GAL4 element transcription occurs. **B**) The UAS/GAL4 system to express htau in all neurons, used in this thesis. Driver lines expressing the panneuronal driver, Elav-GAL4 (Elav C155-GAL4) are crossed to UASlines with genomic inserts of a target gene (shown here as UAS-htau$^{0N3R}$). Fly genetic crosses were carried out using female ElavC155-GAL4 with male flies either UAS-htau$^{0N3R}$, UAS-htau$^{0N4R}$, UAShTau$^{2N4R}$ or Oregon R (WT controls).

# Chapter 2 Investigative Aims

## 2.1 Summary and aims of thesis

The overarching aim of my PhD project is to understand how changes in different tau species can lead to the development of tauopathy. Particularly, this research will investigate how changes in tau species are related to the onset and the progression of the disease in two animal models of tauopathy. The results may provide clues about how this happens in human disease.

**Aim 1. To characterize the emergence of tau phenotypes in two models of tauopathy.**

Objective 1: Evaluate longevity and climbing behavior in the fly model for characterization of the tau phenotype (behavioral defect) and determination of the onset and progression of the disease.

Objective 2: Evaluate locomotor behavior in the rodent model to characterize the tau phenotype and determine the onset and progression of the disease.

**Aim 2. To identify the tau species potentially responsible for the onset and progression of disease in two models of tauopathy.**

Objective 1: To isolate the insoluble granular tau (GTO) species present in our two models of tauopathies at the early and late stages of disease.

Objective 2: To isolate the insoluble larger aggregates/ fibrillary species (NS) of tau present in our two models of tauopathies at the early and late stages of disease.

**Aim 3. To employ a number of biophysical techniques to continue exploring in more detail the characteristics that distinguish each species (GTOs/NS) potentially responsible for the onset and progression of disease**

Objective 1: Determine the structural conformation of the tau species, from the early and late stages of the pathology.

Objective 2: To characterize the overall morphologies of the tau species from the early and advanced stages of disease in our two models.

Objective 3: To determine the size distribution of the tau species from early and advanced stages of disease in our two models.

**Aim 4. To study the effect of a tau aggregation inhibitor in a *Drosophila* model as a future potential disease modifying therapy**

Objective 1: Evaluate the effect of a tau aggregation inhibitor in longevity and climbing behaviour in *Drosophila* model of tauopathy.

Objective 2: To isolate the aggregates of tau (NS) species present in the *Drosophila* model to investigate whether this inhibitor has an effect on tau solubility in our *Drosophila* model.

**Overall hypothesis:** *Intermediate tau oligomers are the pathogenic tau species that might be responsible for tau-mediated dysfunction in the initial stages. Further, I hypothesize that these oligomers polymerize to form longer fibrils and these species form at the later stages of the disease.*

# Chapter 3 Materials and methods

## 3.1 Fly stocks

Assays were conducted using male progeny from genetic crosses of female ElavC155-GAL4 flies with either UAS-htau$^{0N3R}$, UAS-htau$^{0N4R}$, UAShTau$^{2N4R}$ or Oregon R (WT controls) male flies. *Drosophila* was raised and maintained on standard Bloomington media at 23°C with a 12/12 h light/dark cycle.

### 3.1.1 *Drosophila* genotypes

**Table 5. List of fly stocks used in Thesis**

| Drosophila Line | Genotype | Chromosome | Obtained from |
|---|---|---|---|
| Oregon R | +;+;+;+ (wild type no inserts) | N/A | Bloomington Stock Centre |
| Elav GAL4 (pan neuronal driver) | ElavC155-Gal4;+;+;+ | I | Bloomington Stock Centre |
| 3 repeat human tau | w1118;UAS-htau0N3R;+;+ | II | Bloomington Stock Centre |
| 4 repeat human tau | +/+;UAS-htau0N4R/Ser | III | Skoulakis lab |
| 4 repeat human tau | w1118; P{UAS-Tau.wt}7B | III | Bloomington Stock Centre |
| 4 repeat human tau + GKS3β | w1118; P{GMR-htau.Ex}1.1; P{GMR-GSK3β.J}3/T(2;3)SM6a-TM6B, Tb1 | 2N4R-Tau on II GSK3β on III | Bloomington Stock Centre |

## 3.2 Adult climbing assay

Here, 4 cohorts of 10 adult male flies (n= 40) with panneural expression of htau$^{0N3R}$ and htau$^{0N4R}$ and Oregon R wt as a control (wt) were studied. Flies were placed in cylinders in an assay room with controlled lighting conditions, temperature (23°C) and humidity (30–40%) and the assay was conducted by tapping flies 3 times upon a mouse pad to send the flies to the bottom of the cylinder and recording the flies climbing up the sides of the measuring cylinder. The distance climbed by the flies was recorded at 10 s. The assay was repeated three times, with 2 minute rest between each trial and the mean was calculated. Flies were then placed onto fresh food until the following week.

The climbing ability of the htau$^{0N3R}$ and htau$^{0N4R}$ expressing adult lines and OreR wt was measured once a week for a total of 6 weeks. The 2-way ANOVA was used for Statistical Analysis via Graphpad Prism Software.

For the tau inhibitor study, conducted by Hannah Lucas and Dr. Shreyasi Chatterjee, the climbing assay was performed on 5 cohorts of 10 adult male flies (n=50) from each group. Each week 6-9 hours into the 12 hour light cycle of the flies they were anesthetized briefly with CO2 and placed in a measuring cylinder with controlled light, temperature (23°C), and humidity (40%) conditions. They were given about 15 minutes to recover from anesthesia to acclimatize. Next, the measuring cylinder was tapped 3 times upon a mouse pad to send the flies to the bottom and a video recording was carried out for 30 secs as the flies climbed upwards due to negative geotaxis. These cohorts were allowed to rest for 2 minutes and the procedure was repeated 2 more times and the flies were placed onto fresh drug food the following week. 2-way ANOVA was used for Statistical Analysis via Graphpad Prism Software.

## 3.3 Longevity

For this assay, 0-3 days post-eclosion old adult male flies from each genotype were separated and 10 cohorts of 10 flies (n=100) to new food twice a week. Dead animals were scored three times a week. Flies were housed in a room with controlled lighting conditions, temperature (23 °C) and humidity (30–40%). Dead animals were scored and three times a week (Sealy et al., 2017). Survival analysis was carried out using GraphPad Prism software and a Kaplein-Meir curve was plotted. A Log-rank (Mantel-Cox) test was performed on the data.

## 3.4 Tau inhibitor

For the evaluation of the tau inhibitor the peptide RI-AG03 was kindly provided by Dr. Anthony Aggidis and the studies were conducted by Hannah Lucas and Dr. Shreyasi Chatterjee. For this, RIA G03 was dissolved in distilled water to prepare a 5 mg/ml stock from which dilutions were prepared at concentrations of 0.08µM and 0.8µM. RIA G03 concentrations were used at a low dose (0.08 mM) and high dose (0.8 µM). These drugs were added to the fly-food vials and crosses were set up in duplicates for each genotype and each drug concentration. The adult climbing and longevity assays were performed with standardized protocols from our laboratory (Sealy et al., 2017) and mentioned above, every week for a period of 6 weeks.

## 3.5 P301S transgenic mice model of tauopathy

P301S transgenic mice were developed by Prof. Michel Goedert, Division of Neurobiology, University of Cambridge (Cambridge, UK). A detailed description of the animal model can be found in Allen et al. (2002). These transgenic mice express the 0N4R human tau with the P301S mutation controlled by the murine thy1 promoter in mice. Homozygous P301S+/+ and non-transgenic C57Bl/6 wild-type mice were used in this study. Samples were collected at 6, 12, 16, 20, and 24 weeks of age.

## 3.6 Rotarod assay in P301S mice model

Motor coordination, strength, and balance were tested at 6, 12, 20, and 24 weeks of age using rotarod with each time point being an independent cohort. This assay was performed by Dr. Renzo Mancuso.This test consists of placing the animal on a horizontal bar (diameter = 30 mm), that rotates around its major axis at an accelerating speed of 4-40rpm over 5 min. Mice were placed on the rod for up to 5 minutes and the latency to fall was recorded. In this assay, 300s was considered an arbitrary maximum time of remaining on the rotating rod.

## 3.7 Solubility assay to enriching for insoluble granular tau (GTO)

This assay enriches for insoluble oligomeric tau species as described (Cowan et al., 2015; Sealey et al., 2017; Mancunso et al., 2017). A total of 100 adult flies heads expressing either the htau$^{0N3R}$ or htau$^{0N4R}$ (as well as Ore R wt control) and cerebral cortex P301S mice representing several stages of tauopathy were homogenised in 400 µL or 100 µL TBS/sucrose buffer (50 mM Tris-HCl pH 7.4, 175 mM NaCl, 1 M sucrose, 5 mM EDTA and protease inhibitor cocktail) respectively (**Figure 22**). The samples were spun for 2 min at 1000 g and the pellet discarded. The supernatant was labelled as tissue lysate (input). Sample from the supernatant was then spun at 100,000 g for 30 min at 4 °C. To enriching for insoluble granular tau (GTOs) the resulting supernatant was spun at 186,000 g for 2 h at 4 °C (**Figure 22 a**). The resulting supernatant includes the aqueous soluble fraction and presumable monomeric tau "S1" (**Figure 22 c**). The pellet was re-suspended at room temperature in 100 µL of 5% SDS/TBS buffer (50 mM Tris-HCl pH 7.4, 175 mM NaCl, 5%SDS) and spun at 186,000 g for 2 h at 25 °C (**Figure 22 c**). The resulting supernatant includes the aqueous insoluble- detergent SDS soluble fraction "S2" (**Figure 22 d**). The pellet was resuspended at room temperature in 5% SDS/TBS buffer (50 mMTris-HCl pH 7.4, 175 mM NaCl, 5% SDS and protease inhibitor cocktail) and spun at 186,000 g for 2 h at 25 °C as a wash spin; following which the supernatant was discarded. This pellet was then re-suspended in 8M urea, 8%SDS buffer (50mMTris-HClpH7.4, 175mMNaCl, 8%SDS, 8 M urea and protease inhibitor cocktail) and agitated for 12–18 h at room temperature to

obtain the SDS the insoluble fraction "S3" (**Figure 22 e**). All samples were diluted in 2× Laemmli buffer and boiled for 5 min. "S1"and "S2" were loaded equally (equivalent volumes) whereas double the amount of "S3" was loaded compared to"S1"and"S2". Western blotting was performed to assess total tau levels and tau solubility state. The total tau levels in the input (tissue lysate samples before being fractionated) were detected using anti-human tau polyclonal antibody and anti-Actin was used as a loading control. The tau solubility state were detected using anti-human tau polyclonal antibody.

The fractions were quantified as a proportion of the total sum of the three fractions ("S1", "S2" and "S3"), and these were expressed as the percentage corresponding to tau present in the input.

LiCor scanner with Odyssey software was used to detect the signal and ImageJ software was used to measure band densities. GraphPad Prism was used for statistical analysis and unpaired, two-tailed t tests were performed on the data.

## 3.8 Solubility assay to enriching for larger/ fibrillar insoluble tau (NS)

A total of 100 adult flies heads expressing either the htau$^{0N3R}$ or htau$^{0N4R}$ (as well as Ore R wt control) and cerebral cortex P301S mice representing several stages of tauopathy were homogenised in 400 µL or 100 µL TBS/sucrose buffer (50 mM Tris-HCl pH 7.4, 175 mM NaCl, 1 M sucrose, 5 mM EDTA and protease inhibitor cocktail) respectively (**Figure 22**). The samples were spun for 2 min at 1000 g and the pellet discarded. The supernatant was labelled as tissue lysate (input).To enriching for insoluble larger/ fibrillar insoluble tau (NFTs) the supernatant was spun at 100,000 g for 30 min at 4 °C (**Figure 22 a**). The resulting supernatant includes the aqueous soluble fraction and presumable monomeric tau "NS1" (**Figure 22 b**). The pellet was re-suspended at room temperature in 5% SDS/TBS buffer (50 mM Tris-HCl pH 7.4, 175 mM NaCl, 5% SDS and protease inhibitor cocktail) and spun at 100,000 g for 30 at 25 °C, following which the supernatant was discarded. This pellet was then re-suspended in 8M urea, 8%SDS buffer (50mMTris-HClpH7.4, 175mMNaCl, 8%SDS, 8 M urea and protease inhibitor cocktail) and agitated for 12–18 h at room temperature to obtain the SDS the insoluble fraction "NS2". All samples were diluted in 2× Laemmli buffer and boiled for 5 minutes. Double the amount of "NS2" was loaded compared to "NS1". Western blotting was performed to assess total tau levels and tau solubility state. The fraction were then quantified as a proportion of the sum total of the 2 fractions and these were expressed as the percentage corresponding to tau present in the input (brain homogenate samples before being fractionated).

LiCor scanner with Odyssey software was used to detect the signal and ImageJ software was used to measure band densities. GraphPad Prism was used for statistical analysis and unpaired, two-tailed t tests were performed on the data.

To carry out the biophysical methods, instead of dissolving this sediment in urea to obtain the fraction “S3” or “NS2”, the pellets “P2” or “NP1” were washed three times with water to remove the remaining SDS detergent from the fractionation and dissolved in 1X PBS. A solid glass beads were added to the samples and incubated overnight in a rotor at 4 ° C for ThT, AFM and DLS.
For biophysical methods, protein concentration was determined by BCA protein assay against BSA standards using an absorbance of 690 nm. Additionally, tau protein concentration was determined from the absorption at 280 nm with an extinction coefficient of 7450 $cm^{-1}$ $M^{-1}$. Using the molecular weight for either 0N3R or 0N4R samples, concentration was determined by the average value from 5 individual 2 µl droplets.

For important consideration, the composition of both fractions (GTOs and NS) may contain proteins (other than endogenous tau, such as *Drosophila* tau (dtau)) and lipids, as contaminants of the fractionation process.

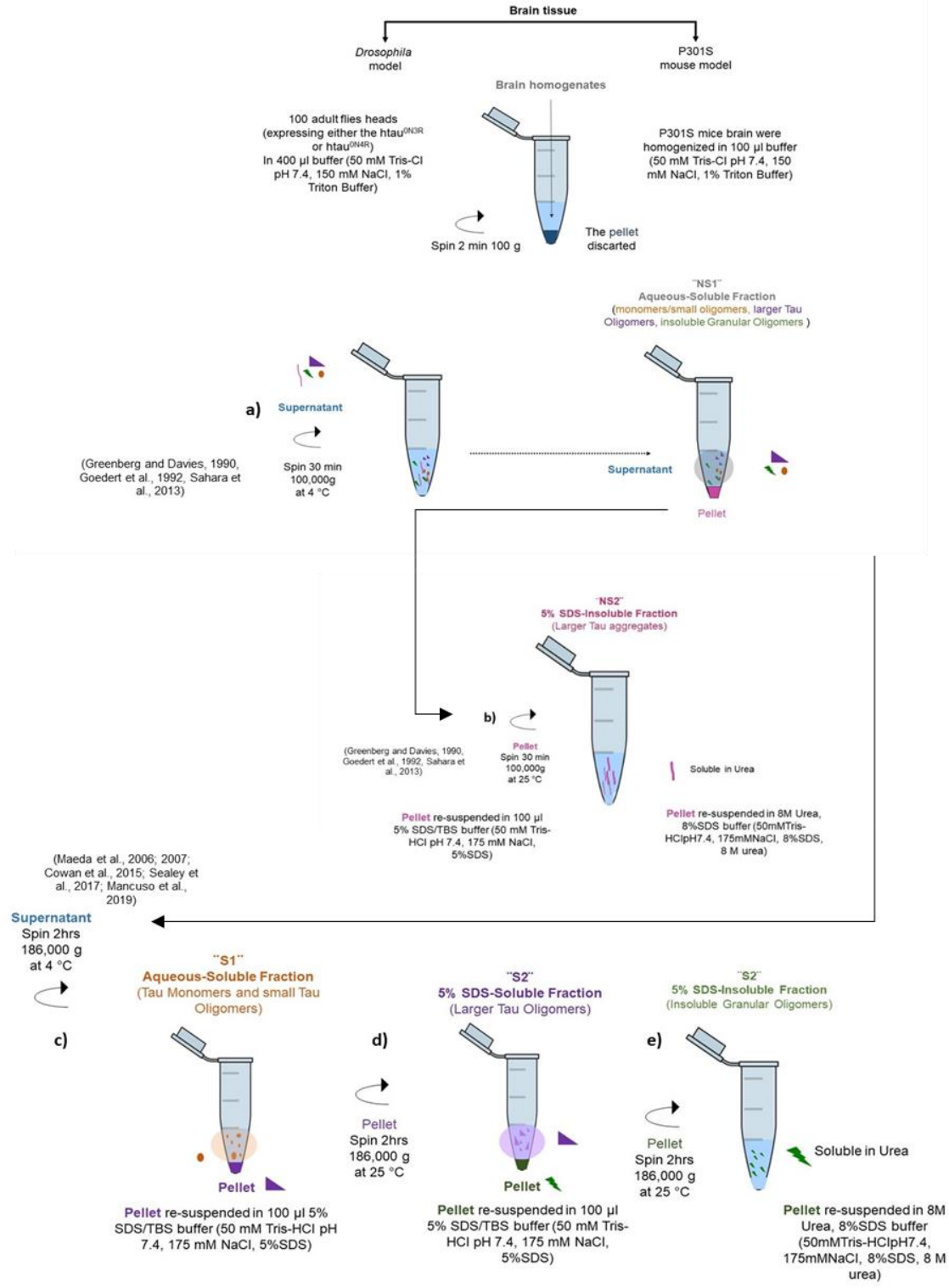


**Figure 22. Schematic representation of Solubility assay.**

The schematic representation shows **a)** Solubility assay to enriching for larger / fibrillary insoluble tau (NS) or **b)** Solubility assay to enriching for insoluble granular tau (GTOs).

## 3.9 Western Blotting

Western blotting was performed to assess total tau solubility state. Adult fly heads were homogenised in buffer in a ratio of 10 heads: 40µl buffer (50 mM Tris-HCl pH 7.4, 175 mM NaCl, 1 M sucrose, 5 mM EDTA and protease inhibitor cocktail). Samples were centrifuged at 1000 *g* for 2 min and unhomogenised material was discarded. The samples prepared for the tau solubility assay s were diluted in 2× Laemmli buffer and boiled at 95°C for 5 min. Then, the samples were run on 10% SDS PAGE gels and transferred to nitrocellulose membrane. Total tau levels were detected using anti-human tau polyclonal antibody (1:15,000, Dako) and anti-beta actin (1:500) was used as a loading control. Signal was detected using fluorescent secondary antibodies against rabbit (IRDye, LI-COR) or mouse (Alexa-Fluor, Invitrogen), both used at 1: 20,000. A LiCor scanner with Odyssey software was used to detect the signal and ImageJ software was used to measure band densities. GraphPad Prism, version 7.0 Software was used for statistical analysis and unpaired, two-tailed t tests were performed on the data.

**Table 6. Antibodies used in this thesis**

| | Supplier | Product no. | Dilution | Species | Extra information |
|---|---|---|---|---|---|
| Tau | Dako | A0024 | 1:15,000 | Rabbit pAb | - |
| Anti-beta Actin | Abcam | ab8224 | 1:500 | Mouse mAb | - |
| Anti-mouse | IRDye, LI-COR | ab216773 | 1:20,000 | Goat pAb | 700 nm channel |
| Anti-rabbit | IRDye, LI-COR | ab216773 | 1:20,000 | Goat pAb | 800 nm channel |

## 3.10 Thioflavin T fluorescence

The thioflavin dye was mixed with the samples to a final concentration of 50 µM ThT dye and ~5 µM protein. 50 µL were taken from this mixture and added to the wells, in a 96-well plate (Costar) and incubated at 37 ˚C for 5 minutes before taking a reading. Fluorescence measurements were taken using a 440, bandwidth of 30 nm excitation filter and a 485, bandwidth of 12 nm emission filter. The experiment was done for at least 2 individual experiments and measurements were carried out in duplicates. For data analysis, fluorescence of each equivalent blank solution (buffer + dye) was subtracted from each protein. The signal from the fluorescence intensity of each samples was divided by the fluorescence intensity of the ThT-only sample. The signal from ThT-only sample has been taken as value 1. To calculate the fold change in fluorescence intensity over the moromer,

the fluorescence intensity of the sample corresponding to the monomer was divided by the fluorescence intensity of the sample (Sample / monomer). The value from the “S1” fraction at 0 weeks in flies and 12 weeks in mice were considered as the monomeric tau to compare the fold increase with the GTOs and NFTs at the different representative stages of the disease. GraphPad Prism, version 7.0 Software was used for statistical analysis and unpaired t tests were performed on the data.

## 3.11 Dynamic Light scattering

The tau fractions, “S1” or “NS1”, “S2” and “P2” or “NP1” (re-suspended in 1xPBS). For the measurement, 40µl of sample in a low-volume quartz batch cuvette (ZEN2112) was used and the samples were thermally equilibrated at 25 °C for 2 min. The Particle size was obtained as an average of 3 measurements with 20 runs each and expressed as volume distribution. The experiment was done for at least 2 individual experiments. The measurement was performed with a Zetasizer Nano ZS (Malvern, Herrenberg, Germany) containing a 5-milliwatt Helium-neon 633-nm laser at 173° measurement angle. The system was calibrated with the latex calibration sample from Malvern. GraphPad Prism, version 7.0 Software was used for statistical analysis and unpaired t tests were performed on the data.

## 3.12 Atomic force microscopy

5 µL of each tau species previously obtained using the protein fractionation method (solubility assay) to isolate granular tau oligomers (GTOs) or fibrils (filaments) at different stages of diseases from brain homogenate in our two models were diluted in 500µL of water. Then 25µL of sample were placed in freshly cleaved 10 mm mica disc (Agar Scientific). These were incubated at room temperature for 5 minutes. After that, samples were rinsed 4 times with ultrapure water and dried with compressed air. Samples were imaged in air with a digital multimode Nanoscope IV AFM operating in tapping mode with an Aluminum coated non-contact/Tapping mode probe with a resonance frequency of 320 kHz and force constant of 42N/m were used for images (Nanoworld, POINTPROBE NHCR). As for the ThT and DLS experiments, at least 2 individual experiments were done. The images are representative of the sample and were taken at random points on the sample with a scan rate of 1Hz-2Hz. The sizes were determined by cross-sectional height analysis. AFM analysis was carried out using WSXM software.

## 3.13 Using immunoprecipitation technique to isolate tau protein from mice

The protocol to immunoprecipitate tau species from P301S mice and mice lacking microtubule associated protein tau (Mapt−/−) tau knockout (KO) as a negative control was carried out with the help of Dr. Katrin Deinhardt and Dr. Mariana Vargas-Caballero.

### 3.13.1 Cross-linking antibody (Tau-5) to beads

The Thermo Scientific Pierce Crosslink Immunoprecipitation (IP) method was employed to covalently cross link the antibody onto the beads was used. Then analysed by dot blot using a generic anti IgG antibody. A 25 µL of the agarose beads were incubated with 10 µg of antibody Tau-5 on a rotator at room temperature for 1, 5 hrs. After shaking, the beads were collected by centrifugation for 1 minute at 1000 xg and the ¨flow-through¨ collected to verify antibody coupling by dot blot analysis. Next, the beads were washed three times, the first and third FT from the washes were saved for dot blot to verify the presence of antibody in the supernatant after wash.

To make sure that antibody bound to beads is not eluted with the antigen during the IP elution step, it is necessary to cross-link the complex. For the reaction, 50 µL of a solution with DSS (5X) was incubated with the beads-antibody for 30 minutes at room temperature on a rotator half an hour and centrifuge for 1 minute at 1000 xg. After incubation, 50 µL of elution buffer was added to the beads and they were centrifuged. The ¨flow-through¨ was collected to verify antibody crosslinking. After the elution, the flow through was eluted twice to remove the non-crosslinked antibody and quench the crosslinking reaction and washed three times with wash buffer and to eliminate the uncoupled antibody. The FT from last wash was saved to analyse by dot blot. Finally, the material that has not been attached to the beads has been eluted and detected in the dot blot. After the elution, this flow through was washed twice to eliminate uncoupled antibody.

### 3.13.2 Tau immunoprecipitated from P301S tau mice

For the immunoprecipitation reactions, brain lysate (333 µL) was previously precleared with 80 µL of protein Control Agarose Resin. The precleared sample was mixed with the previously coupled beads with the antibody (25 µL of beads and 10µg of Tau 5) and the mixture was shaken end-over-end overnight at 4°C. Next, the tau bound to the antibody was eluted from the antibody beads complex by adding 60µL of elution buffer and incubate for 5 min at room temperature. The flow-through was collected and then analysed by SDS-PAGE and Western blot.

To improve capturing as much tau protein three more IP reactions were carried out on each flow through elution buffer.For this, 60 µL of the flow through collected (contained the unbound protein) from the first IP reaction was incubated for 2hrs with the coupled antibody-beads. The tau-bounded protein was eluted and collected individually for the analysis. The flow through from this reaction was incubated with the beads for 2hrs and eluted again. This was repeated two more times. Each time, the IP reaction (IP elute) and the Flow-through (FT) were collected independently to test the presence of tau.

## 3.14 Data analysis

Graphs were generated using GraphPad Prism, version 7.0 Software (Graph Pad Software Inc.). Statistical analysis was conducted using GraphPad Prism, version 7.0 Software. In detail, for longevity experiments conducted in *Drosophila* model, survival analysis was carried out using as mentioned, GraphPad Prism software and a Kaplein-Meir curve was plotted. A Log-rank (Mantel-Cox) test was performed on the data to investigate the difference between the three genotypes tested.For climbing (locomotor) experiments conducted in *Drosophila* model, a two-way analysis of variance (ANOVA) was performed on the climbing data to investigate the difference between the three genotypes tested.

For rotarod assay in P301S mice model: The two-way repeated measurements ANOVA with Tukey post hoc test was performed on the data.

For western blotting, unpaired, two-tailed t tests were performed on the data. Values are presented as the mean ± standard error. $P<0.05$ was considered to indicate a statistically significant difference.

For thioflavin fluorescence, the experiment was done for at least 2 individual experiments and measurements were carried out in duplicates. Fluorescence of each equivalent blank solution (buffer + dye) was subtracted from each sample. The signal from the fluorescence intensity of each samples was divided by the fluorescence intensity of the ThT-only sample. The signal from ThT-only sample has been taken as value 1. To calculate the fold change in fluorescence intensity over the moromer, the fluorescence intensity of the sample corresponding to the monomer was divided by the fluorescence intensity of the sample (Sample/monomer). For DLS measurement the Particle size was obtained as an average of 3 measurements with 20 runs each and expressed as volume distribution. The experiment was done for at least 2 individual experiments. For ThT and DLS data analysis, unpaired t tests were performed on the data to investigate the difference between the fractions tested over time.

# Chapter 4 Tau phenotypes in two models of tauopaty

## 4.1 Introduction

The overarching aim of my PhD project is to understand how changes in different tau species can lead to the development of tauopathy in different animal models. Particularly, this research will investigate how changes in tau species relate to the onset and the progression of the disease in our two models, and by extension in humans with tauopathy. In order to do this, it is important to first **characterise emergence of tau phenotypes in the models of tauopathy I will study.** Only then can these models be used to identify the tau species responsible for the emergence and progression of tau phenotypes at early and late stages of disease.

Several transgenic animal models expressing human tau and mutant tau in neurons have been generated to investigate tauopathies *in vivo* (as reviewed in Lee et al., 2005). Such well stablished models exist in both rodents (Allen et al., 2002; Lewis et al., 2000; Tanemura et al., 2001; Tatebayashi et al., 2002) and *Drosophila melanogaster* (Mudher et al., 2004; Chatterjee et al., 2009; Folwell et al., 2010; Quraishe et al., 2013; Sealey et al., 2017). These models mimic the essential features of human tauopathies for investigating tau behavioural phenotypes and pathogenicity (Lee et al., 2005). Therefore, in this study we decided to use two *Drosophila* and one rodent models of tauopathy.

In *Drosophila* model, two different isoforms of human tau, one expressing 3-repeat (htau$^{0N3R}$) and one expressing 4-repeat human tau (htau$^{0N4R}$) will be expressed in the nervous system and assessed for longevity and climbing behaviour. These are two established tau phenotypes in these models (Mudher et al., 2004; Folwell et al., 2010; Quraishe et al., 2013; Sealey et al., 2017). In addition, a transgenic mice line expressing the 4-repeat human tau (htau$^{0N4R}$) with the P301S mutation in the nervous system will be assessed for emergence of locomotor behaviour, a tau phenotype observed in this particular model using a rotarod assay in mice (Scattoni et al., 2010; Xu et al., 2014).

## 4.2 Summary of aims and objectives:

**Aim 1. To characterize emergence of tau phenotypes in two models of tauopathy.**

Objective 1: Evaluate longevity and climbing behavior in the fly model for characterization of the tau phenotype (behavioral defect) and determination of the onset and progression of the disease.

Objective 2: Evaluate locomotor behavior in the rodent model to characterize the tau phenotype and determine the onset and progression of the disease.

## 4.3 Results

The primary aim of the research described in this chapter is to characterize tau phenotype (behavioral defect) in two models of tauopathy. So that in the next chapter I can explore which tau species is responsible for the disease phenotype at each stage of disease.

*My hypothesis is that Intermediate tau oligomers are the pathogenic tau species that might be responsible for tau-mediated dysfunction in the initial stages. Further, I hypothesize that these oligomers polymerize to form longer fibrils and these species form at the later stages of the disease.*

As mentioned before, in AD, one of the risk factors is age and the symptoms develop slowly and get worse over time (Schmidt et al., 2011). Therefore, age related phenotypes, such as lifespan and climbing in flies, and motor coordination in mice were performed to detect the onset and progression of behavioural phenotypes that correlate with dysfunction and degeneration with increasing age.

In this study we decided to express two different isoforms of htau in *Drosophila* based on the fact that others have found that the expression of htau$^{0N3R}$ and htau$^{0N4R}$ in *Drosophila* exert different phenotypes (Kosmidis et al., 2010; Sealey et al., 2017). It has also been found that the expression of hTau$^{0N3R}$ is associated with dysfunction in the absence of neuronal death (Mudher et al., 2004; Cowan et al., 2010). Conversely, expression of hTau$^{0N4R}$ is associated with degeneration (Sealey et al., 2017). This suggests that there are biochemical and biophysical differences between the tau aggregates generated from these two isoforms that would be interesting to study in more detail (Sealey et al., 2017).

The transgenic mice line expressing the 4-repeat human tau (htau$^{0N4R}$) with the P301S mutation in the nervous system has been used as a model since it develops the tangle pathology similar to that seen in human tauopathies (Allen et al., 2002; Delobel et al., 2008). In addition, a locomotor behavioural phenotype has been observed in this particular model using a rotarod assay in mice

(Scattoni et al., 2010; Xu et al., 2014). For this study, the locomotor behavioural experiments were conducted by Dr. Renzo Mancuso and his data clearly shows how locomotor dysfunction emerges at early stage of disease and progressively worsens at late stages of disease (Scattoni et al., 2010; Xu et al., 2014).

### 4.3.1 Expression of both htau$^{0N3R}$ and htau$^{0N4R}$ is related to a shorter lifespan in *Drosophila*

The longevity assay (lifespan) has been used to evaluate tau-toxicity caused in flies and many studies have reported a shortened lifespan upon expression of various human tau isoforms in *Drosophila* (Mudher et al., 2004; Folwell et al., 2010; Quraishe et al., 2013; Sealey et al., 2017). For this reason, the longevity assay was used to characterize and assess the emergence of this phenotype following expression of two isoforms of human tau.

Ten cohorts of 10 male flies (n=100) with pan-neural expression of htau$^{0N3R}$ and htau$^{0N4R}$ and OreR wt as a control (wt) were separated 0-3 days' post eclosion and transferred to new food twice a week. Dead animals were scored three times a week. Survival analysis was carried out using GraphPad Prism software and a Kaplein-Meir curve was plotted. A Log-rank (Mantel-Cox) test was performed on the three different groups (OreR wt, htau$^{0N3R}$ and htau$^{0N4R}$).

There is a difference between the all three genotypes tested (OreR wt, htau$^{0N3R}$ and htau$^{0N4R}$) ($p<0.0001$) (**Figure 23**). The wild type flies live longer compared with both htau-expressing lines. The lifespan of OreR wt flies is reduced by 50% at 8 weeks and all flies die at 10.5 weeks post-eclosion (**Figure 23**-**B**). In particular, the OreR wt flies begin to decline at around 4 weeks when 90% are alive.

Flies expressing the htau$^{0N3R}$ isoform have a significantly shorter lifespan compared to controls ($p<0.0001$). The median lifespan of htau$^{0N3R}$ flies is 5 weeks whereas that of the control flies is 8 weeks. Survival of htau$^{0N3R}$ flies begins to decline at 2.5 weeks when 90% are alive. Half of the flies are dead at 5 weeks post-eclosion. The percentage of survival goes down with age and only 1% of flies survive at 9.5 weeks of age.

Similarly, the expression of htau$^{0N4R}$ isoform also induces a significant reduction in lifespan compared to control, though it is not as profound as htau$^{0N3R}$. The survival of htau$^{0N4R}$ flies begins to decline at 3.5 weeks post-eclosion and decline to 90%. Whereas the same reduction in OreR wt flies it is observed after 4.2 weeks post-eclosion. In particular, htau$^{0N4R}$ flies have a median lifespan of 6.5 weeks whereas the median lifespan of wt flies is 8 weeks. The survival decline to 10 % at 7 weeks and all flies have died after 7.5 weeks post-eclosion.

A)

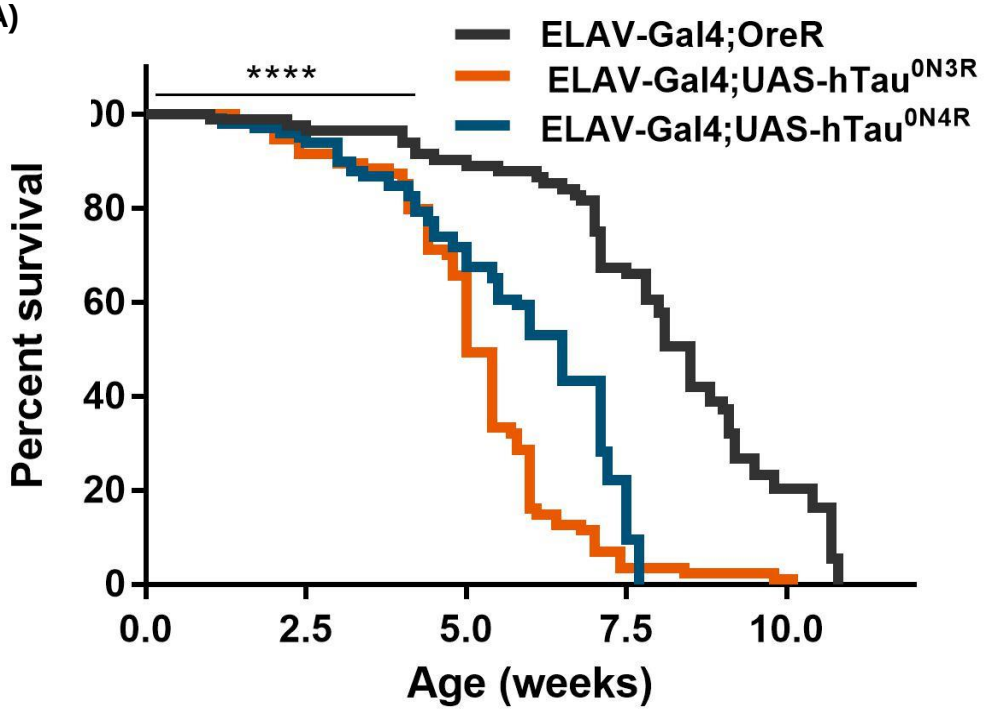


B)

| Median Survival (weeks) | | |
|---|---|---|
| WT | htau$^{0N3R}$ | Htau$^{0N4R}$ |
| 8 | 5 | 6.5 |

**Figure 23. Expression of tau produces premature death.**

**A)** Survival curves for Elav-GAL4 driven htau$^{0N4R}$ and htau$^{0N3R}$ and OreR wt male flies (n=100 separated in 10 different cohorts). Only males were used to avoid possible gender-specific differences. Lifespan of flies is significantly different between the three groups tested (Log-rank, Mantel-Cox test, $p < 0.0001$). **B)** Table showing median survival. Htau$^{0N3R}$ flies die quicker than both htau$^{0N4R}$ and Ore wt control flies. OreR wt and htau$^{0N4R}$ have a median lifespan age of 8 weeks and 6.5 weeks respectively whereas htau$^{0N3R}$ has a median lifespan of 5 weeks.

Overall, this data shows that the expression of both htau$^{0N3R}$ and htau$^{0N4R}$ causes a shorter lifespan and the phenotype emerges around 2 weeks post-eclosion. In addition, this data also shows tau$^{0N3R}$ isoform have a more sever tau phenotype in survival compared to htau$^{0N4R}$ flies. These results are similar to those reported by Sealey et al., 2017, in that they have shown that the expression of the 3R isoform causes deeper axonal transport defects, which result in behavioral defects (Sealey et al., 2017).

The next step is to evaluate the effect of the expression of tau on the locomotor ability of the same fly lines and identify the time point when the climbing phenotype emerges.

### 4.3.2 Expression of both htau$^{0N3R}$ and htau$^{0N4R}$ is related to locomotor dysfunction at a relatively early age in *Drosophila*

The locomotion (climbing) assay has been commonly used to sensitively assess the dysfunction potentially caused to flies due to the expression of tau in the nervous system (Mudher et al., 2004; Folwell et al., 2010; Quraishe et al., 2013; Sealey et al., 2017). The information on locomotor dysfunction is complementary to the information obtained on the impact of the expression of tau on survival in *Drosophila*.

For this study the climbing behaviour of four cohorts of 10 flies (n=40) with pan-neural expression of htau$^{0N3R}$ and htau$^{0N4R}$ and OreR wt as a control (WT) was studied. Flies were placed in cylinders and the assay was conducted by tapping flies to the bottom of the cylinder and recording the time taken for flies to climb up the sides of the measuring cylinder. The distance climbed by the flies was recorded at 10s. The assay was repeated three times, with 1 minute rest between each trial and the mean was calculated. The climbing ability of the htau$^{0N3R}$ and htau$^{0N4R}$ expressing adult lines and OreR wt was measuring once a week for a total of 6 weeks. Two-way ANOVA test test was performed on the three different groups (OreR wt, htau$^{0N3R}$ and htau$^{0N4R}$) (**Figure 24**).

As with the longevity assay, a clear difference between the three groups was evident (**** $p<0.0001$). The climbing ability of OreR wt flies is slightly affected over time. During the first weeks after eclosion, OreR wt flies showed no deficit in climbing ability and this persisted until week 5 when climbing ability began to decline (**Figure 24**). However, even at 6 weeks the flies remain mobile. For instance, the results show that wt flies have the ability to climb up to 49 mm at 0 week-

old and this decreases to 42mm at week 4 and 30 mm at week 5. Finally, after 6 weeks the climbing ability of the flies has decreased to 26 mm.

In contrast to the controls, the climbing ability of flies expressing the htau$^{0N3R}$ isoform begins to deteriorate at 2 week-old and decreases rapidly as flies progress to 5 weeks post-eclosion. At 6 weeks, the htau$^{0N3R}$ flies are virtually immobile. Specifically, young 1-3d htau$^{0N3R}$ flies climb 45 mm. This ability decreases to 35 mm at 2 weeks. After this time, this decrease in climbing ability mobility of htau $^{0N3R}$ flies declines drastically and the phenotype is more profound as flies progress to week 4, when the flies are able to climb around 6 mm and ultimately 2 mm at 5 weeks post-eclosion.

Flies expressing htau$^{0N4R}$ also showed significant loss of climbing ability compared to control flies but less than that seen for htau$^{0N3R}$ flies. The climbing ability of flies expressing htau$^{0N4R}$ starts to decline around 2 weeks and it decreases slightly and progressively until 4 weeks (**Figure 24**). It is not until 5 weeks post-eclosion when the ability to climb falls drastically. Specifically, flies expressing htau$^{0N4R}$ have the ability to climb 42 mm at 0 weeks of age and this decrease slightly to 33 mm around 2 weeks. Around 4 weeks post-eclosion the flies have the ability to climb 23.4 mm, 16.2 mm at 5 weeks and finally 2mm at 6 week-old, whereas the control have decreased the climbing ability to 26 mm at the same age.

The differences in climbing ability of both tau flies (htau$^{0N3R}$ and htau$^{0N4R}$) compared to wt controls is displayed in **Figure 24**. From this table it is clear that the climbing ability of flies is significantly different between the three groups tasted. Two-way ANOVA test shows that both htau$^{0N3R}$ and htau$^{0N4R}$ flies are significantly different to OreR wt at all-time points ($p<0.001$). By comparison, the decline in climbing ability of both htau$^{0N3R}$ and htau$^{0N4R}$ is significantly greater than the control but that of htau$^{0N3R}$ greater than that of htau$^{0N4R}$. Two-way ANOVA test shows that the climbing ability of htau$^{0N3R}$ and htau$^{0N4R}$ flies are significantly different at 4 weeks ($p=0.0242$) and 5 weeks ($p=0.0362$).

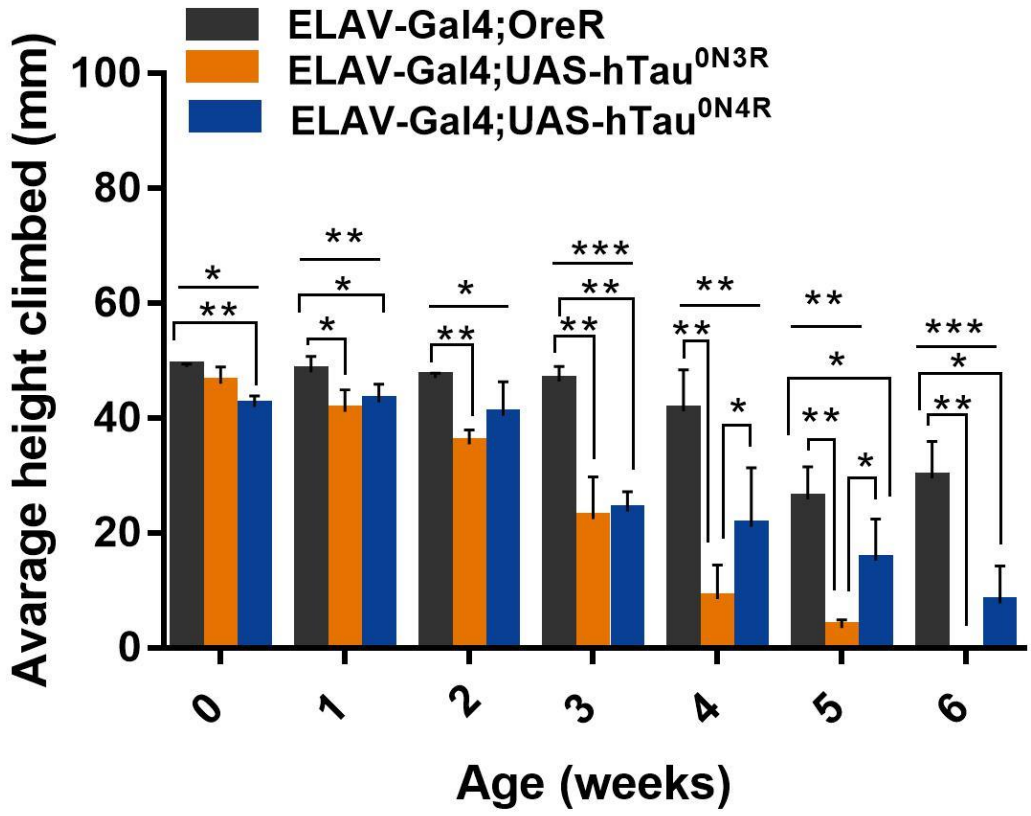


**Figure 24. Expression of tau cause locomotor dysfunction**

Climbing assay for Elav-GAL4 driven htau$^{0N4R}$ and htau$^{0N3R}$ and OreR wt male flies (n=40 separated in 10 different cohorts). Only males were used to avoid possible gender-specific differences. The climbing ability is significantly different between the three groups tested (Two-way ANOVA, $p<0.0001$). The decline in climbing ability of both htau$^{0N3R}$ and htau$^{0N4R}$ is significant greater than the control but that of htau$^{0N3R}$ greater than that of htau$^{0N4R}$. Two-way ANOVA test shows that the climbing ability of htau$^{0N3R}$ and htau$^{0N4R}$ flies are significantly different at 4 weeks ($p=0.0242$) and 5 weeks ($p=0.0362$).

Overall, this data shows that the expression of both htau$^{0N3R}$ and htau$^{0N4R}$ causes locomotor dysfunction at a relatively early age. This phenotype emerges around 2 and 3 weeks post-eclosion. Similarly to longevity assay, the effect caused by htau$^{0N3R}$ is more severe than the effect caused by htau$^{0N4R}$.

Based on both the lifespan and climbing assay, one can identify 2.5 weeks as the time point at which the tau phenotypes begin to emerge and 5 weeks as the time point when it is manifest. The 2.5 week time point will therefore be used as the early stage time point (when disease emerges) and 5 weeks will be used as the late stage time point (when disease is established).

### 4.3.3 Expression of the P301S tau mutation produces locomotor dysfunction at early age in mice

The rotarod assay has been used to evaluate toxicity caused by expression of the 0N4R human tau with the P301S mutation controlled by the murine thy1 promoter in mice (Scattoni et al., 2010; Xu et al., 2014). In these studies, the expression of P301S mutation leads to locomotor impartment (Scattoni et al., 2010; Xu et al., 2014). For that reason, using the same mice model, the rotarod assay was performed by Dr. Renzo Mancuso and the results provided by him were used for assessing emergence of locomotor phenotype.

Motor coordination, strength and balance were tested at 6, 12, 20 and 24 weeks of age using rotarod with each time point being an independent cohort. This test consists of placing the animals on a horizontal bar (diameter = 30 mm), that rotates around its major axis at an accelerating speed of 4-40rpm over 5 min. Mice were placed on the rod for up to 5 minutes and the latency to fall was recorded. In this assay 300s was considered an arbitrary maximum time of remaining on the rotating rod.

**Figure 25** shows that there is a difference between the two groups tested. In this study, control mice perform better when assessing balancing in the rotarod test compared with the P301S. In particular, the maximum time of remaining on the rotating rod is constant (300s) at every time point tested indicating that in the wild type mice (C57Bl/6) the latency to fall is not affected over time.

In contrast the P301S mutant tau-expressing animals have a reduction in the balancing ability. These mice begin to exhibit difficulties in maintaining balance on the rotarod at 10 and 12 weeks of age (**Figure 25**). The balancing ability of P301S decreases and deteriorates rapidly as mice progress to 12 and 16 weeks of age. The time to remain on the rotation is markedly reduced between 16 and 20 weeks when the latency to fall decreases sharply. Finally, at 24 weeks of age, the mice are immobile. The balancing ability of P301S mice is significantly different from the controls at 20 and 24 weeks of age.

This data show that the expression of P301S mutation leads to locomotor impairment at an early age. This phenotype emerges around 12 weeks at early stages and is fully established at 24 weeks of age. Based on this the 12 week time point will be used as the early stage of disease when

phenotype begins to emerge, and the 24 week will be used as the late stage of disease when the phenotype has become established.

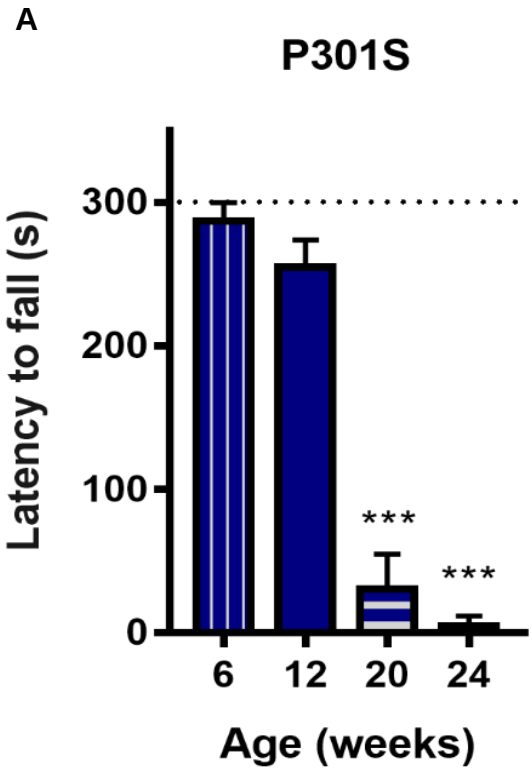


**Figure 25. P301S mutant tau expressing animals showed decreased locomotor behaviour**

Rotarod assay was performed by Dr. Renzo Mancuso. Comparison of balancing ability with age over 20 weeks for expression of the 0N4R human tau with the P301S mutation controlled by the murine thy1 promoter in mice and non-transgenic wild type mice (C57Bl/6) (n=15 per group). Locomotor ability is significantly different to WT at 14, 16 and 20 weeks (two-way repeated measurements ANOVA with Tukey post-hoc test $p < 0.05$).

## 4.4 Discussions

### 4.4.1 Summary

The aim of this chapter was to characterize emergence of tau phenotypes in the two models of tauopathy. The data presented here shows that the expression of tau in the two models produces a phenotype that can be characterized to identify time points for the emergence and progression of the disease.

### 4.4.2 Identification of the appearance and progression of tau phenotypes

In *Drosophila*, it was shown here that flies expressing pan-neurally the two tau isoforms (htau$^{0N3R}$ and htau$^{0N4R}$) have an effect on survival and locomotion and the phenotype has an early and late stage. At the early stages the phenotypes emerge around 2 and 3 weeks post-eclosion. At the late stages the phenotype is more severe at 5 and 6 weeks. The data presented here, also indicates that toxicity caused by htau$^{0N3R}$ is more severe than that caused by htau$^{0N4R}$. However once the phenotype emerges, as in the longevity assay, the decline in 4R tau flies is steeper than that of 3R flies with all the 4R flies dying faster than the 3R flies. This suggests that the 3R has a greater effect at early stage of disease and the 4R tau may potentially have a greater effect at last stage of disease. One explanation for this may due to the greater neuronal dysfunction caused by 3R isoforms compared to 4R isoforms, which may play a greater role at the early stage of disease (Sealey et al., 2017). At later stages of disease, attributes of 4R, such as their greater propensity for aggregation may play a more prominent role. These results confirmed previous observations that expression of these two isoforms present differential effects when compared in similar behavioural assays (Sealey et al., 2017).

The expression in neurons of the human tau 0N4R with the P301S mutation in mice has an effect on locomotion. This phenotype also has an early and late stage. In this model the phenotype emerges at 12 weeks and is more severe at 16 and 20 weeks. These results confirmed the same progression of the phenotype due to expression of tau in the same model (Scattoni et al., 2010; Xu et al., 2014).

## 4.5 Conclusions and future directions

The data presented here demonstrated that in both models the expression of human tau produces a phenotype that can be correlated with some of the pathological characteristics observed in human tauopathies. In these, the phenotypes evaluated manifest in an early stage and in an advanced stage and, therefore, these can be considered time points for the onset and progression of the disease. I can now explore which tau species is responsible for the phenotype at each stage of the disease.

# Chapter 5 Tau species potentially responsible for the onset and progression of phenotypes

## 5.1 Introduction

This chapter seeks to focus on **Aim 2,** which is **to identify the tau species potentially responsible for the onset and progression of disease in the models described in chapter 4.**

*My hypothesis is that Intermediate tau oligomers are the pathogenic tau species that might be responsible for tau-mediated dysfunction in the initial stages. Further, I hypothesize that these oligomers polymerize to form longer fibrils and these species form at the later stages of the disease.*

Different tau species have been implicated in AD and other tauopathies. Some of these species include soluble/ insoluble oligomers, granular insoluble oligomer and larger filaments (Maeda et al., 2006; 2007; Cowan and Mudher, 2013). These species have been isolated and described from AD brains and the presence of some of them have been correlated with the stages of the diseases. For instance, tau species such granular tau oligomers (GTOs) are present at early and moderate Braak stages and neurofibrillary tangles (NFTs) are evident at latest stages of the disease (SantaCruz et al., 2005; Maeda et al., 2006; Spires et al., 2006).

These different species can be obtained by fractionation/purification protocol based on sedimentation, solubility properties and morphology (Maeda et al., 2006; 2007; Cowan et al 2015) as described in **Materials and methods** in section **3.7** and **3.8** (**Figure 22**) . Therefore, these different properties will be used to differentially identify them at different stages of diseases in our two models of tauopathy.

### 5.1.1 Using solubility assays to differentiate between species

#### 5.1.1.1 Solubility assay to enriching for insoluble granular tau (GTOs)

The protocol I have employed to isolate GTOs was described by Maeda et al in 2007 and commonly used for identifying insoluble tau oligomers (Maeda et al., 2007; Cowan et al., 2015; Sealey et al., 2007; Mancunso et al., 2017). These studies have shown that GTO sedimentation requires a 200,000g and 186, 000g spin for 2 h. The presence of GTOs was confirmed by Maeda et al., 2007 using AFM and by immuno electron microscopy (EM), of the GTOs pellet. Further work by Maeda

et al., 2007 demonstrate that the standard protocols to sediment insoluble proteins using 100,000g of spin for 30-60 minutes do not sediment GTOs so they remain in suspension representing the soluble fraction despite their demonstrable insolubility in SDS (Maeda et al 2007). They also characterized the GTOs as positive for MC1 and for thioflavin, although they are clearly not filamentous in any way. They conclude that GTOs have a β-sheet structure and suggest that they may be composed of the partially folded (misfolded) form of the tau monomer (Maedaet al 2007).

For this study, 100 heads of adult flies expressing htau$^{0N3R}$ or htau$^{0N4R}$ (n=3, different crosses/genotype for independent experiments) were homogenized. Since this study is not inclined to study gender differences, it was decided to use 50 females and 50 males for all biochemical experiments. In addition, cerebral cortex P301S mice (n=3) representing several stages of tauopathy were homogenized as described in **Chapter 3**, **section 3.7** (see **Figure 22**). Sample from the homogenized material was processed in SDS gels as input, to analyze the total of tau protein in relation to actin, before fractionation. The homogenized material was fractionated to enriching for insoluble granular tau (GTOs) species and obtain “S1”, “S2” and “S3” fractions.

The composition of the fractions includes, an aqueous soluble fraction and presumable monomeric tau "S1", an aqueous insoluble- detergent SDS- soluble fraction “S2” (SDS-soluble oligomers). Finally, a detergent-SDS-insoluble fraction “S3” (SDS-insoluble granular tau oligomers). As described in **Chapter 3**, **section 3.7** (see **Figure 22**), all samples were diluted in 2× Laemmli buffer and boiled for 5 min. “S1”and “S2” were loaded equally (equivalent volumes) whereas double the amount of “S3” was loaded compared to“S1”and“S2”. Western blotting was performed to assess total tau levels and tau solubility state. The total tau levels in the input (tissue lysate samples before being fractionated) were detected using anti-human tau polyclonal antibody and anti-Actin was used as a loading control. The tau solubility state were detected using anti-human tau polyclonal antibody.The fractions were quantified as a proportion of the total sum of the three fractions (S1, S2 and S3) and these were expressed as the percentage corresponding to tau present in the input. LiCor scanner with Odyssey software was used to detect the signal and ImageJ software was used to measure band densities. GraphPad Prism was used for statistical analysis and unpaired, two-tailed t tests were performed on the data, to compare differences between each fraction over time.

#### 5.1.1.2 Solubility assay to enriching for larger aggregates/ fibrillar species (NS)

The protocol I have employed to isolate larger aggregates/ fibrillar species is based on the standard protocols to sediment insoluble proteins using 100,000g of spin for 30-60 minutes. For instance, Greenberg and Davies first reported a protocol to isolate insoluble tau from paired helical filament

(PHF)-enriched fraction from human AD brain homogenates (Greenberg and Davies, 1990). The authors isolated and described these species by taking advantage of their insolubility in the presence of sarkosyl detergent. Similar methods using the same range of spins and detergent have been standardized and are commonly used for isolating insoluble filaments (Greenberg and Davies, 1990; Sahara et al., 2013) in which the presence of filaments have been confirmed by immune EM microscopy.

For *Drosophila* model, it was decided to use 100 heads of adult flies expressing htau$^{0N3R}$ or htau$^{0N4R}$ (n=3, different crosses/genotype for independent experiments). As for the GTOs, since this study is not inclined to study gender differences, it was decided to use 50 females and 50 males for all biochemical experiments.

The fly heads mentioned above and cerebral cortex P301S mice (n=3) representing several stages of tauopathy were homogenized and fractionated using a series of centrifugation steps to enrich for larger tau aggregates/fibrillar species (NS), as described in **Chapter 3**, section **3.8** (see **Figure 22**). The composition of the fractions includes, a fraction that includes aqueous and detergent soluble tau species "NS1" (such as monomeric tau and some aqueous soluble and insoluble oligomeric species). A second fraction from the NS species includes a detergent-insoluble enriched fraction "NS2" (larger tau aggregates/fibrillar species). All samples were diluted in 2× Laemmli buffer and boiled for 5 minutes. Double the amount of "NS2" was loaded compared to "NS1".

As described in **Chapter 3**, the fractions were then quantified as a proportion of the sum total of the 2 fractions and these were expressed as the percentage corresponding to tau present in the input. LiCor scanner with Odyssey software was used to detect the signal and ImageJ software was used to measure band densities. GraphPad Prism was used for statistical analysis and unpaired, two-tailed t tests were performed on the data, to compare differences between each fraction over time.

## 5.2 Summary of aims and objectives:

Objective 1: To isolate the insoluble granular tau (GTO) species present in our two models of tauopathies at the early and late stages of disease.

Objective 2: To isolate the insoluble larger aggregates/ fibrillary species (NS) of tau present in our two models of tauopathies at the early and late stages of disease.

## 5.3 Results

### 5.3.1 Tau solubility decreases over time in both htau$^{0N3R}$ and htau$^{0N4R}$ in *Drosophila*

#### 5.3.1.1 Formation of tau oligomers: changes in GTO fraction

In flies, whether expressing htau$^{0N3R}$ or htau$^{0N4R}$ isoform it was found that the total tau, in the sample corresponding to the input, in relation to actin does not change significantly over time (**Figure 26**). In these, the representative band of tau migrate around 55kDa in flies expressing htau$^{0N3R}$ and around 60kDa in flies expressing the htau$^{0N4R}$ isoform (**Figure 26**). The fractions were then quantified as a proportion of the sum total of the 3 fractions and these were expressed as the percentage corresponding to tau present in the input.

In the control flies, wt , no reactive species with anti-htau antibody was detected in western blot in any of the samples, both for the adult fly head tissue homogenates (input) and for those corresponding to the fractionation (as shown in **Figure 65**, in **appendix B**).

In all flies, there are differences in tau solubility between the early and late stages of disease. In both transgenic flies, the majority of tau was in the aqueous-soluble fraction S1 or detergent-soluble fractions S2 at early stages (**Figure 27 A** and **B**). However, this S1 fraction decreases at later stages, suggesting that tau becomes insoluble over time. In line with this, the detergent-insoluble fraction S3 increases at early stages and decreases at late stages. This suggests oligomerization of tau as disease progresses.

In flies expressing the htau$^{0N3R}$ there are differences in the tau solubility between the three representative stages of the pathology tested. The representative band of tau migrates around 55kDa (**Figure 27 A-a**). In these flies, the fraction of tau (expressed as a percentage of total tau) found in S1 is around 60% (of total tau) in newly eclosed young (**Figure 27 A-a** and **Figure 27 B-a**). Indicating that the majority of tau is aqueous soluble. The relative amount of this fraction decreases as flies progress to a late stage (5 weeks post-eclosion). This indicates that tau is becoming insoluble.

In agreement with this, the amount of tau detected in the detergent- insoluble fraction, S3, is small compared with both S1 and S2 fraction (**Figure 27 A-a** and **Figure 27 B-b-c**). Quantification of S3 shows that the S3 mount is significantly different between 0 and 2.5 weeks ($p= 0.0118$) and between 2.5 and 5 weeks ($p=0.0164$). In newly eclosed flies, the amount of tau detected in S3 is around 6% and this amount increases to 25% at early stage and decreases to 15% at late stage (5 weeks post-eclosion). This collectively shows progressive aggregation of tau leading to its insolubility as disease evolves.

Interestingly, in all flies, whether they express htau$^{0N3R}$ or htau$^{0N4R}$, the presence of molecular weights of less than 43 kDa was found in the S2 fraction.This may represent a fragmentation of tau, but could also have an implication in the aggregation of tau, (**Figure 27 A-a**), although this suggestion would have to be investigated further.

In flies expressing htau$^{0N4R}$, the amount of tau found in the S1 fraction is around 50% in newly eclosed young flies (**Figure 27 A-b** and **Figure 27 B-a**). The relative amount of this fraction decreases as flies progress to the later stage of disease (5 weeks post-eclosion). In these flies, there is a significant difference between the amount of tau found in the various fractions at early and late stages of disease (**Figure 27**). Quantification of S2 fraction is significantly different between 0 and 5 weeks (p=0.0109). This suggests that soluble tau decrease with age. This suggests that soluble tau decrease with age.

This is supported by the amount of tau found in the S3 insoluble fraction in the htau$^{0N4R}$ flies (**Figure 27 A-b** and **Figure 27 B-c**). Although the amount of tau detected in this fraction is small at the three representative stages, there is a significant difference between 0 and 5 weeks (p= 0.0068) and 2.5 and 5 weeks post-eclosion (p=0.0415). In newly eclosed flies, the detected amount of S3 is around 15% and increases to 40% at the early stage (2.5 weeks). However, this amount decreases to 10% at the late stage (5 weeks post-eclosion). This indicates that GTOs are present at early stages and then decrease at latest stages as insoluble tau aggregates are increasing in sizes due to their oligomerization and further formation of larger aggregates in the 4R flies.

Overall, this data indicates that in both lines, either expressing the htau$^{0N3R}$ or htau$^{0N4R}$ tau becomes more insoluble with age. At early stage, there is an increase in the amount of GTOs. At late stages there is a decrease in the amount of GTOs.

The data also implies that GTOs are responsible for the phenotype at early stages of disease. This data also indicates that htau$^{0N4R}$ is more susceptible to become insoluble-prone to aggregation because this change in GTOs was more evident in these flies than in the 3R flies.

After determining the presence of insoluble granular tau oligomers using this solubility assay, the second assay to probe the presence of larger aggregates/fibrils was used for assessing detection of larger species of tau.

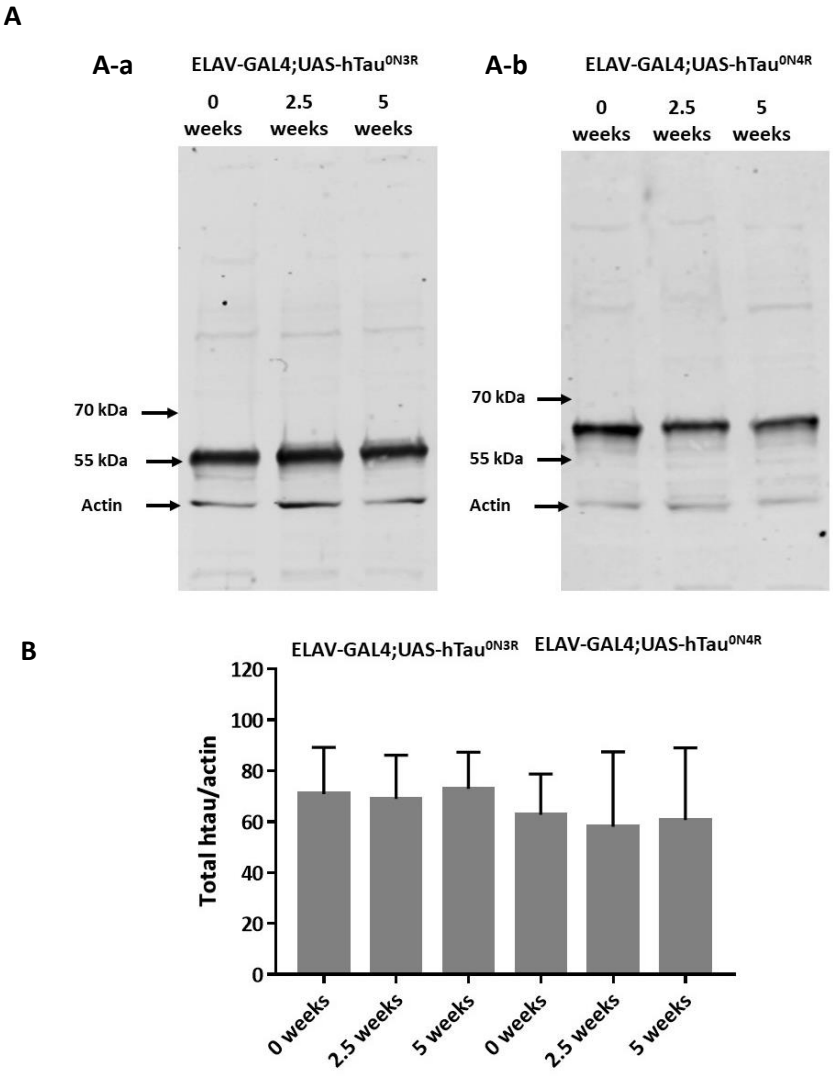


**Figure 26. Tau levels in *Drosophila* model of tauopathy**

Comparison of total levels of tau in relation to actin at different ages (0, 2.5 and 5 weeks-post eclosion) for Elav-GAL4 driven htau$^{0N3R}$ and htau$^{0N4R}$ (n=3, different crosses/ genotype; 100 fly heads for each experiment). **A)** Representative blot of total tau/actin. **B)** Quantification of the amount of tau in htau$^{0N3R}$ and htau$^{0N4R}$ flies shows that total levels do not change significantly over time, ($p<0.05$).Unpaired, two-tailed t tests were used to test for significance. Error bars are plotted as ± S.E.M

# GTOs Fractions

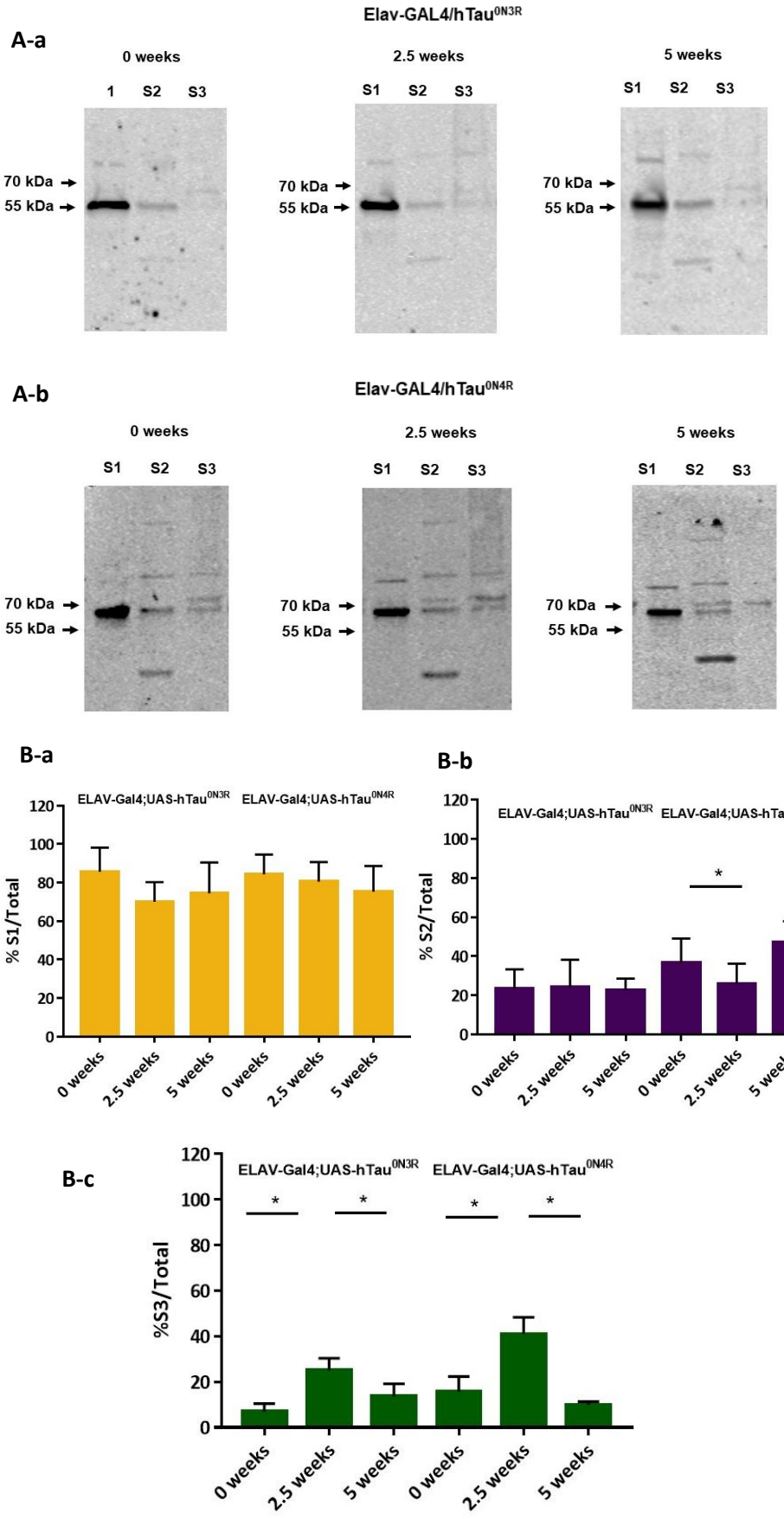

**Figure 27. Tau solubility decrease over time in both htau$^{0N3R}$ and htau$^{0N4R}$ flies as evidenced by the increase of GTOs formation.**

Comparison of solubility fractions at different ages (0, 2.5 and 5 weeks-post eclosion) for Elav-GAL4 driven htau$^{0N3R}$ and htau$^{0N4R}$ (n=3, different crosses/ genotype; 100 fly heads were homogenized for each experiment). **A)** Shows western blots of adult heads flies on S1, S2 and S3 fractions. **B)** Shows quantification on S1, S2 and S3 fractions compared relative to sum total of all fractions and expressed as the percentage corresponding to tau present in the input. **B-c**) Quantification of the amount of insoluble tau in htau$^{0N3R}$ flies shows that the S3 is significantly different between 2.5 and 0 weeks (p=0.0118) and 2.5 and 5 weeks (p=0.0164). In htau$^{0N4R}$ flies, the S2 is significantly different between 0 and 5 weeks (p=0.0109).The S3 mount is significantly different between 2.5 and 0 weeks (p= 0.0086) and 2.5 and 5 weeks (p=0.0415). Unpaired, two-tailed t tests were used to test for significance. Error bars are plotted as ± S.E.M.

#### 5.3.1.2 Formation of tau fibrils: Changes in NS fraction

Given that granular tau oligomers were detected at early time points and assuming that these insoluble species are precursors of larger protofibrils and neurofibrillary tangles, we performed a tau solubility assay to probe the presence of these larger aggregates/ fibrillar species (NS). The fractions contained here includes aqueous and detergent soluble (might contain aggregates of different sizes and monomers) tau, NS1, and detergent-insoluble fraction which is enriched for larger insoluble aggregates/fibrillary species, NS2 fraction. For this experiment, the fractions were quantified as a proportion of the sum total of the 2 fractions and these were expressed as the percentage corresponding to tau which is present in the input.

Similarly, to the detection of globular tau oligomers, there are differences in tau solubility between the early and late stages of the pathology in the solubility assay to detect larger aggregates. In both genotypes, at early stages the majority of tau was found in the fraction containing the aqueous soluble tau, NS1, with less in the fraction containing the larger insoluble tau, NS2. However, this larger insoluble fraction shows an increase with age in both lines (**Figure 28**).

In flies expressing the htau$^{0N3R}$ isoform there are differences in the tau solubility between the three representative stages of the pathology tested. In this, the representative bands of tau migrate around 55-64kDa (**Figure 27 A-a**). Here, the blots show the presence of smooth bands at high molecular weight, around 100kDa and 130 kDa. In addition, lower molecular weight around 52kDa,

43kDa, and 25kDa are detected in the western blot. This may represent a tau fragmentation (**Figure 28 A-b**).

The amount of tau found in the NS1 soluble fraction is around 90% in newly eclosed young flies (**Figure 28 B-a**). This result indicates that the majority of 3R tau is aqueous soluble. However, the amount of tau in this fraction decreases as flies progress to a late stage (5 weeks post-eclosion), indicating that tau is becoming insoluble over time.

In agreement with this, the amount of 3R tau detected in the detergent- insoluble fraction (NS2) is very small at 0 weeks compared with the NS1 fraction at the same age (**Figure 28 A-a** and **Figure 28 B-a**). In newly eclosed flies, the amount of tau detected in the NS2 fraction is around 9% and this increases to 30% at the early stage and to 40% at the late stage (5 weeks post-eclosion) (**Figure 28 A-a** and **Figure 28 B-a-b)**. This is suggestive of oligomerization starting at early stages and progressing to generate larger insoluble aggregates in the late stage.

In flies expressing the 4R isoform (htau$^{0N4R}$) there are also changes in tau solubility between the three representative stages of the pathology tested. This isoform of tau migrates around 60-64kDa. As in the flies expressing (htau$^{0N3R}$), the blots show the presence of smooth bands at high molecular weight, around 100kDa and 130 kDa. In addition, lower molecular weight around 52kDa, 43kDa, and 25kDa are detected in the western blot. As mentioned before, this may represent a tau fragmentation (**Figure 28 A-b**).

The result shows that the amount of tau found in the NS1 fraction is around 70% in newly eclosed young flies (**Figure 28 B-a**). The amount of this fraction decreases as flies progress to a later stage (5 weeks post-eclosion) when the percentage detected is around 40%. Suggesting that the amount of soluble tau is decreasing with age. In line to this, in newly eclosed flies the detected amount NS2 is around 17% and this increase to 40% at the early stage and to 55% at the late stage (5 weeks post-eclosion) (**Figure 28 A-b**).

As for the GTOs, in the control flies, wt, no reactive species with anti-htau antibody was detected in the NS fractionations (as shown in **Figure 65**, in **appendix B**).

Overall, this data indicates that in both tau-expressing lines, there is decrease in tau solubility with time. This suggest oligomerization in pathway to produce larger aggregates and can be related to the decrease of GTOs at latest stages shown in the previous assay and the increase of NS observed at the same late stage using this NS solubility assay. The data presented here also show that in the fly model, the htau$^{0N4R}$ is more susceptible to become insoluble-prone to aggregation than flies expressing htau$^{0N3R}$. This indicates that expression of these two isoforms in flies might have differential effects in the aggregation.

# NS Fractions

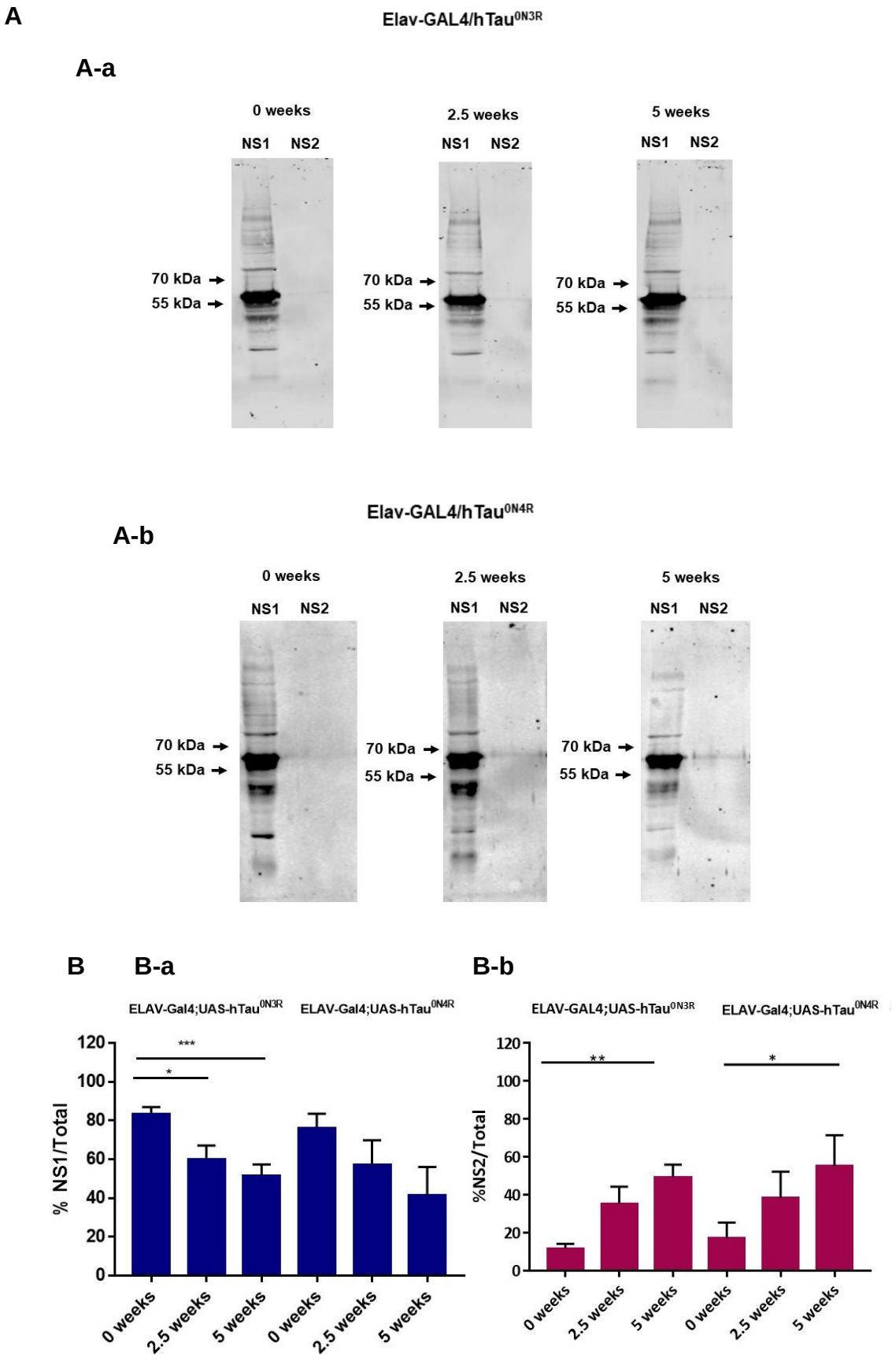

**Figure 28. Tau solubility decrease over time in both htau$^{0N3R}$ and htau$^{0N4R}$ flies as evidenced by the increase of NFTs formation**

Comparison of solubility fractions at different ages (0, 2.5 and 5 weeks-post eclosion) for Elav-GAL4 driven htau$^{0N3R}$ and htau$^{0N4R}$ (n=3, different crosses/ genotype; 100 fly heads were homogenized for each experiment). **A)** Shows western blots of soluble NS1 and NS2 insoluble fractions from adult heads. **B)** Shows quantification of soluble NS1 and NS2 insoluble fractions, relative to sum total of all fractions (NS1 and NS2) and expressed as the percentage corresponding to tau present in the input. **B-a**) Larger soluble fractions shows that the amount of soluble tau in htau$^{0N3R}$ flies shows that the NS1 mount is significantly different between 0 and 5 weeks ($p=0.0055$) and between 2.5 and 0 weeks ($p=0.0419$). **B-b**) Quantification of the amount of insoluble tau in htau$^{0N3R}$ flies shows that the NS2 mount is significantly different between 0 and 5 week ($p=0.0055$). Quantification of the amount of insoluble tau in htau$^{0N4R}$ flies shows that the NS2 mount is significantly different between 0 and 5 week ($p=0.0430$). Unpaired, two-tailed t tests were used to test for significance. Error bars are plotted as ± S.E.M.

### 5.3.2 Tau solubility decrease over time in mice

#### 5.3.2.1 Changes in GTOs:

The brain lysates from the cerebral cortex of P301S mice model show the presence of tau immuno-positive material within the stacking gel and a smooth band through the gel, as shown in the western blot that corresponds to the cerebral lysates (input) (**Figure 29 A**). This suggests the presence of insoluble species including species of tau that were unable to enter the SDS-resolving gel. The fractionation of these samples allows the further exploration of the tau species present in these brains.

The cerebral lysates of the cerebral cortex of P301S show a trend of increase in the levels of total tau over time (**Figure 29 A** and **Figure 29 B**). The tau fractions extracted from cerebral cortex of P301S mutant tau-expressing animals, show differences between the different fractions isolated using the solubility assay enriching for GTOs. In these results, a strong tau band of 55–64kDa is present in each fraction. A thin band around 52kDa are also present in the three fractions at both early stages (12 weeks) and late stages (24 weeks) (**Figure 29 A**). In addition, smooth bands around 43kDa and 25kDa are detected in the western blot. This might represent a tau fragmentation (**Figure 29 A**)

For this experiment, the fractions were quantified as a proportion of the sum total of the fractions and these were expressed as the percentage corresponding to tau present in the input (cerebral lysates). In these animals, the majority of tau is present in the aqueous soluble fraction, S1, at early stages (**Figure 29 A-B**). For instance, the amount of S1 found at 12 weeks of age is 70%. Whereas the amount of this fraction present at 24 weeks of ages is 60% (**Figure 29 A-B**). This suggests that the tau is becoming more insoluble over time. In line with this, the amount of detergent-soluble fraction S2 shows about 30% at early stages (12 weeks), and the amount slightly decreases at a later stage (24 weeks) (**Figure 29 A-B-b**). This could suggest the presence of detergent soluble oligomers.

The amount of the S3 insoluble fraction at early stage is about 50%, suggesting the presence of GTOs at this stage. In addition, there is a significant difference in the amount of insoluble tau, such that it decreases with age between 12 and 24 weeks ($p= 0.0039$) (**Figure 29 A-B-c**). This collectively shows progressive aggregation of tau leading to its insolubility as disease evolves and suggests oligomerization of tau.

As in the fly model, in P301S mice model shows that S1 fraction decrease over time. In this model the quantification of S3 fraction shows the presence of insoluble oligomers at early stage (12 weeks) and this decrease at late stage (24 weeks). This indicates that GTOs are found at early stages and

these species decrease at late stages.The data also implies that GTOs are responsible for the phenotype at early stages of disease.

After determining the presence of insoluble granular tau oligomers in mice model, an assay to probe the presence of larger aggregates/fibrils was used for assessing detection of larger species of tau.

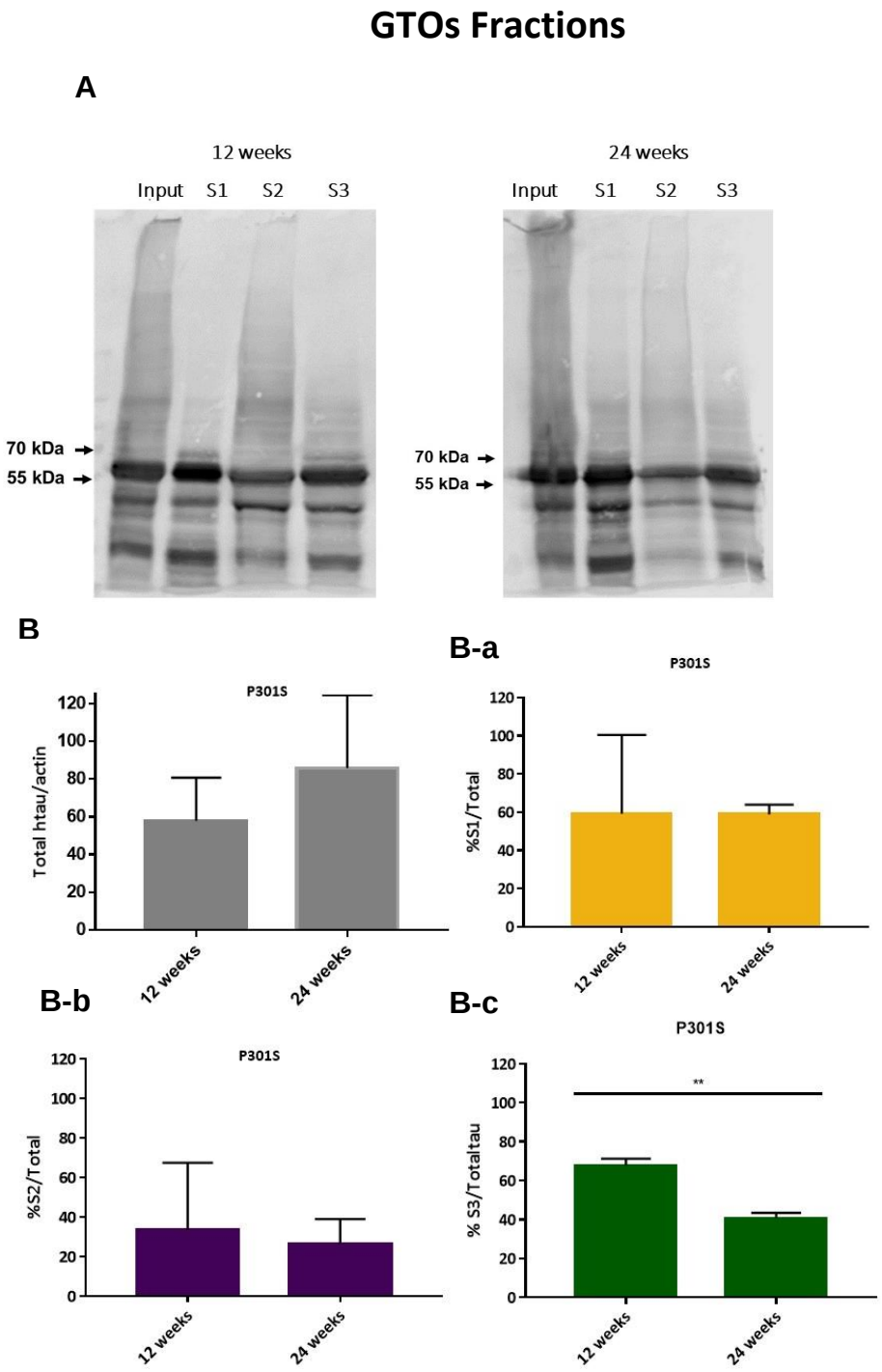


**Figure 29. Tau solubility decrease over time in P301S mutant tau expressing animals**

Comparison of solubility fractions from cerebral cortex from young (12 wk) and old (24wk) P301S mice (n=3, individual experiments). **A**) Shows representative blots of brain lysate (input) and S1, S2 and S3 fractions. **B**) Shows quantification of brain lysate (input) and 3 fractions.**B-c**) Quantification of S3 fraction relative to sum total of all fractions shows that the S3 mount is significantly different between early and late stage (p= 0.0039). Unpaired, two-tailed t tests were used to test for significance. Error bars are plotted as ± S.E.M.

#### 5.3.2.2 Formation of tau fibrils: Changes in NS:

The tau fraction extracted from cerebral cortex of P301S mutant tau-expressing animals show differences between the different fractions NS1 and NS2 isolated using the solubility assay enriching for the larger aggregates/fibrillar species (NS). In this, a broad tau band of 50–64 kDa is present in both fractions (**Figure 30 A**). In addition, in the NS1 fraction, a thin band around 52kDa, 43kDa and 25kDa are detected in the western blot. As mentioned before, this could represent a tau fragmentation.

Like the solubility assay to probe the presence of GTOs, the detection of NFTs also show an age-dependent decrease in tau solubility. Here, the quantification of NS1 fraction shows a decrease at 24 weeks (late stage) compare to the early stage (**Figure 30 B-a**). However, the larger insoluble fraction NS2 increase at this same stage late stage (**Figure 30 B-b**).

In these animals, the amount of tau detected in the NS1 soluble fraction is around 60% at early stages (12 weeks). This result indicate that the majority of tau is aqueous soluble. However, the amount of this fraction decreases to 47% at late stage indicating that tau is becoming insoluble over time (**Figure 30 B-a**). In agreement with this, the amount of tau detected in the detergent- insoluble fraction (NS2) detected at early stage is 40%; whereas the detected amount at late stage is 52% (**Figure 30 B-a-b**).

The results obtained with this solubility assays in the P301S tau expressing transgenic mice model corroborate that the accumulation of insoluble species of tau increases with age and is suggestive of oligomerisation. The increase with time of the NS2 fraction suggest the path of aggregation leading to the elongation and formation of fibrils and tangles.

It is important to mention that the composition of these brain fractions may contain other components. For instance, other proteins (including endogenous tau) and lipids, such as sphingolipids, cholesterol, and glycerophospholipids, as other detergent-resistant components (Schuck et al., 2003) as contaminants of the fractionation process. For this, it is important to consider other methods such as immunoprecipitation or to take into account the possible presence of other components in these fractions.

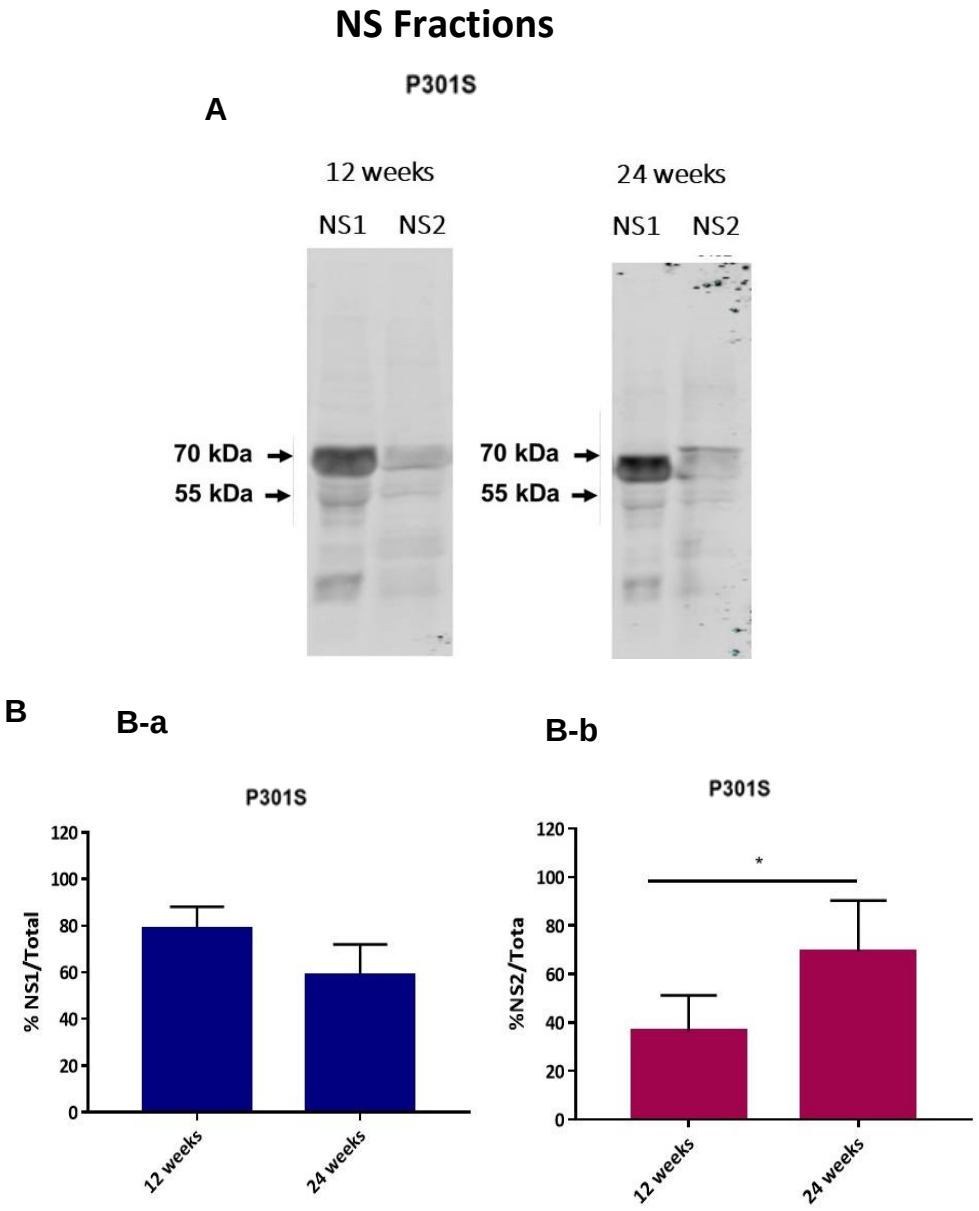


**Figure 30. Tau solubility decrease over time in P301S mutant tau expressing animals.**

**A**) Shows western blots of cerebral cortex from young (12 wk) and old (24wk) mice on NS1and NS2 (n=3, individual experiments) . **B**) Shows quantification of fractions compared to relative total sum of all fractions (NS1 and NS2) and expressed as the percentage corresponding to tau present in the input. Larger insoluble tau aggregates are detected at the two different ages. Quantification shows that the NS1 and NS2 are significantly different between early and late stage (p= 0.0349). Unpaired, two-tailed t tests were used to test for significance. Error bars are plotted as ± S.E.M.

### 5.3.3 Using immunoprecipitation technique to isolate tau protein from mice

Having described the solubility of the tau species generated at early and late stage and their correlation with behavioural phenotype the next step was to isolate the tau protein to characterise their morphology. To do it, it was necessary to isolate tau from transgenic animal models

As mentioned before, different tau species such as oligomers and larger filaments (Maeda et al., 2006; 2007; Cowan and Mudher, 2013) have been implicated in AD and other tauopathies. Similarly, to the fractionation/purification method described before for some of the oligomeric species have been isolated from brain homogenate using immunoprecipitation methods in both rodents (Maeda et al., 200; Lasagna-Reeves et al., 2012) and fly models (Cowan et al., 2015). Previous studies from our lab show that the species enriched for by the GTO fraction are indeed oligomeric tau as evidenced by immune EM.

Therefore, the protocol I will employ to isolate pure tau oligomers is the immunoprecipitation (IP) technique. For my study, it was decided to firstly assess the IP method using brain lysate of tissue from P301S mice and mice lacking microtubule associated protein tau (Mapt−/−) tau knockout (KO) as a negative control.

This protocol was developed with the help of Dr. Katrin Deinhardt and Dr. Mariana Vargas-Caballero.

#### 5.3.3.1 Cross-linking antibody (Tau-5) to beads

For the IP technique to work it is necessary to effectively associate a tau antibody to the agarose beads to capture the protein target. The Thermo Scientific Pierce Crosslink Immunoprecipitation (IP) method was employed to covalently cross link the antibody onto the beads was used. Then analysed by dot blot using a generic anti IgG antibody.

A 25 µL of the agarose beads were incubated with 10 µg of antibody Tau-5 on a rotator at room temperature for 1, 5 hrs as described in **Figure 31 A**. After shaking, the beads were collected by centrifugation for 1 minute at 1000 xg and the ¨flow-through¨ collected to verify antibody coupling by dot blot analysis (**Figure 31 B**). Next, the beads were washed three times (**Figure 31 C**), the first and third FT from the washes were saved for dot blot to verify the presence of antibody in the supernatant after wash.

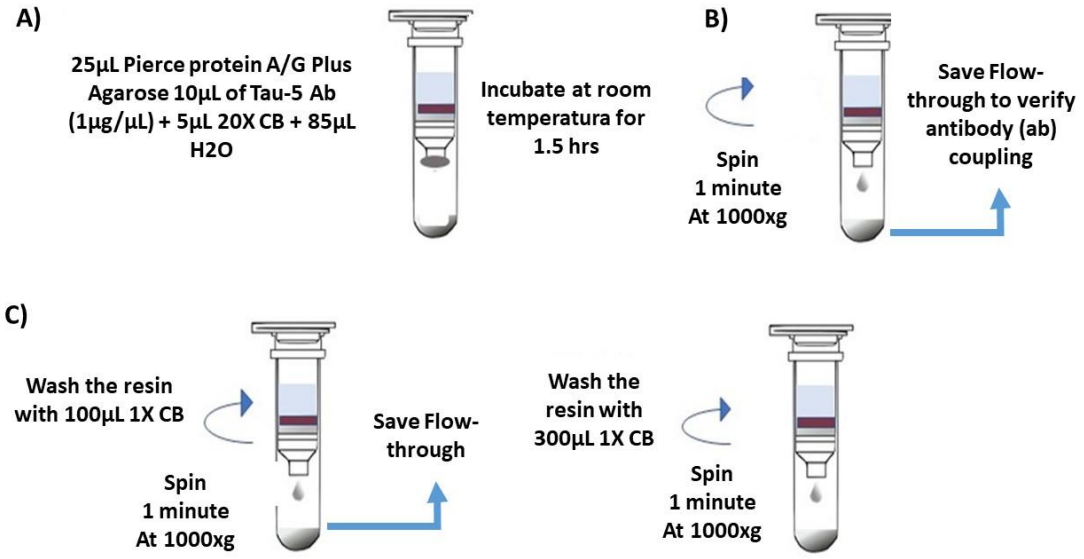


**Figure 31. Schematic representation of binding of antibody Tau-5 to agarose beads**

**A)** Shows the incubation of the agarose beads and the antibody; **B**) shows and the ¨flow-through¨ collected to verify antibody coupling by dot blot analysis; **C)** shows the washes of the beads.

To make sure that antibody bound to beads is not eluted with the antigen during the IP elution step, it is necessary to cross-link the complex. To do this, DDS cross linker was used. For the reaction, 50 µL of a solution with DSS (5X) was incubated with the beads-antibody for 30 minutes at room temperature on a rotator half an hour and centrifuge for 1 minute at 1000 xg as describe in **Figure 32 A**. After incubation, 50 µL of elution buffer was added to the beads and they were centrifuged as shown in **Figure 32 B**. The ¨flow-through¨ was collected to verify antibody crosslinking. After the elution, the flow through was eluted twice to remove the non-crosslinked antibody and quench the crosslinking reaction and washed three times with wash buffer and to eliminate the uncoupled antibody (**Figure 32 C**). The FT from last wash was saved to analyse by dot blot (**Figure 32 D**).

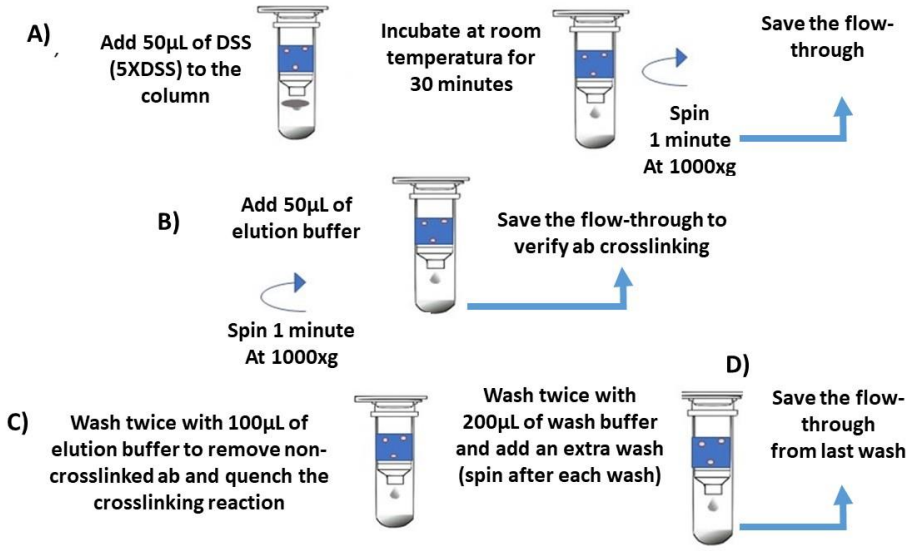


**Figure 32.Schematic representation of crosslinking reaction**

**A**) Shows the incubation of the DDS cross linker with the antibody-beads; **B**) Shows the elution after the incubation. The sample was centrifuged and the ¨flow-through¨ collected to verify antibody crosslinking; **C**) shows the second elution and the different washes of the antibody-beads.

The dot blot analysis is shown in **Figure 33**. Here the dot corresponding to the coupling buffer used to perform the washings (dot #1) and dot # 2 corresponds to the 10 µg of Tau-5 antibody used for the IP reaction are shown. **Figure 33** show, the ¨flow-through¨ collected after the centrifugation to verify antibody coupling by dot blot analysis (**Figure 33** dot #3). The dot blot #3 looks very clean indicating that that the antibody is coupled to the beads. Next, the beads that were washed show that in the first wash (point # 4) and the third (point # 5) they are clean, indicating that the antibody is not present in the supernatant.

**Figure 33** dot#6 show that after centrifugation the incubated beads, there is no immuno-positive material indicating that the antibody is attached to the beads. Next, dot#7 show that after the addition of 50 µL of elution buffer and centrifuge them, very little immuno-positive material is present in the eluted. This indicate that a large amount of antibody was cross-linked onto beads.

Finally, the material that has not been attached to the beads has been eluted and detected in the dot blot. After the elution, this flow through was washed twice to eliminate uncoupled antibody. The last watch is show in dot#8 and uncoupled antibody is present. However, the intensity is very

low compared to the intensity of the antibody observed in dot blot # 2. This suggest that an appropriated amount of antibody is crosslink onto the beads.

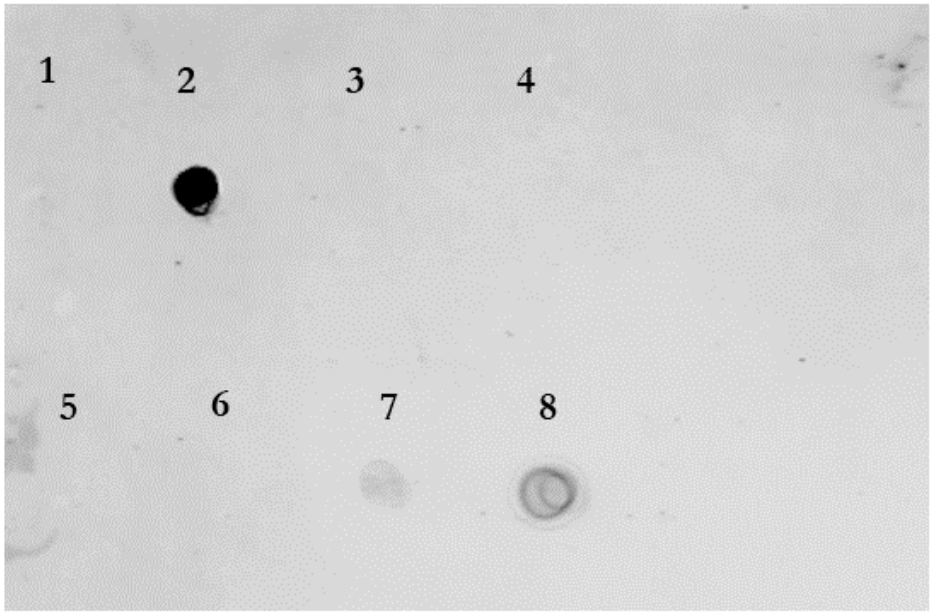


**Figure 33. The antibody (Tau-5) were covalently crosslink onto the beads**

Thermo Scientific Pierce Crosslink Immunoprecipitation (IP) to covalently cross-linked (using 5XDDS cross linker) Tau-5 (10 µg) antibody onto the agarose beads was used. Dot blot was probed with anti IgG antibody. The dot blot shows the dots corresponding to **1** 1X Coupling Buffer (CB) and **2** 10 µg of Tau-5 used for IP reaction. **Dot 3** shows Flow through (FT) after incubating antibody to the beads, here the negative reaction suggest that the antibody (ab) is coupled to the beads. **4** shows first wash with 1X CB and **5** shows the third wash with 1X CB, both indicate that the antibody is not present in the supernatant reaffirming that ab is coupled. Next, **6** FT after incubating antibody+beads in 5XDSS, here negative reaction indicates that antibody is attached to the beads. **7** FT after wash in 50 µL of Elution Buffer, here very little immuno-positive material is present in the eluted indicating that the majority of ab is attached to beads. **8** show the Flow through after third wash in wash buffer to clean the uncoupled antibody. Here, the intensity is very low compared to the intensity of the antibody observed in dot blot **2**. This suggest that a good amount of antibody is crosslink onto the beads.

### 5.3.3.2 Tau immunoprecipitated from P301S tau mice

Having cross-linked the antibody onto the beads, the next step was to immunoprecipitate the tau protein from trangenoc mouse brains to characterise their morphology by AFM.

For this study, the transgenic P301S mice brain and tau knockout (KO) mice brain as, a negative control, were homogenised. The lysate of the brain tissue was isolated using the procedure for the Pierce Crosslink IP Kit mentioned before.

For the immunoprecipitation reactions, brain lysate (333 µL) was previously precleared with 80 µL of protein Control Agarose Resin. The precleared sample was mixed with the previously coupled beads with the antibody (25 µL of beads and 10µg of Tau 5) and the mixture was shaken end-over-end overnight at 4°C as described in **Figure 34 A**. Next, the tau bound to the antibody was eluted from the antibody beads complex by adding 60µL of elution buffer and incubate for 5 min at room temperature (**Figure 34 B** and **Figure 34 C**). The flow-through was collected (**Figure 34 D**) and then analysed by SDS-PAGE and Western blot.

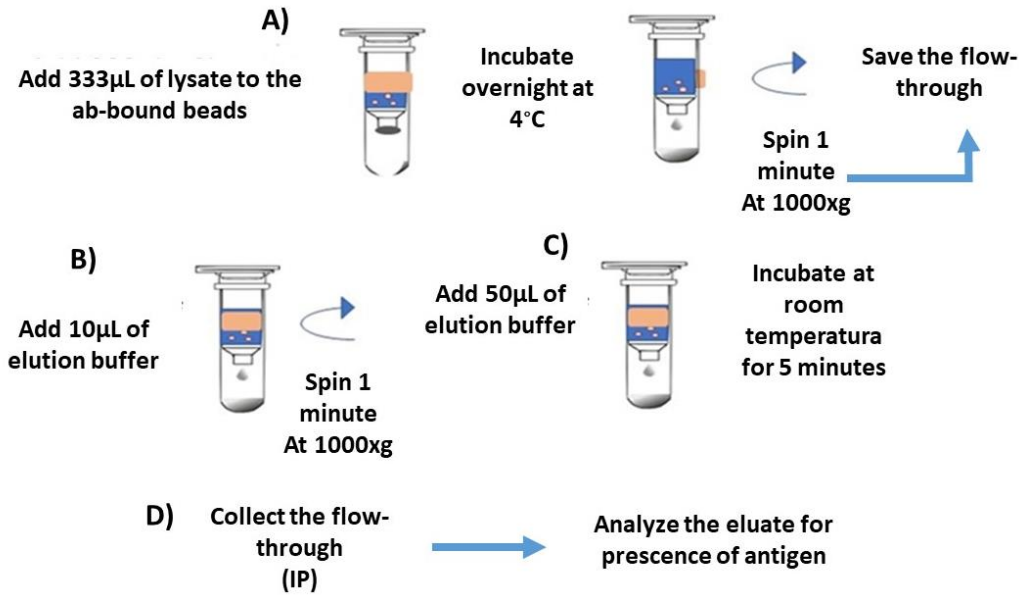


**Figure 34. Schematic representation of crosslinking reaction**

**A**) Shows the incubation of the DDS cross linker with the antibody-beads; **B**) Shows the elution after the incubation. The sample was centrifuged and the ¨Flow-through¨ collected to verify antibody crosslinking; **C**) shows the second elution and the different washes of the antibody-beads.

The western blot detection of immunoprecipitated tau protein show that there is a difference between the IP reactions undertaken in P301S and tau KO brain (**Figure 35**). In the western blot, the first lane indicates the tissue source (input), the second lane indicates the IP reaction (elute IP), and the third lane indicates the supernatant stored as "Flow through", this supernatant contains the unbound protein to the complex.

In particular, lysate that has been immunoprecipitated from tau knockout mice show no tau immuno-positive reaction at any of the lane tested for the presence of tau. This is shown as a negative control. This demonstrates that the IP work to specifically pull-down human tau.

The western blot from P301S brain lysates show the detection of tau immuno-positive material indicating the presence of tau in the three lanes corresponding to the input, elute IP reaction, and Flow through (unbound protein). In these results, a broad tau band of 55–64 kDa is present in each lane. In addition, smooth bands around 95kDa, 130kDa and 43kDa are detected in the lanes and a thin band around 25kDa.

In particular, the immuno-positive tau material within the stacking gel has been detected in both, the lane corresponding to the input and the lane corresponding to the flow-through. This result indicates the presence of insoluble species of tau that were unable to enter the SDS-resolving gel and possibly too large to be captured by the beads.

These results indicate that although protein tau was immunoprecipitated from the P301S mice brain lysates, the IP reaction from P301S brain lysates is not very efficient in capturing large amounts of the tau present in the samples. This is suggested by the presence of large amount of tau protein detected in the unbound corresponding lane "Flow through" which indicates that there was more tau than antibody to capture it.

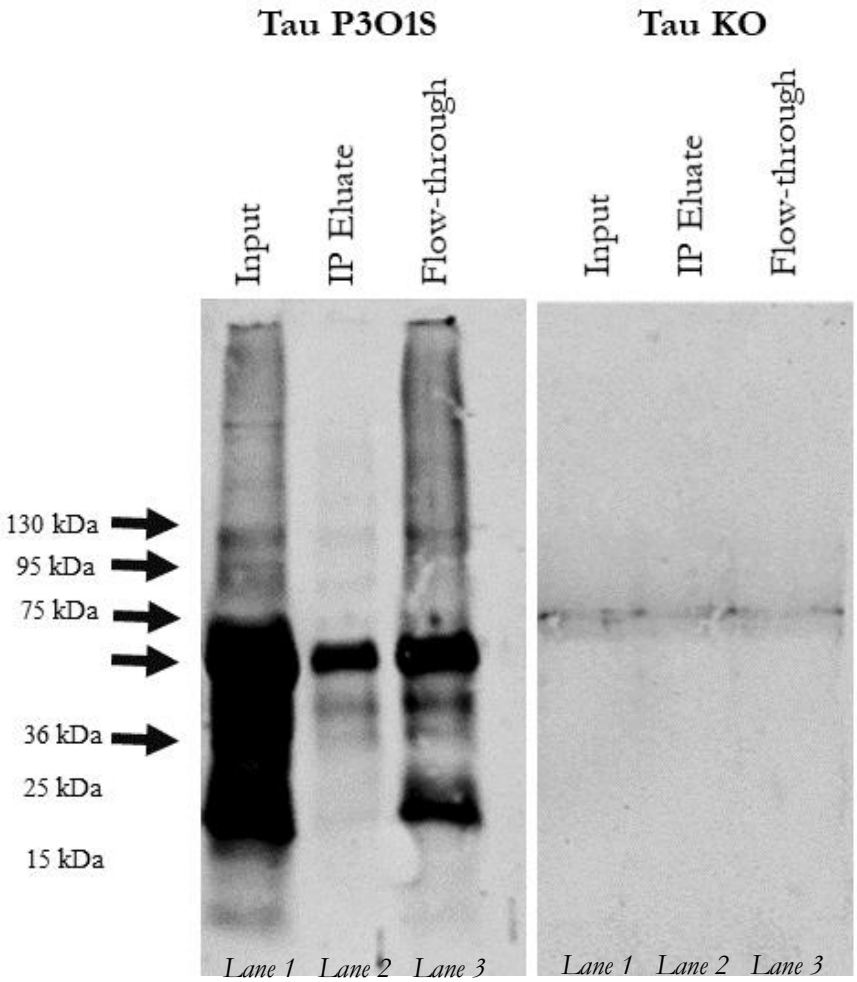


**Figure 35. Validation of identified tau protein by immunoprecipitation**

Western blot show the comparison of Tau immunoprecipitated from brain lysate obtained from P301S mouse model of tauopathy and Tau KO, using 10µg of Tau-5 antibody. Dako polyclonal anti-hTau was used for the WB. The input is shown in **lane 1** as the extraction of mouse brain tissue in IP Buffer; the elute IP reaction is shown in **lane 2**, and "Flow through" in **lane 3**. The tau KO lysate that has been immunoprecipitated is shown as a negative control. The western blot from P301S brain lysates show the detection of tau immuno-positive material indicating the presence of tau in the three lanes corresponding to the input, elute IP reaction, and Flow through (unbound protein).The WB from lysate immunoprecipitated from tau knockout mice show no tau immuno-positive reaction at any of the lane tested for the presence of tau. This is shown as a negative control.

To improve capturing as much tau protein three more IP reactions were carried out on each flow through elution buffer.

For this, 60 µL of the flow through collected (contained the unbound protein) from the first IP reaction was incubated for 2hrs with the coupled antibody-beads. The tau-bounded protein was eluted and collected individually for the analysis. The flow through from this reaction was incubated with the beads for 2hrs and eluted again. This was repeated two more times. Each time, the IP reaction (IP elute) and the Flow-through (FT) were collected independently to test the presence of tau.

The western blot detection of immunoprecipitated tau from P301S show differences between the IP reactions (**Figure 36**). In the western blot, similarly to the previous results, the first lane indicates the tissue source (input), the second lane indicates the IP reaction (elute IP) and the third lane indicates the supernatant stored as "Flow through" (which contains the unbound protein).

Lysate that has been immunoprecipitated in the first reaction (**Figure 36 A**) show the presence of large amount of tau protein detected in the unbound protein corresponding to lane "Flow through"(FT) (**lane 2**). After carrying out the second IP reaction (**Figure 36 B IP2 lane 5**) the presence of a smooth band that migrates around 50-64kDa is detected. The lane corresponding to the flow through of the second reaction (**lane 6**), it shows the presence of smoother bands compared with those of the first reaction (**Figure 36 A lane 3**) suggesting that less amount of tau is present compared to the first IP reaction.

In line with this, the presence of a similar smooth band migrating around 50-64kDa is observed in the lane corresponding to the third IP reaction (**lane 7**). Again, the presence of immuno-positive material is detected in the FT lane of IP3 (**lane 8**), which is softer than the previous reaction (lane 6). Suggesting that less tau is present in this FT.

Finally, in the fourth reaction, an even smoother band around 50-64kDa is still detected in the IP (**lane 9**). Whereas, in the lane corresponding to the FT of this last reaction (**lane 10**), no signal was detected. This indicates that there is not enough tau in this FT to be detected. Suggesting that the tau protein from this lysate has been collected in the previous reactions.

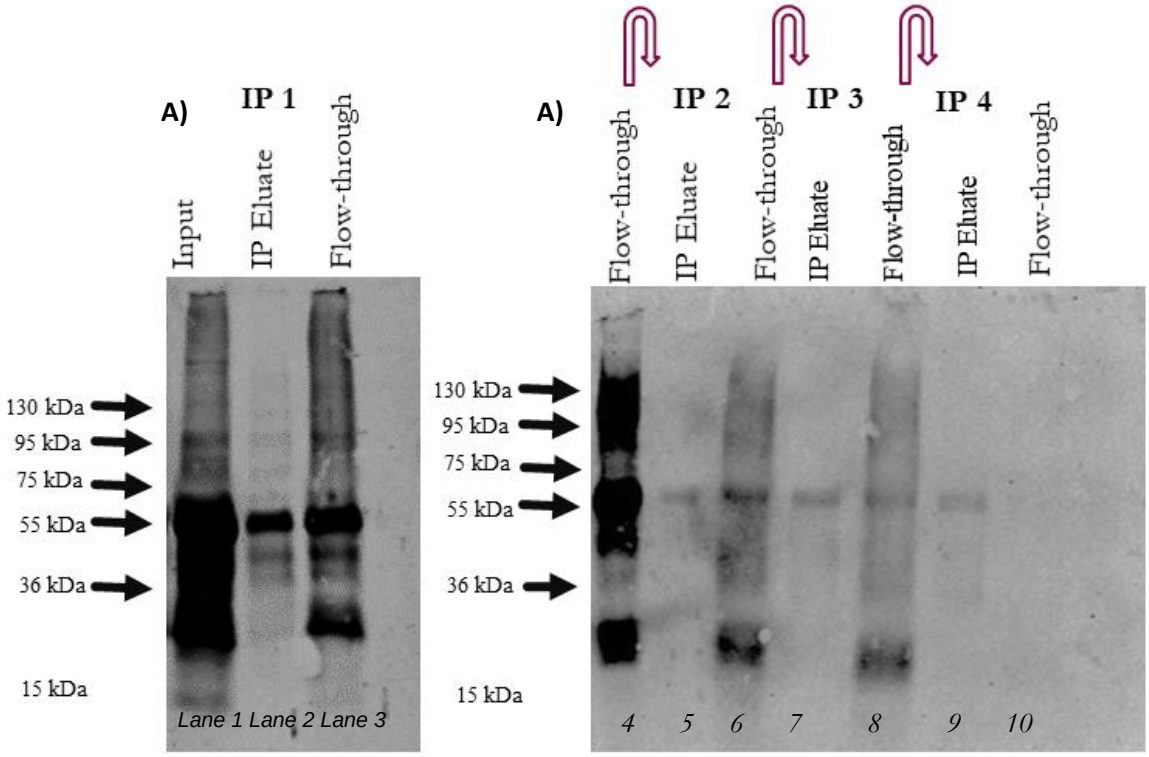


**Figure 36. Multiple immunoprecipitation reactions**

Western blot of tau immunoprecipitated from P301S brain lysate using 10µg of Tau-5 antibody. Dako polyclonal anti-htau was used for the WB a) Shows IP first reaction. The **lane 1** indicates the tissue source; **lane 2** indicates IP reaction 1; **lane 3** indicate the supernatant saved as "flow-through" and contain the unbound protein. b) Shows **lane 4** which indicates the flow through from the first reaction; **lane 5** indicates the second IP reaction; **lane 6** indicates the flow through from the second IP reaction; **lane 7** indicates the third IP reaction. **Lane 8** the flow through from the third IP; **lane 9** shows the fourth IP reaction and finally lane 10 indicates the flow through of the last reaction. In western Blot the presence of immuno-positive material is detected in the consecutive reactions (**IP1**, **IP2**, **IP3** and **IP4**).The lane corresponding to FT of the reactions show the presence of softer bands in comparison with the previous reaction. Suggesting that there is less tau present in this FT. This result indicates that it is possible to obtain the highest amount of tau from the lysates by carrying out multiple IP reactions instead of one.

Now, after having carried out the IP method described above, the following was to characterize the morphology of P301S brain lysates and tau knockout (KO) mice.

To study the morphology, both tau fibrils (Maeda et al., 2006; 2007; Lasagna-Reeves et al., 2012) and oligomers (Maeda et al., 2006; 2007; Lasagna-Reeves et al., 2012 ; Cowan et al., 2015) have been studied and characterized by atomic force microscopy (AFM). Therefore, for my study I will use this technique to characterize the morphology of the samples obtained after the multiple IP reactions described above. The samples were collected in an individual tube to later be observed under a microscope. Elution buffer and tau-5 antibody samples used for IP were also analysed.
The precipitates were placed in freshly excised mica discs (Agar Scientific). These were incubated for 5 minutes. After that, samples were rinsed 4 times with ultrapure water and dried with compressed air. Samples were imaged in air with a digital multimode Nanoscope IV AFM operating in tapping mode with an Aluminum coated non-contact/Tapping mode probe with a resonance frequency of 320 kHz and force constant of 42N/m were used for images (Nanoworld, POINTPROBE NHCR). The mages are representative of the sample and were taken at random points on the sample with a scan rate of 1Hz-2Hz. The sizes were determined by cross-sectional height analysis. AFM analysis was carried out using WSXM software.

The topographic surface of AFM of elution buffer, antibody tau 5, and samples from lysate that has been immunoprecipitated from tau knockout mice and P301S mice show that there are differences between all the samples analysed by AFM.

The topography of the image corresponding to tau-5 antibody alone also shows the formation of a monolayer covering the entire surface of the mica. The **Figure 37** corresponds to the two-dimensional view. Here, the topography shows the formation of small regular structures with similar morphology. These appear to be oriented uniformly covering the entire surface of the mica. In particular, the topography shown heights from ~0.62nm to ~3nm and sizes around ~4-10 nm (**Figure 37**). Scale bar 400 nm. This suggest that the antibody is characterized by the presences of small and rough structures that are distributed regularly on the surface of the mica. This result also suggest that the morphology of the antibody do not resemble the expected oligomeric structures and can be shown.


**Figure 37. Characterization by AFM of Elution Buffer and Tau-5 antibody**

Samples were place in mica and imaged in air with a digital multimode Nanoscope IV AFM operating in tapping mode with an Aluminum coated non-contact/Tapping mode probe with a resonance frequency of 320 kHz and force constant of 42N/m were used for images (Nanoworld, POINTPROBE NHCR). The sizes were determined by cross-sectional analysis. Scale bar 400nm. a) Shows 2D morphology of Tau-5.

The AFM images corresponding to the immunoprecipitated brain lysate of tau knockout (KO) mice revealed a smooth surface composed of irregular and amorphous structures. **Figure 38 A**, correspond to the two-dimensional topographic image and the **Figure 38 B** correspond to the three-dimensional topographic image.

In particular, the topographic surface of the sample (KO) reveals the presence of smooth and amorphous structures with heights from ~0.42nm ~2.58 nm (**Figure 38 B**). These structures vary in sizes between 10 and 70 nm. Scale bar 400 nm. By comparison with the topographic surfaces in images of antibody (**Figure 37**), the topographic surface of the tau knockout is less uniform. However, the background is similar in height between these samples. This suggests that the composition of the KO IP samples is characterized by the presence of amorphous structures that resemble the morphologies of the controls (elution buffer and tau-5 antibody).

It is important to clarify that, it was decided to analyze only the AFM images obtained from the elution buffer as well as the tau-5 antibody, as a control. This was done with the intention of mainly comparing the topography of these two important components used on the IP protocol and the topography of the material isolated (IP eluate). On the other hand, in this study it was only considered the use of mice lacking tau (KO) as a negative control. However, it would have been

interesting to analyze a non-transgenic mice model, such as wild-type mice (C57BI / 6), for comparison.

Since it has been previously shown by WB analysis that immunoprecipitated KO lysates do not show immuno-positive tau reaction, the presence of tau is not expected to be found in these topographic images. However, it is necessary to characterize the topography of these IP samples to ensure that the structures present in these samples do not resemble to oligomers of tau or other amyloid-like proteins analysed by AFM. The results obtained here suggest that oligomer-like structures have not been found in the analysed sample.

By comparison, the AFM images corresponding to the immunoprecipitated brain lysate of P301S mice (**Figure 38 B**) shows differences between the topographic images of the previously analysed samples. In particular, the P301S sample shows the presence of globular and amorphous structures that are irregularly distributed over the surface of the mica. The analysis reveals the presence of structures with heights from ~0.53nm ~6 nm. Scale bar 400 nm. In these, although it is possible to observed individual spheroidal structures, some structures are shown as aggregates, possibly due to high concentration.

After determining clear differences between the topographic surfaces of the control samples and the P301S, the sample corresponding to P301S was diluted and analysed again (**Figure 39**). Here, the surface topography of the image corresponding to the P301S mice diluted (**Figure 39 A**) show a very homogeneous layer on the background of the mica. This is comparble with the surface of the control samples including the antibody used and the samples isolated from the tau knockout mice (**Figure 38 A-B**). However, different structures are distributed irregularly on the surface of the mica. These structures have a different topography and morphology to the background. In addition, is different from the rest of the samples analysed and established as controls.

The cross section of individual structures shows sizes that vary between ~15 and ~30 nm and the widths are around ~20 and ~60 nm with a height from ~2.07 to ~7 nm. Scale bar 400 nm. These results suggest the characteristic oligomeric sizes and structure by analysis with AFM.

The results obtained here indicate morphological differences in the topographies of the samples analyzed by AFM. In particular, P301S mouse brain lysate samples contain tau species that resemble tau oligomers reported by other authors (Maeda et al., 2007; Lasagna-Reeves et al., 2012; Cowan et al., 2015). However, after immunoprecipitation and subsequent observation of the material by AFM, the presence of tau filaments could not be detected. One possible explanation is that the Tau-5 antibody-bound beads used for IP are not effective at precipitating high molecular weight aggregates. Therefore, fractionation could be a more suitable method to isolate these species.

On the other hand, it is important to consider that another possible disadvantage of the immonoprecipitation method is the selectivity of the method. For example, as mentioned, the observed results indicate that certain structures can be isolated with the appearance of oligomers but not of filaments. This could also suggest the possibility that not the entire population of oligomers, which may be present in the brains of model animals, are effectively isolated. Furthermore, as the use of antibodies is required to isolate tau, these antibodies could also act selectively.

In general, in this particular study it has been decided to use the solubility fractionation method to isolate the tau species.

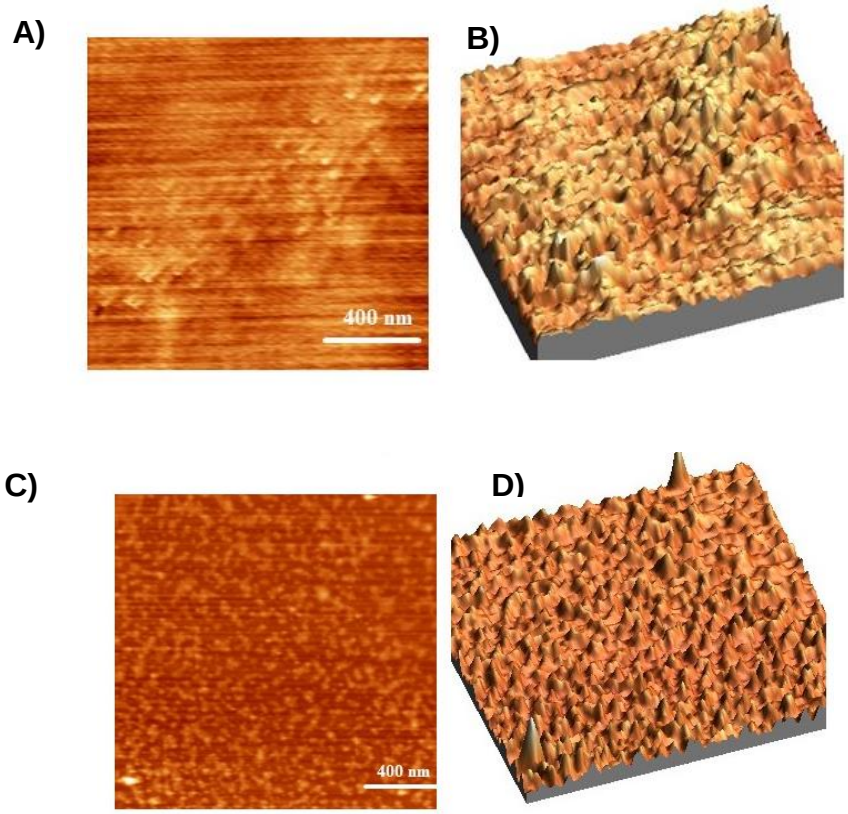


**Figure 38.Characterization by AFM was carried out in the samples obtained after the multiple IP reactions from brain lysates of tau knockout (KO) and P301S mice**

Samples were place in mica and imaged in air with digital multimode Nanoscope IV AFM operating in tapping mode with an Aluminum coated non-contact/Tapping mode probe with a resonance frequency of 320 kHz and force constant of 42N/m were used for images (Nanoworld, POINTPROBE NHCR). The sizes were determined by cross-sectional analysis. Scale bar 400nm. The sizes were determined by cross-sectional height analysis. **A)** Shows 2D morphology of tau knockout (KO); **B)** shows the 3D of the same sample. By comparison **C)** shows the morphology in 2D of P301S mice not diluted; **D)** shows the 3D of the same sample.

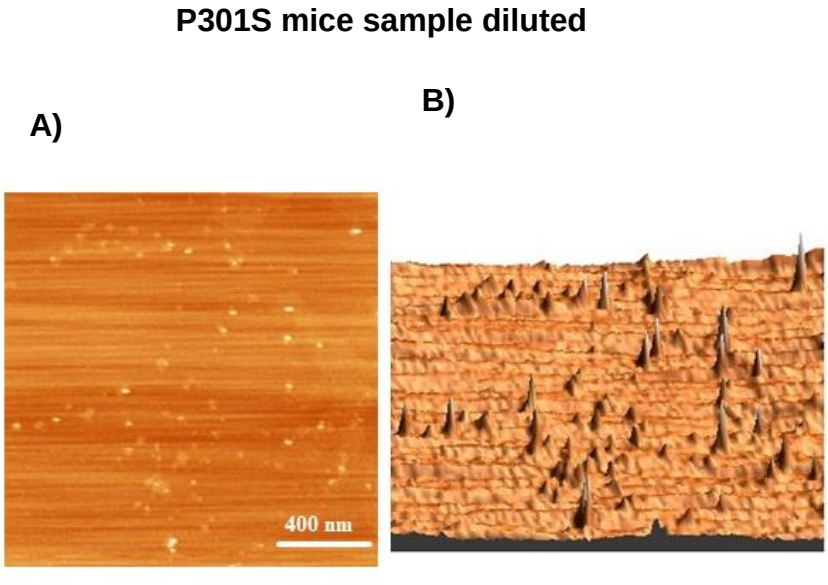


**Figure 39. Characterization by AFM was carried out in the samples obtained after the multiple IP reactions from brain lysates of P301S mice**

Samples were place in mica and imaged in air with digital multimode Nanoscope IV AFM operating in tapping mode with an Aluminum coated non-contact/Tapping mode probe with a resonance frequency of 320 kHz and force constant of 42N/m were used for images (Nanoworld, POINTPROBE NHCR).The sizes were determined by cross-sectional analysis. Scale bar 400nm. The sizes were determined by cross-sectional height analysis. **A)** Shows 2D morphology of P301S mice diluted; **B)** shows the 3D of the same sample.

## 5.4 Discussions

### 5.4.1 Summary

The overarching aim of this chapter was to identify which tau species might be responsible for the early and late stages of phenotype reported in **Chapter 4**. In the current study, I hypothesized that the onset of progression is due to granular tau oligomers (GTOs) while the progression of phenotype is due to larger tau aggregates (pre-NFT). To address this, the properties of these tau species at early and advanced stages of the disease in two *in vivo* models of tauopathy were interrogated using an established solubility assay. The results indicate that in both models, the expression, accumulation, and further aggregation of tau is critical for the emergence and progression of the phenotype.

### 5.4.2 Tau aggregation underpins phenotype in our two models even though some studies suggest tau does not aggregate in *Drosophila*

The microtubule-associated protein tau is natively unfolded. Abnormal aggregation of tau and subsequent neuronal dysfunction are key pathological features in many neurodegenerative diseases as such Alzheimer's disease (AD) frontotemporal dementia (FTD) and other related disorders collectively referred to as tauopathies.

Previous studies have shown that in *Drosophila* models, human tau overexpression is sufficient to induce behavioral deficits as a result of neuronal dysfunction. For example, as described in **Table 7**, when evaluating the climbing ability of flies after the expression of tau, it has been reported that the expression of tau produces deficits in locomotion both in adult flies (Folwell et al., 2010; Ali et al., 2012; Roy and Jackson, 2014; Cowan et al., 2015; Sealey et al., 2017) and in larvae (Mudher et al., 2004; Quraishe et al., 2013). In addition, a reduction in life expectancy after tau expression has also been reported (Wittmann et al., 2001; Khurana et al., 2010; Folwell et al., 2010; Colodner and Feany, 2010; Sealey et al., 2017; Pasarella and Goedert, 2018). These studies show that the overexpression of tau is sufficient to induce phenotypes related to the disease. However, not all of these studies follow the phenotype and its progression over time.

For instance, only some of the studies report subsequent degeneration over time(Wittmann et al., 2001; Jackson et al., 2002; Colodner and Feany, 2010; Ali et al., 2012; Wu et al., 2013; Sealey et al. , 2017; Passarella and Goedert, 2018). This was evident in our study where the pan-neural expression of htau$^{0N3R}$ and htau$^{0N4R}$ had an effect on adult life and locomotor behavior progresses with age.

While in most studies conducted in *Drosophila* model, pathological changes associated with disease, such as hyperphosphorylation are evident, tau aggregation and tangle formation in contrast are not often observed (Wittmann et al., 2001; Mudher et al., 2004; Cowan et al., 2010; Sealey et al., 2017).

There are only a few studies in which tau aggregation and oligomer formation have been reported (Ali et al., 2012; Cowan et al., 2015; Wu et al., 2013). In addition, a couple of studies have reported filaments that resemble early tangle formation (pre-NFT) (Jackson et al., 2002; Colodner and Feany 2010; Wu et al., 2013). The reasons for these apparent discrepancies in *Drosophila* models are not well understood, but one can speculate that they are related either to conditions of tau expression, such as tissue susceptibility to form abundant aggregation; as to limitations of the methods for detection and characterization.

Another reason for this could be that the methods employed to visualise or detect tau aggregates are not sensitive enough. I employed a method which was based on fractionation which enriches for tau aggregates, prior to detection. The commonly used protocols to fractionate proteins based on detergent extraction (sarcosyl or SDS) have proven to be suitable for sediment tangle components, such as insoluble filaments (Greenberg and Davies, 1990; Maeda et al., 2006).

Conversely, it has been suggested that these methods have limitations when it comes to sediment small oligomers (Maeda et al., 2006; 2007; Cowan and Mudher, 2013). Considering these different approaches, here it was decided to use a method described for the first time by the Takashima group (Maeda et al 2006), and previously reported in our laboratory (Cowan et al., 2015; Sealey et al., 2017; Mancuso et al., 2019), to extract the GTO and NS tau species from our *in vivo* models.

My data provides evidence to suggest that pan-neural overexpression of $hTau^{0N3R}$ and $hTau^{0N4R}$ leads to gradual accumulation and formation of insoluble tau species and this is causally related to the emerging age-related phenotypes. Further polymerization of the oligomeric species found in this study produced larger insoluble aggregates/fibrillary species (NS) with increasing age. This similar process has been reported as a key feature of polymerisation during fibrillation pathway (Maeda et al., 2006; 2007).

These findings are validated by comparable results from our P301S mice model, where such tau aggregates have routinely been detected by other, less sensitive methods (Mancuso et al., 2019). This collectively suggests that the mechanism for aggregation and filament formation follow a

similar rout to pathology in these two models. Demonstrating that aggregation is essential for the development of the disease and suggesting that different species are responsible for the appearance and progression of the phenotype.

### 5.4.3 Tau oligomers are associated with early phenotypes and fibrils cause late stage phenotypes

The presence of neurofibrillary tangles (NFTs) forms has been considered for many years as the primary cause of disease. However, more recent evidence suggests that intermediate species such as oligomers are the tau species responsible for toxicity. These, oligomers are likely precursors to tau filaments and important players in events that precede neurodegeneration (Mudher et al., 2004; Cowan et al., 2010; 2015; Passarella and Goedert, 2018).

The presence of oligomers has been previously described in the early and moderate stages of the disease. In human brain tissue from patients with AD, FTDP-17 and PSP, prominent levels of oligomers have been correlated with the onset of clinical symptoms (Maeda et al., 2006, 2007; Patterson et al., 2011; Lasagna-Reeves et al., 2012; Ercan-Herbst et al., 2019).

In rodent models, these oligomers and non-filamentous forms have been closely related to both early neuronal dysfunction and memory impairment (Santacruz et al., 2005; Spires et al., 2006; Berger et al., 2007; Yoshiyama et al., 2007; Sahara et al., 2013; Xu et al., 2014). On the other hand, tau filaments and tangles have been described at advanced stages of the disease and correlated with neuronal cell loss (Allen et al., 2002; SantaCruz et al., 2005; Spires et al., 2006; Berger et al., 2007; Xu et al., 2014; Sahara et al., 2013; Macdonald et al., 2019). However, details about the nature of these tau species are not entirely clear, nor is their direct relationship with the behavioural phenotype in models of tauopathy.

My data provides evidence that supports what others have suggested before. I also confirm that in our two models, the detectable appearance of the insoluble granular tau oligomers (GTOs) correlates with the onset of phenotype preceding the detection of larger aggregates and degenerative phenotype, which is evident at late stages of disease. Thus, details on solubility suggest a relationship with the phenotype in these tauopathy models. Furthermore, our data also suggest differences related to the isoforms and the characteristics of the aggregates. This suggests that the different isoforms have different roles in disease. This study suggests that that 4R-tau may be more pathogenic compared to 3R.

### 5.4.4 Different isoforms of tau can induce differences in phenotypes

A few studies have shown differential pathological roles between the 3R and 4R isoforms of tau. For example, when comparing and contrasting directly these differences in a human tau mouse model, it was observed that the 4R isoform induces more severe pathological changes (Schoch et al., 2016). For instance, when analysing brain tissue from mice, the increase in expression of 4R-tau, a significant formation of high molecular weight tau species (HMW) and strongly phosphorylated was reported. In addition, a decrease in the solubility of the tau species was also described due major expression of 4R-tau. These results demonstrate that the increase in 4R produced greater phosphorylation, insolubility and aggregation of tau. In addition, it produces more severe seizures and abnormalities in nesting behavior (Schoch et al., 2016).

Likewise, in cellular models, the 4R isoform has a greater effect on both mitochondrial transport. For instance, Stoothoff et al., 2009, reported that both tau 3R and tau 4R tau have effects of tau on mitochondrial transport when studying them in H4 neuroglioma cells as in primary neurons. However, these authors found that the 4R isoform produces a greater effect compared to the 3R isoform (Stoothoff et al., 2009). Similarly, some differences in microtubule dynamics have been reported. For example, by exogenously introducing tau protein, either 4R isoform or 3R isoform, into MCF7 cells, it was found that there is a differential effect on the dynamic modulation of microtubules. In particular, the 4R isoform reduces the rate and extent of growth and shortening events. While the 3R isoform, in general stabilizes the dynamics with less efficiency compared to the 4R isoform (Bunker et al., 2004). In line with this, *in vitro* studies has been shown that 4R-tau suppress the rate and extent of microtubule shortening (Panda et al., 2003). These studies demonstrates that different tau isoform exert different pathological role phenotype. Collectively, these studies suggest that different tau isoforms play a different role in tau pathology.

In a few other studies conducted on *Drosophila*, it has been found that expression of htau$^{0N3R}$ and htau$^{0N4R}$ in *Drosophila* also exert different phenotypes (Kosmidis et al., 2010; Sealey et al., 2017). A description of some of these models are listed in **Table 7**. When the 3R isoform has been expressed, a clear dysfunction is commonly observed in the absence of overt neuronal death (Mudher et al., 2004; Cowan et al., 2010; Kosmidis et al., 2010; Quraishe et al. , 2013; Papanikolopoulou and Skoulakis, 2015; Sealey et al., 2017). In contrast, in models in which clear neuronal death and degeneration have been observed, the 4R isoform has been expressed (Wittmann et al., 2001; Jackson et al., 2002; Colodner and Feany 2010; Kosmidis et al., 2010; Ali et al., 2012; Wu et al., 2013; Papanikolopoulou and Skoulakis, 2015; Sealey et al., 2017; Pasarella et al., 2018).

Our results from **Chapter 4** show that the 3R flies are more severely impacted in climbing ability than 4R flies, and begin to die at an early age compared to the 4R flies, though once the 4R flies

begin to die, they decline more quickly than the 3R flies. This has led us to speculate that 3R isoform induce more severe dysfunction whilst the 4R isoform promote greater degeneration.

Additionally, studies showing that the propensity of the 4R isoform to aggregate plays an important role in degeneration further support this notion that different isoforms of tau exert a different role in tau pathology. This association has been demonstrated in both *Drosophila* and mouse models of tauopathy (Passarella and Goedert, 2018; Macdonald et al., 2019).

In this regard, our study show a similar correlation. When studying the solubility properties, flies expressing the 4R isoform showed slightly higher levels of insoluble species compared to flies expressing the 3R isoform. This observation leads us to speculate that the property of the 4R isoform to aggregate and elongate is more efficient compared to the 3R isoform. Also, the slower propensity of 3R to polymerize (as evident from the reduced insolubility) suggest that it remains for a longer period of time in a hyper-phosphorylated soluble state, which is amenable to loss of function-led to neuronal dysfunction (Mudher et al 2004; Chee et al 2005).

These differences may be due to structural differences between the isoforms. For instance, 4R isoforms have been reported to bind to microtubules more strongly than 3R isoforms; This due to the insertion of 31-amino acid sequence in the second microtubule binding domain, which is absent in 3R isoforms (Butner and Kirschner, 1991; Goode et al., 2000). In addition, some of these amino acid sequences important for microtubule binding play important roles in aggregation due its ability to form β-sheet structure (Von Bergen et al., 2000; von Bergen et al., 2001; Li and Lee, 2006; Bulic et al., 2010).

These sequences are the hexapeptide VQIVYK at the beginning of the third repeat domain, and VQIINK at the N-terminus of the second repeat domain. NMR spectroscopy has shown that these hexapeptides adopt a rigid β-sheet structure forming the core of filaments (Daebel et al., 2012). Some published studies have shown that the modulation or total elimination of hexapeptides with the ability to form β-sheet structure, counteracts the pathology caused by tau. For example, this been shown in a *Drosophila* model that expresses human 0N4R that the elimination of the regions necessary for the aggregation of tau into β-sheet (Δ306-311) completely rescues the neurodegenerative phenotype (Passarella and Goedert, 2018).

In our study, the presence of these two hexapeptides necessary for aggregation in the 4R isoform could be the reason that gives it greater ability to aggregate compared to the 3R isoform. This could also explain the differences in the observed phenotype in **Chapter 4**. Further analysis to demonstrate this would remain to be seen.

**Table 7. Examples different tau isoforms and mutations and their phenotypes in *Drosophila***

| Tau isoform | Phenotype | Reference |
|---|---|---|
| 0N3R | L3 locomotion defects<br>L3 axonal transport dysfunction<br>Locomotor defects in adults | Mudher et al., 2004 |
| 0N3R | L3 defects in NMJ morphology<br>L3 abnormal exo/endocytosis in NMJ<br>L3 abnormal transmission at NMJ<br>Defects in mitochondria | Chee et al., 2005 |
| 0N3R | Disruption of MT.<br>Reduced binding ability of dtau to MTs (L3 and young adults) | Cowan et al., 2010 |
| | | |
| 0N3R | No effect on MBs | Kosmidis et al., 2010 |
| 0N3R | Defects in larval locomotor activity<br>Microtubule destabilisation<br>Axonal transport defects | Quraishe et al., 2013 |
| 0N3R | Young adults and L3 locomotor impairment and L3 disrupted axonal transport | Cowan et al., 2015 |
| 0N3R | Axonal transport defects locomotor alterations<br>Shorter life.<br>Reduced learning and memory | Sealey et al., 2017 |
| 0N4R<br>R406W-(0N4R) mutant | Reduce lifespan<br>Reduce lifespan<br>Vacuolization and degeneration of cells.<br>The phenotypes are greater in mutant tau. | Wittmann et al., 2001 |
| 0N4R | Deficits olfactory learning and memory | Mershin et al., 2004 |
| 0N4R | Reduced lifespan | Colodner and Feany 2010 |
| 0N4R<br>2N4R<br>R406W-(0N4R) mutant | Increased apoptosis<br>Expression of 0N4R R406W induces neuronal death | Khurana et al., 2010 |
| 1N4R | L3 Axonal transport dysfunction<br>Morphology defects in NMJ<br>Adult reduce lifespan<br>Adults locomotor dysfunction<br>Vesicular aggregation | Folwell et al., 2010 |
| 0N4R<br>2N4R | Loss of mushroom body (MB). 2N4R induces more severe deficits compared to 0N4R | Kosmidis et al., 2010 |
| V337M-(2N4R) mutant<br>R406W-(2N4R) mutant<br>$Tau^{E14}$ - (0N4R) | Expression of mutant V337M induces milder defects in MB compared with WT 0N4R.<br>Expression of mutant R406W were significantly more severe in MB compared with WT.<br>$Tau^{E14}$ induces abnormal MB more severe than 0N4R | Kosmidis et al., 2010 |

| | | |
|---|---|---|
| mutant | | |
| 2N4R and R406W-(2N4R) mutant | Decline in memory performance<br>Decrease in locomotor activity<br>Vacuolisation | Ali et al., 2012 |
| 2N4R | Motor and learning deficits<br>Loss of neurons<br>Rough eye phenotype | Wu et al., 2013 |
| 2N4R | Reduced climbing phenotype<br>Microtubule/cytoskeleton disorganisation<br>Reduced axonal transport<br>Reduced synapsis in synaptic boutons<br>Rough eye phenotype | Roy and Jackson 2014 |
| 0N4R | Locomotor dysfunction<br>Reduced lifespan<br>Structural abnormalities in the Mushroom bodies | Passarella and Goedert al., 2018 |
| Third instar larvae (L3); Neuromuscular junction (NMJ); R406W and V337M- FTDP-17-linked mutants | | |

## 5.5 Conclusions and future directions

It has been demonstrated here a relationship between the phenotypes and changes in solubility of tau. The decrease in solubility of tau paralleled the appearance of phenotype in both models. These data might suggest that small aggregates of tau might be related to the emergence of phenotype as previously reported in other studies. In addition, these data indicate that changes in solubility could suggest oligomerization and further polymerization. In order to further examine this conversion of tau, I intend to characterize the morphology of oligomeric and larger species of tau in both models for each time point. Finally, to define experimental conditions for performing DLS and THT assay on oligomers and larger filaments obtained from fractions of *Drosophila* and mice models.

# Chapter 6 Biochemical and biophysical characterization of tau species using a number of biophysical techniques

## 6.1 Introduction

So far, I have characterized and identified the onset and progression of the disease phenotype in two models. In both models my data shows that granular tau oligomers (GTO) appear in the early stages of the disease and mostly larger aggregates/fibrillary species (NS) are evident in the late stages of the disease.

Given that my main goal is to understand how changes in tau species relate to the onset and progression of disease, the **Aim 3** of this chapter is t**o employ a number of biophysical techniques to characteristics each species (GTOs/NS) potentially responsible for the onset and progression of disease in the models described in Chapter 4 – to shed light on their structural conformation (especially β-sheet content), their morphology and their size.**

*The hypothesis of this chapter is that, given the conformational alteration, intermediate tau oligomers are the pathogenic tau species that might be responsible for tau-mediated dysfunction in the initial stages and that lead to consequent aggregation and polymerization of tau. Further conformational alteration towards elongated and fibrillary structures might be responsible for degeneration during the advanced stage of the disease.*

As discussed before, the granular tau oligomers and short or large filaments are conformational and structurally different. They can contain a range of different species, such a dimer to prefibrillar and fibrillary forms (Dobson 1999; Maeda et al., 2006; 2007; Cowan and Mudher, 2013). For this reason, they have different biophysical properties including solubility, size and morphology. These different properties can be used to characterise them and identify them at different stages of diseases using a number of biochemical and biophysical techniques.

In line with the above, the structural conformation of the tau species can be investigated by fluorescence spectroscopy using the compound thioflavin. Thioflavin serves as a signal sensor for binding of the β-sheet structure contained in aggregates. In general, thioflavin fluorescence has been used more specifically to monitor the formation of filaments in solution. For example, to investigate the formation of recombinant tau (full-length human 2N4R) filaments generated *in vitro*

(Maeda et al., 2007; Flach et al., 2012). However, its use has been reported to be useful for identifying intermediate species of tau as oligomers. As an example of this, the presence of granular tau oligomers generated in vitro has been identified for both full-length human 2N4R tau (Maeda et al., 2007) and pro-aggregation tau constructs (K18 repeat domain with the ΔK280 mutation) generated *in vitro* (without using inducers such as heparin) (Kaniyappan et al., 2017) .In addition, the use of thioflavin has also been used to identify both oligomers and tau filaments, derived from AD brains (Lasagna-Reeves et al., 2012). These published studies, which will be mentioned later, demonstrate the potential of this method to characterize and identify tau species, at different stages of aggregation, from the measurement of thioflavin fluorescence emission.

On the other hand, information on the morphology and size of both oligomers (Maeda et al., 2006; 2007; Lasagna-Reeves et al., 2012; Cowan et al., 2015; Kaniyappan et al., 2017;) and tau filaments (Maeda et al., 2007; Lasagna-Reeves et al., 2012; Kaniyappan et al., 2017; Chandupatla et al., 2020) can be revealed by atomic force microscopy (AFM). As an example of this, Maeda et al. have analysed granular tau oligomers by AFM, both isolated from AD brains and formed *in vitro* (full-length human 2N4R in the presence of heparin to induce aggregation) (Maeda et al., 2006). Later, this authors also showed the morphology of filaments isolated from brains with AD and from recombinant tau (2N4R) formed *in vitro* (Maeda et al., 2007). Similarly, other authors have isolated tau oligomers and filaments from AD brains and analysed them using AFM (Lasagna-Reeves et al., 2012). Kaniyappan et al., 2017 investigated the small and highly purified tauRDΔK oligomers (K18 repeat domain with the ΔK280 mutation) generated *in vitro* (Kaniyappan et al., 2017). More recently, Chandupatla et al., Analysed filaments formed by recombinant tau prone to aggregation (Tau-P301L) (Chandupatla et al., 2020). Together, these studies demonstrate that size and morphological details can be revealed by atomic force microscopy (AFM).

In addition to AFM technique, Dynamic light scattering (DLS) is another method to analyse differences between monomers, oligomers, and filaments (Maeda et al., 2006; 2007; Kaniyappan et al., 2017, Chandupatla et al., 2020) in terms of the size derived from the sample in solution. The size distribution of granular recombinant tau oligomers (2N4R) formed *in vitro* has been investigated using DLS (Maeda et al., 2007). Likewise, the sizes of both oligomers (Flach et al., 2012; Hill et al., 2019) and larger aggregates (Flach et al., 2012) of this recombinant tau isoform generated *in vitro*, has been previously reported also using the DLS technique. Similarly, DLS has been used to study pro-aggregating tau formed *in vitro* (Kaniyappan et al., 2017; Chandupatla et al. 2020). These studies are examples that show that DLS is a technique that allows to discriminate between species of tau aggregates by their size distribution.

Therefore, the range of biophysical methods described above were used in this study to characterize the structural nature and sizes/morphologies of the tau species to differentially identify them at different stages of diseases in our models of tauopathy.

## 6.2 Method to isolate tau fractions: cross fractionation into granular tau oligomers (GTOs) or larger aggregates aggregates/fibrillary species NS

The biophysical characterization was done on the species identified using biochemical methods described in **Chapter 3**.

### 6.2.1 Using thioflavin T (ThT) fluorescence method to assess β-sheet content of tau species (GTOs and NS)

The oligomers and large filaments have been frequently identified and analysed using the fluorescence dye thioflavin T (ThT) as a detection method (Dobson, 1999). Therefore, since its first description in 1959 as a potent fluorescent marker of amyloid in histology (Vassar and Culling, 1959) it has become a standard method to analyse the kinetic and structural properties of amyloid-like structures, such fibrils, *in vitro* and selectively identifying and staining them *in vivo* (as reviewed in Biancalana and Koide, 2010).

In particular, the fluorescence dye thioflavin T (ThT) has the ability to detect the β-sheet structure in aggregates (cross- β), such fibrils, and act as a sensor (Friedhoff et al., 1998). When the ThT binds to β-sheet structures, the dye displays enhanced fluorescence (**Figure 40**). This enhanced fluorescence produces a shift in the emission spectrum, from approximately 510 nm (when is in the Free State) to 480 nm when bound to aggregates with β-sheet structures (Naiki et al., 1989; LeVine, 1993; Biancalana and Koide, 2010).

As mentioned before, some species of oligomers and filaments of a variety of proteins have been investigated by fluorescence spectroscopy using thioflavin. For instance, Chen et al. have described that *in vitro* generated α-synuclein oligomers contain β-sheet structure that interact with thioflavin T (ThT) molecules. However, the authors report a 10-fold less interaction compared to fibrils (Chen et al., 2015). Similar results have been reported in the case of tau protein oligomers, derived from AD brains and from recombinant tau. Some of these studies are described in **Figure 42** in which it is shown that small oligomers, formed in the initial stage of aggregation, have a low interaction with

thioflavin compared to filaments. This has been described for oligomers isolated from AD brains (Lasagna-Reeves et al., 2012) and recombinant tau (Maeda et al., 2007; Hill et al., 2019; Kaniyappan et al., 2017; Chandupatla et al., 2020) as shown in **Figure 43**. As example, the low interaction between thioflavin and oligomers has been reported in small and highly purified pro-aggregating tau repeat domain (TauRD-ΔK280) oligomers generated *in vitro* (Kaniyappan et al., 2017). This and other studies show that oligomers exhibit altered conformation compared to monomers and demonstrate that it is possible to monitor and characterize the transition of tau monomers, oligomers and fibrils based on the measurement of thioflavin fluorescence emission.

Maeda et al. showed that both tau granules (GTOs) and fibrils have a β-sheet structure and that tau granules are fibril intermediates. According to the authors, both forms of tau show similar fluorescence emission levels derived from the interaction with thioflavin (Maeda et al., 2007). However, as others have reported, the early formation of GTOs (small oligomers) also contain low affinity for ThT (**Figure 42**). Suggesting that it is also possible to identify an early and late stage prior to the formation of filamentous structures with affinity for ThT. Therefore, these and other studies demonstrate that it is possible to characterize differences between tau monomers, oligomers and fibrils from tau from the measurement of thioflavin fluorescence emission (Maeda et al., 2007; Kaniyappan et al., 2017 ; Chandupatla et al., 2020).

For this reason, this method based on the measurement of the thioflavin T (ThT) fluorescence was used to achieve **objective 1: determine the structural conformation of the tau species, as they evolve from the early to the late stages of pathology**.

The method to study the thioflavin T fluorescence is described in the materials and methods section.

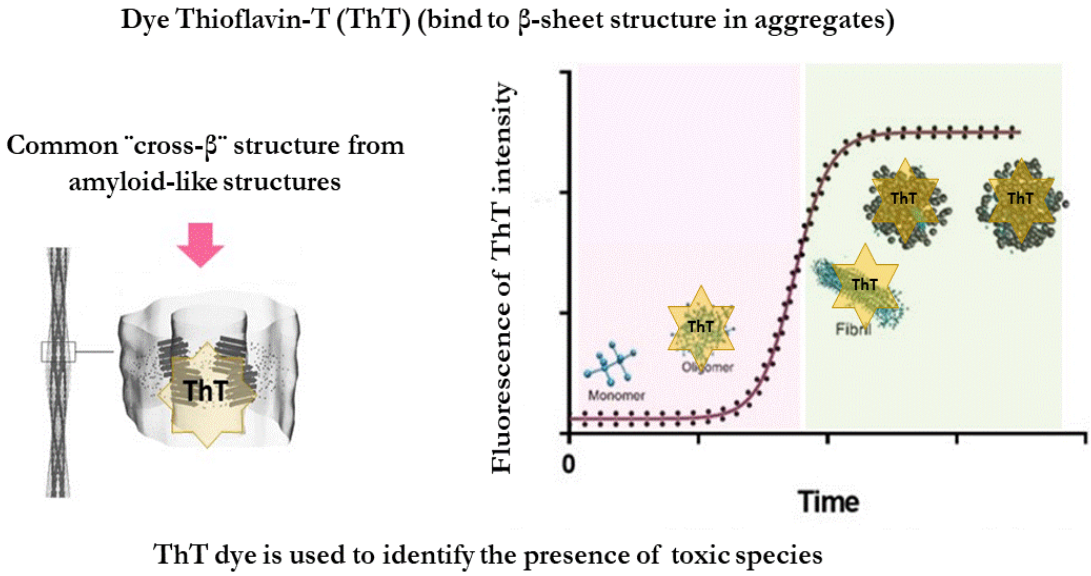


**Figure 40. Schematic representation of Thioflavin-T assay.**

Shows the β-sheet structure in amyloid-like aggregates. Fluorescence of ThT when bound to aggregates with β-sheet conformation.

### 6.2.2 Using Atomic force microscopy (AFM) to characterize morphology of tau species (GTOs/NS) and differentiate them

Atomic force microscopy (AFM) technique has been frequently used to characterize the morphological properties of oligomers and filaments, demonstrating the particular differences between these different species of aggregates as described below.

The principle of the Atomic Force Microscope is similar to the scanning probe microscope in which a topographical image of the surface of the sample is achieved based on the interactions between a tip and the sample surface. Since their introduction in 1986 (Binnig and Quate 1986) the Atomic force microscopy (AFM) has been proved to be one of the most powerful tools to acquire three-dimensional morphology with nanometric resolution of biological In particular, this technique has been widely used to visualize and analyse misfolded proteins during protein aggregation process (Chiti and Dobson, 2006)

Conventional analysis of AFM topography provides valuable information on the shape / morphology of tau species. In published studies, tau species have been analysed and differentiated between tau oligomers and fibrils using AFM. Some of these studies have been carried out with samples derived

from human brains (Maeda et al., 2006: Lasagna-Reeves et al., 2012; Ercan-Herbst et al., 2019) or samples generated *in vitro* Maeda et al., 2007; 2018; Kaniyappan et al. , 2017; Chandupatla et al., 2020) as shown in **Figure 42.** As an example, the characterization of granular tau oligomers from human brains in different Braak stages, Braak stage 0 (non-AD) and Braak stage V (AD) (Maeda et al., 2006;2007) as well as oligomers generated *in vitro* (full-length human 2N4R tau) has been reported (Maeda et al., 2007). The authors report that granular tau oligomers, both isolated from brains with AD or generated *in vitro*, ranges between 5 and 50 nm with a height of up to 30 nm (Maeda et al., 2006; 2007). As can be seen in (**Figure 42)** the ranges are similar in early Braak stage or advanced braak stage. These authors also reported the presence of PHFs and straight filaments in AD brain at late stage. These filaments are very similar to those generated *in vitro*, reaching lengths of up to 950 nm and diameters of 15-25 nm (Maeda et al., 2007) (**Figure 43**).

Lasagna-Reeves et al. have also reported the characterization of tau species derived from AD brains using AFM. In this study, the authors used the immunoprecipitation (IP) technique to specifically isolate oligomeric structures (using the anti-tau T22 oligomeric antibody) from AD brains. The authors reported small oligomers with a diameter of 4-8 nm. Because of the small sizes of oligomers, the dimensions reported by AFM were positioned in the column of early stage of the disease in **Figure 42**; given that, as reported by Maeda et al., 2006, the majority of structures of small sizes are related to the early stage of the disease. Additionally, they also analysed detergent-insoluble fractions obtained from AD brains and reported the presence of classic paired helical filament (PHF) morphology (**Figure 43**). These studies are examples that demonstrate that this technique allows to identify and characterize between oligomeric and fibrillar species of tau.

In a more recent study, the AFM analysis of oligomers isolated from human brains by IP technique (using Tau12 antibody), has been reported. Particularly, the presence of oligomeric structures was demonstrated even in early Braak stage 0-I of (non- AD), when most species are reported between 5 and 10 mn in height. While in Braak stage III-IV (non- AD), most of the tau aggregates are reported as larger oligomeric structures, varying from 10 to 30 nm in height (Ercan-Herbst et al., 2019). These observations suggest that oligomers appear from very early stages and that the size of the oligomers increases with time. Since published studies suggest that small oligomeric structures are related to toxicity and appear in very early stages of the disease, relatively recent studies have focused on investigating the characteristics of these small oligomers *in vitro* **Figure 42**, For example, Kaniyappan et al., 2017, have investigated small and highly purified tauRD-ΔK280 toxic oligomers (K18 repeat domain construct with the ΔK280 mutation) generated *in vitro* using AFM. These authors report that the toxic species have a height of ~ 3.2 and a width distribution of 3-15 nm (Kaniyappan et al., 2017).

Additionally to these studies, AFM has also been used in the characterization of granular tau (GTOs) in the *Drosophila* mode (Cowan et al., 2015) (**Figure 42**). In this model, it was demonstrated that expression of human tau (0N3R) in neurons and treatment with an inhibitor of GSK 3β tau kinase results in the formation of GTOs species. The morphology of these oligomers was analysed using AFM, showing that these structures resembled the oligomeric structures in AD. These structures were reported as having widths from 5–50 nm, with an average width and height of 20 nm (Cowan et al., 2015).

Together, these studies show that the AFM technique makes it possible to differentiate between heterogeneous species, such as oligomers and filaments, of tau aggregates. Therefore, AFM was used to achieve **Objective 2: To characterize the overall morphologies of the tau species from early and advance stage of disease in our models**.

The method is described **Chapter 3**, the materials and methods section.

### 6.2.3 Using Dynamic Light Scattering (DLS) to assess relative size of tau species (GTOs/NS) and differentiate them

Differences in size between oligomers and filaments of tau can also be analyzed using the dynamic light scattering technique (Maeda et al., 2007; Flach et al., 2012; Kaniyappan et al., 2017; Hill et al., 2019; Chandupatla et al., 2020). For this reason, this method was used to characterize the size of the tau fractions in this thesis.

Dynamic Light Scattering (DLS) is a method that can be used to study aggregates in macromolecular solutions (Lorber et al., 2012). This method allows determining the size distribution profile of molecules such as proteins, nucleic acids, and other complexes (Lorber et al., 2012). This technique is based on the fluctuation of dispersed particles, caused by Brownian motion, which depends on both the size and shape of the particles in the sample. The DLS measures the Brownian motion in the sample solution when illuminated with a laser and analyses the intensity fluctuations in the scattered light (**Figure 41)**. This technique has been used to analyse different types of particles such as monomers, oligomers, and tau fibrils (Maeda et al., 2007; Flach et al., 2012; Kaniyappan et al., 2017; Hill et al., 2019; Chandupatla et al. al., 2020) (**Figure 42**). Showing that it is possible to study differences in the size parameters between monomers, oligomers and tau fibrils by means of dynamic light scattering.

For example, it has been described that granular recombinant tau oligomers (2N4R) formed *in vitro*, in the presence of heparin, have an average size distribution of 55 nm (**Figure 42**). While, the monomers have a distribution with an average size of 12nm in diameter (Maeda et al., 2007). As described in **Figure 42**, in this study these granular species are reported as species formed during initial stage of fibrillation process (Maeda et al., 2007). In a relatively recent study, the recombinant tau monomers were described as between 7.5 and 10 nm in diameter. While early formed oligomers have a wide size distribution that varies between 18 and 32 nm (**Figure 42**, column corresponding to the early stage) (Hill et al., 2019).

Similarly, DLS has been used to study tau pro-aggregation constructs formed *in vitro*. For example, tauRDΔK monomer sizes of 12 nm in diameter have been reported, while the sizes of small highly purified oligomers of tauRDΔK formed, *in vitro* without heparin, have been reported with sizes of 20 nm in diameter (Kaniyappan et al., 2017) also shown at the early stages during fibrillation process (**Figure 43**). Recombinant full-length Tau-P301L aggregates formed *in vitro* (with heparin), have been also analysed using DLS. The authors report size distributions ranging from ~ 4 to 10 nm in diameter for monomers, and 10 to 200 nm in diameter for aggregates (**Figure 42** early stage) such as high molecular weight oligomeric forms (**Figure 42** late stage) or filaments (**Figure 43**) (Chandupatla et al. 2020). These studies are examples that show that DLS is a technique that allows discriminating between species of tau aggregates.

This provides the basis for **objective 3: To determine the size distribution of the tau species from early and advance stage of disease in our models.**

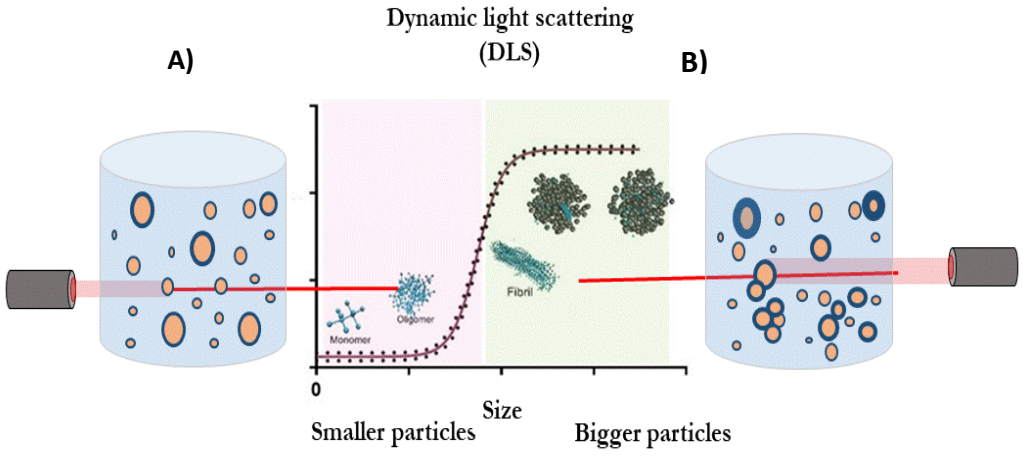


**Figure 41. Schematic representation of Dynamic light scattering**

**A**) Shows the intensity fluctuations in the scattered light that is analysed and correspond to smaller particles in the solution. **B**) Shows the intensity fluctuations in the scattered light that is analysed and correspond to bigger particles.

| Oligomers from model: | Thioflavin (Fluorescence intensity) | | DLS (nm ) | | AFM (nm) | | Reference |
|---|---|---|---|---|---|---|---|
| | Early time point | Late time point | Early time point | Late time point | Early time point | Late time point | |
| Human AD Brain (GTOs) | -n/a | -n/a | -n/a | -n/a | 5-50 diameter (Braak stage 0) | 5-50diameter (Braak stage 0) | Maeda et al.,2006; 2007 |
| | | | | | 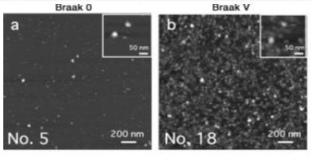  | | |
| Human Brain | --n/a | --n/a | --n/a | -n/a | 5-10 Height (0-I of Braak) | 10-30 height (Braak stage III-IV) | Ercan-Herbst et al., 2019 |
| | | | | | 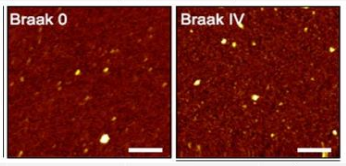  | | |
| Human AD brain (small oligomers) | Low | | n/a | n/a | ~ 4-8 (diameter) | n/a | Lasagna-Reeves et al., 2012 |
| | 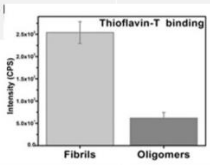  | | | | 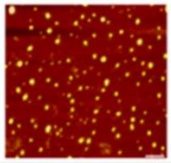 | | |
| Recombinant full-length human 2N4R tau (GTOs) | Low | High | Avarage of 55 | n/a | 5-50 diameter Avarage 25-50 (diameter) | 5-50 diameter Avarage 25-50 (diameter) | Maeda et al 2007 |
| | | 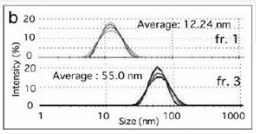  | | | 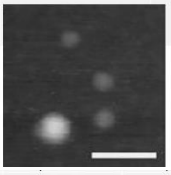 | | |
| Recombinant full-length human 2N4R tau | Low | n/a | 18 and 32 nm in diameter | n/a | | | Hill et al., 2019 |
| TauRDΔ K18 repeat domain construct with the ΔK280 mutation | Low | | 20 nm in diameter | | | | Kaniyappan et al., 2017 |
| | 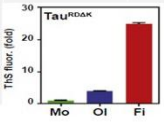  | | 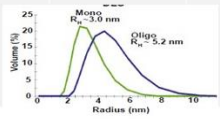  | | 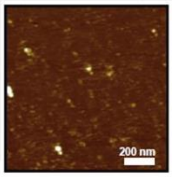  | | |

| | | | | | | | |
|---|---|---|---|---|---|---|---|
| Recombinant full-length Tau-P301L | Low | | 20 nm in diameter | | ~2 to 3 nm heights | >10 nm heights | Chandupatla et al., 2020 |
| Human 0N3R Fly model Treated with inhibitor of GSK 3β tau kinase | n/a | n/a | n/a | n/a | Widths from 5–50 nm average width and height of 20 nm | n/a | Cowan et al., 2015 |

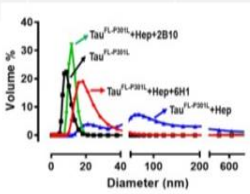


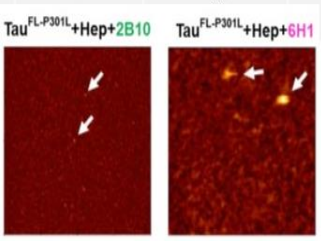


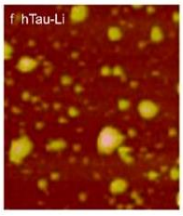


**Figure 42. Examples of published studies that have characterized tau oligomers using techniques similar to those used in this study**

| Filaments from model: | Thioflavin (Fluorescence intensity) | | DLS (nm ) | | AFM (nm) | | Reference |
|---|---|---|---|---|---|---|---|
| | Early time point | Late time point | Early time point | Late time point | Early time point | Late time point | |
| Human AD Brain | n/a | High | -n/a | -n/a | -n/a | 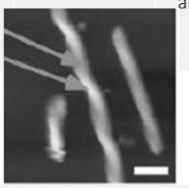 | Maeda et al., 2007 |
| Human Brain | -Low | High | --n/a | -n/a | -n/a | Classical morphology PHF 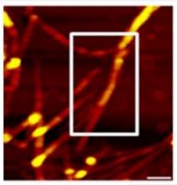 | Lasagna-Reeves et al., 2012 |
| | Early time point | Late time point | Early time point | Late time point | Early time point | Late time point | |
| Recombinant full-length human 2N4R tau | Low | High | -n/a | -n/a | -n/a | Lengths of up to 950 nm and diameters of 15-25 nm 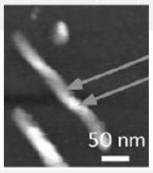  | Maeda et al., 2007 |
| Recombinant full-length Tau-P301L | -Low | High | --n/a | Up to 10 to 200 nm in diameter | -n/a | 10 to 18 nm 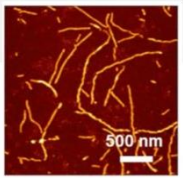  | Chandupatla et al., 2020 |

**Figure 43. Examples of published studies that have characterized tau filaments using techniques similar to those used in this study**

## 6.3 Summary of aims and objectives:

**Aim 3. To employ a number of biophysical techniques to continue exploring in more detail the characteristics that distinguish each species (GTOs/NS) potentially responsible for the onset and progression of disease**

Objective 1: Determine the structural conformation of the tau species, from the early and late stages of the pathology.

Objective 2: To characterize the overall morphologies of the tau species from the early and advanced stages of disease in our two models.

Objective 3: To determine the size distribution of the tau species from the early and advanced stages of disease in our two models.

## 6.4 Results

For this study, a total of 100 heads of adult flies expressing htau$^{0N3R}$ or htau$^{0N4R}$, as well as the cerebral cortex of P301S mice representing different stages of the disease, were homogenized and fractionated using the solubility method described in **Chapter 3**, to obtain either the GTOs fractions or NS fractions (species described in **Chapter 5**). The experiment was done at leas for 2 individual experiments. This protocol was also carried out on controls. Next, a series of physical techniques were used to characterize the fractions obtained (GTO / NS) during the different stages of the disease.

### 6.4.1 Changes in β-sheet using ThT

The structural characteristics of the fractions (S1, S2, S3, NS1 and NS2) were studied by means of the spectroscopic fluorescence method using thioflavin T (ThT). For data analysis, fluorescence of each equivalent blank solution (buffer + dye) was subtracted from each protein. The signal from the fluorescence intensity of each samples was divided by the fluorescence intensity of the ThT-only sample. The signal from ThT-only sample has been taken as value 1. To calculate the fold change in fluorescence intensity over the moromer, the fluorescence intensity of the sample corresponding to the monomer was divided by the fluorescence intensity of the sample (Sample / monomer). The value from the ¨S1¨fraction at 0 weeks in flies and 12 weeks in mice were considered as the monomeric tau to compare the fold increase with the GTOs and NFTs at the different representative stages of the disease. GraphPad Prism, version 7.0 Software was used for statistical analysis and

unpaired t tests were performed on the data to investigate differences between the fractions tested during the different stages.

In both models of tauopathy, it was observed significant differences in the intensity of the ThT fluorescence between the stages representative of the pathology tested. In *Drosophila*, whether expressing htau$^{0N3R}$ or htau$^{0N4R}$ isoform induces changes associated with the β-sheet structure compared to control flies. And these changes are significantly prominent in hTau$^{0N4R}$ than the hTau$^{0N3R}$ (**Figure 45** and **Figure 46 A-a**). First, in OreR wt flies, a minimal increase in ThT fluorescence intensity was observed at early time points and no further increase in the intensity of ThT was evident at any of the subsequent time points, in any of the three fractions. This suggests the absence of β-sheet structure in any proteins found in brains of these control flies (**Figure 44 A-a**). Unpaired, two-tailed t test show that the fold increase of ThT shows no significant difference between the fractions tested during the different stages.

In contrast, in both htau-expressing lines, significant differences in the intensity of the ThT between the fractions at the early and advance stages were observed. The S1 fraction at 0 weeks showed minimal increase in the intensity of ThT (**Figure 45B-a** and **Figure 46 C-a**).This data suggests that both htau-expressing lines, protein is primarily monomeric at this stage (with absence of β-sheet structure) and this ThT value was used as the baseline to which subsequent ThT values were compared to.

As flies progressed to the early stage of disease, both htau-expressing lines begins to show structural changes associated with the β-sheet content in the fraction containing the detergent-insoluble fractions (S3). However, the intensity of the ThT to this fraction from htau$^{0N3R}$ flies is ~3 times lower in comparison to the hTau$^{0N4R}$ (**Figure 45 B-a** and **Figure 46 C-a**). This suggests that the hTau$^{0N4R}$ possess more β-sheet structure in the S3 fraction during the early stage and this increase to ~9-fold increase compared to control during the advance stage of disease. Unpaired t test shows shows that the three fractions are significantly different at early and advance stage of disease.

In particular, in 3R flies, the S1 fraction is significantly different than S2 fraction at 0 weeks ($p=0.0031$), 2.5 weeks ($p=0.0290$) and at 5 weeks ($p=0.0295$) post-eclosion. In addition, the S1 is significantly different between the S3 fraction at 0 weeks ($p=0.0041$), 2.5 weeks ($p=0.0243$) and 5 weeks ($p=0. 0008$). In flies expressing 4R tau, In particular, the S1 fraction is significantly different than S2 fraction at 0 weeks ($p=0.0002$) 2.5 weeks ($p=0.0032$) and at 5 weeks post eclosion ($p=0.0074$). In addition, the S1 is significantly different between the S3 fraction at all stages ($p<0.0001$). The S2 fraction is signigicantly different between S1 and S2 at 0 weeks ($p<0.0001$), 2.5 weeks ($p= 0.0701$) and 5 weeks ($p=0.0737$) post eclosion.

Similarly to the fly model, in the P301S mice model, the S1 fraction also showed a minimal fold increase (~0.6) (**Figure 47 A-a**), suggesting the presence of mostly soluble and monomeric tau at both representative stages of disease. The fluorescence intensity of ThT showed an increase in the fractions containing insoluble species compared to the monomers. During the advanced state of pathology, the intensity of ThT fluorescence show a strong ~10-fold increase **Figure 47 A-a**). In this model, unpaired t test shows that the fold increase of ThT is significantly different between S1 and S2 at advance stage ($p<0.0001$). In addition, the fold increase of ThT is significantly different between S1 and S3 at early ($p= 0.0416$) and at an advance stage ($p<0.0001$). In addition, at advance stage, the fold increase between the S2 and S3 is significantly different ($p= 0.0050$). This data suggests the transition from oligomers to polymeric aggregates is in line with the solubility assay.

Overall, these data indicate that the expression of htau induces a temporal structural reorganization of tau species associated with the β-sheet structure irrespective of the model in which it is expressed. This data also shown that in the *Drosophila* model, the affinity of the ThT marker is stronger to species from htau$^{0N4R}$ flies in comparison to the hTau$^{0N3R}$. Suggesting that the hTau$^{0N4R}$ possess more β sheet structure in than the hTau$^{0N3R}$. Likewise, the increase in the affinity of ThT and aggregates from flies expressing htau$^{0N4R}$ in advanced stage, resembles the increase achieved in the P301S mouse model, in advanced stage.

In general, the results obtained are like previously reported observations (as shown previously in **Figure 42**). For example, low levels of thioflavin intensity like those reported here have been reported in small oligomers from AD brain (Lasagna-Reeves et al., 2012) and small oligomers characteristic of initial stages of aggregation, as shown in TauRDΔK oligomers generated *in vitro* (Kaniyappan et al., 2017). On the other hand, elevated levels of ThT fluorescence intensity have been reported for recombinant (2N4R) tau granules generated *in vitro* (Maeda et al., 2007) that resemble isolates from AD brains (Maeda et al., 2006; 2007). These observation suggest that the temporal increase in ThT intensity levels are due to the tau granules being direct intermediates of larger aggregates and filaments.

### 6.4.2 Investigating size of tau species (GTOs) using DLS

To investigate the size distribution of the fractions (S1, S2 and S3), dynamic light scattering (DLS) was used. Here temporal changes in the size distribution at early and advance stage were also observed in both tested models.

In general, most of the S1 fraction was characterized by a population with a hydrodynamic diameter smaller than ~1 nm and another population slightly larger than ~1 nm. This data suggest that this fraction contains monomeric and soluble species and agrees with previous ThT results in which low affinity for ThT was shown (Lasagna-Reeves et al., 2012; Kaniyappan et al., 2017)

In the Ore R wt flies, the DLS results revealed a low increase in size over time, although this increase does not suggest oligomerisation (**Figure 44 A-b**). For example, the S1 fraction showed a larger population with a diameter of ~ 5nm after 2.5 weeks. However, this distribution correspond to small and soluble species. As for the size distribution of both the detergent-soluble (S2) and detergent-insoluble (S3) fractions, the size distribution increased from ~6 to ~12nm in diameter as time progressed to 5 weeks (**Figure 44 A-b-c**). It is likely that endogenous dtau, and other proteins, are pulled out in these fractions from the brain of the wt flies. However, these sizes correspond to small and mostly soluble species suggesting not aggregation.

By comparison, the expression of htau induced a clear increase in the size distribution over time, compared to controls. Although much prominent in flies that express $hTau^{0N4R}$ than in those that express $hTau^{0N3R}$. For instance, in $hTau^{0N3R}$ flies, the size distribution of the detergent-insoluble (S3) fraction showed a major population with a diameter of ~1nm followed by a second population with a diameter of ~12nm during the early stages of disease. As the disease progress to an advance stage, the distribution shift to a diameter of ~2nm, ~9nm and ~20 to ~35nm. As for the $hTau^{0N4R}$ flies, the size of the S3 fraction, showed a large population with a diameter of ~1nm, followed by three populations with a diameter of ~4, ~9 to ~13nm during the early stages of the disease (**Figure 45** and **Figure 46. C-b-c**). At advance stage, these distribution shift to a diameter of ~10nm, ~20nm and ~50 to 70nm. These values suggest the presence aggregates and may suggest that the 4R form is more prone to aggregate. In addition, unpaired t test shows that in flies expressing $hTau^{0N3R}$ size distribution is significantly different between S1 and S2 ($p=0.0040$); S1 and S3 ($p=0.0243$) at 0 weeks.

As in the fly model, the GTO fractions generated from the P301S mouse model at early and advance stage of disease showed an increase in the size distribution. Here, the DLS revealed that at early stage (12weeks) the S1 fraction slightly increase to from <1 and ~2nm to ~3nm at the advance stage of disease (**Figure 47 D-b-c**). This fraction contains a majority of soluble and monomeric species with low affinity to ThT. Additionally, the size distribution of the S3 fraction increases from a size distribution ranging from ~1nm, ~4 and nm diameter to a distribution size ranging from ~1nm, ~20nm to up to 300 nm. This data revealed a pronounced increase in the size for the species over time compared to the monomers, suggesting aggregation due to oligomerization and further polymerization.

Overall, this data shown that in both models the expression of tau caused temporal changes in the size distribution, suggestive of aggregation and agrees with the increase in both, the insolubility and ThT interaction. This data suggests that species among groups of sizes from 0 to 10nm in diameter correspond to monomers and soluble proteins. Larger groups of 10 to 100nm (<200) corresponds to association / aggregation of proteins. For example, *in vitro* generated recombinant tau oligomers (2N4R) with a diameter ranging from 20 to 55 nm have been reported (Maeda et al., 2007; Flach et al., 2012; Hill et al., 20019) (as described in **Figure 42**). In addition, aggregates of higher molecular weight and filaments with sizes between 84 nm in diameter have been reported in recombinant tau (2N4R) (Flach et al., 2012) and up to 200 nm in aggregates of recombinant tau-P301L (Chandupatla et al. 2020). Additionally, the results shown here, also suggest that the 4R isoform is more susceptible to aggregation.

### 6.4.3 Studying the morphology of species in the GTO fraction from flies using AFM

The morphology of the sediment (P2) obtained from the detergent-insoluble fractions (S3) (See **Chapter 3**, section **3.12**) was evaluated by AFM. For AFM different random images from at least 3 different experiments were performed and analyzed using WSXM software. The data is presented as the topography of the image corresponding to the two-dimensional view of the fractions. Scale bar 200nm.

Here, it was observed that the expression of tau also produces temporary changes in the morphology. When investigating the control flies (OreR wt), the topography of the image showed a homogeneous monolayer with the presence of smooth shapes distributed over the surface of the mica (short arrows). These structures have an average height of ~2 nm suggesting the presence of small and monomeric proteins. At a late stage, the images showed slightly larger and amorphous structures irregularly distributed over the surface of the mica (large arrows) (**Figure 44 A-d**). The analysis of the cross-section of these images shows that these structures have a width of around ~0-10nm (small arrows) and ~ 20-30nm with a maximum height of around ~4nm during the late stages. However, the minimal increase in ThT shown above suggests that these structures do not suggest aggregation.

It is important to mention that all flies, as in control flies, the composition of these fractions may contain proteins (other than *Drosophila* tau (dtau)) and lipids, such as sphingolipids, cholesterol and glycerophospholipids, as other detergent-resistant components (Schuck et al., 2003) as contaminants of the fractionation process. For this reason, it is possible that the slight increase in

the size observed in some fractions is due to the interaction of protein-lipids-producing a solution more similar to that of a solution colloidal but with a lack of β-sheet structure, as the ThT data suggests.

In both htau-expressing flies, the topography of the AFM images at early stages, is characterized by the presence of small puncta homogeneously distributed on background and some slightly larger and globular structures irregularly distributed over the surface. The analysis of the cross section of these images shows that in both lines, these structures have a width of around ~0-10nm for the small puncta and ~20-60nm with a maximum height around ~4nm for the amorphous structures during the early stages of the disease (**Figure 45** for htau$^{0N3}$ **Figure 46 B-d** for htau$^{0N4}$short arrow). As the disease progresses, amorphous structures are characterized by having widths of ~20nm to a range of ~100nm with a maximum height of about ~10nm (**Figure 45** and **Figure 46 B-d** larger arrows). These widths are larger in htau$^{0N4R}$ flies (**Figure 45 B-d** larger arrows). This increase in height suggest aggregation and is in line with increase in size shown by DLS and the increase in the ThT assay.

Similarly, in P301S mice model, the analysis of the cross section of these images at early stage, showed that the amorphous structures have a width of around ~20nm (short arrows) with a maximum height around ~2nm. In addition to some bigger structures with a ~50nm (large arrows) with a maximum height around ~10nm (**Figure 47 D-d**). At advance stage of disease, the analysis of the cross section showed that these structures have a width of around ~10nm (Short arrows) with a maximum height around ~10nm. In addition, bigger structures have up to ~100 nm with a maximum height around ~20nm for the amorphous structures during advance stages of the disease (large arrows) (**Figure 47 D-d**).

In general, this data further confirm that the expression of htau produces temporal changes in morphology and size in both models. In support of our results, Maeda et al demonstrated that Braak stage V AD brains present a higher proportion of GTO compared to Braak stage 0 (not AD) (Maeda et al., 2006) (**Figure 42**). Furthermore, they showed that the GTOs of the Braak stage I brains were smaller than the Braak stage III or V GTOs. On the other hand, Ercan-Herbst et al, reported that most of the oligomers isolated from the entorhinal cortex in the Braak 0-I stage (not AD) contain small oligomers between 5 and 10 nm in height by AFM. While the Braak III-IV stage (not AD), contains larger oligomers that vary from 10 to 30 nm in height (Ercan-Herbst et al., 2019) (**Figure 42**). These results are in line with our observations suggesting a similar increase in size during disease progression to an advanced stage.

**Elav-GAL4/Ore R**

**A-a**

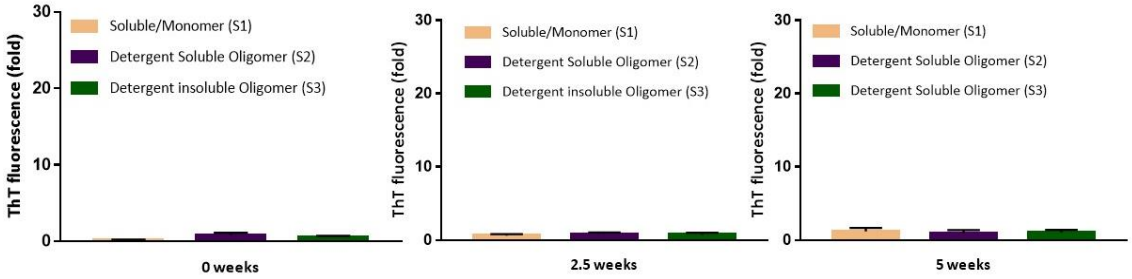


**A-b**

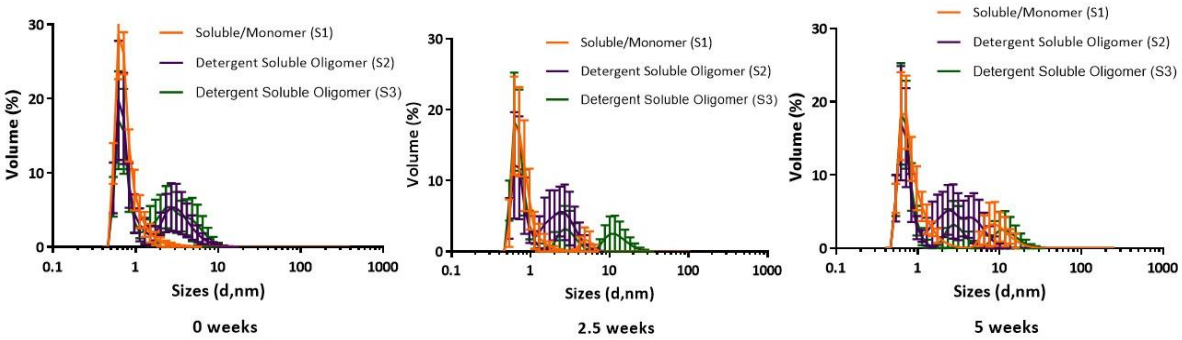


**A-c**

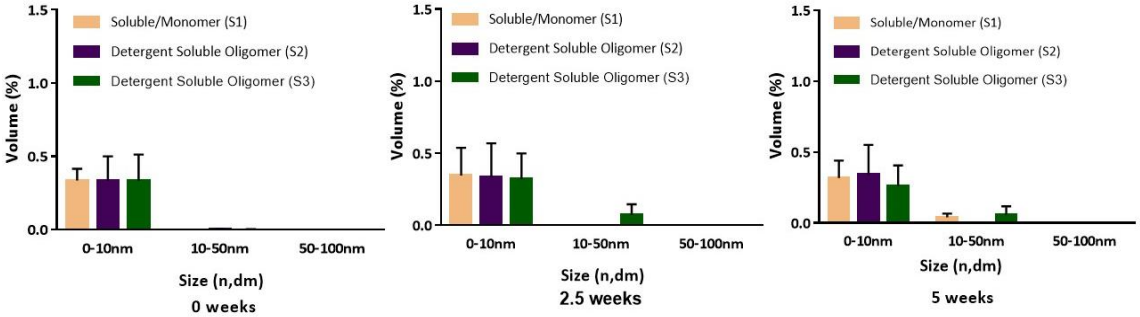


**A-d**

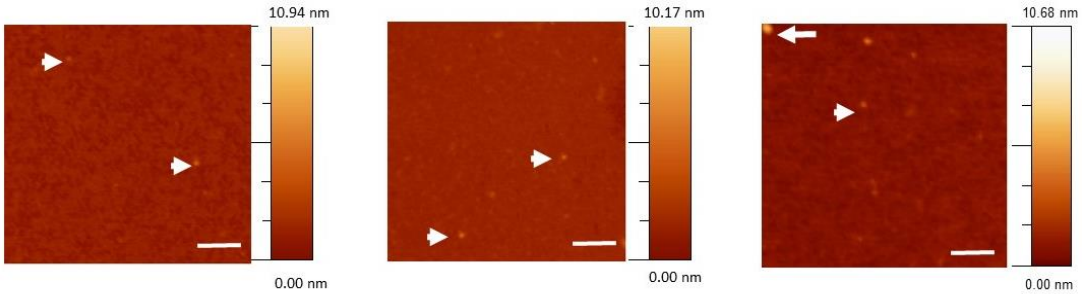

**Figure 44**. **Temporal structural and morphological changes in protein species at the early stage and advance stage of disease in OreR wt flies**

**A-a**) ThT fluorescence intensity of fractions from adult heads flies on S1, S2 and S3 fractions at 0, 2.5 and 5 weeks-post eclosion for Elav-GAL4 driven OreR wt, obtained by solubility. The experiment was done for 2 individual experiments (n=2, from different crosses; using 100 fly heads for fractionation). Measurements were carried out in duplicates. ThT fluorescence of fractions displayed as fold change over monomer fluorescence. Unpaired t test shows no significant difference between the three fractions (S1, S2 and S3) tested over time. Error bars are plotted ±S.E.M. **A-b**) Hydrodynamic diameter of tau species measured by DLS and result expressed as a volume graph. **A-c**) Size distribution measured by DLS and expressed as the fraction of components in the total sample evaluated. The particle size was obtained as an average of 3 measurements with 20 runs each, from 2 individual experiments (n=2, from different crosses). Unpaired t test shows that the size distribution is not significantly different between the fractions at any stage studied. **A.d**) Detergent-insoluble species (S3) from adult flies at 0, 2.5 and 5 weeks post eclosion and imaged by AFM in tapping mode.

## Elav-GAL4/ htau$^{0N3R}$

**B-a**

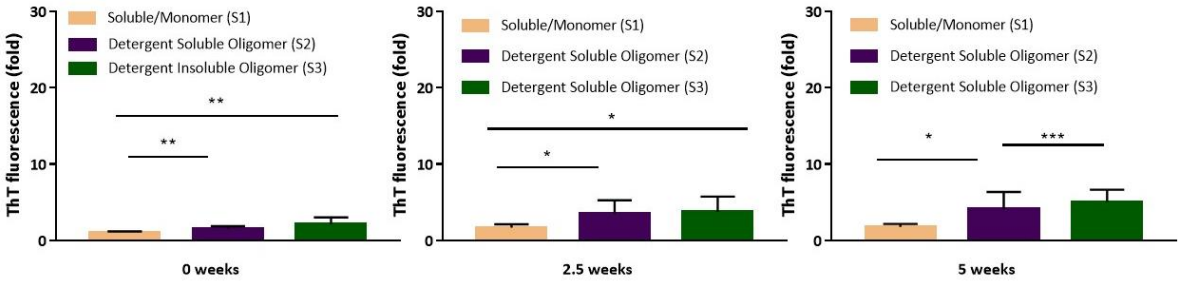


**B-b**

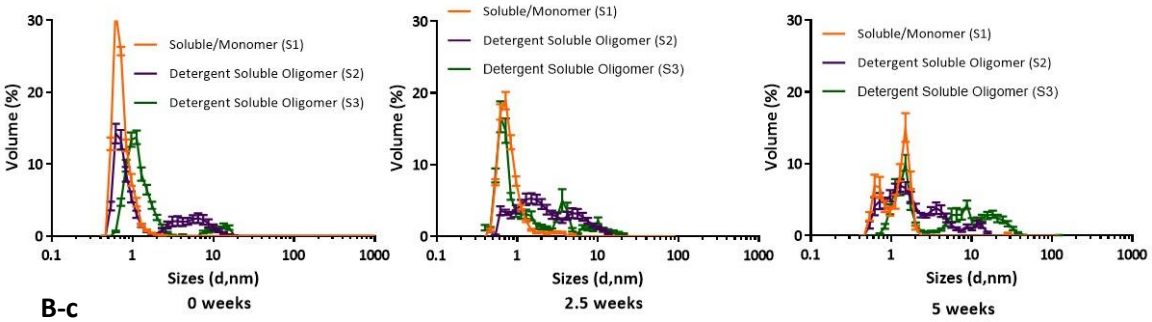


**B-c**

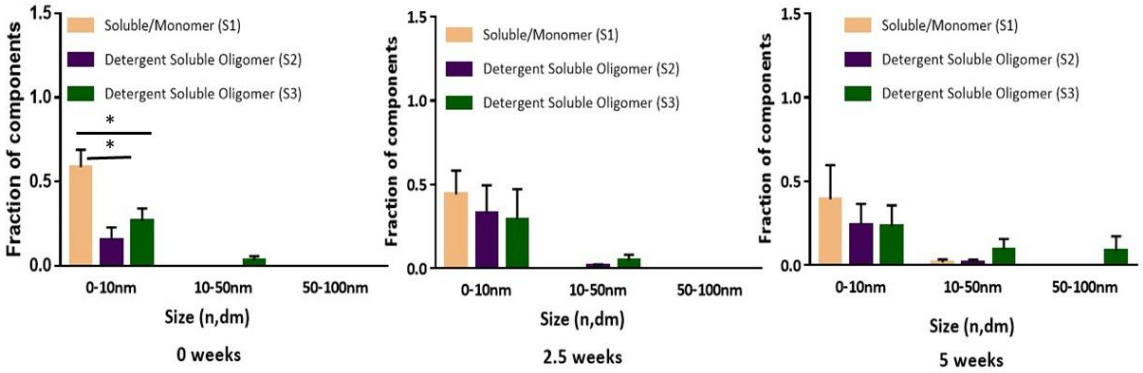


**B-d**

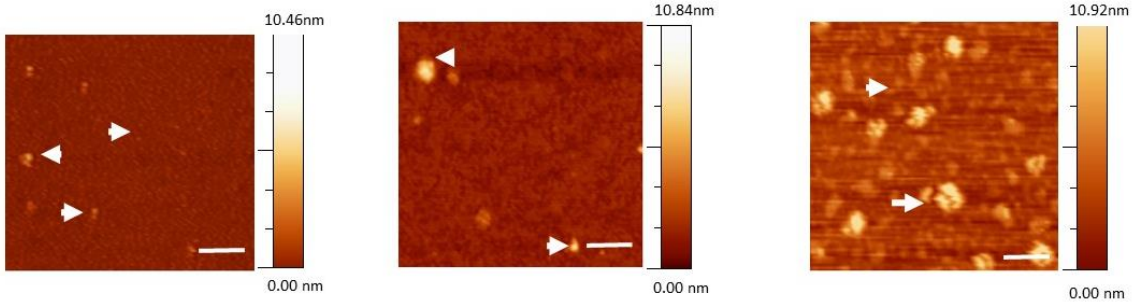

**Figure 45. Temporal structural and morphological changes in tau species at the early stage and advance stage of disease in htau$^{0N3R}$**

**B-a**) Comparison of ThT fluorescence intensity of fractions from adult heads flies on S1, S2 and S3 fractions at 0, 2.5 and 5 weeks-post eclosion for Elav-GAL4 driven htau$^{0N3R}$ obtained by solubility assay. The experiment was done for 3 individual experiments (n=3, from different crosses; using 100 fly heads for fractionation).Measurements were carried out in duplicates. ThT fluorescence of fractions displayed as fold change over monomer fluorescence. Unpaired t test was used for analysis. S1 fraction is significantly different than S2 fraction at 0 weeks (p=0.0031), 2.5 weeks (p=0.0290) and at 5 weeks (p=0.0295) post-eclosion. In addition, the S1 is significantly different between the S3 fraction at 0 weeks (p=0.0041), 2.5 weeks (p=0.0243) and 5 weeks (p=0. 0008).The **B-b**) Hydrodynamic diameter of tau species measured by DLS and result expressed as a volume graph. **B-c**) Size distribution measured by DLS and expressed as the fraction of components in the total sample evaluated.The particle size was obtained as an average of 3 measurements with 20 runs, each from 3 individual experiments (n=3, from different crosses). Unpaired t test shows that size distribution is significantly different between S1 and S2 (p=0.0040); S1 and S3 (p=0.0243) at 0 weeks. B.d) Detergent-insoluble species (S3) from adult flies at 0, 2.5 and 5 weeks post eclosion and imaged by AFM in tapping mode.

## Elav-GAL4/ htau$^{0N4R}$

**C-a**

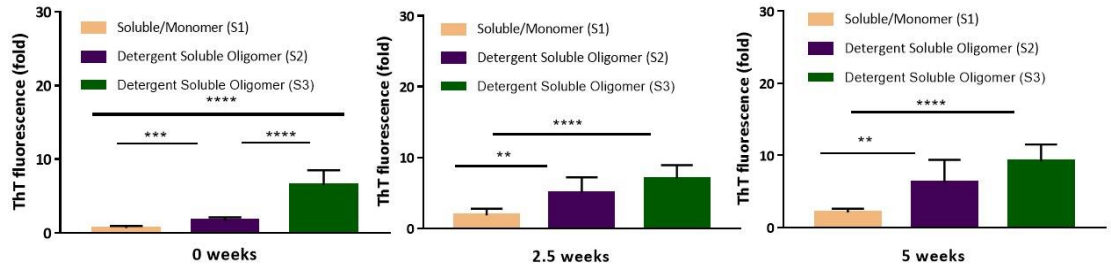


**C-b**

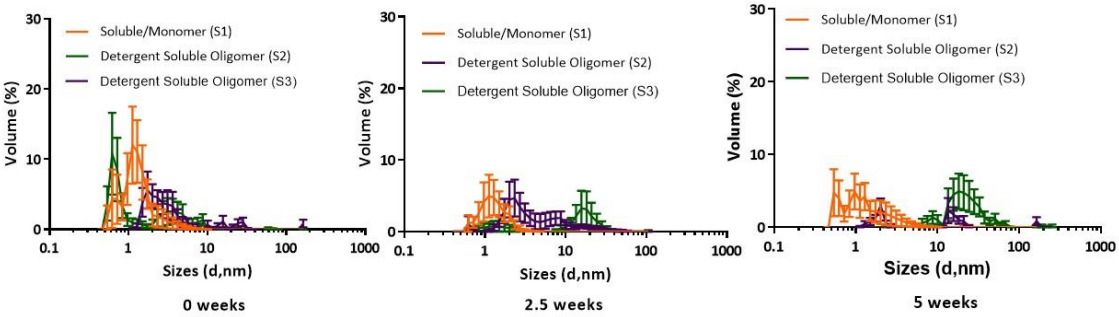


**C-c**

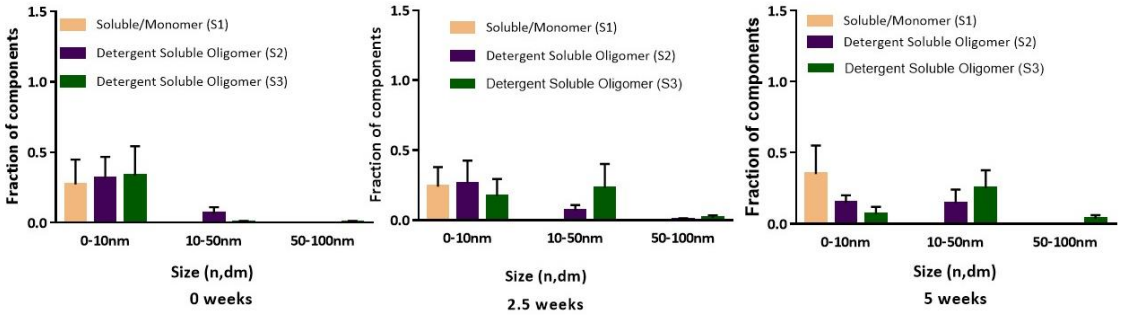


**C-d**

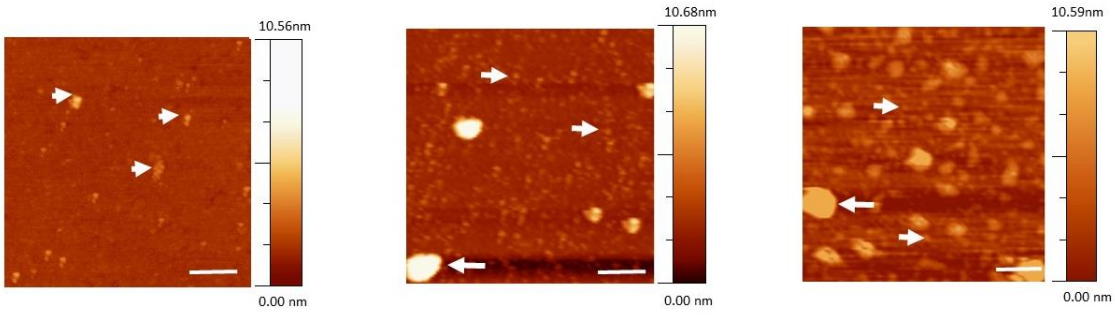

**Figure 46. Temporal structural and morphological changes in tau species at the early stage and advance stage of disease in htau$^{0N4R}$**

**C-a**) Comparison of ThT fluorescence intensity of fractions from adult heads flies on S1, S2 and S3 fractions at 0, 2.5 and 5 weeks-post eclosion for Elav-GAL4 driven htau$^{0N4R}$ obtained by solubility. The experiment was done for 3 individual experiments (n=3, from different crosses; using 100 fly heads for fractionation). Measurements were carried out in duplicates. ThT fluorescence of fractions displayed as fold change over monomer fluorescence. The fold increase of ThT is significantly different between the three fractions tested. Error bars are plotted ±S.E.M. Unpaired t test shows that the S1 fraction is significantly different than S2 fraction at 0 weeks ($p=0.0002$) 2.5 weeks ($p=0.0032$) and at 5 weeks post eclosion ($p=0.0074$). S1 is significantly different between the S3 fraction at all stages ($p<0.0001$). The S2 fraction is signigicantly different between S1 and S2 at 0 weeks ($p<0.0001$), 2.5 weeks ($p= 0.0701$) and 5 weeks ($p=0.0737$) post eclosion. **C-b**) Hydrodynamic diameter of tau species measured by DLS and result expressed as a volume graph. **C-c**) Size distribution measured by DLS expressed as the fraction of components in the total sample evaluated. The particle size was obtained as an average of 3 measurements with 20 runs, each from 3 individual experiments (n=3, from different crosses/ genotype). The unpaired t test shows that the size distribution is not significantly different between the fractions at any stage studied. C-d) Detergent-insoluble fractions (S3) from adult flies at 0, 2.5 and 5 weeks post eclosion and imaged by AFM in tapping mode.

## P301S mice

**D-a**

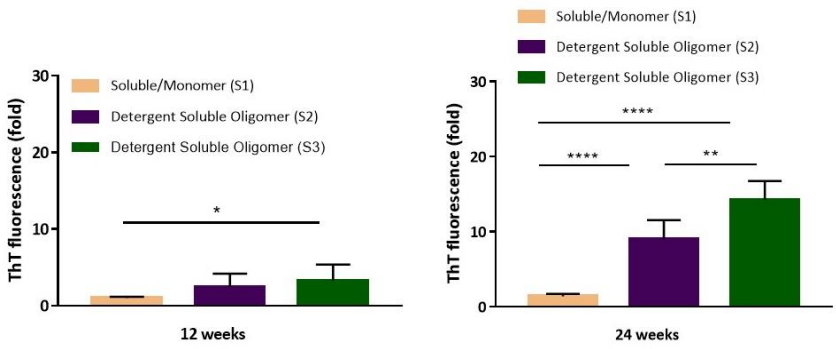


**D-b**

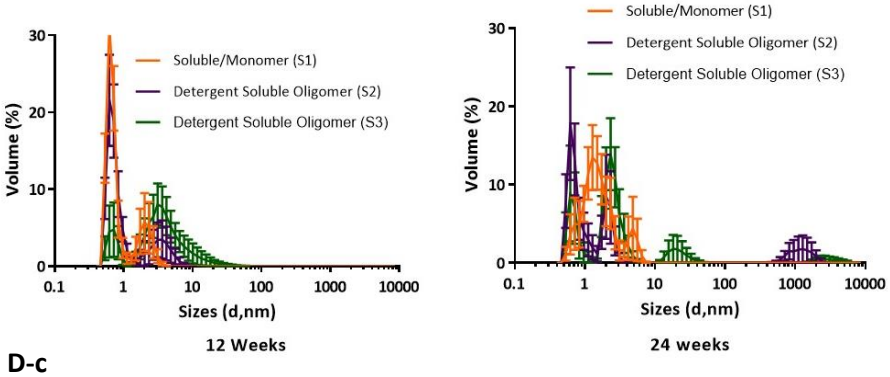


**D-c**

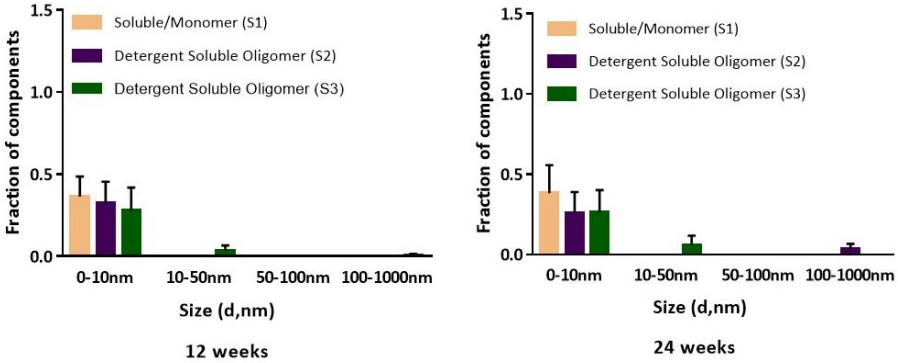


**D-d**

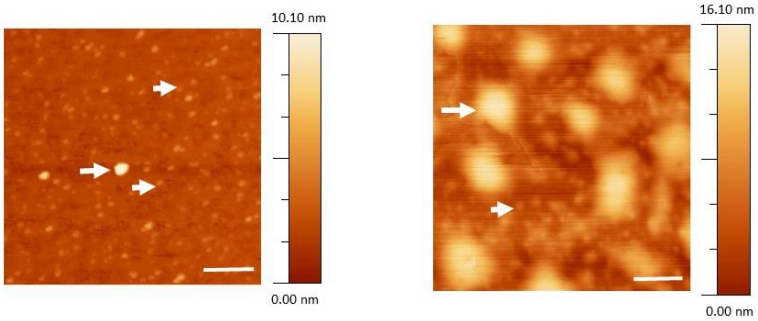

**Figure 47. Temporal structural and morphological changes in tau species at advance stage of disease in P301S**

**D-a)** Comparison of ThT fluorescence intensity of fractions from brain on S1, S2 and S3 fractions at 24 weeks obtained by solubility assay. Error bars are plotted ±S.E.M. The experiment was done for 3 individual experiments (n=3).Measurements were carried out in duplicates. ThT fluorescence of fractions displayed as fold change over monomer fluorescence. Unpaired t test shows that the fold increase of ThT is significantly different betwee the three fractions tested at 12 ($p=0.0189$) and 24 weeks of age ($p<0.0001$).The fold increase is significantly different between S1 and S2 at advance stage ($p<0.0001$). The fold increase of ThT is significantly different between S1 and S3 at early ($p= 0.0416$) and at an advance stage ($p<0.0001$). In addition, at advance stage, the fold increase between the S2 and S3 is significantly different ($p= 0.0050$). **D-b**) Hydrodynamic diameter of tau species measured by DLS and result expressed as a volume graph. **D-c)** Size distribution measured by DLS expressed as the fraction of components in the total sample evaluated. The particle size was obtained as an average of 3 measurements with 20 runs each (from 3 individual experiments n=3). Unpaired t test shows that the size distribution is not significantly different between the fractions at any stage studied. **D-d)** Detergent-insoluble specie (S3) from mice at early (12 weeks) and advance (24 weeks) stage of disease and imaged by AFM in tapping mode.

Now, the conformational changes between the largest aggregates / fibrillary species (NS) were examined using the same approaches as were used for the oligomeric preps.

### 6.4.4 Changes in β-sheet using ThT

When investigating structural changes associated in the NS fractions it was observed that the expression of tau also induce changes associated with the β-structure over time.

In the *Drosophila* model, a difference was observed between the three genotypes studied (OreR wt, htau$^{0N3R}$ and htau$^{0N4R}$). As previously observed with the GTO fractions in OreR wt flies, the fluorescence intensity of ThT in NS fractions is little affected with time, suggesting the absence of β-sheet structure. (**Figure 48 A-a**). In detail, the ThT fluorescence of both fractions (NS1 and NS2), is only a ~ 1-fold increase compared to the baseline (S1 at 0 weeks). As the time progress to 5 weeks, the ThT fluorescence of the NS2 fraction increases twice (**Figure 48 A-a**). This low fold increase suggests minimal interaction between the fractions and ThT at the different time points tested, suggesting the absence of the β-sheet structure. Unpaired t test was show no significant difference between the fractions tested during the distinct stages.

In flies expressing either the htau$^{0N3R}$ (**Figure 49**) or htau$^{0N4R}$ (**Figure 50**), the ThT fluorescence intensity of the NS1 fraction is ~ 3 times greater compared to the monomer fraction at early stage (**Figure 49 B-a** and **Figure 50 C-a**). However, the affinity of the NS1 fraction to ThT is ~ 6 times greater compared to monomer at an advanced stage in 4R-expressing flies (**Figure 50 C-a**), whereas in 3R flies the intensity remains the same (**Figure 49 B-a**). As for the NS2 fraction, the ThT affinity of 3R flies is ~ 3 times lower when compared to hTau$^{0N4R}$. This data also suggest that htau$^{0N4R}$ flies gave a higher β-sheet content. Unpaired t test shows that there is a significant difference between early and advance stages of disease. In particular, in the htau$^{0N3R}$ flies, the three fractions are significantly different between the stages at 0 and 5 weeks post-eclosion (p=0.0195 and p=0.0352 respectively).In htau$^{0N4R}$ flies the fractions are significantly different at 0 weeks post-eclossion (0.0069).

As for the P301S mutant tau-expressing animals, the NS1 fraction showed a minimal ~0.6-fold increase **(Figure 51 C-a**), suggesting the presence of mostly soluble and monomeric tau at both representative stages of disease. However, the fluorescence intensity increase in the fractions containing detergent-insoluble species (NS2). For instance, during the early stages of disease, the ThT fluorescence of the NS2 is ~4-fold higher compared to the monomers. These data suggest the structural reorganization of tau species at this early stage and may suggest that these fractions contain some β-sheet structure. Similarly, during the advanced state of pathology, the intensity of ThT fluorescence continues to increase significantly to a strong ~16-fold increase (**Figure 51 C-a**). Unpaired t test shows that the fold increase is significantly different between NS1 and NS2 at early stage (p= 0.0130).

Overall, this data suggests the transition from oligomers to polymeric aggregates is in line with the solubility assay.

### 6.4.5 Investigating size of tau species (NS) using DLS

In control flies, both NS fractions (NS1 and NS2) showed peaks with a diameter of <1 nm to ~ 3 nm (**Figure 48 A-b**), with an additional larger of ~12nm in the NS2 fraction. However, the small distribution size and the lack of interaction with ThT indicate the presence of mostly soluble non-aggregated species. In these Ore R wt flies, the populations remain constant over time (**Figure 48-a-b**).

In comparison, the expression of either htau$^{0N3R}$ (**Figure 49**) or htau$^{0N4R}$ (**Figure 50**) revealed a pronounced increase in the distribution size over time. In hTau$^{0N3R}$ flies, the NS1 fraction showed peaks with a diameter <1nm that remain constant over time. Followed by a larger population of ~15.54nm that increase to~42nm as the disease progress (**Figure 49 B.b**). This suggest that both monomers, oligomers and larger soluble aggregates might be contained in these fractions. Finally, a third population increases to an average diameter of ~851nm as the disease progress suggesting the presence of bigger proteins (**Figure 49 B-b-c**). As for the hTau$^{0N4R}$ flies, the NS1 fraction showed a small population with a diameter lower than 1nm and a larger population with a diameter of ~42nm that increase to ~400nm as the disease progress (**Figure 50 C-b**).

In htau$^{0N3R}$ flies (**Figure 49**), the size distribution of the NS2 fraction showed a major population with a diameter of lower than 1nm followed by a second population with a diameter of ~5nm, and a minimal population with a diameter up to 100nm during the early stages of disease. As the disease progress to an advance stage, the distribution shift to a diameter of ~1nm, ~200nm and ~500 to ~1000nm. In htau$^{0N4R}$ flies the size distribution of the NS2 showed a minimal population with diameter of ~2 to 15nm and a major distribution from ~200nm to 1000nm and up to 10000nm. In flies expressing the 4R isoform, the changes towards larger size distribution occur early (2.5 weeks) compared to 3R flies.

Similar to the observed in the fly model, the NS1 fraction generated from the P301S mouse model at early stages is characterized by the presence of a small population ranging from <1, 2 and 10nm (**Figure 51 D-b-c**). In addition to two larger populations from ~200 and ~400nm. As the disease progress, these distribution shift to a diameter of ~400, 900 and a population greater than 1000nm. When investigating the NS2 fraction, the presence of populations with a diameter of ~1nm, 3 to ~10nm. In addition to a larger population of ~20 followed by a distribution size ranging from 200 and grater ~1000nm. At the advance stage of disease, the size distribution showed diameters of ~50, ~300 to ~1000nm and grater.

Overall, this data shows that in both models, the expression tau causes an increase of the tau species compared to the monomers, suggesting aggregation and further polymerization. In addition, this data also shows that the formation of bigger aggregates caused by htau$^{0N4R}$ is greater than htau$^{0N4R}$.

### 6.4.6 Studying the morphology of tau species (NS) using AFM

Next, the morphology of the fraction from the pellet (NP1) obtained from the detergent-larger insoluble fractions (NS2) at early and advance stage, was evaluated using the AFM.

First, in OreR wt flies, the initial stage image topography showed the presence of smooth shapes irregularly distributed on the mica surface with an average height of ~ 2nm and a width of around ~ 0-10nm (**Figure 48 A-d** small arrows) suggesting the presence of small and possibly monomeric proteins. At advanced time points, similar small structures with a width of around ~ 0-10 nm (small arrows) and average height of ~ 2n were evident. In addition to the presence of some slightly larger structures with a width of around ~ 20-30nm (larger arrows) with a maximum height of around ~ 4nm. This data revealed structures similar to those observed in the fractions obtained in GTO that do not suggest oligomerisation given the lack of evidence of conformational alteration associated with β-sheet structure.

In the htau$^{0N3R}$ flies, it was observed that the topography of the image in early stage is characterized by the presence of globular and amorphous structures distributed irregularly. This globular structures have a cross sections ranging from ~10 to 50nm with a maximum height of about ~4nm (**Figure 49 B-d** small arrows). While in the htau$^{0N4R}$ they have a cross-sections ranging from ~40 to 80nm (**Figure 50 C-d-** small arrows and large arrows) (200nm scale bar) with a maximum height around ~10nm. In both expressing flies, the images also shown the presence of bigger amorphous structures with a cross section of up to 100nm (**Figure 49 B-d** and **Figure 50 C-d** large arrows) and a maximum height around ~16nm.

In addition, some structures with elongated characteristics were observed in htau$^{0N4R}$ flies at 2.5 weeks of age. These structures have widths of around ~60 to 80nm (**Figure 50 C-d** black arrows). As the disease progresses the structures showed across section ranging from 70 to 90nm. While in flies expressing the 3R isoform, these elongated structures with widths of around ~20nm and up to ~40nm were evident at advanced stages of the disease. These results suggest that the initially globular structures elongate with time, given the presence of abundant elongated structures at an advanced stage compared to the early stage.

In the P301S model, at the initial stage, most structures are globular and amorphous (**Figure 51 C-d**). These structures were characterized by widths of around 40-80 nm and even greater than 100 nm and a maximum height of ~13nm. By contrast, in the advanced stage, the most abundant structures are elongated aggregates. These elongated structures are between ~ 30 to 80 nm wide

(heights around ~ 8 nm) and some other structures also present at these late stage have larger widths up to ~ 170 nm and heights around ~ 20 nm.

In general, these data show that in both models, tau expression induces temporary changes in morphology. In particular, the early stages are characterized by the presence of a globular shape that increases in size with time. The advanced stage is characterized by the appearance of larger amorphous structures as well as the formation of elongated structures.

As mentioned above, it is important to consider the presence of several different components present in the analyzed fractions. Although, methods for isolating the fractions have been reported to enrich for tau proteins. It is important to consider the potential presence of other proteins and lipids as contaminants. For this reason, in this work, it is not entirely clear whether lipid forms or endogenous tau, such as dTau, play a role in our results. And for that, this remains to be determined in future studies.

**A-a** **Elav-GAL4/Ore R**

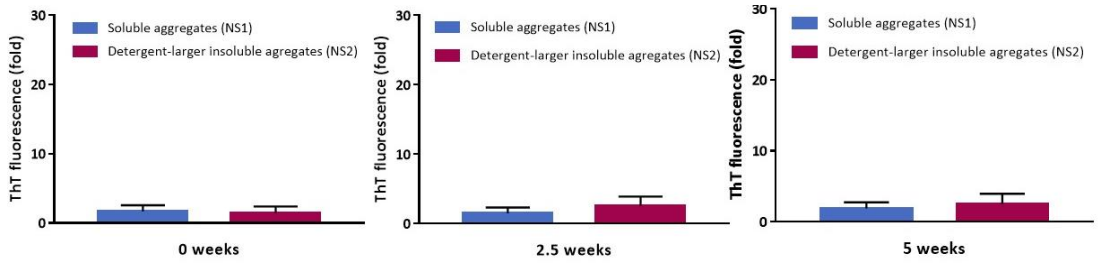


**A-b**

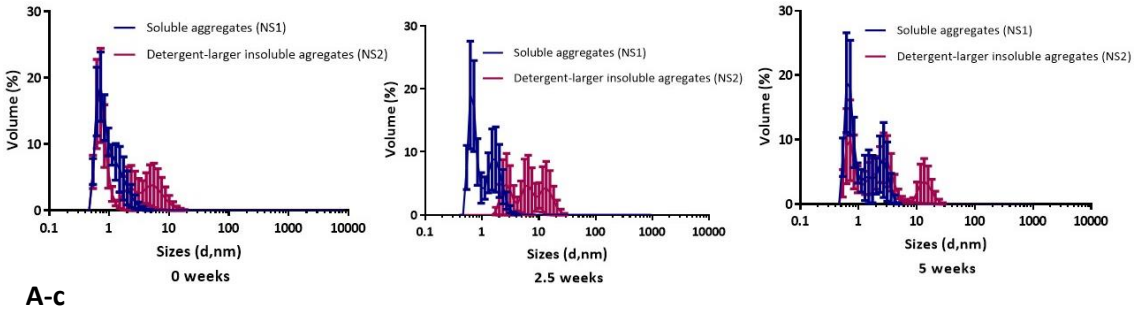


**A-c**

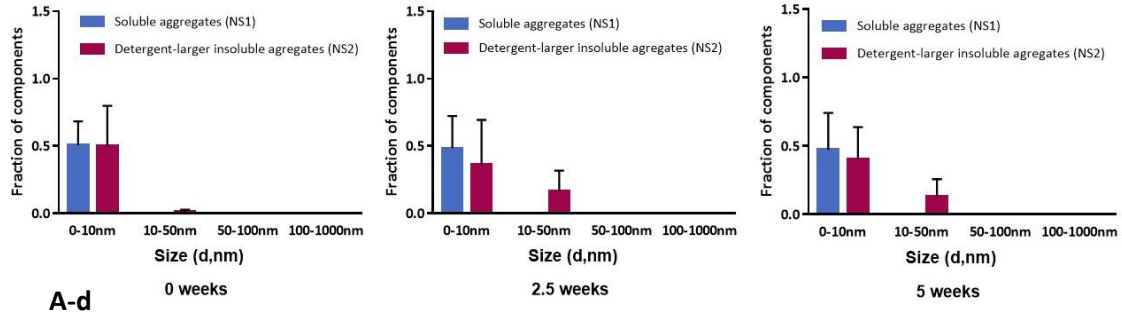


**A-d**

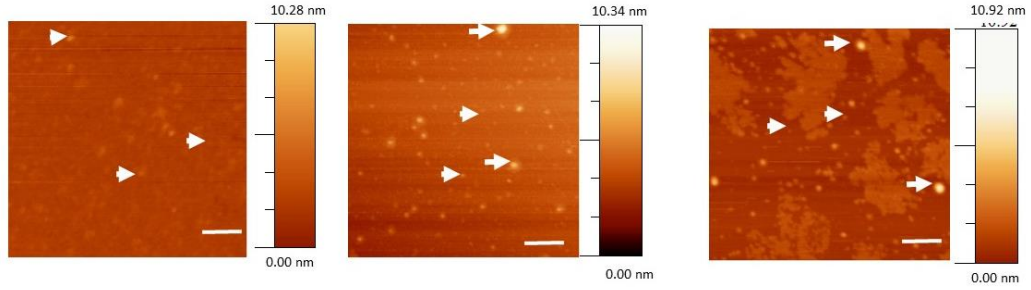

**Figure 48. Temporal structural and morphological changes in NS species at the early stage and advance stage of disease in OreR wt flies**

**A-a**) Comparison of ThT fluorescence intensity of fractions from adult heads flies on NS1 and NS2 fractions at 0, 2.5 and 5 weeks-post eclosion for Elav-GAL4 driven OreR wt obtained by solubility assay. The experiment was done for 2 individual experiments (n=2, from different crosses; using 100 fly heads for fractionation). Measurements were carried out in duplicates. ThT fluorescence of fractions displayed as fold change over monomer fluorescence.The Fold increase of ThT shows no significant difference between the fractions tested. Error bars are plotted ±S.E.M. Unpaired t test was used for analysis**. A-b**) Hydrodynamic diameter of tau species measured by DLS and result expressed as a volume graph. **A-c**) Size distribution measured by DLS and expressed as the fraction of components in the total sample evaluated. The particle size was obtained as an average of 3 measurements with 20 runs each, from 2 individual experiments (n=2, from different crosses). The unpaired t test shows that the size distribution is not significantly different between the fractions at any stage studied. **A-d)** Detergent-larger insoluble species (NS2) from adult flies at 0, 2.5 and 5 weeks post eclosion and imaged by AFM in tapping mode.

## Elav-GAL4/ htau$^{0N3R}$

**B-a**

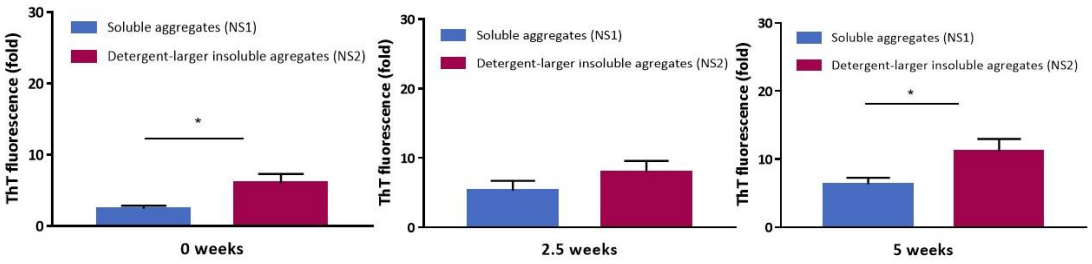


**B-b**

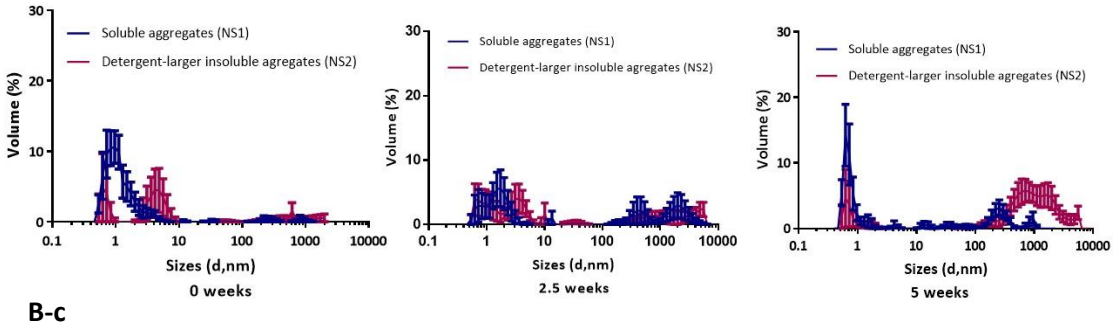


**B-c**

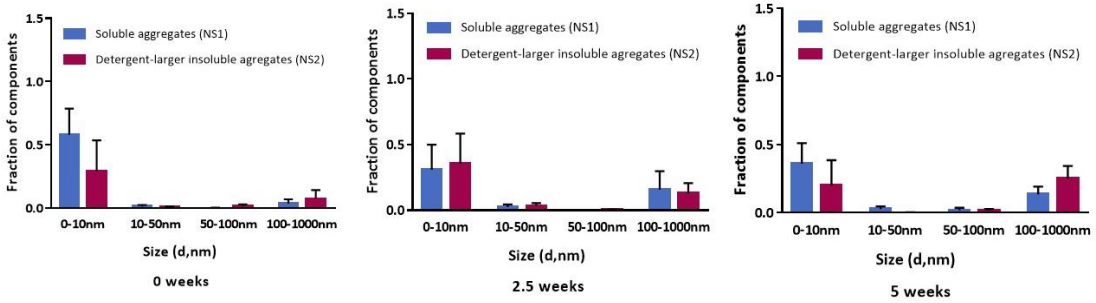


**B-d**

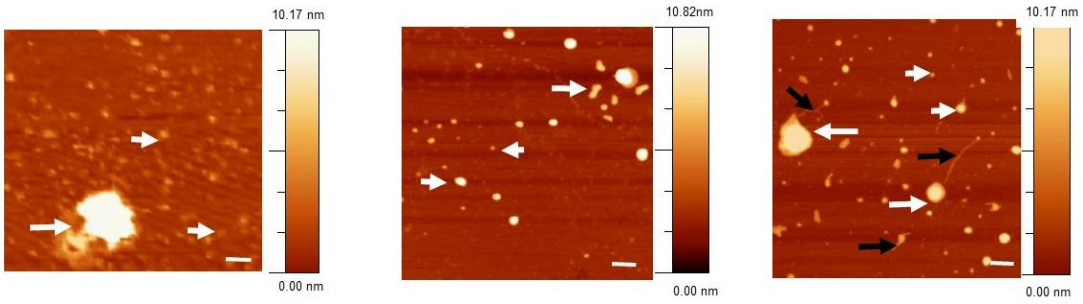

**Figure 49. Temporal structural and morphological changes in tau species at early stage of disease in htau$^{0N3R}$**

**B-a)** Comparison of ThT fluorescence intensity of fractions from adult fly heads on NS1 and NS2 fractions at 0, 2.5 and 5 weeks-post eclosion for Elav-GAL4 driven htau$^{0N3R}$ obtained by solubility assay. The experiment was done for 3 individual experiments (n=3, from different crosses; using 100 fly heads for fractionation). Measurements were carried out in duplicates. ThT fluorescence of fractions displayed as fold change over monomer fluorescence. Error bars are plotted ±S.E.M. Unpaired t test shows that the three fractions are significantly different between the stages at 0 and 5 weeks post-eclosion (p=0.0195 and p=0.0352 respectively). The **B-b)** Hydrodynamic diameter of tau species measured by DLS and result expressed as a volume graph. **B-c)** Size distribution measured by DLS and expressed as the fraction of components in the total sample evaluated. The particle size was obtained as an average of 3 measurements with 20 runs each, from 3 individual experiments (n=3, from different crosses). The unpaired t test shows that the size distribution is not significantly different between the fractions at any stage studied. **B-d)** Larger insoluble aggregate (NS2) from adult flies at 0, 2.5 and 5 weeks post eclosion and imaged by AFM in tapping mode.

## Elav-GAL4/ htau$^{0N4R}$

**B-a**

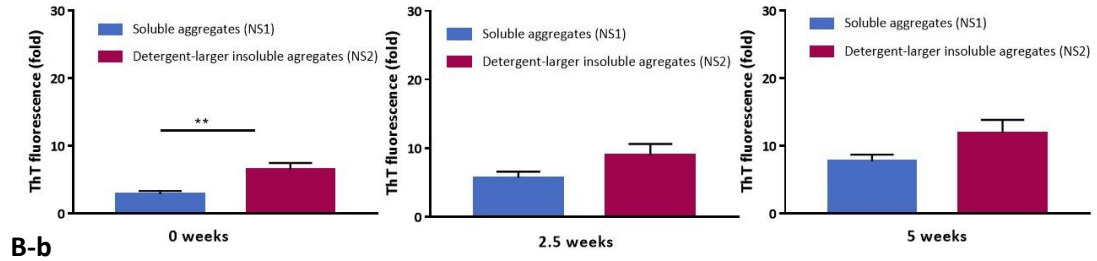


**B-b**

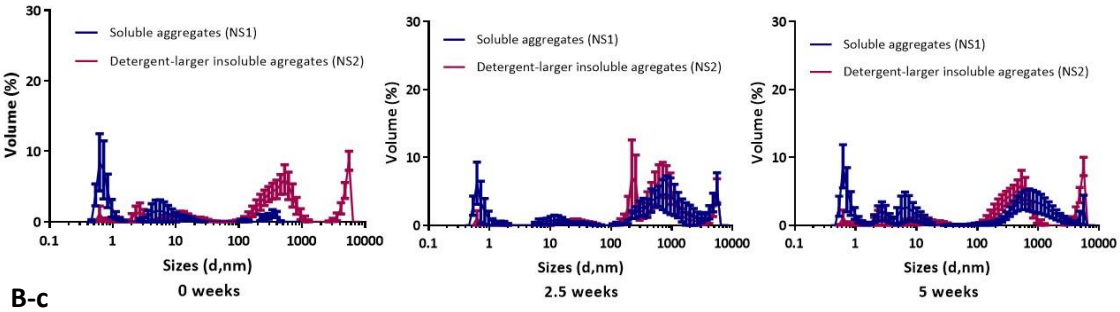


**B-c**

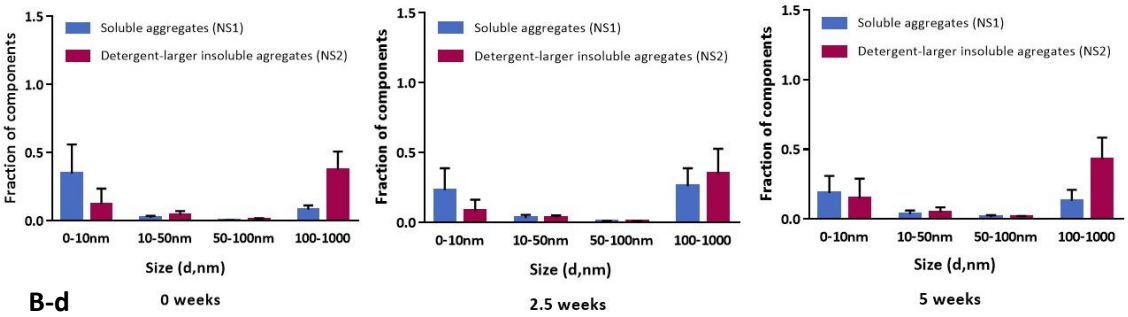


**B-d**

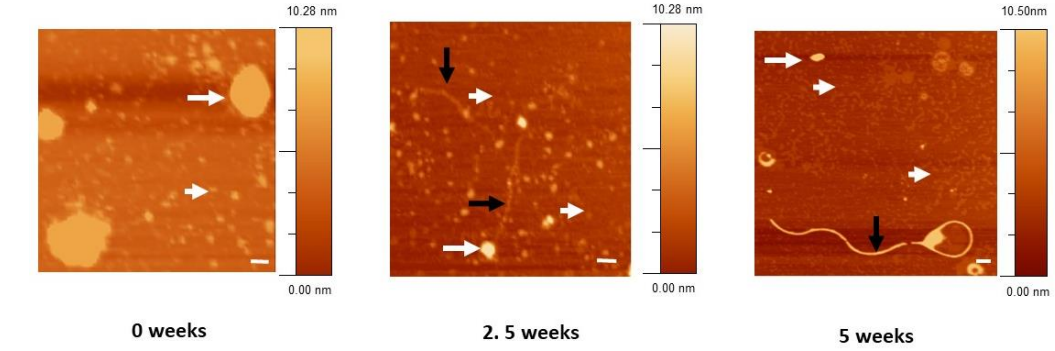

**Figure 50.Temporal structural and morphological changes in tau species at early stage of disease in htau$^{0N4R}$**

**C-a**) Comparison of ThT fluorescence intensity of fractions from adult fly heads on NS1 and NS2 fractions at 0, 2.5 and 5 weeks-post eclosion for Elav-GAL4 driven htau$^{0N4R}$ obtained by solubility assay. The experiment was done for 3 individual experiments (n=3, from different crosses, using 100 fly heads for fractionation). Measurements were carried out in duplicates. Measurements were carried out in triplicates (n=3). ThT fluorescence of fractions displayed as fold change over monomer fluorescence. Error bars are plotted ±S.E.M. Unpaired t test shows that the fractions (NS1 and NS2) are significantly different at 0 weeks post-eclossion (0.0069). **C-b**) Hydrodynamic diameter of tau species measured by DLS and result expressed as a volume graph. **C-c**) Size distribution measured by DLS expressed as the fraction of components in the total sample evaluated. The particle size was obtained as an average of 3 measurements with 20 runs each, for 3 individual experiments (n=3, different crosses).The unpaired t test shows that the size distribution is not significantly different between the fractions at any stage studied. **C-d)** larger insoluble aggregates (NS2) from adult flies at 0, 2.5 and 5 weeks post eclosion and imaged by AFM

**P301S**

**D-a**

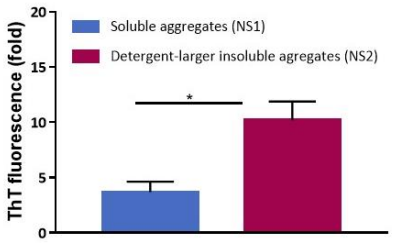


12 weeks

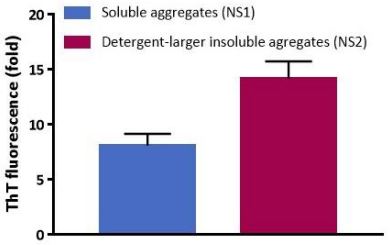


24 weeks

**D-b**

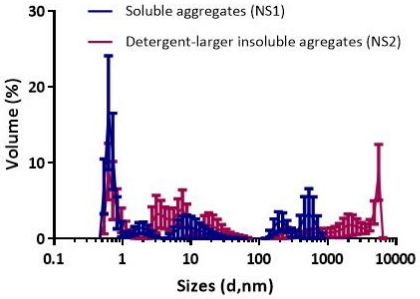


12 weeks

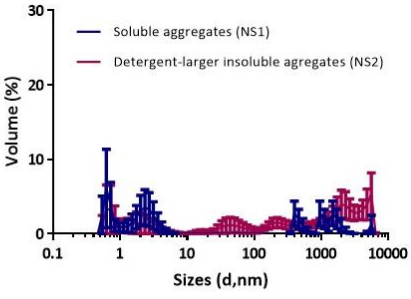


24 weeks

**D-c**

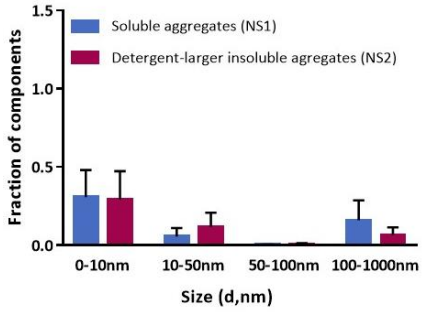


12 weeks

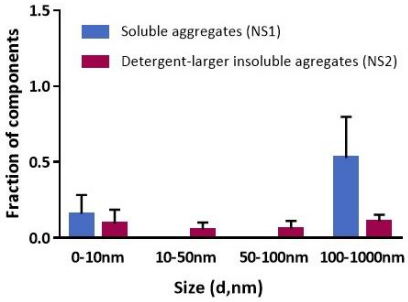


24 weeks

**D-d**

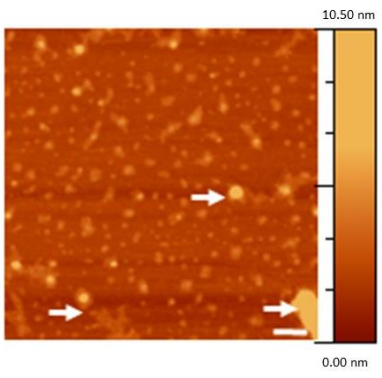


12 weeks

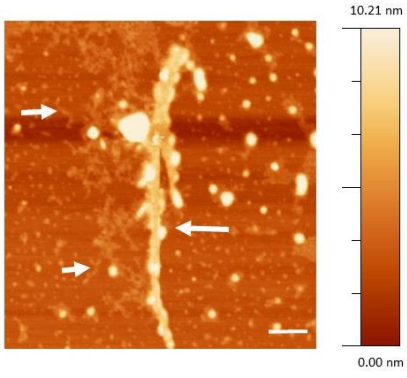


24 weeks

**Figure 51. Temporal structural and morphological changes in tau species at advance stage of disease in P301S**

**D-a**) Comparison of ThT fluorescence intensity of fractions from brain on NS1, and NS2 fractions at 24 weeks obtained by solubility assay (from 3 individual experiments, n=3). Error bars are plotted ±S.E.M. Unpaired t test shows that the fold increase is significantly different between NS1 and NS2 at early stage (p= 0.0130). **D-b**) Hydrodynamic diameter of tau species measured by DLS and result expressed as a volume graph. **D-c**) Size distribution measured by DLS expressed as the fraction of components in the total sample evaluated.The particle size was obtained as an average of 3 measurements with 20 runs each (3 individual experiments, n=3). **D-d**) Larger insoluble aggregates (NS2) from mice at early (12 weeks) and advance (24 weeks) stage of disease and imaged by AFM in tapping mode.

## 6.5 Discussions

### 6.5.1 Summary

The aim of this chapter was to explore in more detail the characteristics of the tau species responsible for the phenotypes observed in **Chapter 4**. The data presented here provide evidence suggesting that in both animal models, the expression of human tau induced gradual accumulation, aggregation and formation of tau species that resemble tau oligomers (GTOs). As described in **Figure 52**). These oligomers are evident at early stage when the phenotype appear and have altered conformation, low β-sheet content, and globular shape. During advance stage, the size and the β-sheet content of these species increase although the globular shape remains. Further polymerization produces larger insoluble aggregates / fibrillary species (NS) with increasing age, that resemble filaments when a degenerative phenotype is evident. The results obtained in this work are in line with oligomerization and fibrillation processes reported in the literature (as shown in **Figure 53** and **Figure 54**). Furthermore, this data suggest that the formation of elongated tau aggregates rich in β-sheets correlate better with neurodegeneration which is often seen at later stages of disease.

Additionally, our results also indicate that htau$^{0N4R}$ is more susceptible to aggregation because the biophysical changes in tau species were more evident in these flies than in flies expressing the 3R isoforms.

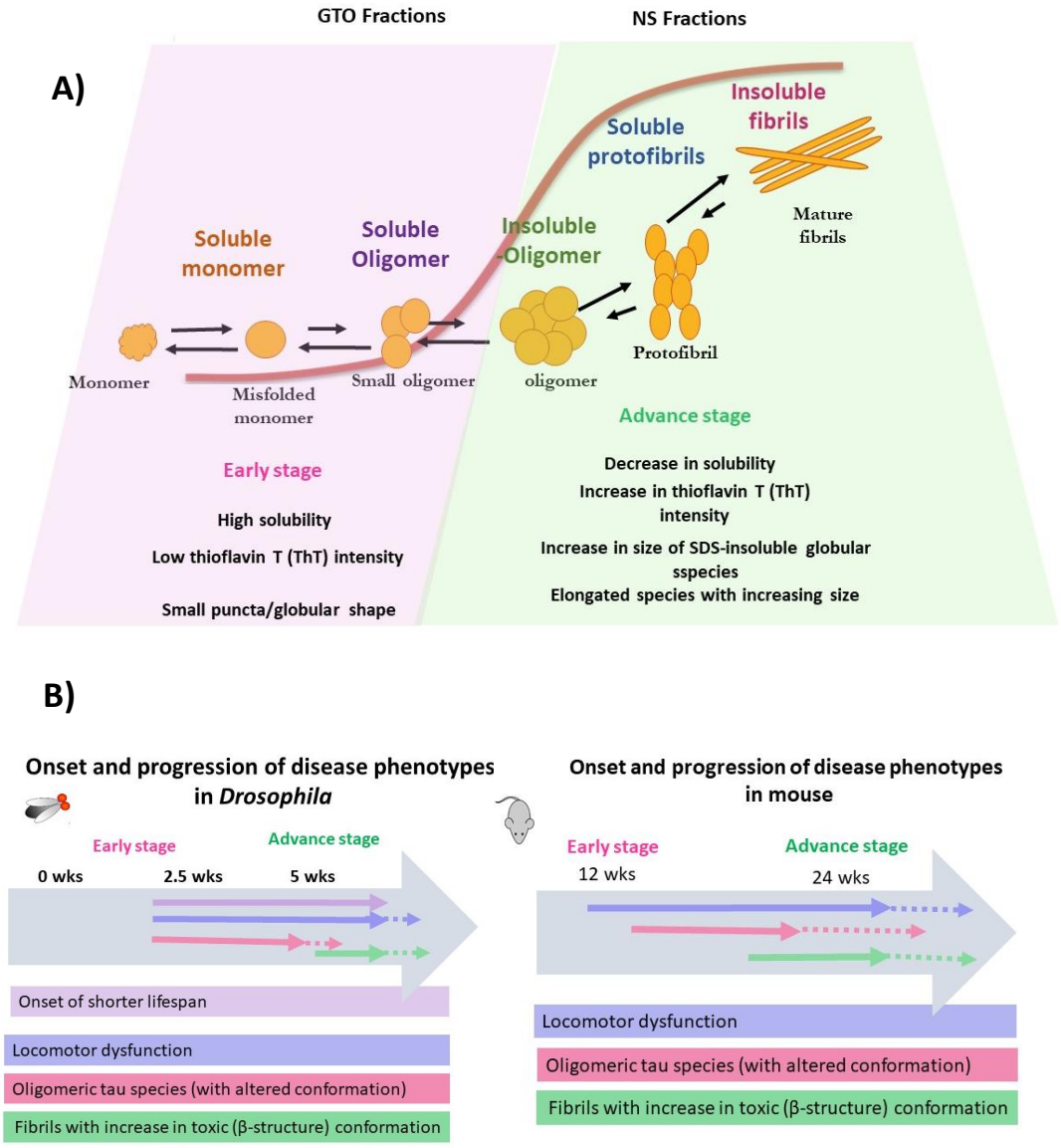


**Figure 52. Schematic representation of progression of the phenotype and changes in tau in models of tauopathy**

**A**) Shows a schematic representation of the oligomerization and fibrillation process in different stages. In the early stage, monomers undergo a conformational change, incorrectly fold, and associate to form oligomers. In advanced stage, formed granular oligomers grow rapidly to form elongated aggregates/larger fibrils rich in β sheet (high ThT intensity). **B**) shows the progression of the phenotype and tau changes. In both animal models, the expression of human tau induces the formation of oligomers (with low content of β sheets and globular form) which are evident at an early stage when the phenotype appears. During the advancement stage, the size and content of β sheets of these species increase although the globular shape is maintained. Further polymerization produces larger insoluble aggregates / fibrillar species (NS) with increasing age, resembling filaments when a degenerative phenotype is evident.

### 6.5.2 Degenerative phenotype is associated with increased β-sheet structure

Most neurodegenerative disorders such as tauopathies in humans are sporadic. Therefore, to model the disease in animals it is necessary to use transgenic lines that express mutations in the tau gene, found in FTDP-17, to accelerate neurodegeneration (Hutton et al., 1998; Goedert and Jakes. 2005). In line with this, this mutation has been shown to accelerate both oligomerization (Maeda et al., 2018) and the formation of the tau filament (Goedert et al., 1999; von Bergen et al., 2001). Specifically, tau filaments and tangles have been correlated with neuronal cell loss (Allen et al., 2002; SantaCruz et al., 2005; Maeda et al., 2006; Spires et al., 2006; Berger et al., 2007; Delobel et al., 2008; Xu et al., 2014; Sahara et al., 2013; Macdonald et al., 2019). These studies suggest that neurodegeneration is related to the ability of tau to aggregate abnormally.

The association between abnormal aggregation in abundant β-rich structures and degeneration has been demonstrated in both *Drosophila* and mouse model of tauopathy (Pasarella and Goedert, 2018; Macdonald et al., 2019). These studies collectively provide clues also suggesting that propensity of tau to aggregate and form abundant β-sheet-rich aggregates has a common pathway with neurodegeneration. A similar correlation has been shown in the two tauopathy models studied here, in which degeneration is evident as levels of β structure increase. For example, our results previously reported in **Chapter 4** suggest that flies that overexpress the 4R isoform show signs that could indicate greater degeneration compared to flies that express the 3R isoform. The observations in **Chapter 5** and this chapter suggest that the aggregates from flies expressing the 4R isoform have more insoluble species and more β-structure. This leads us to speculate that the propensity of the 4R isoform to aggregate plays a significant role in neurodegeneration.

As discussed in **Chapter 5**, in our *Drosophila* model in which the 3R and 4R isoform are compared the 4R isoform produce slightly more insoluble species suggesting that 4R tau is more susceptible to aggregation compared to 3R. Continuing with this notion, in this chapter it was found that the β structure of tau aggregates in 4R flies appears to interact with thioflavin T (ThT) approximately 3 times more than in flies expressing the 3R isoform. Furthermore, the bigger sizes and elongated species that promote the filaments were more evident in the $hTau^{0N4R}$ flies; these correlated well with the appearance of degeneration.

Quantification of the AFM topographic images corresponding to larger aggregates indicates that the number of species of aggregates increases slightly over time. Furthermore, the number of aggregates quantified in flies expressing the 4R isoform is slightly higher than the number of aggregates present in flies expressing the 3R isoform (**Figure 66** in **appendix C**). These data

demonstrate that aggregation in flies expressing $hTau^{0N4R}$ occurs slightly faster than in flies expressing $hTau^{0N3R}$ and correlate better with degeneration.

These differences between ability to aggregate and form the β-sheet rich structures in the isoforms could be explained by structural differences. It has been shown that the hexapeptides VQIVYK at the beginning of the third repeat domain, R3, and VQIINK in the second repeat domain, R2, are required for tau aggregation (Li and Lee, 2006, von Bergen et al., 2000). Removal of both hexapeptides prevents β-sheet assembly and seeding activity of full-length recombinant tau (Falcon et al., 2015). For instance, For example, it has been shown in both pro-aggregation inducible cell and mouse model (TauRD carrying the ΔK280 mutation) that aggregation and toxicity are related to the propensity of tau adopt β –structure (Khlistunova et al., 2007; Moncanu et al., 2008). In addition, hese authors demonstrated that the addition of proline, I277P and I308P mutations in the repeat domain (that nucleate β-structure), alters the formation of the β-structure preventing tau aggregation and neurodegeneration (Khlistunova et al., 2007; Moncanu et al., 2008).

For example, in the study by Khlistunova et al., 2007, it was reported that the expression of four repeated domains of the human tau construct that contains the two hexapeptide motifs (TauRD) and that carry the FTDP17 (ΔK280) mutation influences cell viability. By adding prolines in the repeat domain (nucleating the β structure), the inhibition of tau aggregation and toxicity was reported (Khlistunova et al., 2007). Similarly, in the study conditioned by Mocanu et al., it was reported that the expression of the pro-aggregating mutant TauRDΔ in the rodent brain induces the formation of aggregates (pre-tangle) and tau tangles at 2 months and evident neuronal loss at 5 months of age.

While the addition of proline mutations prevents the formation of NFT, the formation of the beta sheet structure, even in 22-month-old mice (Mocanu et al., 2008). Similarly, it has been shown in a *Drosophila* model expressing the human Tau-383 that eliminating the regions required for tau aggregation into β-sheet (Δ306–311) completely rescues the neurodegenerative phenotype (Pasarella and Goedert, 2018). These studies confirm that these hexapeptides play a critical role in the aggregation and formation of β-sheet, and that it, in turn, is directly associated with neurodegeneration. Thus, prevention of β-sheet formation prevents aggregation and neurodegeneration.

This could explain why 3R oligomerise and forms filaments but not as quick as in 4R-expressing flies. The ability of 4R to accelerate fibril formation could be explained due to the hexapeptide motifs

capable of form β-sheet rich structures. This could also explain the differences in the observed phenotype in **Chapter 4**.

### 6.5.3 The animal models studied here recapitulate the human disease process

Tau oligomers associated with AD and other tauopathies have been previously reported and characterized. These are in line with our observations where it was indicated a similar temporal increase in size during progression of disease to an advanced stage (**Figure 53**). For instance, Maeda et al demonstrated that the sizes of GTO purified from the human frontal cortex brain, Braak-stage 0 (non-AD) brain and a Braak-stage V (AD), vary from 5 to 50 nm in diameter, and the peak in size was around 35 nm in diameter under AFM (Maeda et al., 2007). These oligomers were β-sheet rich and insoluble as compared to filaments (Maeda et al., 2006). In addition, Ercan-Herbst et al, indicate that most of the oligomers isolated from the entorhinal cortex in the Braak 0-I stage (non-AD) contain structures between 5 and 10 nm in height by AFM. While the Braak III-IV stage (non-AD), includes larger oligomer varying from 10 to 30 nm in height (Ercan-Herbst et al., 2019). According to these studies, the results obtained in this thesis show that in the fly model, the oligomers range from 10 to 50 nm in width with a height around ~ 4 nm during the early stages. While heights of ~ 10 nm and sizes up to 100 nm wide were described for advanced disease stages. Similarly, in the P301S mouse model, the early stage oligomers have widths of about 20 and 50 nm and heights of about ~ 2 to 10 nm. Whereas, the largest structures have up to ~ 100 nm and heights of around ~ 20 nm during the advanced stages of the disease. Showing similarities with the reported oligomers.

Lasagna-Reeves et al. reported that tau oligomers from AD human brains with diameters from 5 to 15 nm under AFM were associated with toxicity *in vivo*. These were β-sheet rich and more hydrophobic compared to monomeric tau (Lasagna-Reeves et al., 2012). Some studies report a similar correlation between size, shape, β-sheet content, solubility and toxicity (Maeda et al., 2006; 2007; Kaniyappan et al., 2017; Hill et al., 2019). Overall, the results presented here are in line with previous observation about the major characteristic properties of a variety of tau at early and moderate stages of the disease (SantaCruz et al., 2005; Maeda et al., 2006; Spires et al., 2006; Kaniyappan et al., 2017) that also remain at late stages of disease (Maeda et al., 2006).

Oligomers generated *in vitro* from the recombinant human tau protein and associated with toxicity have been described and characterized. In a study by Kaniyappan et al. small and highly purified oligomers from a pro-aggregated tau repeat domain were reported to be the species responsible for synaptic toxicity without affecting cell viability, when exposed in the extracellular space, in cell

culture models and neural tissues (Kaniyappan et al. al., 2017). According to the authors, these oligomers represent early stages of aggregation and correspond to dimers to only a few larger oligomers. They have a globular/granular shape that corresponds from 2 nm to 15 nm with an average size of 20nm in diameter by AFM (as described in **Figure 53**), which were 5 times more hydrophobic and richer in a β-sheet structure compared to monomers (Kaniyappan et al., 2017)

In a more recent study, it was reported that recombinant tau oligomers from the 2N4R isoform induce synaptic dysfunction when injected directly into the brain of mice. The authors also reported a globular/granular shape by EM and an increase in β-structure compared to monomers. And a wide size distribution in which most of the particles measure between 18 and 32 nm by DLS (Hiil et al., 2019). These oligomers show similar characteristics to the distribution sizes of the oligomers (particularly insoluble fractions ¨S3¨) in this study, coming from both models. For example, size distributions were previously described in the *Drosophila* model, ranging from ~ 4 to 13nm during early stages. While the distribution increases to ~ 50 and ~ 70 nm in advanced stages. On the other hand, in the mouse model the oligomers increase their size distribution from ~ 4 to up to 300 nm, suggesting an increase in size due to the formation of high molecular weight aggregates. This suggests that structures with these similar characteristics could be responsible for the dysfunction in the *in vivo* models in the present study.

Filaments associated with AD and other tauopathies have been also isolated and described. Some of these filaments characterized by EM are shown in **Figure 55.**These studies have been reported paired helical filaments (PHFs) as a predominant component of tangles in Alzheimer's disease (Kidd 1963). These PHFs have widths between 8 and 20nm (Crowther 1991) and a cross section of 70–80 nm when studied on AFM (Crowther 1991; Maeda et al., 2007). Straight filaments (SF) (another component of tangles) were also observed to share similar sizes to PHFs when studied on EM (10 and 15nm width) (Crowther 1991) (**Figure 55**).

Similarly, filaments from P301S model have been described as half-twisted structure with an apparent width ranging from 5 to 10 nm in widths and a highly variable size in cross-section analysis when studied on EM (Allen et al., 2002) (**Figure 55**). These filaments were reported as high β-structure content, comparable to oligomers isolated from AD brains characterized by AFM (Maeda et al., 2007; Lasagna-Reeves et al., 2012) (as described in **Figure 54**).

According to the data presented here, it was identified that the cross-section of AFM images from *Drosophila* shows globular shapes with widths of around 10-60nm with a maximum height of ~4nm at early stages (**Figure 53**). These structures resemble oligomeric species from AD brain, as previously described by other groups as shown in **Figure 53**. As the disease progresses, the widths

increase to ~20nm-80nm with a maximum height of about ~10nm. Interestingly, although the shapes are similar between flies expressing 3R and 4R tau, larger sizes were slightly more frequent in flies expressing the 4R isoform. In the P301S mice model, the GTOs were characterized by widths of around 40-80 nm and even greater than 100 nm and a maximum height of ~13nm. These results suggest that our model shares some characteristics with the reported by Maeda et al., 2006; 2007; Hill et al., 2019, as described in **Figure 53**. Further *in vitro* characterization of GTOs from the AD brain using DLS has indicated that a single granular tau oligomer with a DLS peak around 55 nm consists of 40 tau molecules (Maeda et al., 2007). This observation suggests that large oligomer structures in our models could be made up of more than 40 tau molecules formed during the aggregation process as described by Maeda et al., 2007 (**Figure 53**).

As for the filaments, data suggest the presence of filaments in htau$^{0N4R}$ flies at 2.5 weeks of age. These structures have a variable most closely resembles that of straight, unpaired filaments, size in cross-section and widths of around ~10nm at wides point and up to~80 nm at advanced stages of the disease. While in flies expressing the 3R isoform, these elongated structures with widths between~ 20 and ~40nm are evident only at advanced stages of the disease. Similar characteristics have been reported in some *Drosophila* models when characterized by EM (Jackson et al., 2002; Colodner and Feany 2010; Wu et al., 2013) (**Figure 55**). In the P301S model these elongated structures with a cross section of ~ 30 to 80 nm wide and heights around ~ 8 nm, these species resemble the filaments described by EM in this model (**Figure 55**).

In both models these measurements are within the size range of 75 to 550nm length, 8 to 40nm width observed in human filaments and other models (**Figure 54** and **Figure 55**). We provide evidence suggesting that our two models recapitulate the human disease process. Additionally, compared to other approaches used to study tau assembly, the tau species extracted directly from the brains of animals using GTO and NFT enrichment protocols were interrogated.

| Oligomers from model: | Thioflavin (Fluorescence intensity) | | DLS (nm ) | | AFM (nm) | | Reference |
|---|---|---|---|---|---|---|---|
| | Early time point | Late time point | Early time point | Late time point | Early time point | Late time point | |
| Human 0N3R Fly model | Low | High | 12 diameter | 32 diameter | 5-50 width | 10-60 width | This thesis |
| | | | | | 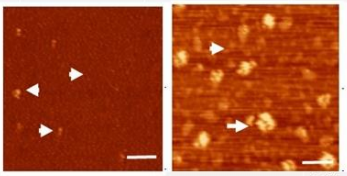 | | |
| Human 0N4R Fly model | Low | High | 10 diameter | 35 diameter | 5-60 width | 20-80 width | This thesis |
| | | | | | 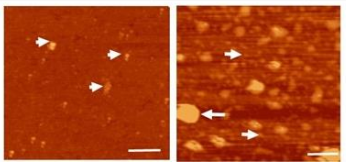 | | |
| | Early time point | Late time point | Early time point | Late time point | Early time point | Late time point | |
| P301S Mouse model | Low | High | 9 diameter | 35-300 diameter | 10-60 width | >80 width | This thesis |
| | | | | | 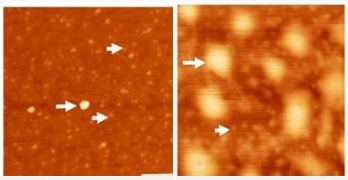 | | |
| Human AD Brain (GTOs) | -n/a | -n/a | -n/a | -n/a | 5-50 diameter (Braak stage 0) | 5-50diameter (Braak stage 0) | Maeda et al.,2006; 2007 |
| | | | | | 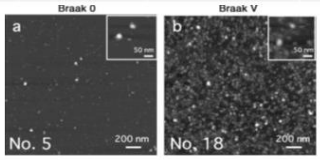 | | |
| Human Brain | --n/a | --n/a | --n/a | -n/a | 5-10 Height (0-I of Braak) | 10-30 height (Braak stage III-IV) | Ercan-Herbst et al., 2019 |
| | | | | | 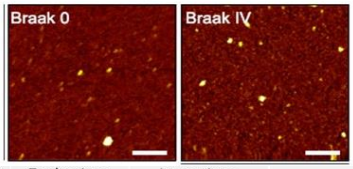 | | |
| | Early time point | Late time point | Early time point | Late time point | Early time point | Late time point | |
| Human AD brain (small oligomers) | Low | | n/a | n/a | ~ 4-8 (diameter) | n/a | Lasagna-Reeves et al., 2012 |
| | 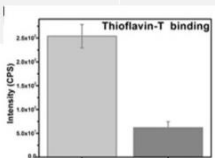 | | | | 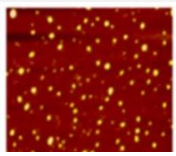 | | |

**Figure 53. Characterization of tau oligomeric species reported in this thesis and examples of published studies**

| Filaments (pre-filaments) from model: | Thioflavin (Fluorescence intensity) | | DLS (nm ) | | AFM (nm) | | Reference |
|---|---|---|---|---|---|---|---|
| | Early time point | Late time point | Early time point | Late time point | Early time point | Late time point | |
| Human 0N3R Fly model | High | High | <200 | >200 | Globular ~20 to >40 widht | Elongated species with ~20 widht | This thesis |
| Human 0N4R Fly model | High | High | <200 | >200 | Globular >60 Elongates 10 width | And elongated ~80 nm width | This thesis |
| P301S Mouse model | High | High | <200 | >200 | Globular shape~ 30 to 80 nm widht | Elongated species with 30>80 widht | This thesis |
| Human AD Brain | n/a | High | -n/a | -n/a | -n/a | PHF 10-11 and 14-16 heiths | Maeda et al., 2007 |
| Human Brain | -Low | High | --n/a | -n/a | -n/a | Classical morphology PHF | Lasagna-Reeves et al., 2012 |

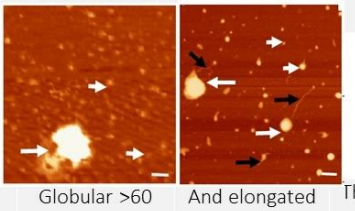

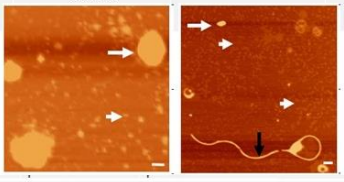

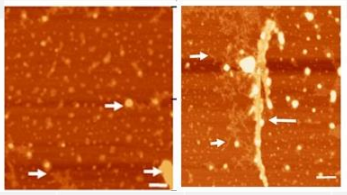

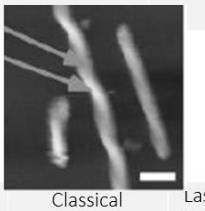

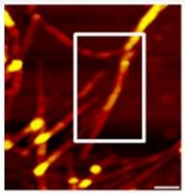

**Figure 54. Characterization of tau filaments reported in this thesis and examples of published studies**

| Filaments (pre-filaments) from model: | Thioflavin (Fluorescence intensity) | | DLS (nm ) | | EM (nm) | | Reference |
|---|---|---|---|---|---|---|---|
| | Early time point | Late time point | Early time point | Late time point | Early time point | Late time point | |
| P301S Mouse model twister ribbons and PHF | n/a | n/a | n/a | n/a | n/a | ~5-10 Width EM 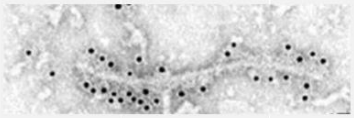 | Allen et al., 2002 |
| Human AD Brain PHF (P) and SF (S) | n/a | n/a | n/a | n/a | n/a | PHF ~8-20 nm (Width) EM SF:width from 10 to 15 nm 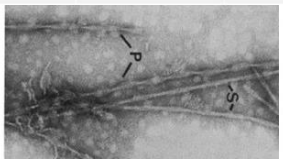  | Crowther 1991 |
| Human 0N4R Fly model SF | n/a | n/a | n/a | n/a | n/a | >410 long 40-60 widht 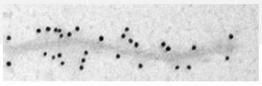 | Colodner and Feany 2010 |
| Human 2N4R Fly model PHF and SF | n/a | n/a | n/a | n/a | n/a | >410 long 15–40 widht  | Wu et al., 2013 |
| Human 2N4R Fly model PHF and SF | n/a | n/a | n/a | n/a | n/a | PHF:410 nm long and 30nm wide 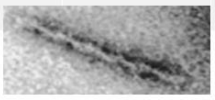 | Jackson et al., 2002 |

**Figure 55. Examples of published studies characterizing filaments from AD brains, fly models and P301S mouse model**

## 6.6 Conclusions and future directions

This study provides evidence to suggest that our two models recapitulate the disease process observed in humans. Additionally, this data suggests that dysfunction may be due to granular tau oligomers (GTOs) while degeneration may be induced to larger tau aggregates (pre-NFT) with abundant β-sheet structure. Furthermore, this study provides information on detailed properties of the tau aggregate species that are related to the phenotype in our two models of tauopathies.

In this thesis, now that both the initial and advanced stages of the disease have been identified in *Drosophila*, and the biochemical and biophysical characteristics of the tau species responsible for the onset and progression of the disease have been elucidated, it is now possible to evaluate a potential inhibitor of tau aggregation as a treatment for tauopathies. For this an additional line of *Drosophila* model expressing the UAS-htau$^{2N4R}$ transgene in the brain will be used.

# Chapter 7 Tau aggregation inhibitor

## 7.1 Introduction

Having shown that the overexpression of htau$^{0N3R}$ and htau$^{0N4R}$ in the central nervous system (CNS) induces characteristic phenotypes of the disease and that these are accompanied by accumulation of tau protein aggregates, the **Aim** of this chapter is **to study the effect of a tau aggregation inhibitor in a *Drosophila* model as a potential treatment of tauopathy.**

*My hypothesis in this chapter is that a peptide-based tau aggregation inhibitor (*RI-AG03) *prevents progression of disease phenotype in a Drosophila model of tauopathy*

Tauopathies are a complex spectrum of heterogeneous neurodegenerative disorders that affect millions of people around the world. Currently, there are no disease-modifying treatments available clinically. As exception, two drugs, Riluzole (an inhibitor of glutamatergic neurotransmission) and Edaravon (an antioxidant drug) are currently approved for clinical use in the treatment of amyotrophic lateral sclerosis disorder-FTD (ALS). However, they have limited efficacy in delaying the deterioration of motor function (Jaiswal, 2019). Therefore, development of drugs to treat tauopathies remains urgent.

The association between abnormal tau aggregation and pathogenesis has led to the design of treatments focused on the inhibition of tau aggregation. To this end, some approaches have focused on the study of compounds with aggregation inhibitory properties *in vitro* and in animal models. For example, N-phenylamine compounds (B4D3, D1C11, and B4A1) have been shown to inhibit tau aggregation and disassemble preformed aggregates in a cell model of tau aggregation (N2a neuroblastoma cell lines) expressing the domain of tau repeat with deletion mutant ΔK280. (TauRD ΔK280) (Khlistunova et al., 2005). In this particular study, cell lines were created expressing different variants of the tau repeat domain (TauRD), wild-type, pro-aggregation, and anti-aggregation mutants. What the authors have concluded is that aggregation is toxic and that the degree of toxicity is dependently related to β-sheet propensity. It therefore shows that the development of inhibitors aimed at preventing β-sheet formation can have positive effects on tau aggregation and cell degeneration.

Another example, long-term phenothiazine treatment, such as methylthioninium chloride (methylene blue), has been found to reduce abnormal accumulation of phosphorylated tau, altered conformation, and insoluble tau, in a P301L transgenic mouse model of tauopathy (Hosokawa et al., 2012).Therefore, it is suggested that methylene blue has disease-modifying activity to attack tauopathy.

Similarly, in another study carried out by Hochgräfe et al., it was shown that methylene blue reduces tau phosphorylation, insoluble tau and pathological conformation in an inducible pro-aggregating mice model of tauopathy. In their study, two variations of the mouse model were used. One line expressing full-length pro-aggregating human 2N4R tau with deletion mutant ΔK280 (TauΔK) and another expressing the pro-aggregating tau repeat domain TauRD-ΔK280 (TauRDΔK). The authors also showed that cognition can be preserved when treatment begins before the onset of cognitive deficits in the TauΔK mouse model. However, these results cannot be achieve in second line expressing the tau repeat domain TauRD-ΔK280 (TauRDΔK) that cause a more severe aggregation and phenotype, even when applied at young age before the onset of cognitive deficit (Hochgräfe et al., 2015). These results suggest that the efficacy of methylene blue is related to the stage of the disease and the propensity for tau to aggregate (Hochgräfe et al., 2015).

Despite the demonstrable efficacy of methylene blue in these models, these treatments failed in subsequent clinical trials (Gauthier et al., 2016; Medina, 2018). More recently, a new formulation of a stable reduced form of methylthioninium has reached phase 3 clinical trials under the name LMTM (TauRx Therapeutics). However, new treatments are urgently needed to improve the course of diseases.

Over the years, different approaches to identifying effective strategies against tauopathies have emerged. Some reported inhibitors of tau aggregation have been designed based on the recognition and subsequent modulation of certain amino acid sequences in the tau protein. These amino acid sequences are two hexapeptide segments in the repeat domains that interact with microtubules but also play an important role in pathological tau aggregation.

In particular, the $^{306}$VQIVYK$^{311}$ hexapeptide at the beginning of the third repeat domain and $^{275}$VQIINK$^{280}$ at the N-terminus of the second repeat region is known to be critical in driving tau protein aggregation and the ability to form a β-sheet structure (Von Bergen et al., 2000; von Bergen et al., 2001; Li and Lee, 2006; Bulic et al., 2010). Through studies based on NMR spectroscopy, it has been shown that these hexapeptides adopt a rigid structure of β-sheet forming the core of

filaments (Daebel et al., 2012). Additional studies have shown that these hexapeptides adopt a different conformation when bind to microtubules. This indicates that the conformation of the hexapeptide regions must be destabilized so tau misfold into a pathogenic β-sheet structure during aggregation (Kadavath et al., 2015).

Since the ability of these hexapeptides to form a β-sheet structure and lead to pathology, it has been demonstrated that their modulation can be achieved by mutations. For example, it has been shown in both pro-aggregation inducible cell and mouse model (TauRD carrying the ΔK280 mutation) that by adding proline, I277P and I308P mutations in the repeat domain (that nucleate β-structure) the aggregation of tau is inhibited. These authors suggest that the addition of proline alters the formation of the β-structure preventing tau aggregation (Khlistunova et al., 2007; Moncanu et al., 2008).

Following the same line Haj and colleagues demonstrated that the palmatine chloride alkaloid (PC) compound interacts with the key residues (VQIVYK) responsible for the formation of the β sheet, in this way the compound inhibits the assembly and disassembles already formed aggregates *in vitro* (Haj et al., 2018). Similarly, the structure of the VQIVYK has also served to design inhibitors, such peptides, capable of blocking the ends of the filaments and thus preventing the progression of tau aggregation (Sievers et al., 2011; Seidler et al., 2018). More recently, the crystal structure of VQIINK of the 4R domain has been studied in order to design inhibitors effective in stopping the aggregation and seeding of tau containing 3 repeats (3R) and full-length tau under *in vitro* conditions (Seidler et al., 2018). Collectively these studies demonstrate that these motifs serve as a platform for understanding pathology and for the design of aggregation inhibitors

Consequently, this chapter seeks to study the potential of an inhibitor as a possible treatment of tauopathies in a *Drosophila* model. This tau inhibitor is based on a peptide effective against the above relevant sequences in order to avoid pathogenic aggregation. The tau aggregation inhibitor (RI-AG03) was synthesized, tested and kindly provided by Dr. Anthony Aggidis, as a novel treatment for tauopathies in a *Drosophila* model. Dr. Aggidis found that under *in vitro* conditions RIA-G03 was found to inhibit more than 90% of tau aggregation Tau251-441 (TauΔ1-250) fragment in the presence of heparin. The inhibition of TauΔ1-250 was confirmed by thioflavin-T fluorescence assay, transmission electron microscopy, circular dichroism, and Congo red birefringence. Furthermore, when tested in a *Drosophila* model of a rough eye, a suggestion was found that RIA-G03 partially rescued the phenotype in this model which was caused by degeneration following expression of 2N4R tau. Therefore, to study in more detail the effect of RIA-G03 *in vivo*, it was decided to use a *Drosophila* model expressing the longest isoform of human tau, htau$^{2N4R}$, in the central nervous

system. The effect of the inhibitor was studied on the two phenotypes longevity and locomotor behaviour (described in **Chapter 4**). Finally, the impact of the inhibitor on the tau species present in the *Drosophila* model was evaluated using the solubility assay (described in **Chapter 3**).

## 7.2 Summary of aims and objectives:

**Aim 4. To study the effect of a tau aggregation inhibitor in a *Drosophila* model as a future potential disease modifying therapy**

Objective 1: Evaluate the effect of a tau aggregation inhibitor in longevity and climbing behaviour in *Drosophila* model of tauopathy.

Objective 2: To isolate the aggregates of tau (NS) species present in the *Drosophila* model to investigate whether this inhibitor has an effect on tau solubility in our *Drosophila* model.

## 7.3 Results

### 7.3.1 Tau-aggregation inhibitor rescues tau-induced longevity deficits in a *Drosophila* model of tauopathy

The effect of RI-AG03 tau aggregation inhibitor on the phenotype was studied in an additional *Drosophila* model selected in order to follow up a previous study conducted in our laboratory expressing the UAS-htau$^{2N4R}$ transgene in the eye. In this chapter, the effect of RI-AG03 tau aggregation inhibitor on both, the longevity and locomotor activity was studied in *Drosophila* expressing the -htau$^{2N4R}$ in the brain (n=50). The studies were conducted by Hannah Lucas and Dr. Shreyasi Chatterjee. These drugs were added to the fly-food and crosses were set up in duplicates for each genotype and each drug concentration which was a low (LD) and high (HD) dose of the RI-AG03 tau aggregation inhibitor (0.08 µM and 0.8 µM). The concentrations were selected after preliminary studies.

Their longevity and climbing behavior were performed with standardized protocols from our laboratory and described in detail in **Chapter 3**, every week for a period of 6 weeks. Survival analysis was carried out using GraphPad Prism software and a Kaplein-Meir curve was plotted. A Log-rank (Mantel-Cox) test was performed on the data. As described below the expression of htau$^{2N4R}$ resulted in a disease phenotype and treatment with both the low (LD) and high (HD) dose of RIA-

G03 resulted in a significant improvement in the observed phenotype, though it did not take it back to control levels.

In this study, both untreated and treated htau$^{2N4R}$ expressing flies have a significantly shorter lifespan compared to controls (<0.0001) (**Figure 56**). Here, the phenotype begins around 1 weeks (7 days) post-eclosion when htau expressing flies start to die. Whereas in OreR wt flies the onset of the phenotype is observed at 3 weeks (21 days) post-eclosion. The median lifespan of htau$^{2N4R}$ flies without treatment is 3.7 weeks (26 days) and it is at 7.5 weeks (53 days) post-eclosion when all flies die (as shown in **Figure 56**). In contrast, the median lifespan in wt flies is 9.5 weeks (67 days) and all these flies die after 12 weeks (84 days) post-eclosion.

By comparison, treatment with inhibitor significantly delayed the onset of the phenotype. Htau$^{2N4R}$ flies treated with low and high doses have a median lifespan of 4.7 weeks (33 days) and 5 weeks (35 days) respectively. In both treated tau flies, the survival decline to 10 % at 8.5 weeks (60 days) and all flies died after 10 weeks (70 days) post-eclosion. Overall flies expressing the htau$^{2N4R}$ have a significantly shorter lifespan compared to htau$^{2N4R}$ post treatment with low doses (LD) (p=0.0007) and high doses (HD) (p=0.0004) (**Figure 56**).

Overall, this data shows that treatment with both low (LD) and high (DH) doses of inhibitor significantly improved the lifespan of hTau$^{2N4R}$ flies, extending it by 2.5 weeks (almost 20 days) but did not take it back to control levels.

A)

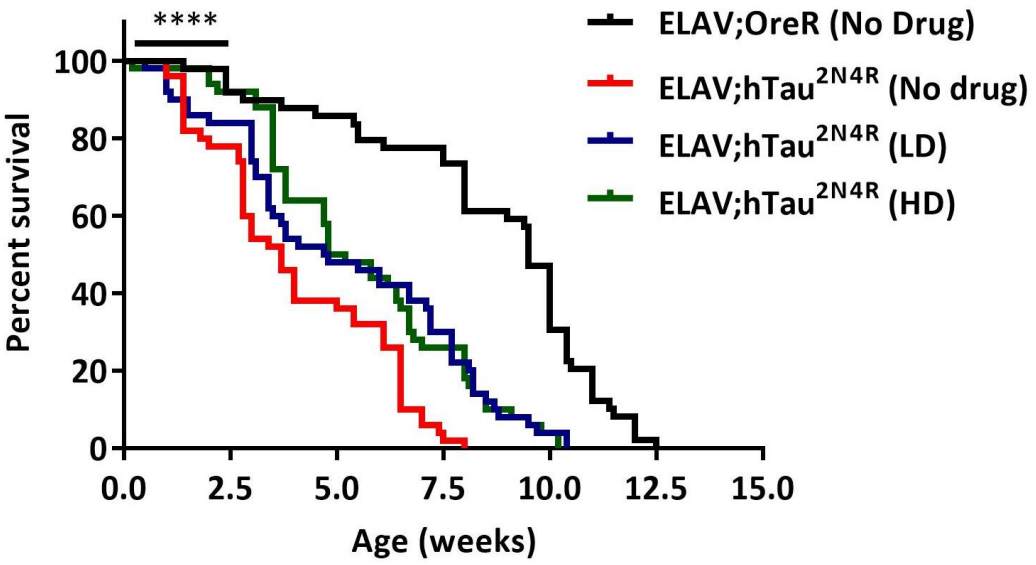


B)

| Median Survival (weeks) | | | |
|---|---|---|---|
| WT | Htau$^{2N4R}$ (ND) | Htau$^{2N4R}$ (LD) | Htau$^{2N4R}$ (HD) |
| 9.5 (Weeks) 67 (Days) | 3.7 (Weeks) 26 (Days) | 4.7 (Weeks) 33.5 (Days) | 5 (Weeks) 35.5 (Days) |

**Figure 56. Tau aggregation inhibitor delays premature death in flies expressing htau**

A) Survival curves for Elav-GAL4 driven htau$^{2N4R}$ performed over a period of 6 weeks shows that the lifespan of control flies are not significantly improves post drug treatment. The lifespan of the tau flies are increased significantly post treatment by 0.08µM and 0.8µM concentration of RI-AG03 (n=50). (Log-rank, Mantel-Cox test p <0.0001). Control= (Elav-Gal4/UASOreR), tau= (Elav-GAL4/UAShtau$^{2N4R}$).B) Table showing median survival. By comparison, htau$^{2N4R}$ flies without treatment die quicker than both htau$^{2N4R}$ post treatment and OreR wt control flies. OreR wt and htau$^{2N4R}$ (ND) have a median lifespan age of 9.5 weeks and 3.7 weeks respectively whereas htau$^{2N4R}$ post treatment either with high or low doses has a median lifespan of around 5 weeks. This results, indicates that treatment with RI-AG03 delays premature death in the flies expressing htau$^{2N4R}$.

### 7.3.2 Tau-aggregation inhibitor rescues tau-induced locomotor deficits in a *Drosophila* model of tauopathy

The climbing assay was performed on 5 cohorts of 10 adult male flies from each group housed in their testing cohorts (n=50). Flies were placed in cylinders and the assay was conducted by tapping flies to the bottom of the cylinder and recording the time taken for flies to climb up the sides of the measuring cylinder. The distance climbed by the flies was recorded at 10s. The assay was repeated three times, with 2 minute and the procedure was repeated 2 more times and the flies were placed onto fresh drug food the following week. 2-way ANOVA was used for Statistical Analysis via Graphpad Prism Software.

As with the longevity assay, the climbing ability of flies expressing $hTau^{2N4R}$ pan-neurally displays severe deficit compared to control flies (**Figure 57**). Here, the phenotype begins as soon as they eclosed when the ability to climb is about 40% less compared to control flies and decreases rapidly as flies age to 4 weeks (28 days) post-eclosion. By 5 weeks (35 days) the flies are virtually immobile, displaying a severe motor dysfunction.

In contrast, the climbing ability of flies expressing $hTau^{2N4R}$ treated with LD of RI-AG03 , deficit begin to emerge around 1 week (7 days) post-eclosion, when the ability to climb is about 20% less compared to control flies and progresses over time. Whilst the untreated $hTau^{2N4R}$ flies are immobile at 5 weeks (35 days) of age, treated $hTau^{2N4R}$ flies continue to maintain some locomotor ability at this age. This suggests an improvement in their locomotor behaviour although not significant at this time point. Two-way ANOVA test shows that the climbing ability of untreated $htau^{2N4R}$ and $htau^{2N4R}$ flies treated with LD of RI-AG03 are significantly different at 0-3 days ($p=0.0002$) and 1 weeks (7days) ($p= 0.0487$) weeks post-eclosion.

Similar results with a small but significant improvement in the phenotype is observed in flies expressing $hTau^{2N4R}$ reared on high doses (HD) of RI-AG03 tau aggregation inhibitor. Importantly, the treatment did not have an effect on locomotion in control flies, indicating that the protective effect is specific to tau protein aggregation (**Figure 57**). Further demonstrating that RI-AG03 tau aggregation inhibitor appears to counter tau-specific, possibly aggregation of tau in this *Drosophila* model. Two-way ANOVA test shows that the climbing ability of untreated $htau^{2N4R}$ and treated $htau^{0N4R}$ flies treated with HD of RI-AG03 are significantly different at 0-3 days ($p=0.0379$), at 1 week (7 days) ($p= 0.0263$), at 2 weeks (14 days) ($p=0.0445$), 4 and 5 weeks post- eclosion ($p=0.0347$) ($p=0.0255$) respectively.

Overall this data shows that treatment with both low (LD) and high (DH) doses of RI-AG03 in htau$^{2N4R}$ flies significantly improves the locomotion phenotype induced by expression of tau.

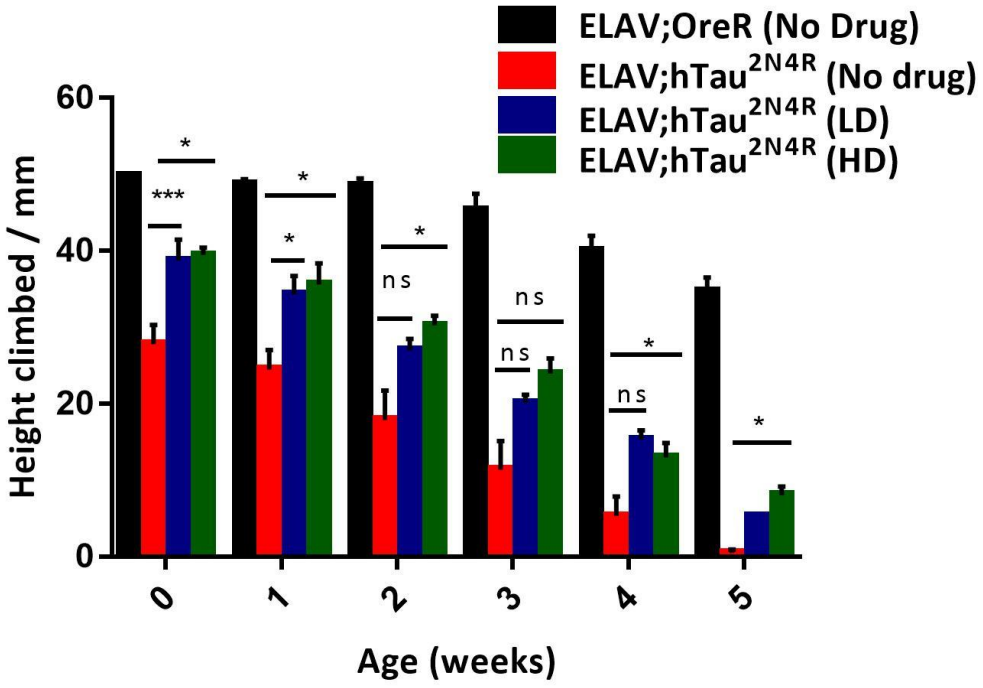


**Figure 57. Tau aggregation inhibitor improves climbing ability in flies expressing tau**

Comparison of the climbing ability with age from 1 weeks to 6 weeks for control and tau flies treated with 0.08µM and 0.8µM dosage of tau-aggregation inhibitor RI-AG03. Error bars are plotted as ± S.E.M. Control= (Elav-Gal4/UASOreR), tau= (Elav-GAL4/UAShtau$^{2N4R}$). Two-way ANOVA; p<0.0001), the difference in the climbing ability of tau flies treatment with RI-AG03 was found to be significant. The climbing ability of untreated htau$^{2N4R}$ and htau$^{0N4R}$ flies treated with LD of RI-AG03 are significantly different at 0-3 days (p=0.0002) and 1 weeks (7days) (p= 0.0487) weeks post-eclosion. Untreated htau$^{2N4R}$ and treated htau$^{0N4R}$ flies treated with HD of RI-AG03 are significantly different at 0-3 days (p=0.0379), at 1 week (7 days) (p= 0.0263), at 2 weeks (14 days) (p=0.0445), 4 and 5 weeks post- eclosion (p=0.0347) (p=0.0255) respectively.

### 7.3.3 Tau-aggregation inhibitor increase solubility of tau species in a *Drosophila* model of tauopathy

After characterizing the effect of treatment with RI-AG03 on the phenotype, the next thing to investigate was whether this inhibitor has an effect on tau solubility in our *Drosophila* model. I hypothesize that the rescue mediated by the inhibitor is due to suppression of tau aggregation in this model and if this is the case tau solubility should increase. To investigate this, the tau species were isolated using the solubility assay described in **Chapter 3** to obtain the NS1 fraction and characterized by western blotting.

There are differences in tau solubility between the flies with and without treatment with RI-AG03 in different stages of pathology. This was first indicated by assessing the total amount of tau in whole brain homogenates which would generally contain mostly soluble protein species. Here the amount of total tau evident in this fraction was dramatically greater in flies treated with RI-AG03 at both early and late stages of disease when compared to untreated flies (**Figure 58 A**). This result suggests the presence of more tau soluble species, potentially monomeric tau, in flies after exposure with inhibitor treatment (**Figure 58 A-a**).

To probe this further, I analysed the tau levels in the NS1 fraction, which enriches for soluble tau species as the insoluble tau aggregates are sedimented out (**Figure 58 A-1**). In treated flies there was significantly more soluble tau (NS1) compared to untreated flies. In untreated flies, 50% of total amount of soluble tau (NS1) is found in this fraction in newly eclosed young flies which suggests that the majority of tau is aqueous soluble and might contain both monomeric and oligomeric species at this early stage. However, the amount of tau in this fraction decreases to around 30% as flies progress to 6 weeks post-eclosion, indicating that tau is becoming insoluble over time possibly due to oligomerisation and further formation of more insoluble tau aggregates.

In comparison, the amount of the NS1 tau fraction from treated flies with RI-AG03 slightly decreases to 60% as flies progress to 6 weeks post-eclosion, indicating that the treatment with the inhibitor delays the increase in insolubility of tau, suggesting that have an effect on preventing tau aggregation.

In general, these results confirm what was observed in **Chapter 5**, since the expression of tau induces a decrease in the solubility of tau with time. This suggests oligomerization and subsequent polymerization in pathway to produce elongated aggregates. The data presented here also suggest

that RI-AG03 treatment increases the soluble species compared to flies without treatment. Suggesting that the inhibitor might has an effect partially preventing tau aggregation. Here, it is not entirely clear whether the treatment could be affecting tau expression levels, which remains to be determined in future studies.

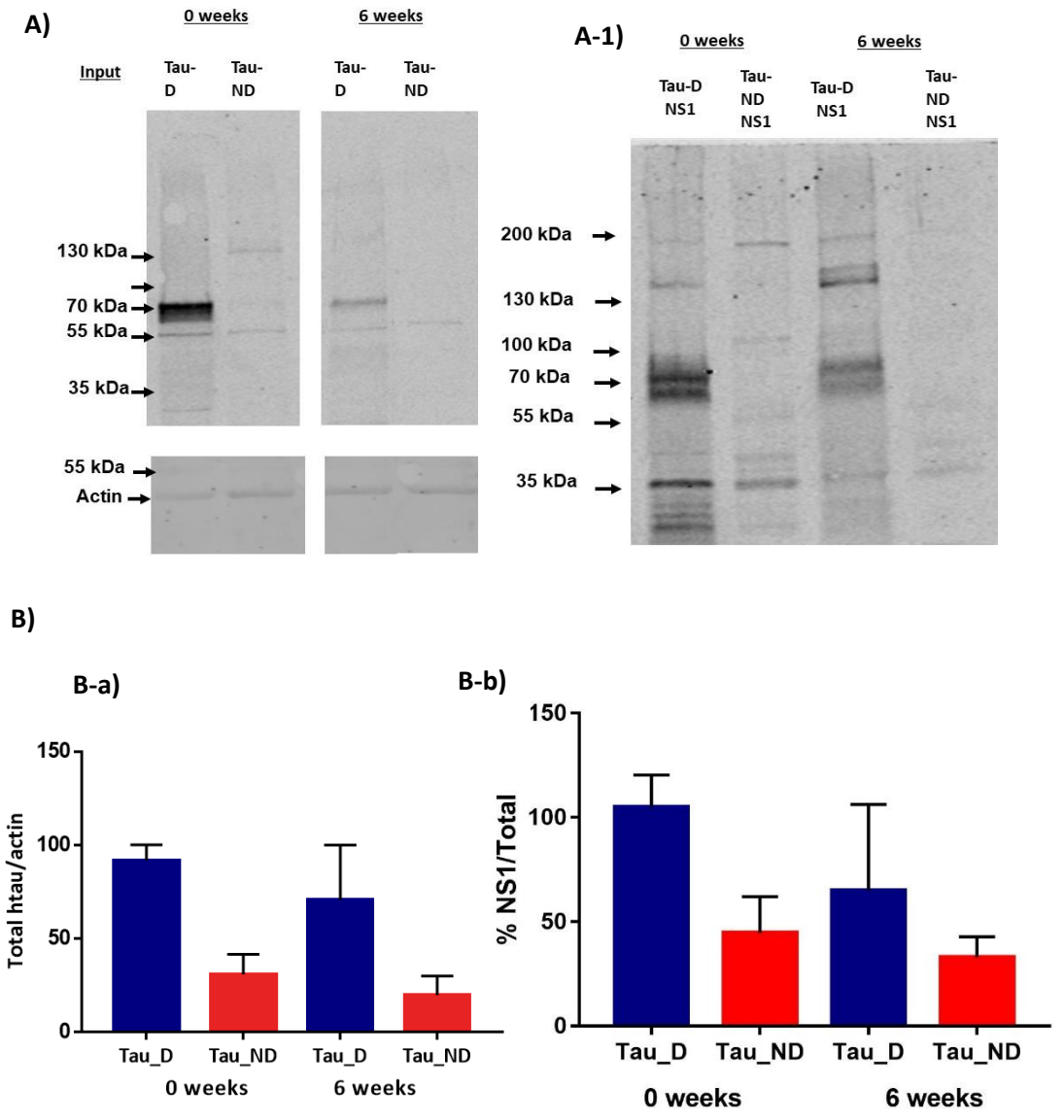


**Figure 58**. **Treatment with RI-AG03 increase solubility of tau species in a *Drosophila* model of tauopathy**

Comparison of solubility fractions at different ages (0 and 6 weeks-post eclosion) for Elav-GAL4 driven htau$^{2N4R}$ with (Tau_D) and without (Tau_ND) treatment with RI-AG03 (n=2, different crosses; 20 fly heads from used for different experiments). **A)** Shows western blots of inputs and soluble NS1 soluble fractions from adult heads. **B-a)** Quantification of amount of tau relative to actin. **B-b)** Shows quantification of soluble NS1 fractions to total of inputs.

## 7.4 Discussions

### 7.4.1 Summary

The aim of this chapter was to study the effect of the RI-AG03 aggregation inhibitor in a *Drosophila* model where aggregation is believed to underpin the disease phenotypes. The data presented here suggests that treatment with the inhibitor prevents the progression of the disease phenotype, possibly by reducing aggregation of the tau.

### 7.4.2 Tau-aggregation inhibitor rescues tau-induced phenotype in a *Drosophila* model of tauopathy

It was shown here that the expression of $hTau^{2N4R}$ exhibits several phenotypes similar to the models described in **Chapter 4** and other fly models of tauopathy (Ali et al., 2012; Wittmann et al., 2001). Overall treatment with either low or high doses of RI-AG03 aggregation inhibitor delayed the onset of both the climbing and longevity phenotype and significantly reducing them, though they did not rescue them back to control levels. In addition, treatment with RI-AG03 appeared to increase the amount of soluble tau species, suggesting that reduces aggregation of tau.

Since the formation and increase of the tau aggregates levels leads to the formation of fibrillary structures rich in β-sheet structure with potential impact on neuronal death, suggests that the prevention or reduction of aggregation could be a therapy for tauopathies. Supporting this notion, it has been shown that the addition of proline mutations, 277P and I308P, in the hexapeptide motifs of the tau repeat domain (TauRD) carrying the ΔK280 mutation, results in the inhibition of pathological β structure formation, thus inhibiting completely the aggregation of tau in a cellular model of tau aggregation (Khlistunova et al., 2006) and in an inducible mouse model (Moncanu et al., 2008).

Similarly, it has been shown in a *Drosophila* model expressing the human Tau-383 that eliminating the regions required for tau aggregation into β-sheet (Δ306–311) completely rescues the neurodegenerative phenotype (Passarella and Goedert, 2018). These study examples demonstrate that the reduction or the elimination of pathogenic tau counteracts the pathology of tau. Further demonstrate that the elimination of toxic tau expression through genetic modulation results in the complete rescue of the tau pathology, through the general elimination of toxic tau.

In the *Drosophila* model used in this thesis, overexpression of tau is not modulated or eliminated at any time, so this constant expression of tau could explain the partial rescue of the phenotype

after treatment with RI-AG03. In line with this, there is evidence that suggests that aggregation inhibitors interfere with the aggregation process but do not affect the continuous expression of tau with the potential for aggregating and form β-structure. This has been reported in methylene blue treatment and points to the importance of administering the treatment at an early time to avoid the formation of new β-structured seeds in TauΔK mice (Hochgräfe et al., 2015)

Our data presented here, also suggest that RI-AG03 treatment increases the soluble species compared to flies without treatment. These results suggest that the inhibitor have an effect partially preventing tau aggregation. The inhibition can be explained due to the characteristics of RI-AG03, which is designed with the incorporation of solubilizing residues to its amino acid sequence to avoid self-assembly, and inhibiting further formation of the β-sheet (**Figure 59**). However, as mentioned before, it is possible that the incomplete rescue of the phenotype is due to the formation of new oligomeric aggregates produced by overexpression of tau or due to sequestration of oligomeric forms of tau in which further polymerization and fibril formation is prevented by RI-AG03.

In line with this, the work done by Dr. Aggidis shows that the presence of RI-AG03 during the *in vitro* fibrillation process of tau, prevents the characteristic formation of disordered structure to structure of β sheet (Unpublished data). In addition, Dr. Aggidis data demonstrated that the presence of RI-AG03 during the fibrillation process prevents fibril formation. By means of TEM, the presence of spherical structures of ~ 36 nm in diameter is demonstrated, which suggests the presence of oligomeric structures such as GTOs (**Figure 60**) (Unpublished data). From the above observation, it is possible to suggest that RI-AG03 could interact with both monomers and oligomers stopping subsequent polymerization and fibril formation. These results are consistent with the improvement or delay of the phenotype and with the partial increase in solubility in fractions from flies treated with the inhibitor. This may explain the increased low molecular weight tau species that are evident after treatment, possibly because further polymerisation into toxic oligomers and fibrils is prevented in our model.

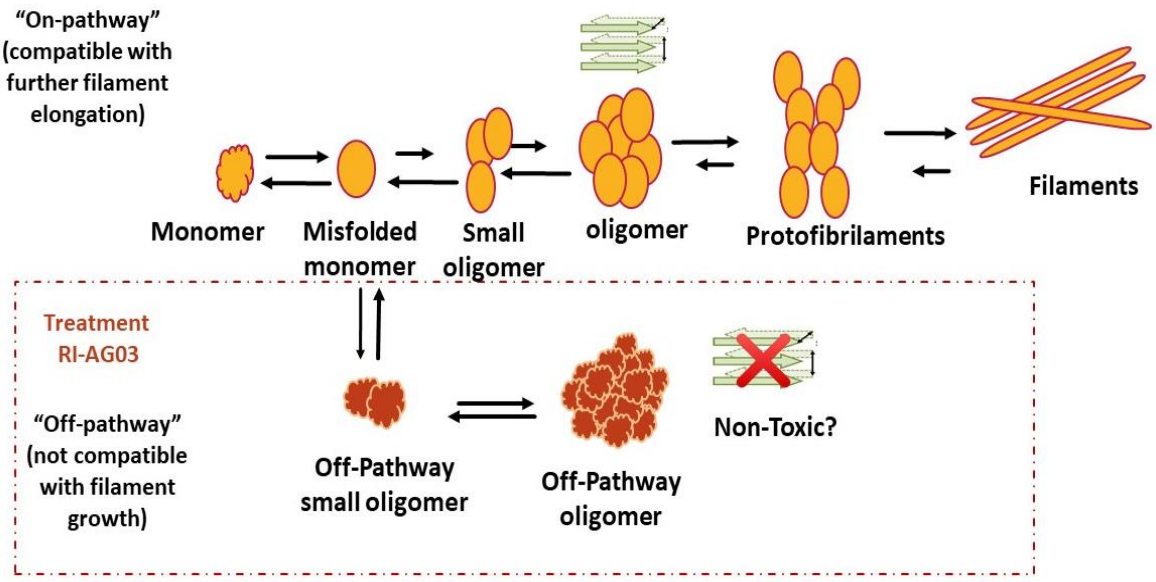


**Figure 59. Schematic representation of the potential effect of RIA-G03 on tau aggregation**

Moreover, to ascertain if tau aggregates were reduced in the flies that had the improved survival after inhibitor treatment, atomic force microscopy (AFM) was carried out on the NS2 species. In untreated htau2N4R flies there was evidence of both oligomeric and fibrillar tau species (arrowheads and arrows respectively in **Figure 68** in **appendix D** (Unpublished data). There was a 73% reduction in both oligomeric and fibrillar species after 6wk treatment with inhibitor (**Figure 68-B** in **appendix D**). Interestingly the fibrillar species of tau that were prevented from forming *in vivo* were the same species that were reduced after inhibitor treatment of recombinant tau aggregation *in vitro* (**Figure 60**). This data demonstrates the ability of RI-AG03 to act in the same manner *in vitro* and *in vivo*, reducing formation of toxic tau aggregates responsible for tau-dependent phenotypes.

### 7.4.3 Conclusions and future directions

Our results showed that $hTau^{2N4R}$ expression resulted in a disease phenotype, and both low and high doses of tau-aggregation inhibitor rescue the tau-induced phenotype. This results further confirms that tau aggregation is critical for the emergence and progression of phenotype. And point towards the urgency of studies to explore in more detail, the tau aggregates formed *in vivo* to better understand their toxicity as well as highlighting the potential role of the *Drosophila* model for the development of pharmacological studies against degenerative diseases.

In particular future studies should investigate more in detail the biochemical and biophysical properties, such as size, morphology and β-sheet content, of the tau species forming after RI-AG03 treatment and therefore investigate which species of tau are targeted by RI-AG03.

In addition, it would also be interesting to investigate the effect of the inhibitor during different stages of pathology to further investigate if RI-AG03 is also capable of modulate aspects as such conformation of the secondary structure by disassembling filaments already formed.

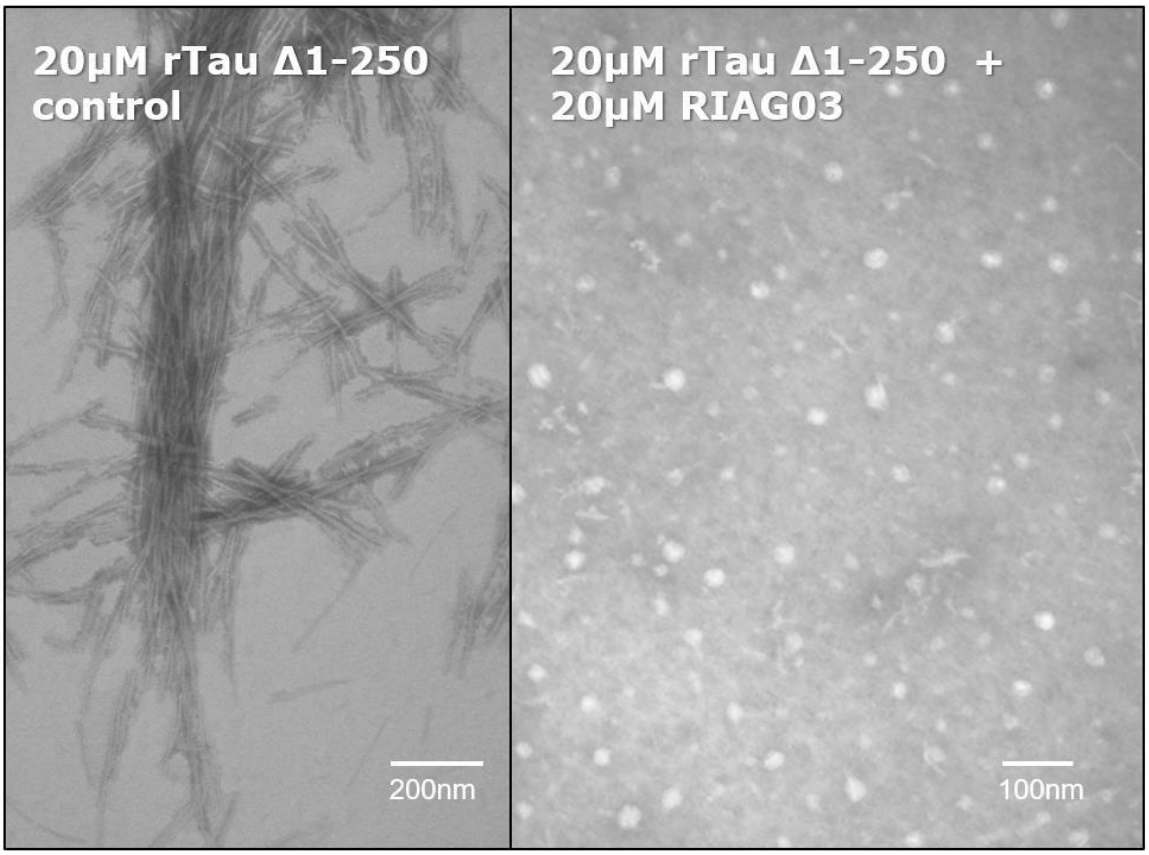


**Figure 60. RIAG03 prevents fibril formation under *in vitro* conditions**

Negative stain TEM images using a Joel JEM 1010 following aggregation of Tau Δ1 250 20 µM) at pH 7.4 in the presence of Tris buffer (30 mM), DTT (1 mM), heparin, (5 µM), without (Left) and with RI AG03 (20 µM) (right) and incubated at 37 ° C for 24 hr. Figure from A. Aggidis, PhD thesis, 2019.

# Chapter 8 General discussion

## 8.1 Summary

The research described in this thesis focused on studying how changes in tau species are related to the onset and the progression of the disease in two animal models of tauopathy. The results may provide clues about how this happens in human disease.

As there is currently no disease-modifying treatment for AD and related tauopathies, there is a need to understand the underlying mechanisms of the disease to find new therapeutic interventions. Therefore, investigating the pathogenic tau species responsible for the toxicity initially, and how this tau species progresses to an advanced stage of the disease, can provide useful information for the development of effective disease-modifying drugs to treat tauopathies. Thus, drugs can then target and eliminate the crucial species at the appropriate stage of the disease. The data described in this thesis has contributed to this research by exploring the tau species potentially responsible for dysfunction at the onset of the disease and neurodegeneration at the advanced stage of the disease. Some properties of these tau species that could have an impact on the pathology are also described here. Specifically, aspects such as solubility, morphology, size and β-structure content. These structural properties have been investigated here in both mouse and *Drosophila* models of tauopathies.

## 8.2 Identification of the onset and progression of tau phenotype

In order to investigate the species of tau that become pathogenic initially and at late of stage disease, it was important to first characterize the emergence and progression of tau phenotypes in the models of tauopathy used in this study. To do this, two lines of *Drosophila* expressing either 3R or 4R isoforms of human tau in the nervous system were assessed for age-related changes in longevity and locomotor behaviour. Similarly for the P301S mouse model, age-related changes in the locomotor behavior were assessed. As shown in **Chapter 4**, it was found that in both models, the expression of human tau produces a phenotype that can be correlated with some of the pathological features observed in human tauopathies. In these, the phenotypes assessed manifest at an early stage and at an advanced stage and might therefore be considered time points for the emergence and progression of the disease (**Figure 61**). In the *Drosophila* model the phenotype emerges at 2.5 weeks post-eclosion, whilst the late stage was established at 5 weeks, when the

phenotype worsens. In the mouse model, the early stage was established at 12 weeks of age and the advanced stage at 24 weeks of age.

It was also found that in *Drosophila* model, the expression of 3R isoform caused more severe behavioural phenotypes compared with 4R-expressing flies at initial stage, as the phenotypes appears earlier (**Figure 61 A**). However, once the phenotype becomes evident in 4R-expressing flies, the decline is steeper than that of 3R flies. These data implicate the isoform 3R in mediating dysfunction at an early stage of disease and the 4R isoform in mediating degeneration at a late stage of the disease. These results confirmed previous observations in these *Drosophila* models that indicated that 3R tau expression resulted in a reduction in longevity and a more rapid decrease in climbing ability when compared to flies expressing 4R (Sealey et al., 2017) . Likewise, 3R expression has been shown to be associated with dysfunction in the absence of neuronal death (Mudher et al., 2004, Cowan et al., 2010; Sealey et al., 2017). While on the contrary, the expression of 0N4R in neurons has been associated with degeneration (Sealey et al., 2017). This has also been demonstrated after the expression of 4R isoforms expressed in the MBs (Papanikolopoulou et al. 2010, Kosmidis et al. 2010).

These observations suggest that there are biochemical and biophysical differences between tau isoforms. These differences could be key to explain why different isoforms of tau are involved in different tauopathies. Further investigation into the different roles and toxicities of different tau isoforms may lead to a better understanding of these different tauopathies.

It has not been determined whether the presence of endogenous tau could be playing a role in our results. For this reason, it is important to consider its possible role in our results described and in a future study to determine the potential impact of endogenous tau in our model.

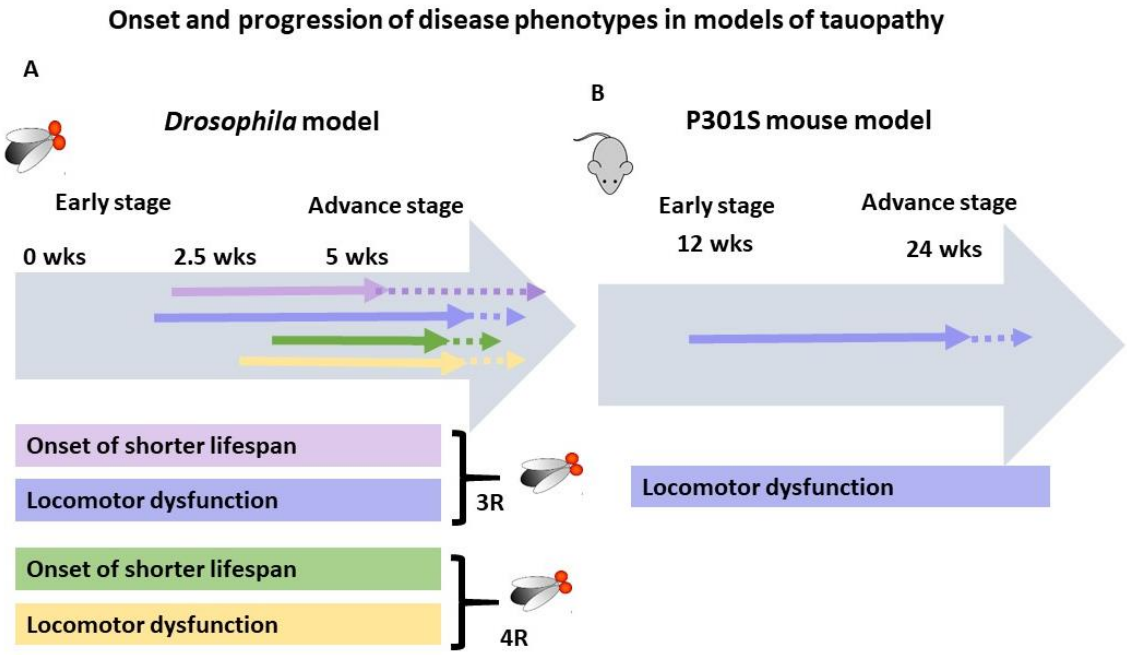


**Figure 61. Schematic representation of progression of the phenotype**

In both animal models, the expression of human cause a phenotype. **A)** In Drosophila model, the expression of both 3R and 4R human tau causes a reduction of lifespan and locomotor. The survival of flies begins to decline at 2.5 weeks in 3R-expressing flies and at 3.5 weeks 4R- expressing flies. At 5 weeks, 50% of 3R flies have died, while flies expressing 4R, this reduction is observed at 6.5 weeks and worsens at 7.5 weeks. 90% of 3R flies have died at 9.5 weeks. In both *Drosophila* lines, the onset of locomotor dysfunction begins at 2 weeks and decreases rapidly as flies progress to 5 weeks. However, at initial stage, dysfunction is more severe in 3R flies. **B)** In P301S mouse mode, mice begin to exhibit locomotor dysfunction at 12 weeks of age and deteriorates rapidly as mice progress to 16 weeks of age. At 24 weeks of age, the mice are immobile.

## 8.3 Which species of tau could be related to the appearance of the phenotype during the early stage and which to the late stage of the disease?

Despite many studies conducted in animal models, details about the nature of the species responsible for the toxicity are not entirely clear, nor is it known how their structural characteristics relate to the behavioral phenotype. Studying the properties of oligomeric species is a complex process, this is particularly true for the early oligomeric forms. This is because there are highly heterogeneous and dynamic species. Therefore, this work focused on identifying the time points relevant in terms of the emergence of the phenotype to characterize the biochemical and biophysical properties of the tau species present at that stage and how these properties progress

to an advance stage of disease. The description of these species provides information for understanding how these properties could be related to toxicity.

When investigating which species of tau could be related to the appearance and progression of the phenotype, it was found that in both models, the emergence of the earliest phenotype was accompanied by appearance of species that resemble oligomers with altered conformation and partial solubility (**Figure 62**). In particular, these species have globular shapes with widths of around 10-60nm, resembling oligomeric species isolated from human brains at Braak 0 and Braak III-IV stage identified by others (Maeda et al., 2006; Ercan-Herbst et al., 2019). This result indicate that these are the toxic species that caused dysfunction at the early stage of disease. While insoluble larger tau aggregates (pre-NFT) with a higher β-structure content, ranging from 75 to 550nm length and 8 to 40nm width as observed in human filaments and other models ( Crowther 1991; Maeda et al., 2007), are the toxic species that cause degeneration and are formed at the advance stage of disease. The data presented in this thesis indicated that in both models, the expression and further aggregation of tau is critical for the emergence and progression of the phenotype (**Figure 62**). In addition, the data suggest that the mechanism for aggregation and filament formation follow a similar pathway in these two models.

Furthermore, an interesting observation in this study is that in the fly model, the presence of globular structures of very large sizes seems to overcome the formation of elongated and well-defined structures such as tau filaments (as shown in **Figure 67 appendix C**). This could indicate a different mechanism of oligomerization and subsequent aggregation, perhaps similar to aggregation not compatible with filament growth (as in **Figure 59**) (see **Figure 14**). This is an interesting aspect to consider for later experiments.

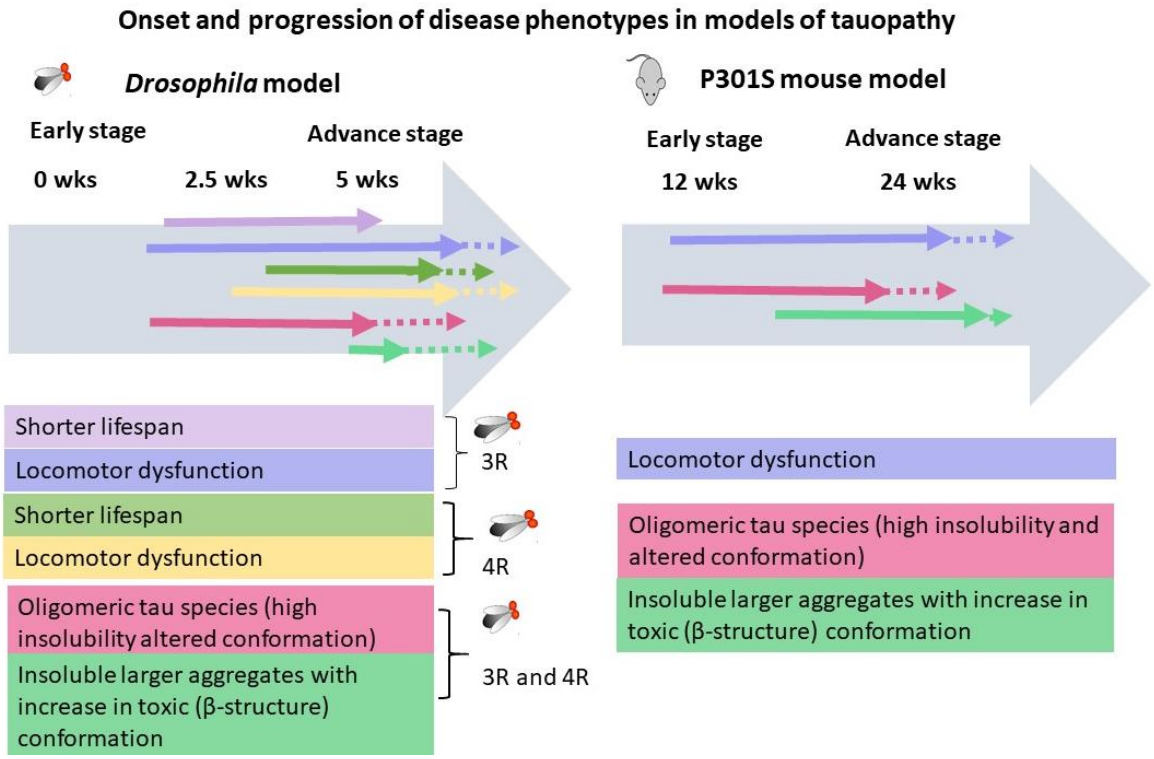


**Figure 62. Schematic representation of progression of the phenotype and biochemical changes in tau**

In both animal models, the expression of human tau induces the formation of oligomers (with low content of β sheets and globular form) which are evident at an early stage when the phenotype appears. During the advancement stage, the size and content of β sheets of these species increase although the globular shape is maintained. Further polymerization produces larger insoluble aggregates / fibrillar species (NS) with increasing age, resembling filaments when a degenerative phenotype is evident.

Furthermore, it was found that that different isoforms of tau, expressed in our *Drosophila* model, might cause differences in the polymerisation pathway. Specifically, our data suggest that 4R-tau is more prone to aggregation compared to 3R. As shown in **Chapter 4**, our data suggest that flies that overexpress the 4R isoform show greater lethality compared to flies that express the 3R isoform. In addition, the data shown in **Chapter 5**, indicates that the aggregates of flies expressing the 4R isoform have higher insolubility and a higher affinity for ThT (suggesting a higher content of β-structure). This leads us to speculate that the 4R isoform has a greater propensity to aggregate than the 3R isoform. And this propensity to aggregate and form the β structure of the 4R isoform could explain the degeneration with which this isoform is associated as described in **Chapter 4.**

The abundant aggregates rich in β-structure that form at a late stage seem to play a key role in neurodegeneration. Therefore, the ability of 4R isoform to aggregate and form β-structure faster

than 3R, could explain the differences between the isoforms and their role in the observed phenotype.

These observations provide clues that suggest biochemical and biophysical differences exist between the tau isoforms. It would be interesting to further analyse other biochemical properties of the different tau isoforms. For instance, it might be interesting to use proteinase k digestion assays or guanidine hydrochloride disaggregation. The resistance to protease or stability to disaggregation have been applied to study differential seeding potency of preformed aggregates of different tau variants. Therefore, this could be used to investigate differences in stability from different tau isoform aggregates in our tauopathy models that may explain differences in aggregation propensity. This could also provide relevant information on how different conformers with different stability properties can dictate toxicity.

## 8.4 How does β -sheet structure and filament formation could relate to degeneration?

Previous studies have suggested that abnormal aggregation in abundant β-rich filaments is related to neurodegeneration. However, the mechanism involved are not understood.

As only few studies have reported filament formation (Jackson et al., 2002; Colodner and Feany 2010; Wu et al., 2013) in *Drosophila* model it is arguable the suitability of these model to study the role of β-sheet structure and filament formation in degeneration. However, a strong evidence supporting the association between abnormal aggregation, propensity to form β-structure and degeneration has been demonstrated in *Drosophila* model (Pasarella and Goedert, 2018). In a study conducted by Pasarella and Goedert, flies that express non aggregating 4R tau, (due deletion of the hexapeptide motifs that are required for tau aggregation and β-sheet formation) completely rescue the tau-mediated neurodegenerative phenotype (Pasarella and Goedert, 2018).

A similar correlation has been shown in the two tauopathy models studied in this thesis, in which degeneration is evident as aggregation and levels of β-structure increase. More interestingly, as shown in **Chapter 6**, in this thesis we provide evidence suggesting tau aggregation and formation of structures that resemble tau oligomers on pathway to further form elongated aggregate aggregates that resemble filaments with increasing age. These structures have similar levels of β-structure to P301S mouse model. Suggesting that the mechanism for aggregation and filament formation follow a similar pathway in these two models. These findings are important to highlight the great potential of fly models of AD and tauopathies.

For future studies, it would be interesting to investigate in more detail the secondary structure adopted by the different species of tau generated in our models. As the only conformational information studied in this thesis is based on affinity of aggregates to dye ThT (suggesting the presence of cross-β-beta conformation). It would be interesting to be able to characterise and quantify temporal changes in secondary structure using other informative technique such as Infrared Spectroscopy (IR) or Raman spectroscopy. This could be particularly interesting as it has been demonstrated that differences in β-sheet geometry adopted by early aggregates might influence aggregation kinetics and filament formation, as well as toxicity. In particular this has been demonstrated by investigating oligomers from α-synuclein using Fourier transform infrared (FTIR) spectroscopy (Chen et al., 2015). It was found that oligomers that adopt a parallel β-sheet geometry elongate faster and have a lower degree of toxicity when expose to cells (Chen et al., 2015). Conversely, oligomers that adopt antiparallel β-sheets, highly hydrophobic and become partially stable remaining in that oligomeric state for longer resulting in and higher toxicity (Chen et al., 2015). In this regard, it might be interesting to analyse differences in β-sheet geometry in different isoforms. Perhaps this could also provide valuable information to understand differences in aggregation capabilities from 3R and 4R.

Previous studies have shown that pathological tau with β-structure is capable of triggering soluble tau aggregation through templated seeding. This has been demonstrated in cell models in which, by exposing pathological tau from the sarkosyl-insoluble tau fraction isolated from the brains of P301S transgenic mice in the extracellular medium, this insoluble tau is able to enter cells and promote soluble tau aggregation (Falcon et al., 2015). Based on this, it would be interesting to evaluate the seeding capacity of tau aggregate from *Drosophila* model to induce recombinant monomeric tau nucleation, aggregation and fibrillation. As the expression of a number of tau variant is *Drosophila* modes is relatively easy it would be also possible to study potential differences in seeding potency in the different tau isoforms expressed in *Drosophila* model (**Figure 63**) shows a schematic representation of this process).

On the other hand, it is possible that *in Drosophila*, there are unidentified components that can act as cofactors accelerating the formation of aggregates and subsequent fibrillation when applied to a recombinant tau substrate and evaluating the seeding capacity using ThT fluorescence. The presence and characterization of these components could well be investigated in *Drosophila*. This could contribute to the understanding of components that lead to spontaneous aggregation in vivo.

It has been previously established that the co-expression of human tau and glycogen synthase kinase-3 (GSK-3β) enhances neurodegeneration in the eye. This also enhance neurofibrillary

pathology formation (Jackson et al., 2002). This observation seems to suggest that hyper-phosphorylation accelerates the aggregation and filament formation that leads to degeneration. For instance, it would be interesting to investigate the biochemical and biophysical properties of these tau species, to analyse if phosphorylation have an effect on the aggregation pathway that can be identify by any of the different techniques used here.

As a preliminary analysis, in this thesis work we validate the previous observations made by Jackson's group, in addition to validating our characterization method. As shown in **Figure 64**, when characterizing, using AFM, the insoluble aggregate species from flies that express human tau isoform 2N4R, structures that resemble oligomeric globular forms were observed. However, when characterizing aggregates generated in flies that co-express the same isoform of human tau in conjunction with GSK-3β, well-defined filamentous structures are observed at the same stage. It would be also interesting to investigate the properties of tau species generated after expression of pseudophosphorylated tau mutant to analyse if phosphorylation have an effect on the aggregation pathway that can be identified by any of the different techniques used here.

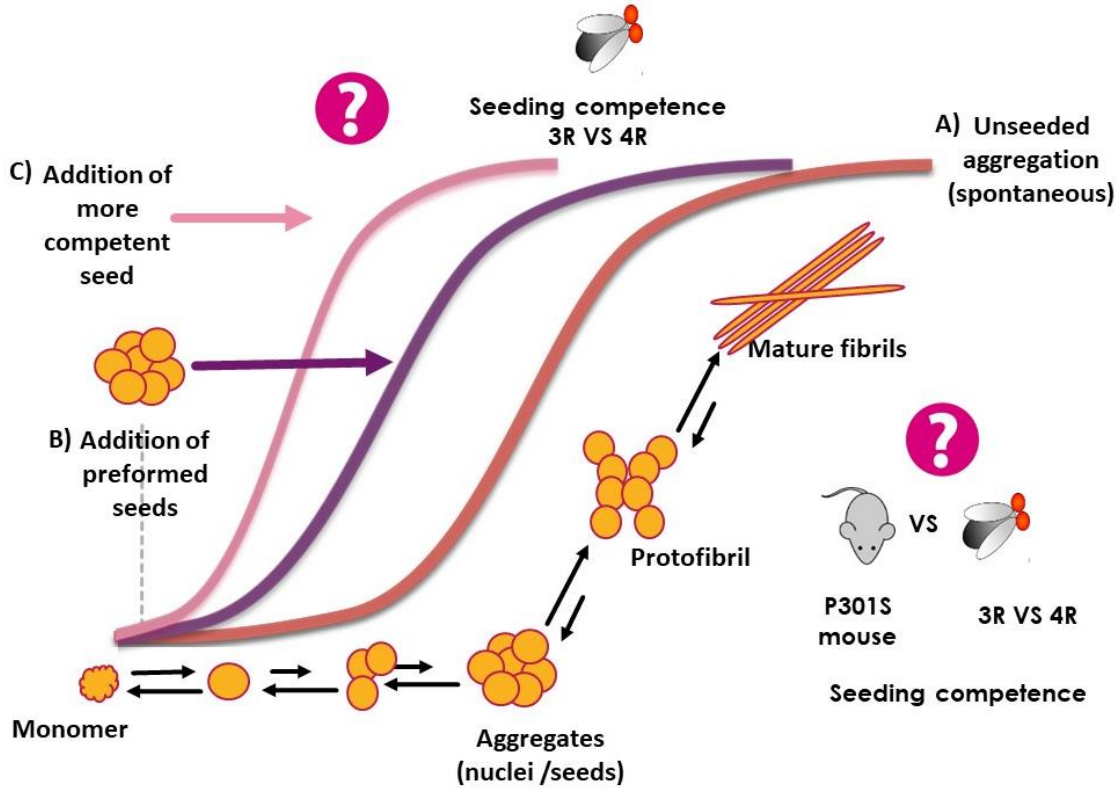


**Figure 63.Schematic representation of potential differences in seeding capacity of pre-formed species of tau variants**

**A)** Red color shows spontaneous tau aggregation and fibrillation. Fibrillation does not depend on the addition of preformed nuclei or seeds. **B)** In purple the formation of aggregates and fibrillation after the addition of pre-formed seeds or nuclei is shown. The presence of seeds speeds up the aggregation process. **C)** In pink the formation of aggregates is shown after the addition of more potent seeds, shortening even more the speed of fibril formation. This fibrillation process is commonly followed by ThT fluorescence. The seeds are incubated in the presence of monomeric recombinant protein (adding heparin) and fibrillation is monitored by measuring the fluorescence intensity of ThT. It would be interesting to evaluate and compare the seeding competence of different species used in this model and other models. For example, it would be interesting to compare this capacity between the different tau isoforms expressed in *Drosophila*.

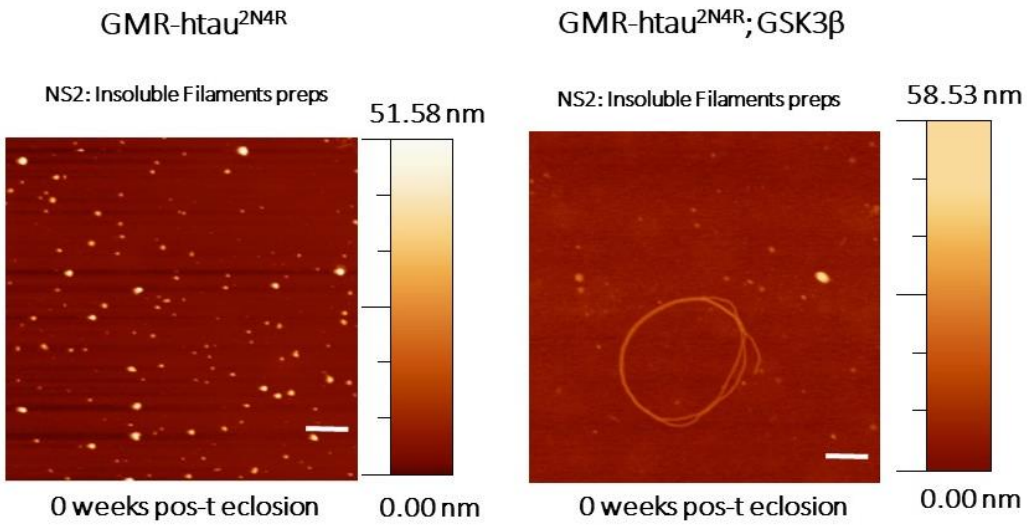


**Figure 64. The co-expression of tau in conjunction with GSK3B accelerates the formation of aggregates**

When investigating the fraction containing insoluble (NS) long aggregates (filaments) generated in flies expressing human tau isoform 2N4R in eyes, the presence of insoluble globular structures is observed. While analysing the same NS generated in flies that co-express human tau isoform 2N4R in conjunction with glycogen synthase kinase-3 (GSK-3β), filaments are observed. The tau species generated in both flies were investigated at 0 weeks post-eclosion.

## 8.5 Targeting aggregation as potential intervention against degenerative diseases

The fact that the increased GTOs levels lead to the formation of NFT and potentially have an impact on neuronal death allows us to speculate that reducing toxic tau oligomers and prevent NFT formation could be a therapy for tauopathies. Supporting this, the data presented in **Chapter 7** suggests that treatment with RI-AG03 prevents progression of disease phenotype in a *Drosophila* model of tauopathy expressing human 2N4R tau in neurons. In detail, treatment with RI-AG03 delayed the onset of both the climbing and longevity phenotype. It was also found that treatment increase the amount of soluble tau species, suggesting that RI-AG03reduces aggregation of tau.

The results presented in this thesis further confirms that tau aggregation is critical for the emergence and progression of phenotype. In addition highlighting the potential role of the *Drosophila* model for the development of pharmacological studies against degenerative diseases.

Future studies should investigate the effect of the inhibitor during different stages of pathology to further investigate if RI-AG03 is also capable of modulating aspects as such conformation, for instance altering preformed β-sheet structure, by disassembling filaments already formed. By doing this, it might provide information on how RI-AG03 can interact in *in vivo* and to what extent it can prevent aggregation.

## 8.6 Conclusions and future directions

In conclusion, I found that in two models of tauopathy that the expression of human tau produces a phenotype and this is manifested in an early and advanced stage of the disease. This satisfies **Aim 1 which was to characterize the appearance of tau phenotypes in two models of tauopathy.** The characterization of the early and advanced stages is useful for the identification of species responsible for dysfunction and degeneration in the models used in this thesis. Knowledge of this species and its properties can be used to develop potential drugs that improve clinical symptoms.
Using a combination of biochemical and biophysical techniques, the tau species potentially responsible for neuronal dysfunction early in the disease and the species responsible for degeneration in the advanced stage of the disease were identified and described. This satisfies **Aim 2 which was to identify the tau species potentially responsible for the onset and progression of the disease, and Aim 3, in which I employed a series of biophysical techniques to further explore the characteristics of each species (GTO / NS) responsible for the onset and progression of the disease.**
This study provides evidence to suggest that the disease process is conserved between invertebrates and vertebrates and likely recapitulates some of the pathogenic events observed in humans. This has the potential to generate clues that allow a greater understanding of tau-mediated toxicity, as well as highlighting disease-modifying targets for this. Thus **Aim 4** can be satisfied in which proof-of-concept for this idea was provided by **studying the effect of a tau aggregation inhibitor in our *Drosophila* model as a potential future disease modifying therapy**.

# Chapter 9 Appendices

## Appendix A Additional methods/ recipes

| **Standard Bloomington fly media (1L)** dH2O (ml) | 1 |
|---|---|
| Agar (g) | 6 |
| Yeast (g) | 17.5 |
| Soya flour (g) | 10 |
| Yellow maize meal (g) | 73.1 |
| Light malt extract (g) | 46.2 |
| Dry weight sucrose (g) | 48 |
| Additional dH2O (ml) | 80 |
| Propionic acid (ml) | 5 |

1. Agar, yeast, soya flour and yellow maize meal are mixed with 1/5 total water into a smooth paste.
2. Boil the remaining water and malt and sucrose are then added. Stir mixture until dissolved.
3. Add malt/sucrose solution to agar/yeast/soya flour/maize paste, mix and boil, stirring constantly. Boil for a few minutes.
4. Allow to cool to 60°C and then add propionic acid and stir through.
5. Pour into vials and leave covered to cool (2hrs-overnight) before plugging with cotton wool bungs and storing in fridge.

# Appendix B Supporting data for Chapter 5

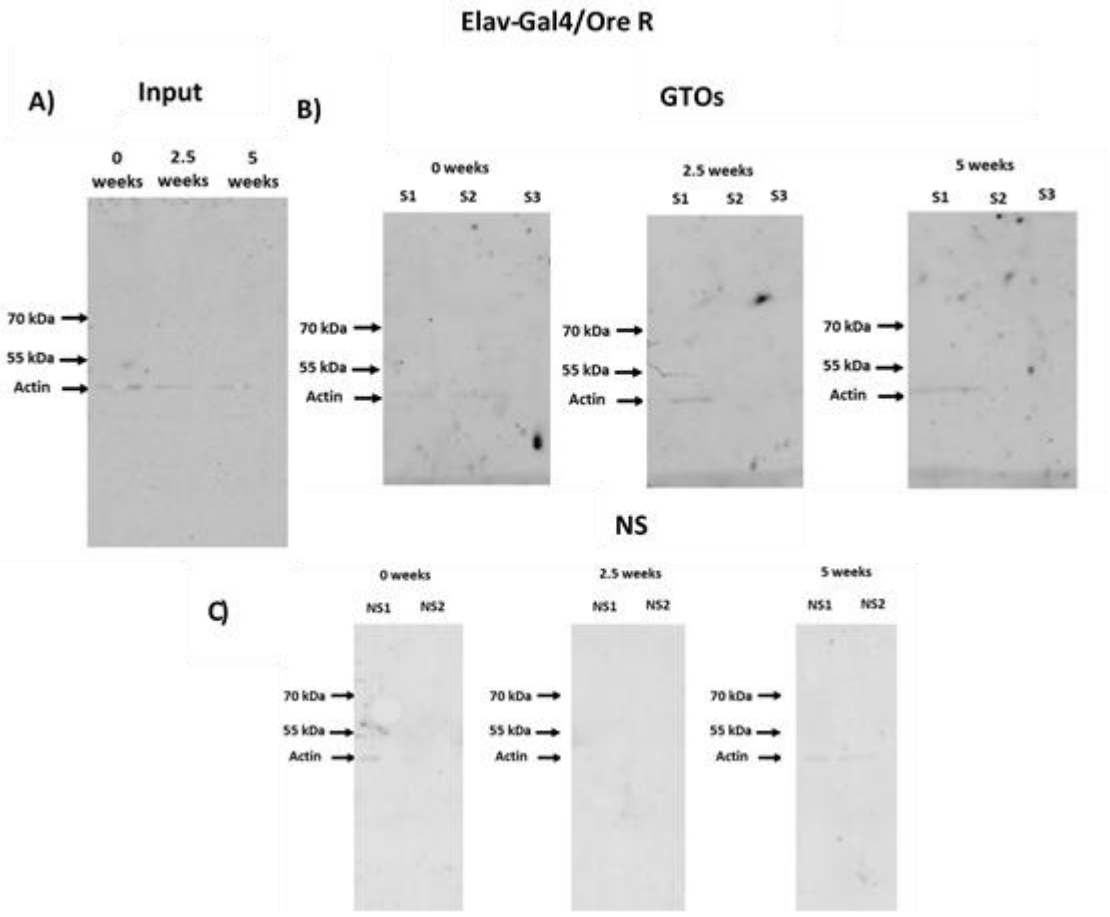


**Figure 65. Control flies show no evidence of tau**

A) Representative blots of adult fly head homogenate (inputs) from Elav-Gal4/Ore R wt flies (n=3, different crosses/ genotype). 100 fly heads were homogenized. Tissue lysate samples show no reactivity to anti-human tau antibody (Dako). B) Shows western blots of S1, S2, and S3 fractions and C) show the NS1 and NS2 fraction. The blots show no reaction to the anti-human tau antibody (Dako).

# Appendix C Supporting data for Chapter 6

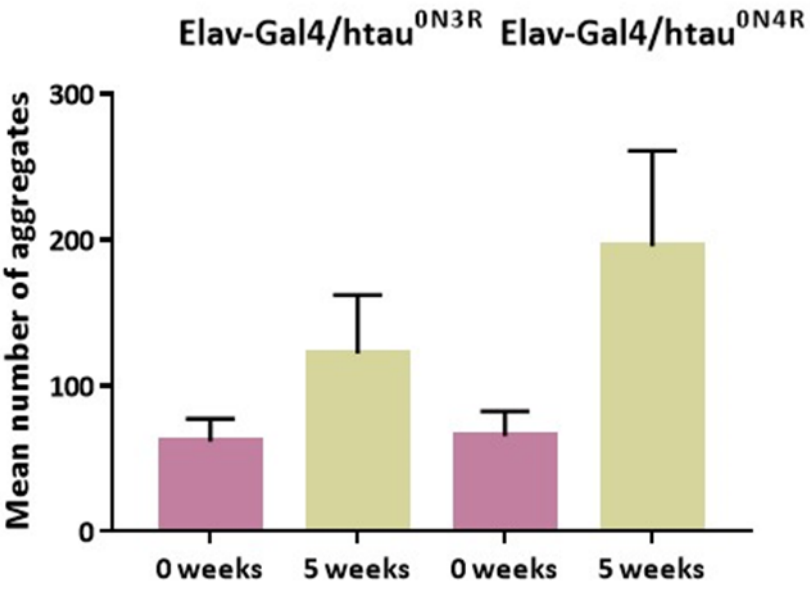


Figure 66. **Expression of htau in *Drosophila* leads to aggregation of tau that slightly increases with time**

The acquired AFM images corresponding to the NS2 tau species obtained from 0 and 5 weeks-old flies were processed by the WSXM software. The quantification of the aggregates was carried out using ImageJ software. Data are expressed as mean ± standard deviation. The unpaired t-test does not show significant differences between the analyzed times, however, a trend towards increase is observed (n=3, different random images from 3 different experiments).

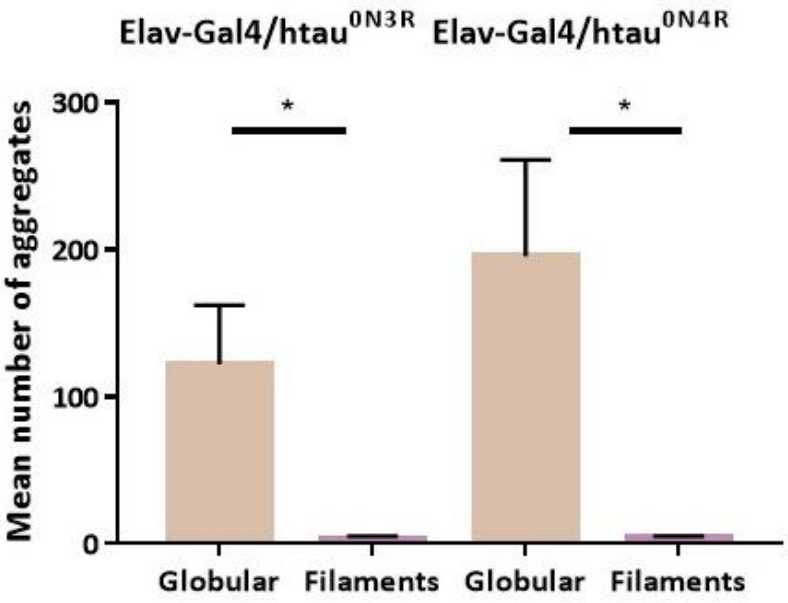


**Figure 67. Expression of htau in *Drosophila* leads to the formation of mainly globular species of tau that increases with time**

The acquired AFM images corresponding to the NS2 tau species obtained from 0 and 5 weeks-old flies, were processed by the WSXM software. The quantification of the aggregates, (globular shape (pixel range 0-200) and and large aggregates (filaments) (pixel range 200 to >1000), was carried out using ImageJ software. Data are expressed as mean ± standard deviation. The unpaired t-test does show significant differences between the analyzed times, however, a trend towards increase is observed (n=3, different random images from 3 different experiments).

# Appendix D Supporting data for Chapter 7

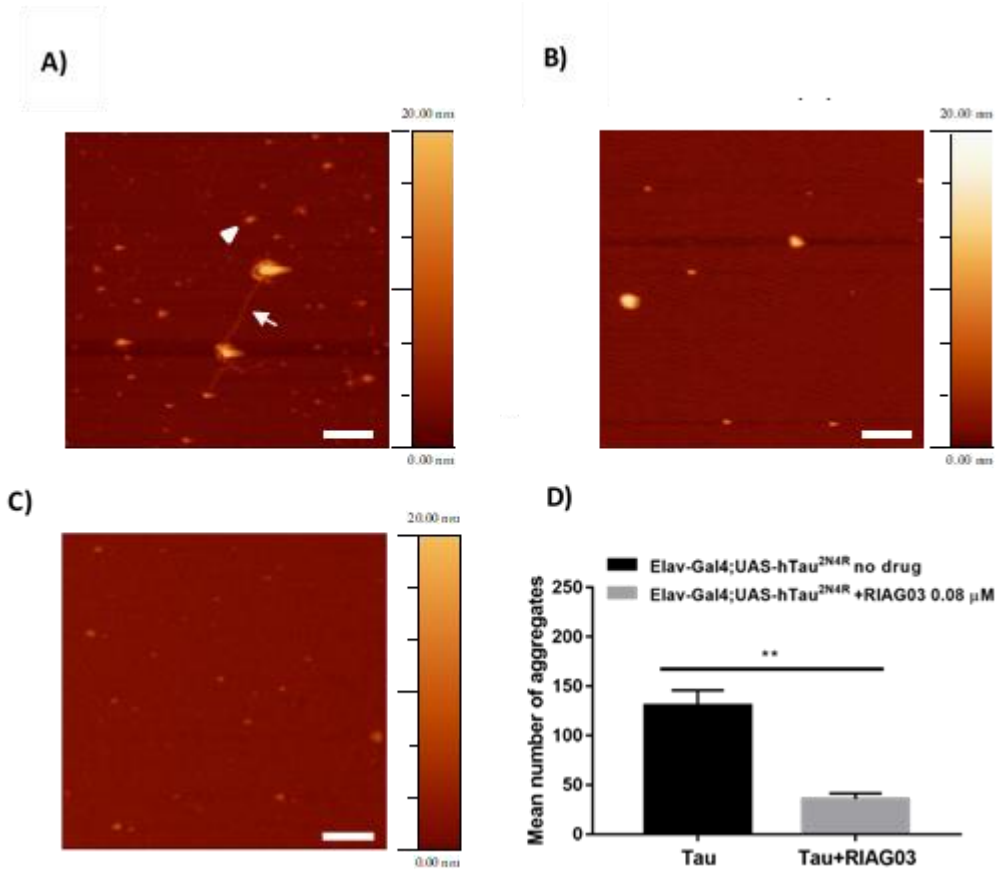


Figure 68. **Treatment with RI-AG03 reduces the number of aggregates.**

**(A)** AFM on an insoluble tau prep obtained from 6wk transgenic flies expressing the hTau2N4R pan-neurally. There is evidence of both oligomeric (arrowheads) and fibrillar (arrows) Tau aggregates. **(B)** AFM on a similar Tau-enriched insoluble prep obtained from 6wk transgenic flies expressing hTau2N4R pan-neurally that had been treated with RI-AG03 0.08 µM show a conspicuous dearth in Tau fibrils as well as a profound reduction in small oligomeric Tau species. No such structures were evident in Elav/Orer controls **(C)**. Scale bar = 200 nm. Quantitation of reduction of tau aggregates after inhibitor treatment **(D)** n=8, unpaired t-test p =0.02.

## Appendix E Research impact

Renzo Mancuso, Gemma Fryatt, Madeleine Cleal, Juliane Obst, Elena Pipi, Jimena Monzón-Sandoval, Elena Ribe, Laura Winchester, Caleb Webber, Alejo Nevado, Tom Jacobs, Nigel Austin, Clara Theunis, Karolien Grauwen, Eva Daniela Ruiz, Amrit Mudher., et al. CSF1R inhibition by JNJ-40346527 attenuates microglial proliferation and neurodegeneration in P301S mice. Brain. 2019

Anthony Aggidis, Shreyasi Chatterjee, David Townsend, Nigel J. Fullwood, Eva Ruiz Ortega, Airi Tarutani, Masato Hasegawa, Hannah Lucas, Amritpal Mudher and David Allsop.Peptide-based inhibitors of Tau aggregation as a potential therapeutic for Alzheimer's disease and other Tauopathies. For consideration at PLOS Biology.

Katy Stubbs, Ben Batchelor, Lovesha Sivanantharajah, Megan Sealey, Miguel R Moreno Eva Ruiz, Brad Richardson, Victor H Perry, Tracey A Newman and Amritpal Mudher. Tau-mediated axonal degeneration is prevented by activation of the WldS pathway. For consideration at Cellular and Molecular Neurobiology.

Shreyasi Chatterjee, Megan Sealey, Eva Ruiz, , Chrysia M. Pegasiou, Sam Green, Anna Crisford, Michael Duque Vasquez, Emma Luckett, Rebecca Robertson, Philippa Richardson, Girish Vajramani, Paul Grundy, Diederik Bulters, Christopher Proud, Mariana Vargas-Caballero and Amritpal Mudher. Age-related changes in Tau and Autophagy in human brain in the absence of neurodegeneration. Submission at Scientific Reports.

Eva Ruiz, George Devitt, Sumeet Mahajan and Amrit Mudher. Tau aggregation in *Drosophila* models of tauopathy is strikingly similar to that evident in rodent models of tauopathy. In preparation.

Arya Chithran, Ben Batchelor, Lovesha Sivanantharajah, Tian, Brad Richardson, Eva Ruiz, Makis Skoulakis, Douglas Alan and A Mudher. A *Drosophila* model depicting Braak-like propagation of Tau pathology. In preparation.

# Bibliography

Adams, S. J., DeTure, M. A., McBride, M., Dickson, D. W., & Petrucelli, L. (2010). 'Three repeat isoforms of tau inhibit assembly of four repeat tau filaments'. PloS one, 5(5), e10810.

Allen, B., Ingram, E., Takao, M., Smith, M. J., Jakes, R., Virdee, K., Yoshida, H., Holzer, M., Craxton, M., Emson, P. C., Atzori, C., Migheli, A., Crowther, R. A., Ghetti, B., Spillantini, M. G., & Goedert, M. (2002). 'Abundant tau filaments and nonapoptotic neurodegeneration in transgenic mice expressing human P301S tau protein'. The Journal of neuroscience: the official journal of the Society for Neuroscience, 22(21), 9340–9351.

Al-Chalabi, A., & Hardiman, O. (2013). 'The epidemiology of ALS: a conspiracy of genes, environment and time'. Nature reviews. Neurology, 9(11), 617–628.

Ali, Y. O., Ruan, K., & Zhai, R. G. (2012). 'NMNAT suppresses tau-induced neurodegeneration by promoting clearance of hyperphosphorylated tau oligomers in a Drosophila model of tauopathy'. Human Molecular Genetics, 21(2), 237-250.

Alonso, A. D., Cohen, L. S., Corbo, C., Morozova, V., ElIdrissi, A., Phillips, G., & Kleiman, F. E. (2018). 'Hyperphosphorylation of Tau Associates with Changes in Its Function beyond Microtubule Stability'. Frontiers in cellular neuroscience, 12, 338.

Alonso, A. C., Grundke-Iqbal, I., & Iqbal, K. (1996). 'Alzheimer's disease hyperphosphorylated tau sequesters normal tau into tangles of filaments and disassembles microtubules'. Nature medicine, 2(7), 783–787.

Alonso, A. C., Zaidi, T., Grundke-Iqbal, I., & Iqbal, K. (1994). 'Role of abnormally phosphorylated tau in the breakdown of microtubules in Alzheimer disease'. Proceedings of the National Academy of Sciences of the United States of America, 91(12), 5562–5566.

Andorfer C, Acker CM, Kress Y, Hof PR, Duff K, Davies P. (2005) 'Cell-cycle reentry and cell death in transgenic mice expressing nonmutant human tau isoforms'. Journal of Neuroscience. 25(22):5446-54.

Andorfer, C. A., & Davies, P. (2000). 'PKA phosphorylations on tau: developmental studies in the mouse'. Developmental neuroscience, 22(4), 303–309.

Alyenbaawi, H., Allison, W. T., & Mok, S. A. (2020). 'Prion-Like Propagation Mechanisms in Tauopathies and Traumatic Brain Injury: Challenges and Prospects'. Biomolecules, 10(11).

Arai, T., Ikeda, K., Akiyama, H., Shikamoto, Y., Tsuchiya, K., Yagishita, S., Beach, T., Rogers, J., Schwab, C., & McGeer, P. L. (2001). 'Distinct isoforms of tau aggregated in neurons and glial cells in brains of

patients with Pick's disease, corticobasal degeneration and progressive supranuclear palsy'. Acta neuropathologica, 101(2), 167–173.

Arriagada, P. V., Growdon, J. H., Hedley-Whyte, E. T., & Hyman, B. T. (1992). 'Neurofibrillary tangles but not senile plaques parallel duration and severity of Alzheimer's disease'. Neurology, 42(3 Pt 1), 631–639.

Avila J., Lucas J.J., Perez M., Hernandez F. (2004). 'Role of tau protein in both physiological and pathological conditions'. Physiological Reviews, 84(2):361–84.

Barghorn, S., & Mandelkow, E. (2002). 'Toward a unified scheme for the aggregation of tau into Alzheimer paired helical filaments'. Biochemistry, 41(50), 14885–14896.

Barghorn, S., Zheng-Fischhöfer, Q., Ackmann, M., Biernat, J., von Bergen, M., Mandelkow, E. M., & Mandelkow, E. (2000). 'Structure, microtubule interactions, and paired helical filament aggregation by tau mutants of frontotemporal dementias'. Biochemistry, 39(38), 11714–11721.

Baudier, J., & Cole, R. D. (1987). 'Phosphorylation of tau proteins to a state like that in Alzheimer's brain is catalyzed by a calcium/calmodulin-dependent kinase and modulated by phospholipids'. The Journal of biological chemistry, 262(36), 17577–17583.

Baumann, K., Mandelkow, E. M., Biernat, J., Piwnica-Worms, H., & Mandelkow, E. (1993). 'Abnormal Alzheimer-like phosphorylation of tau-protein by cyclin-dependent kinases cdk2 and cdk5'. FEBS letters, 336(3), 417–424.

Bengoa-Vergniory, N., Velentza-Almpani, E., Silva, A. M., Scott, C., Vargas-Caballero, M., Sastre, M., Wade-Martins, R., & Alegre-Abarrategui, J. (2021) 'Tau-proximity ligation assay reveals extensive previously undetected pathology prior to neurofibrillary tangles in preclinical Alzheimer's disease'. Acta Neuropathologica Communications, 9(1), 18.

Biancalana, M., & Koide, S. (2010). 'Molecular mechanism of Thioflavin-T binding to amyloid fibrils'. Biochimica et biophysica acta, 1804(7), 1405–1412.

Bier E. (2005). 'Drosophila, the golden bug, emerges as a tool for human genetics'. Nature reviews. Genetics, 6(1), 9–23.

Binnig, G., Quate, C. F., & Gerber, C. (1986). 'Atomic force microscope'. Physical review letters, 56(9), 930–933.

Birks J. (2006). 'Cholinesterase inhibitors for Alzheimer's disease'. The Cochrane database of systematic reviews, (1), CD005593.

Blake, C., & Serpell, L. (1996). 'Synchrotron X-ray studies suggest that the core of the transthyretin amyloid fibril is a continuous beta-sheet helix. Structure'. (London, England : 1993) 4(8), 989–998.

# Bibliography


Blard, O., Frebourg, T., Campion, D., & Lecourtois, M. (2006). 'Inhibition of proteasome and Shaggy/Glycogen synthase kinase-3beta kinase prevents clearance of phosphorylated tau in Drosophila'. Journal of Neuroscience Research, 84(5), 1107-1115.

Braak H., & Braak E. (1991). 'Neuropathological stageing of Alzheimer-related changes'. Acta Neuropathologica.82 (4):239-59.

Braak, H. & Braak, E. (1995). 'Staging of Alzheimer's disease-related neurofibrillary changes'. Neurobiology of Aging, 16, 271-278.

Brand, A. H., & Perrimon, N. (1993). 'Targeted gene expression as a means of altering cell fates and generating dominant phenotypes'. Development (Cambridge, England), 118(2), 401–415.

Bukar Maina, M., Al-Hilaly, Y. K., & Serpell, L. C. (2016). 'Nuclear Tau and Its Potential Role in Alzheimer's Disease'. Biomolecules, 6(1), 9.

Bulic, B., Pickhardt, M., Mandelkow, E. M., & Mandelkow, E. (2010). 'Tau protein and tau aggregation inhibitors'. Neuropharmacology, 59(4-5), 276-289.

Buée, L., Bussière, T., Buée-Scherrer, V., Delacourte, A., & Hof, P. R. (2000). 'Tau protein isoforms, phosphorylation and role in neurodegenerative disorders'. Brain research reviews, 33(1), 95–130.

Bunker, J. M., Wilson, L., Jordan, M. A., & Feinstein, S. C. (2004). 'Modulation of microtubule dynamics by tau in living cells: implications for development and neurodegeneration'. Molecular Biology of the Cell, 15(6), 2720-2728.

Cabezas-Opazo, F. A., Vergara-Pulgar, K., Pérez, M. J., Jara, C., Osorio-Fuentealba, C., & Quintanilla, R. A. (2015). 'Mitochondrial Dysfunction Contributes to the Pathogenesis of Alzheimer's Disease'. Oxidative medicine and cellular longevity, 509654.

Carmel, G., Mager, E. M., Binder, L. I., & Kuret, J. (1996). 'The structural basis of monoclonal antibody Alz50's selectivity for Alzheimer's disease pathology'. The Journal of biological chemistry, 271(51), 32789–32795.

Cash, A. D., Aliev, G., Siedlak, S. L., Nunomura, A., Fujioka, H., Zhu, X., Raina, A. K., Vinters, H. V., Tabaton, M., Johnson, A. B., Paula-Barbosa, M., Avíla, J., Jones, P. K., Castellani, R. J., Smith, M. A., & Perry, G. (2003). 'Microtubule reduction in Alzheimer's disease and aging is independent of tau filament formation'. The American journal of pathology, 162(5), 1623–1627.

Cassimeris, L., & Spittle, C. (2001). 'Regulation of microtubule-associated proteins'. International review of cytology, 210, 163–226.

Chandupatla, R. R., Flatley, A., Feederle, R., Mandelkow, E. M., & Kaniyappan, S. (2020). 'Novel antibody against low-n oligomers of tau protein promotes clearance of tau in cells via lysosomes'. Alzheimer's & dementia (New York, N. Y.), 6(1), e12097.

# Bibliography


Chatterjee, S., Sang, T. K., Lawless, G. M., & Jackson, G. R. (2009). 'Dissociation of tau toxicity and phosphorylation: role of GSK-3beta, MARK and Cdk5 in a Drosophila model'. Human Molecular Genetics, 18(1), 164-177.

Chee, F. C., Mudher, A., Cuttle, M. F., Newman, T. A., MacKay, D., Lovestone, S., & Shepherd, D. (2005). 'Over-expression of tau results in defective synaptic transmission in Drosophila neuromuscular junctions'. Neurobiology of Disease, 20(3),

Chen, S. W., Drakulic, S., Deas, E., Ouberai, M., Aprile, F. A., Arranz, R., Ness, S., Roodveldt, C., Guilliams, T., De-Genst, E. J., Klenerman, D., Wood, N. W., Knowles, T. P., Alfonso, C., Rivas, G., Abramov, A. Y., Valpuesta, J. M., Dobson, C. M., & Cremades, N. (2015). 'Structural characterization of toxic oligomers that are kinetically trapped during α-synuclein fibril formation'. Proceedings of the National Academy of Sciences of the United States of America, 112(16), E1994–E2003.

Cheng, Y., & Bai, F. (2018). 'The Association of Tau With Mitochondrial Dysfunction in Alzheimer's Disease'. Frontiers in Neuroscience, 12, 163.

Chirita, C. N., Congdon, E. E., Yin, H., & Kuret, J. (2005). 'Triggers of full-length tau aggregation: a role for partially folded intermediates'. Biochemistry, 44(15), 5862–5872.

Chiti, F., & Dobson, C. M. (2006). 'Protein misfolding, functional amyloid, and human disease'. Annual review of biochemistry, 75, 333–366.

Clavaguera, F., Akatsu, H., Fraser, G., Crowther, R. A., Frank, S., Hench, J., Probst, A., Winkler, D. T., Reichwald, J., Staufenbiel, M., Ghetti, B., Goedert, M., & Tolnay, M. (2013). 'Brain homogenates from human tauopathies induce tau inclusions in mouse brain'. Proceedings of the National Academy of Sciences of the United States of America, 110(23), 9535–9540.

Clavaguera, F., Bolmont, T., Crowther, R. A., Abramowski, D., Frank, S., Probst, A., Fraser, G., Stalder, A. K., Beibel, M., Staufenbiel, M., Jucker, M., Goedert, M., & Tolnay, M. (2009). 'Transmission and spreading of tauopathy in transgenic mouse brain'. Nature cell biology, 11(7), 909–913.

Colodner, K. J., & Feany, M. B. (2010). 'Glial fibrillary tangles and JAK/STAT-mediated glial and neuronal cell death in a Drosophila model of glial tauopathy'. Journal of Neuroscience, 30(48), 16102-16113.

Congdon, E. E., Kim, S., Bonchak, J., Songrug, T., Matzavinos, A., & Kuret, J. (2008). 'Nucleation-dependent tau filament formation: the importance of dimerization and an estimation of elementary rate constants'. Journal of Biological Chemistry, 283(20), 13806-13816.

Cowan, C. M., Bossing, T., Page, A., Shepherd, D., & Mudher, A. (2010). 'Soluble hyper-phosphorylated tau causes microtubule breakdown and functionally compromises normal tau in vivo'. Acta Neuropathologica, 120(5), 593-604.

# Bibliography


Cowan, C. M., Chee, F., Shepherd, D., & Mudher, A. (2010). 'Disruption of neuronal function by soluble hyperphosphorylated tau in a Drosophila model of tauopathy'. Biochemical Society Transactions, 38(2), 564-570.

Cowan, C. M., Sealey, M. A., Quraishe, S., Targett, M. T., Marcellus, K., Allan, D., & Mudher, A. (2011). 'Modelling tauopathies in Drosophila: insights from the fruit fly'. International journal of Alzheimer's disease, 2011, 598157.

Cowan, C. M., & Mudher, A. (2013). 'Are tau aggregates toxic or protective in tauopathies?' Frontiers in neurology, 4, 114.

Cowan, C. M., Quraishe, S., Hands, S., Sealey, M., Mahajan, S., Allan, D. W., & Mudher, A. (2015). 'Rescue from tau-induced neuronal dysfunction produces insoluble tau oligomers'. Scientific Reports, 5, 17191.

Crowther R. A. (1991). 'Straight and paired helical filaments in Alzheimer disease have a common structural unit'. Proceedings of the National Academy of Sciences of the United States of America, 88(6), 2288–2292.

Crowther, R. A., & Wischik, C. M. (1985). 'Image reconstruction of the Alzheimer paired helical filament'. The EMBO journal, 4(13B), 3661–3665.

Cummings, J. L. (2009). 'Defining and labeling disease-modifying treatments for Alzheimer's disease'. Alzheimer's & Dementia, 5(5), 406-418.

Daebel, V., Chinnathambi, S., Biernat, J., Schwalbe, M., Habenstein, B., Loquet, A., Akoury, E., Tepper, K., Müller, H., Baldus, M., Griesinger, C., Zweckstetter, M., Mandelkow, E., Vijayan, V., & Lange, A. (2012). 'β-Sheet core of tau paired helical filaments revealed by solid-state NMR'. Journal of the American Chemical Society, 134(34), 13982–13989.

Dawson, H. N., Ferreira, A., Eyster, M. V., Ghoshal, N., Binder, L. I., & Vitek, M. P. (2001). 'Inhibition of neuronal maturation in primary hippocampal neurons from tau deficient mice'. *Journal of cell science*, *114*(Pt 6), 1179–1187.

Delobel, P., Lavenir, I., Fraser, G., Ingram, E., Holzer, M., Ghetti, B., Spillantini, M. G., Crowther, R. A., & Goedert, M. (2008). 'Analysis of tau phosphorylation and truncation in a mouse model of human tauopathy'. The American journal of pathology, 172(1), 123–131.

Dickson, D., Crystal, H., Bevona, C., Honer, W., Vincent, I. and Davies, P. (1995) 'Correlations of synaptic and pathological markers with cognitive of the elderly'. Neurobiology of Aging 16:285–304.

DeTure, M. A., & Dickson, D. W. (2019). 'The neuropathological diagnosis of Alzheimer's disease'. Molecular Neurodegeneration, 14(1), 32.

Drewes, G., Trinczek, B., Illenberger, S., Biernat, J., Schmitt-Ulms, G., Meyer, H. E., Mandelkow, E. M., & Mandelkow, E. (1995). 'Microtubule-associated protein/microtubule affinity-regulating kinase

(p110mark). A novel protein kinase that regulates tau-microtubule interactions and dynamic instability by phosphorylation at the Alzheimer-specific site serine 262'. The Journal of biological chemistry, 270(13), 7679–7688.

Doble, B. W., & Woodgett, J. R. (2003). 'GSK-3: tricks of the trade for a multi-tasking kinase'. Journal of cell science, 116(Pt 7), 1175–1186.

Dobson C. M. (1999). 'Protein misfolding, evolution and disease'. Trends in biochemical sciences, 24(9), 329–332.

Dotti, C. G., & Banker, G. A. (1987). 'Experimentally induced alteration in the polarity of developing neurons'. Nature, 330(6145), 254–256.

Dugger, B. N., & Dickson, D. W. (2017). 'Pathology of Neurodegenerative Diseases'. Cold Spring Harbor Perspectives in Biology, 9(7).

Eckermann, K., Mocanu, M. M., Khlistunova, I., Biernat, J., Nissen, A., Hofmann, A., Schönig, K., Bujard, H., Haemisch, A., Mandelkow, E., Zhou, L., Rune, G., & Mandelkow, E. M. (2007). 'The beta-propensity of Tau determines aggregation and synaptic loss in inducible mouse models of tauopathy'. The Journal of biological chemistry, 282(43), 31755–31765.

Ercan-Herbst, E., Ehrig, J., Schöndorf, D. C., Behrendt, A., Klaus, B., Gomez Ramos, B., Prat Oriol, N., Weber, C., & Ehrnhoefer, D. E. (2019). 'A post-translational modification signature defines changes in soluble tau correlating with oligomerization in early stage Alzheimer's disease brain'. Acta neuropathologica communications, 7(1), 192.

Falcon, B., Cavallini, A., Angers, R., Glover, S., Murray, T. K., Barnham, L., Jackson, S., O'Neill, M. J., Isaacs, A. M., Hutton, M. L., Szekeres, P. G., Goedert, M., & Bose, S. (2015). 'Conformation determines the seeding potencies of native and recombinant Tau aggregates'. The Journal of biological chemistry, 290(2), 1049–1065.

Falcon, B., Zhang, W., Murzin, A. G., Murshudov, G., Garringer, H. J., Vidal, R., Crowther, R. A., Ghetti, B., Scheres, S., & Goedert, M. (2018). 'Structures of filaments from Pick's disease reveal a novel tau protein fold'. Nature, 561(7721), 137–140.

Feuillette, S., Miguel, L., Frébourg, T., Campion, D., & Lecourtois, M. (2010). 'Drosophila models of human tauopathies indicate that Tau protein toxicity in vivo is mediated by soluble cytosolic phosphorylated forms of the protein'. Journal of neurochemistry, 113(4), 895–903.

Fischer, D., Mukrasch, M. D., Biernat, J., Bibow, S., Blackledge, M., Griesinger, C., Mandelkow, E., & Zweckstetter, M. (2009). 'Conformational changes specific for pseudophosphorylation at serine 262 selectively impair binding of tau to microtubules'. Biochemistry, 48(42), 10047–10055.

# Bibliography


Fitzpatrick, A., Falcon, B., He, S., Murzin, A. G., Murshudov, G., Garringer, H. J., Crowther, R. A., Ghetti, B., Goedert, M., & Scheres, S. (2017). 'Cryo-EM structures of tau filaments from Alzheimer's disease'. Nature, 547(7662), 185–190.

Flach, K., Hilbrich, I., Schiffmann, A., Gärtner, U., Krüger, M., Leonhardt, M., Waschipky, H., Wick, L., Arendt, T., & Holzer, M. (2012). 'Tau oligomers impair artificial membrane integrity and cellular viability'. The Journal of biological chemistry, 287(52), 43223–43233.

Folch, J., Busquets, O., Ettcheto, M., Sánchez-López, E., Castro-Torres, R. D., Verdaguer, E., Garcia, M. L., Olloquequi, J., Casadesús, G., Beas-Zarate, C., Pelegri, C., Vilaplana, J., Auladell, C., & Camins, A. (2018). 'Memantine for the Treatment of Dementia: A Review on its Current and Future Applications'. Journal of Alzheimer's disease: JAD, 62(3), 1223–1240.

Folwell, J., Cowan, C. M., Ubhi, K. K., Shiabh, H., Newman, T. A., Shepherd, D., & Mudher, A. (2010). 'Abeta exacerbates the neuronal dysfunction caused by human tau expression in a Drosophila model of Alzheimer's disease'. Experimental Neurology, 223(2), 401-409.

Friedhoff, P. Von Bergen, M. Mandelkow, E.M., Mandelkow, E. (2000). 'Structure of tau protein and assembly into paired helical filaments'. Biochimica et Biophysica Acta. 1502 (1),122-132.

Frost, B., Gotz, J., & Feany, M. B. (2015). 'Connecting the dots between tau dysfunction and neurodegeneration'. Trends in Cell Biology, 25(1), 46-53.

Frost, B., Jacks, R. L., & Diamond, M. I. (2009). 'Propagation of tau misfolding from the outside to the inside of a cell'. The Journal of biological chemistry, 284(19), 12845–12852.

Fujio, K., Sato, M., Uemura, T., Sato, T., Sato-Harada, R., & Harada, A. (2007). '14-3-3 proteins and protein phosphatases are not reduced in tau-deficient mice'. Neuroreport, 18(10), 1049–1052.

Gauthier, S., Feldman, H. H., Schneider, L. S., Wilcock, G. K., Frisoni, G. B., Hardlund, J. H., Moebius, H. J., Bentham, P., Kook, K. A., Wischik, D. J., Schelter, B. O., Davis, C. S., Staff, R. T., Bracoud, L., Shamsi, K., Storey, J. M., Harrington, C. R., & Wischik, C. M. (2016). 'Efficacy and safety of tau-aggregation inhibitor therapy in patients with mild or moderate Alzheimer's disease: a randomised, controlled, double-blind, parallel-arm, phase 3 trial'. Lancet (London, England), 388(10062), 2873–2884.

Ghetti, B., Oblak, A. L., Boeve, B. F., Johnson, K. A., Dickerson, B. C., & Goedert, M. (2015). 'Invited review: Frontotemporal dementia caused by microtubule-associated protein tau gene (MAPT) mutations: a chameleon for neuropathology and neuroimaging'. Neuropathology and applied neurobiology, 41(1), 24–46.

Glenner, G. G., Eanes, E. D., & Page, D. L. (1972). 'The relation of the properties of Congo red-stained amyloid fibrils to the -conformation'. The journal of histochemistry and cytochemistry : official journal of the Histochemistry Society, 20(10), 821–826.

# Bibliography


Goedert, M. (2004). 'Tau protein and neurodegeneration'. Seminars in Cell & Developmental Biology, 15(1), 45-49.

Goedert, M. (2016). 'The ordered assembly of tau is the gain-of-toxic function that causes human tauopathies'. Alzheimer's & Dementia, 12(10), 1040-1050

Goedert, M., & Jakes, R. (2005). 'Mutations causing neurodegenerative tauopathies'. Biochimica et biophysica acta, 1739(2-3), 240–250.

Goedert, M., & Hasegawa, M. (1999). 'The tauopathies: toward an experimental animal model'. The American journal of pathology, 154(1), 1–6.

Goedert, M., Spillantini, M. G., Jakes, R., Rutherford, D., & Crowther, R. A. (1989). 'Multiple isoforms of human microtubule-associated protein tau: sequences and localization in neurofibrillary tangles of Alzheimer's disease'. Neuron, 3(4), 519–526.

Goedert, M., & Spillantini, M. G. (2000) 'Tau mutations in frontotemporal dementia FTDP-17 and their relevance for Alzheimer's disease'. Biochimica et Biophysica Acta, 1502 (1),110-121.

Goedert, M., & Spillantini, M. G. (2006). 'A century of Alzheimer's disease'. Science, 314(5800), 777-781.

Gómez-Isla, T., Hollister, R., West, H., Mui, S., Growdon, J. H., Petersen, R. C., Parisi, J. E., & Hyman, B. T. (1997). 'Neuronal loss correlates with but exceeds neurofibrillary tangles in Alzheimer's disease'. Annals of neurology, 41(1), 17–24.

Gorsky, M.K., Burnouf, S., Sofola-Adesakin, O., Dols, J., Augustin, H., Weigelt, C. M., Grönke, S., & Partridge, L. (2017). 'Pseudo-acetylation of multiple sites on human Tau proteins alters Tau phosphorylation and microtubule binding, and ameliorates amyloid beta toxicity'. Scientific Reports, 7, 9984.

Götz, J., Chen, F., van Dorpe, J., & Nitsch, R. M. (2001). 'Formation of neurofibrillary tangles in P301l tau transgenic mice induced by Abeta 42 fibrils'. Science (New York, N.Y.), 293(5534), 1491–1495.

Greenberg, S. G., & Davies, P. (1990). 'A preparation of Alzheimer paired helical filaments that displays distinct tau proteins by polyacrylamide gel electrophoresis'. Proceedings of the National Academy of Sciences of the United States of America, 87(15), 5827–5831.

Grundke-Iqbal, I., Iqbal, K., Tung, Y. C., Quinlan, M., Wisniewski, H. M., & Binder, L. I. (1986). 'Abnormal phosphorylation of the microtubule-associated protein tau (tau) in Alzheimer cytoskeletal pathology'. Proceedings of the National Academy of Sciences of the United States of America, 83(13), 4913–4917.

Guo, T., Noble, W., & Hanger, D. P. (2017). 'Roles of tau protein in health and disease'. Acta neuropathologica, 133(5), 665–704.

Gustke, N., Trinczek, B., Biernat, J., Mandelkow, E. M., & Mandelkow, E. (1994). 'Domains of tau Protein and Interactions with Microtubules'. Biochemistry, 33(32), 9511-9522.

# Bibliography


Haass, C., Schlossmacher, M. G., Hung, A. Y., Vigo-Pelfrey, C., Mellon, A., Ostaszewski, B. L., Lieberburg, I., Koo, E. H., Schenk, D., & Teplow, D. B. (1992). 'Amyloid beta-peptide is produced by cultured cells during normal metabolism'. Nature, 359(6393), 322–325.

Hampton, D. W., Webber, D. J., Bilican, B., Goedert, M., Spillantini, M. G., & Chandran, S. (2010). 'Cell-mediated neuroprotection in a mouse model of human tauopathy'. Journal of Neuroscience, 30(30), 9973-9983.

Hanger, D. P., Byers, H. L., Wray, S., Leung, K. Y., Saxton, M. J., Seereeram, A., Reynolds, C. H., Ward, M. A., & Anderton, B. H. (2007). 'Novel phosphorylation sites in tau from Alzheimer brain support a role for casein kinase 1 in disease pathogenesis'. The Journal of biological chemistry, 282(32), 23645–23654.

Heidary, G. & Fortini, M. E. (2001). 'Identification and characterization of the Drosophila tau homolog'. Mechanisms of Development, 108, 171–8.

Hempen, B., & Brion, J. P. (1996). 'Reduction of acetylated alpha-tubulin immunoreactivity in neurofibrillary tangle-bearing neurons in Alzheimer's disease'. Journal of neuropathology and experimental neurology, 55(9), 964–972.

Hill, E., Karikari, T. K., Moffat, K. G., Richardson, M., & Wall, M. J. (2019). 'Introduction of Tau Oligomers into Cortical Neurons Alters Action Potential Dynamics and Disrupts Synaptic Transmission and Plasticity'. eNeuro, 6(5).

Himmler, A., Drechsel, D., Kirschner, M. W., & Martin, D. W., Jr (1989). 'Tau consists of a set of proteins with repeated C-terminal microtubule-binding domains and variable N-terminal domains'. Molecular and cellular biology, 9(4), 1381–1388.

Hochgräfe, K., Sydow, A., Matenia, D., Cadinu, D., Könen, S., Petrova, O., Pickhardt, M., Goll, P., Morellini, F., Mandelkow, E., & Mandelkow, E. M. (2015). 'Preventive methylene blue treatment preserves cognition in mice expressing full-length pro-aggregant human Tau'. Acta neuropathologica communications, 3, 25.

Hong, M., Zhukareva, V., Vogelsberg-Ragaglia, V., Wszolek, Z., Reed, L., Miller, B. I., Geschwind, D. H., Bird, T. D., McKeel, D., Goate, A., Morris, J. C., Wilhelmsen, K. C., Schellenberg, G. D., Trojanowski, J. Q., & Lee, V. M. (1998). 'Mutation-specific functional impairments in distinct tau isoforms of hereditary FTDP-17'. Science (New York, N.Y.), 282(5395), 1914–1917.

Hosokawa, M., Arai, T., Masuda-Suzukake, M., Nonaka, T., Yamashita, M., Akiyama, H., & Hasegawa, M. (2012). 'Methylene blue reduced abnormal tau accumulation in P301L tau transgenic mice'. PloS one, 7(12), e52389.

Hou, Y., Dan, X., Babbar, M., Wei, Y., Hasselbalch, S. G., Croteau, D. L., & Bohr, V. A. (2019). 'Ageing as a risk factor for neurodegenerative disease'. Nature Reviews Neurology, 15(10), 565-581.

Hutton, M., Lendon, C. L., Rizzu, P., Baker, M., Froelich, S., Houlden, H., Pickering-Brown, S., Chakraverty, S., Isaacs, A., Grover, A., Hackett, J., Adamson, J., Lincoln, S., Dickson, D., Davies, P., Petersen, R. C., Stevens, M., de Graaff, E., Wauters, E., van Baren, J., … Heutink, P. (1998). 'Association of missense and 5'-splice-site mutations in tau with the inherited dementia FTDP-17'. Nature, 393(6686), 702–705.

Ikegami, S., Harada, A., & Hirokawa, N. (2000). 'Muscle weakness, hyperactivity, and impairment in fear conditioning in tau-deficient mice'. *Neuroscience letters*, *279*(3), 129–132.

Iqbal, K., Alonso, A., Chen, S., Chohan, M. O., El-Akkad, E., Gong, C. X., Khatoon, S., Li, B., Liu, F., Rahman, A., Tanimukai, H., & Grundke-Iqbal, I. (2005). 'Tau pathology in Alzheimer disease and other tauopathies'. Biochimica et biophysica acta, 1739(2-3), 198–210.

Iqbal, K., Liu, F., & Gong, C. X. (2016). 'Tau and neurodegenerative disease: the story so far'. Nature reviews. Neurology, 12(1), 15–27.

Irwin, D. J. (2016). 'Tauopathies as clinicopathological entities'. Parkinsonism & Related Disorders, 22 Suppl 1, S29-33.

Ishihara, T., Hong, M., Zhang, B., Nakagawa, Y., Lee, M. K., Trojanowski, J. Q., & Lee, V. M. (1999). 'Age-dependent emergence and progression of a tauopathy in transgenic mice overexpressing the shortest human tau isoform'. Neuron, 24(3), 751–762.

Jackson, G. R., Wiedau-Pazos, M., Sang, T. K., Wagle, N., Brown, C. A., Massachi, S., & Geschwind, D. H. (2002). 'Human wild-type tau interacts with wingless pathway components and produces neurofibrillary pathology in Drosophila'. Neuron, 34(4), 509–519.

Jaiswal, M. K. (2019). 'Riluzole and edaravone: A tale of two amyotrophic lateral sclerosis drugs'. Medicinal Research Reviews, 39(2), 733-748.

Jeganathan, S., Hascher, A., Chinnathambi, S., Biernat, J., Mandelkow, E. M., & Mandelkow, E. (2008). 'Proline-directed pseudo-phosphorylation at AT8 and PHF1 epitopes induces a compaction of the paperclip folding of Tau and generates a pathological (MC-1) conformation'. The Journal of biological chemistry, 283(46), 32066–32076.

Kadavath, H., Hofele, R. V., Biernat, J., Kumar, S., Tepper, K., Urlaub, H., Mandelkow, E., & Zweckstetter, M. (2015). 'Tau stabilizes microtubules by binding at the interface between tubulin heterodimers'. Proceedings of the National Academy of Sciences of the United States of America, 112(24), 7501–7506.

Kampers, T., Friedhoff, P., Biernat, J., Mandelkow, E. M., & Mandelkow, E. (1996). 'RNA stimulates aggregation of microtubule-associated protein tau into Alzheimer-like paired helical filaments'. FEBS letters, 399(3), 344–349.

# Bibliography


Kaniyappan, S., Chandupatla, R. R., Mandelkow, E. M., & Mandelkow, E. (2017). 'Extracellular low-n oligomers of tau cause selective synaptotoxicity without affecting cell viability'. Alzheimer's & dementia: the journal of the Alzheimer's Association, 13(11), 1270–1291.

Kempf, M., Clement, A., Faissner, A., Lee, G., & Brandt, R. (1996). 'Tau binds to the distal axon early in development of polarity in a microtubule- and microfilament-dependent manner'. The Journal of neuroscience: the official journal of the Society for Neuroscience, 16(18), 5583–5592.

Khlistunova, I., Biernat, J., Wang, Y., Pickhardt, M., von Bergen, M., Gazova, Z., Mandelkow, E., & Mandelkow, E. M. (2006). 'Inducible expression of Tau repeat domain in cell models of tauopathy: aggregation is toxic to cells but can be reversed by inhibitor drugs'. The Journal of biological chemistry, 281(2), 1205–1214.

KIDD M. (1963). 'Paired helical filaments in electron microscopy of Alzheimer's disease'. Nature, 197, 192–193.

Khurana, V., Elson-Schwab, I., Fulga, T. A., Sharp, K. A., Loewen, C. A., Mulkearns, E., Tyynelä, J., Scherzer, C. R., & Feany, M. B. (2010). 'Lysosomal dysfunction promotes cleavage and neurotoxicity of tau in vivo'. PLoS genetics, 6(7), e1001026.

Kosik, K. S., Orecchio, L. D., Bakalis, S., & Neve, R. L. (1989). 'Developmentally regulated expression of specific tau sequences'. Neuron, 2(4), 1389–1397.

Kosmidis, S., Grammenoudi, S., Papanikolopoulou, K., & Skoulakis, E. M. (2010). 'Differential effects of Tau on the integrity and function of neurons essential for learning in Drosophila'. Journal of Neuroscience, 30(2), 464-477.

Ksiezak-Reding, H., Liu, W. K., & Yen, S. H. (1992). 'Phosphate analysis and dephosphorylation of modified tau associated with paired helical filaments'. Brain research, 597(2), 209–219.

Kubo, A., Misonou, H., Matsuyama, M., Nomori, A., Wada-Kakuda, S., Takashima, A., Kawata, M., Murayama, S., Ihara, Y., & Miyasaka, T. (2019). 'Distribution of endogenous normal tau in the mouse brain'. The Journal of comparative neurology, 527(5), 985–998.

Kuca, K., Soukup, O., Maresova, P., Korabecny, J., Nepovimova, E., Klimova, B., Honegr, J., Ramalhob, T., França, T. (2016). 'Current Approaches Against Alzheimer's Disease in Clinical Trials'. Journal of the Brazilian Chemical Society, 27(4); 641-649.

Lane, C. A., Hardy, J., & Schott, J. M. (2018). 'Alzheimer's disease'. European Journal of Neurology, 25(1), 59-70.

Lansbury P. T., Jr. 1999. 'Evolution of amyloid: what normal protein folding may tell us about fibrillogenesis and disease'. Proceedings of the National Academy of Sciences of the United States of America, 96(7), 3342–3344

# Bibliography


Lasagna-Reeves, C. A., Castillo-Carranza, D. L., Sengupta, U., Clos, A. L., Jackson, G. R., & Kayed, R. (2011). 'Tau oligomers impair memory and induce synaptic and mitochondrial dysfunction in wild-type mice'. Molecular neurodegeneration, 6, 39.

Lasagna-Reeves, C. A., de Haro, M., Hao, S., Park, J., Rousseaux, M. W., Al-Ramahi, I., Jafar-Nejad, P., Vilanova-Velez, L., See, L., De Maio, A., Nitschke, L., Wu, Z., Troncoso, J. C., Westbrook, T. F., Tang, J., Botas, J., & Zoghbi, H. Y. (2016). 'Reduction of Nuak1 Decreases Tau and Reverses Phenotypes in a Tauopathy Mouse Model'. Neuron, 92(2), 407–418.

Lee, V. M., Balin, B. J., Otvos, L., Jr, & Trojanowski, J. Q. (1991). 'A68: a major subunit of paired helical filaments and derivatized forms of normal Tau'. Science (New York, N.Y.), 251(4994), 675–678.

Lee, V. M., Goedert, M., & Trojanowski, J. Q. (2001). 'Neurodegenerative tauopathies'. Annual review of neuroscience, 24, 1121–1159.

Lee, G., Neve, R. L., & Kosik, K. S. (1989). 'The microtubule binding domain of tau protein'. Neuron, 2(6), 1615–1624.

Lee, G., Thangavel, R., Sharma, V. M., Litersky, J. M., Bhaskar, K., Fang, S. M., Do, L. H., Andreadis, A., Van Hoesen, G., & Ksiezak-Reding, H. (2004). 'Phosphorylation of tau by fyn: implications for Alzheimer's disease'. The Journal of neuroscience: the official journal of the Society for Neuroscience, 24(9), 2304–2312.

Lei, P., Ayton, S., Finkelstein, D. I., Spoerri, L., Ciccotosto, G. D., Wright, D. K., Wong, B. X., Adlard, P. A., Cherny, R. A., Lam, L. Q., Roberts, B. R., Volitakis, I., Egan, G. F., McLean, C. A., Cappai, R., Duce, J. A., & Bush, A. I. (2012). Tau deficiency induces parkinsonism with dementia by impairing APP-mediated iron export. *Nature medicine*, *18*(2), 291–295.

LeVine, H. (1993) 'Thioflavine T Interaction with Synthetic Alzheimer's Disease Beta-Amyloid Peptides: Detection of Amyloid Aggregation in Solution'. Protein Science, 2, 404-410.

Lewis, J., McGowan, E., Rockwood, J., Melrose, H., Nacharaju, P., Van Slegtenhorst, M., Gwinn-Hardy, K., Paul Murphy, M., Baker, M., Yu, X., Duff, K., Hardy, J., Corral, A., Lin, W. L., Yen, S. H., Dickson, D. W., Davies, P., & Hutton, M. (2000). 'Neurofibrillary tangles, amyotrophy and progressive motor disturbance in mice expressing mutant (P301L) tau protein'. Nature genetics, 25(4), 402–405.

Li, S.; Luo, Z.; Zhang, R.; Xu, H.; Zhou, T.; Liu, L.; Qu, J. (2021). 'Distinguishing Amyloid -Protein in a Mouse Model of Alzheimer's Disease by Label-Free Vibrational Imaging'. Biosensors 11, 365.

Li, W., & Lee, V. M. (2006). 'Characterization of two VQIXXK motifs for tau fibrillization in vitro'. Biochemistry, 45(51), 15692–15701.

Lindwall, G., & Cole, R. D. (1984). 'Phosphorylation affects the ability of tau protein to promote microtubule assembly'. Journal of Biological Chemistry, 259(8), 5301-5305.

# Bibliography


Ling, H., Kovacs, G. G., Vonsattel, J. P., Davey, K., Mok, K. Y., Hardy, J., Morris, H. R., Warner, T. T., Holton, J. L., & Revesz, T. (2016). 'Astrogliopathy predominates the earliest stage of corticobasal degeneration pathology'. Brain: a journal of neurology, 139(Pt 12), 3237–3252.

Lorber, B., Fischer, F., Bailly, M., Roy, H., & Kern, D. (2012). 'Protein analysis by dynamic light scattering: methods and techniques for students'. Biochemistry and molecular biology education: a bimonthly publication of the International Union of Biochemistry and Molecular Biology, 40(6), 372–382.

Lovestone, S., Davis, D. R., Webster, M. T., Kaech, S., Brion, J. P., Matus, A., & Anderton, B. H. (1999). 'Lithium reduces tau phosphorylation: effects in living cells and in neurons at therapeutic concentrations'. Biological psychiatry, 45(8), 995–1003.

Lucas, J. J., Hernández, F., Gómez-Ramos, P., Morán, M. A., Hen, R., & Avila, J. (2001). 'Decreased nuclear beta-catenin, tau hyperphosphorylation and neurodegeneration in GSK-3beta conditional transgenic mice'. The EMBO journal, 20(1-2), 27–39.

Macdonald, J.A., Bronner, I., Drynan, L., Fan, J., Curry, A., Fraser, G., Lavenir, I., & Goedert, M. (2019). 'Assembly of transgenic human P301S Tau is necessary for neurodegeneration in murine spinal cord'. Acta Neuropathologica Communications. 7, 44.

Maeda, S., Sahara, N., Saito, Y., Murayama, S., Ikai, A., & Takashima, A. (2006). 'Increased levels of granular tau oligomers: an early sign of brain aging and Alzheimer's disease'. Neuroscience research, 54(3), 197–201.

Maeda, S., Sahara, N., Saito, Y., Murayama, M., Yoshiike, Y., Kim, H., Miyasaka, T., Murayama, S., Ikai, A., & Takashima, A. (2007). 'Granular tau oligomers as intermediates of tau filaments'. Biochemistry, 46(12), 3856–3861.

Mair, W., Muntel, J., Tepper, K., Tang, S., Biernat, J., Seeley, W. W., Kosik, K. S., Mandelkow, E., Steen, H., & Steen, J. A. (2016). 'FLEXITau: Quantifying Post-translational Modifications of Tau Protein in Vitro and in Human Disease'. Analytical chemistry, 88(7), 3704–3714.

Mancuso, R., Fryatt, G., Cleal, M., Obst, J., Pipi, E., Monzón-Sandoval, J., Ribe, E., Winchester, L., Webber, C., Nevado, A., Jacobs, T., Austin, N., Theunis, C., Grauwen, K., Daniela Ruiz, E., Mudher, A., Vicente-Rodriguez, M., Parker, C. A., Simmons, C., Cash, D., … Perry, V. H. (2019). 'CSF1R inhibitor JNJ-40346527 attenuates microglial proliferation and neurodegeneration in P301S mice'. Brain: a journal of neurology, 142(10), 3243–3264. h

McShane, R., Areosa Sastre, A., & Minakaran, N. (2006). 'Memantine for dementia'. The Cochrane database of systematic reviews, (2), CD003154.

Mandelkow, E. M., & Mandelkow, E. (2012). 'Biochemistry and cell biology of tau protein in neurofibrillary degeneration'. Cold Spring Harb Perspect Med, 2(7), a006247.

# Bibliography


Medina, M. (2018). 'An Overview on the Clinical Development of Tau-Based Therapeutics'. International Journal of Molecular Sciences, 19(4).

Mirbaha, H., Holmes, B. B., Sanders, D. W., Bieschke, J., & Diamond, M. I. (2015). 'Tau Trimers Are the Minimal Propagation Unit Spontaneously Internalized to Seed Intracellular Aggregation'. The Journal of biological chemistry, 290(24), 14893–14903.

Mocanu, M. M., Nissen, A., Eckermann, K., Khlistunova, I., Biernat, J., Drexler, D., Petrova, O., Schönig, K., Bujard, H., Mandelkow, E., Zhou, L., Rune, G., & Mandelkow, E. M. (2008). 'The potential for beta-structure in the repeat domain of tau protein determines aggregation, synaptic decay, neuronal loss, and coassembly with endogenous Tau in inducible mouse models of tauopathy'. The Journal of neuroscience: the official journal of the Society for Neuroscience, 28(3), 737–748.

Mondragón-Rodríguez, S., Mena, R., Binder, L. I., Smith, M. A., Perry, G., & García-Sierra, F. (2008). 'Conformational changes and cleavage of tau in Pick bodies parallel the early processing of tau found in Alzheimer pathology'. Neuropathology and applied neurobiology, 34(1), 62–75.

Morishima-Kawashima, M., Hasegawa, M., Takio, K., Suzuki, M., Yoshida, H., Titani, K., & Ihara, Y. (1995). 'Proline-directed and non-proline-directed phosphorylation of PHF-tau'. The Journal of biological chemistry, 270(2), 823–829.

Morris, M., Maeda, S., Vossel, K., & Mucke, L. (2011). 'The many faces of tau'. Neuron, 70(3), 410–426.

Morozova, O. A., March, Z. M., Robinson, A. S., & Colby, D. W. (2013). 'Conformational features of tau fibrils from Alzheimer's disease brain are faithfully propagated by unmodified recombinant protein. 'Biochemistry, 52(40), 6960-6967.

Mudher, A., Colin, M., Dujardin, S., Medina, M., Dewachter, I., Alavi Naini, S. M., Mandelkow, E. M., Mandelkow, E., Buée, L., Goedert, M., & Brion, J. P. (2017). ´What is the evidence that tau pathology spreads through prion-like propagation?' Acta neuropathologica communications, 5(1), 99.

Mudher, A., Shepherd, D., Newman, T. A., Mildren, P., Jukes, J. P., Squire, A., Mears, A., Drummond, J. A., Berg, S., MacKay, D., Asuni, A. A., Bhat, R., & Lovestone, S. (2004). 'GSK-3beta inhibition reverses axonal transport defects and behavioural phenotypes in Drosophila'. Molecular psychiatry, 9(5), 522–530.

Mukrasch, M. D., Bibow, S., Korukottu, J., Jeganathan, S., Biernat, J., Griesinger, C., Mandelkow, E., & Zweckstetter, M. (2009). 'Structural polymorphism of 441-residue tau at single residue resolution'. PLoS biology, 7(2), e34.

Mukrasch, M. D., Biernat, J., von Bergen, M., Griesinger, C., Mandelkow, E., & Zweckstetter, M. (2005). 'Sites of tau important for aggregation populate {beta}-structure and bind to microtubules and polyanions'. Journal of Biological Chemistry, 280(26), 24978-24986.

# Bibliography


Naiki, H., Higuchi, K., Hosokawa, M., & Takeda, T. (1989). 'Fluorometric determination of amyloid fibrils in vitro using the fluorescent dye, thioflavin T'. Analytical biochemistry, 177(2), 244–249.

Necula, M., & Kuret, J. (2004). Pseudophosphorylation and glycation of tau protein enhance but do not trigger fibrillization in vitro. J Biol Chem, 279(48), 49694-49703. doi: 10.1074/jbc.M405527200

Noble, W., Hanger, D. P., Miller, C. C., & Lovestone, S. (2013). 'The importance of tau phosphorylation for neurodegenerative diseases'. Frontiers in neurology, 4, 83.

Panda, D., Samuel, J. C., Massie, M., Feinstein, S. C., & Wilson, L. (2003). 'Differential regulation of microtubule dynamics by three- and four-repeat tau: implications for the onset of neurodegenerative disease'. Proceedings of the National Academy of Sciences of the United States of America, 100(16), 9548–9553.

Papanikolopoulou, K., Kosmidis, S., Grammenoudi, S., & Skoulakis, E. M. (2010). 'Phosphorylation differentiates tau-dependent neuronal toxicity and dysfunction'. Biochemical Society transactions, 38(4), 981–987.

Papanikolopoulou, K., & Skoulakis, E. M. (2015). 'Temporally distinct phosphorylations differentiate Tau-dependent learning deficits and premature mortality in Drosophila'. Human molecular genetics, 24(7), 2065–2077.

Passarella, D., & Goedert, M. (2018). 'Beta-sheet assembly of Tau and neurodegeneration in Drosophila melanogaster'. Neurobiology of aging, 72, 98–105.

Patterson, K. R., Remmers, C., Fu, Y., Brooker, S., Kanaan, N. M., Vana, L., Ward, S., Reyes, J. F., Philibert, K., Glucksman, M. J., & Binder, L. I. (2011). 'Characterization of prefibrillar Tau oligomers in vitro and in Alzheimer disease'. The Journal of biological chemistry, 286(26), 23063–23076.

Pei, J. J., Braak, E., Braak, H., Grundke-Iqbal, I., Iqbal, K., Winblad, B., & Cowburn, R. F. (1999). 'Distribution of active glycogen synthase kinase 3beta (GSK-3beta) in brains staged for Alzheimer disease neurofibrillary changes'. Journal of neuropathology and experimental neurology, 58(9), 1010–1019.

Pei, J. J., Tanaka, T., Tung, Y. C., Braak, E., Iqbal, K., & Grundke-Iqbal, I. (1997). 'Distribution, levels, and activity of glycogen synthase kinase-3 in the Alzheimer disease brain'. Journal of neuropathology and experimental neurology, 56(1), 70–78.

Polydoro, M., Acker, C. M., Duff, K., Castillo, P. E., & Davies, P. (2009). 'Age-dependent impairment of cognitive and synaptic function in the htau mouse model of tau pathology'. Journal of Neuroscience, 29(34), 10741-10749.

Poorkaj, P., Bird, T. D., Wijsman, E., Nemens, E., Garruto, R. M., Anderson, L., Andreadis, A., Wiederholt, W. C., Raskind, M., & Schellenberg, G. D. (1998). 'Tau is a candidate gene for chromosome 17 frontotemporal dementia'. Annals of neurology, 43(6), 815–825.

# Bibliography


Probst, A., Götz, J., Wiederhold, Tolnay, M., Mistl, C., Jaton, A. L., Hong, M., Ishihara, T., Lee, V. M., Trojanowski,., J. Q., Jakes, R., Crowther, R. A., Spillantini, M. G., Bürki, K & Goedert, M. (2000). 'Axonopathy and amyotrophy in mice transgenic for human four-repeat tau protein'. Acta Neuropathologica. 99, 469–481

Prusiner, S.B. (1982) 'Novel proteinaceous infectious particles cause scrapie'. Science, 216(4542), 136-144.

Quraishe, S., Cowan, C. M., & Mudher, A. (2013). 'NAP (davunetide) rescues neuronal dysfunction in a Drosophila model of tauopathy'. Molecular Psychiatry, 18(7), 834-842.

Reiter, L. T., Potocki, L., Chien, S., Gribskov, M., & Bier, E. (2001). 'A systematic analysis of human disease-associated gene sequences in Drosophila melanogaster'. Genome research, 11(6), 1114–1125.

Roberson, E. D., Scearce-Levie, K., Palop, J. J., Yan, F., Cheng, I. H., Wu, T., Gerstein, H., Yu, G. Q., & Mucke, L. (2007). Reducing endogenous tau ameliorates amyloid beta-induced deficits in an Alzheimer's disease mouse model. *Science (New York, N.Y.)*, *316*(5825), 750–754.

Roy, B., & Jackson, G. R. (2014). 'Interactions between Tau and alpha-synuclein augment neurotoxicity in a Drosophila model of Parkinson's disease'. Human Molecular Genetics, 23(11), 3008-3023.

Sahara, N., DeTure, M., Ren, Y., Ebrahim, A. S., Kang, D., Knight, J., Volbracht, C., Pedersen, J. T., Dickson, D. W., Yen, S. H., & Lewis, J. (2013). 'Characteristics of TBS-extractable hyperphosphorylated tau species: aggregation intermediates in rTg4510 mouse brain'. Journal of Alzheimer's disease: JAD, 33(1), 249–263.

Sahara, N., Maeda, S., Yoshiike, Y., Mizoroki, T., Yamashita, S., Murayama, M., Park, J. M., Saito, Y., Murayama, S., & Takashima, A. (2007). 'Molecular chaperone-mediated tau protein metabolism counteracts the formation of granular tau oligomers in human brain'. Journal of neuroscience research, 85(14), 3098–3108.

Santacruz, K., Lewis, J., Spires, T., Paulson, J., Kotilinek, L., Ingelsson, M., Guimaraes, A., DeTure, M., Ramsden, M., McGowan, E., Forster, C., Yue, M., Orne, J., Janus, C., Mariash, A., Kuskowski, M., Hyman, B., Hutton, M., & Ashe, K. H. (2005). 'Tau suppression in a neurodegenerative mouse model improves memory function'. Science (New York, N.Y.), 309(5733), 476–481.

Sanders, D. W., Kaufman, S. K., DeVos, S. L., Sharma, A. M., Mirbaha, H., Li, A., Barker, S. J., Foley, A. C., Thorpe, J. R., Serpell, L. C., Miller, T. M., Grinberg, L. T., Seeley, W. W., & Diamond, M. I. (2014). 'Distinct tau prion strains propagate in cells and mice and define different tauopathies'. Neuron, 82(6), 1271–1288.

# Bibliography

Scattoni, M. L., Gasparini, L., Alleva, E., Goedert, M., Calamandrei, G., & Spillantini, M. G. (2010). 'Early behavioural markers of disease in P301S tau transgenic mice'. Behavioural Brain Research, 208(1), 250-257.

Scheuner, D., Eckman, C., Jensen, M., Song, X., Citron, M., Suzuki, N., Bird, T. D., Hardy, J., Hutton, M., Kukull, W., Larson, E., Levy-Lahad, E., Viitanen, M., Peskind, E., Poorkaj, P., Schellenberg, G., Tanzi, R., Wasco, W., Lannfelt, L., Selkoe, D., … Younkin, S. (1996). 'Secreted amyloid beta-protein similar to that in the senile plaques of Alzheimer's disease is increased in vivo by the presenilin 1 and 2 and APP mutations linked to familial Alzheimer's disease'. Nature medicine, 2(8), 864–870.

Schneider, A., Biernat, J., von Bergen, M., Mandelkow, E., & Mandelkow, E. M. (1999). 'Phosphorylation that detaches tau protein from microtubules (Ser262, Ser214) also protects it against aggregation into Alzheimer paired helical filaments'. Biochemistry, 38(12), 3549–3558.

Schoch, K. M., DeVos, S. L., Miller, R. L., Chun, S. J., Norrbom, M., Wozniak, D. F., Dawson, H. N., Bennett, C. F., Rigo, F., & Miller, T. M. (2016). 'Increased 4R-Tau Induces Pathological Changes in a Human-Tau Mouse Model'. Neuron, 90(5), 941–947.

Schweers, O., Schönbrunn-Hanebeck, E., Marx, A., & Mandelkow, E. (1994). 'Structural studies of tau protein and Alzheimer paired helical filaments show no evidence for beta-structure'. The Journal of biological chemistry, 269(39), 24290–24297.

Sealey, M. A., Vourkou, E., Cowan, C. M., Bossing, T., Quraishe, S., Grammenoudi, S., Skoulakis, E., & Mudher, A. (2017). 'Distinct phenotypes of three-repeat and four-repeat human tau in a transgenic model of tauopathy'. Neurobiology of disease, 105, 74–83.

Seidler, P. M., Boyer, D. R., Rodriguez, J. A., Sawaya, M. R., Cascio, D., Murray, K., Gonen, T., & Eisenberg, D. S. (2018).' Structure-based inhibitors of tau aggregation'. Nature chemistry, 10(2), 170–176.

Sengupta, A., Kabat, J., Novak, M., Wu, Q., Grundke-Iqbal, I., & Iqbal, K. (1998). 'Phosphorylation of tau at both Thr 231 and Ser 262 is required for maximal inhibition of its binding to microtubules'. Archives of biochemistry and biophysics, 357(2), 299–309.

Sergeant, N., Delacourte, A., & Buee, L. (2005). 'Tau protein as a differential biomarker of tauopathies'. Biochimica et Biophysica Acta, 1739(2-3), 179-197.

Serrano-Pozo, A., Frosch, M. P., Masliah, E., & Hyman, B. T. (2011). 'Neuropathological alterations in Alzheimer disease'. Cold Spring Harbor Perspectives in Medicine, 1(1), a006189.

Sievers, S. A., Karanicolas, J., Chang, H. W., Zhao, A., Jiang, L., Zirafi, O., Stevens, J. T., Münch, J., Baker, D., & Eisenberg, D. (2011). 'Structure-based design of non-natural amino-acid inhibitors of amyloid fibril formation'. Nature, 475(7354), 96–100.

# Bibliography


Sillen A., Leroy A., Wieruszeski J. M., Loyens A., Beauvillain J. C., Buee L., Landrieu I. and Lippens G. (2005) 'Regions of tau implicated in the paired helical fragment core as defined by NMR'. ChemBioChem 6, 1849–1856.

Šimić, G., Babić Leko, M., Wray, S., Harrington, C., Delalle, I., Jovanov-Milošević, N., Bažadona, D., Buée, L., de Silva, R., Di Giovanni, G., Wischik, C., & Hof, P. R. (2016). 'Tau Protein Hyperphosphorylation and Aggregation in Alzheimer's Disease and Other Tauopathies, and Possible Neuroprotective Strategies'. Biomolecules, 6(1), 6.

Sivanantharajah, L., Mudher, A., & Shepherd, D. (2019). 'An evaluation of Drosophila as a model system for studying tauopathies such as Alzheimer's disease'. Journal of Neuroscience Methods, 319, 77-88.

Sperfeld, A. D., Collatz, M. B., Baier, H., Palmbach, M., Storch, A., Schwarz, J., Tatsch, K., Reske, S., Joosse, M., Heutink, P., & Ludolph, A. C. (1999). 'FTDP-17: an early-onset phenotype with parkinsonism and epileptic seizures caused by a novel mutation'. Annals of neurology, 46(5), 708–715.

Spillantini, M. G., & Goedert, M. (1998). 'Tau protein pathology in neurodegenerative diseases'. Trends in neurosciences, 21(10), 428–433.

Spillantini, M. G., & Goedert, M. (2013). 'Tau pathology and neurodegeneration'. The Lancet. Neurology, 12(6), 609–622.

Spires, T. L., Orne, J. D., SantaCruz, K., Pitstick, R., Carlson, G. A., Ashe, K. H., & Hyman, B. T. (2006). 'Region-specific dissociation of neuronal loss and neurofibrillary pathology in a mouse model of tauopathy'. The American Journal of Pathology, 168(5), 1598-1607.

Spittaels, K., Van den Haute, C., Van Dorpe, J., Bruynseels, K., Vandezande, K., Laenen, I., Geerts, H., Mercken, M., Sciot, R., Van Lommel, A., Loos, R., & Van Leuven, F. (1999). 'Prominent axonopathy in the brain and spinal cord of transgenic mice overexpressing four-repeat human tau protein'. The American journal of pathology, 155(6), 2153–2165.

Stoothoff, W., Jones, P. B., Spires-Jones, T. L., Joyner, D., Chhabra, E., Bercury, K., Fan, Z., Xie, H., Bacskai, B., Edd, J., Irimia, D., & Hyman, B. T. (2009). 'Differential effect of three-repeat and four-repeat tau on mitochondrial axonal transport'. Journal of neurochemistry, 111(2), 417–427.

Stoothoff, W. H., & Johnson, G. V. (2005). 'Tau phosphorylation: physiological and pathological consequences'. Biochimica et Biophysica Acta, 1739(2-3), 280-297.

Sun, Q., & Gamblin, T. C. (2009). 'Pseudohyperphosphorylation causing AD-like changes in tau has significant effects on its polymerization'. Biochemistry, 48(25), 6002-6011.

Sydow, A., Van der Jeugd, A., Zheng, F., Ahmed, T., Balschun, D., Petrova, O., Drexler, D., Zhou, L., Rune, G., Mandelkow, E., D'Hooge, R., Alzheimer, C., & Mandelkow, E. M. (2011). 'Tau-induced defects in

synaptic plasticity, learning, and memory are reversible in transgenic mice after switching off the toxic Tau mutant'. The Journal of neuroscience : the official journal of the Society for Neuroscience, 31(7), 2511–2525.

Tatebayashi, Y., Miyasaka, T., Chui, D. H., Akagi, T., Mishima, K., Iwasaki, K., Fujiwara, M., Tanemura, K., Murayama, M., Ishiguro, K., Planel, E., Sato, S., Hashikawa, T., & Takashima, A. (2002). 'Tau filament formation and associative memory deficit in aged mice expressing mutant (R406W) human tau'. Proceedings of the National Academy of Sciences of the United States of America, 99(21), 13896–13901.

Takeda S. (2019). 'Tau Propagation as a Diagnostic and Therapeutic Target for Dementia: Potentials and Unanswered Questions'. Frontiers in neuroscience, 13, 1274.

Takeda S, Wegmann S, Cho H, DeVos SL, Commins C, Roe AD, Nicholls SB, Carlson GA, Pitstick R, Nobuhara CK, Costantino I, Frosch MP, Müller DJ, Irimia D, Hyman BT.(2015) 'Neuronal uptake and propagation of a rare phosphorylated high-molecular-weight tau derived from Alzheimer's disease brain'. Nature Communications. 13; 6:8490.

Tanemura, K., Akagi, T., Murayama, M., Kikuchi, N., Murayama, O., Hashikawa, T., Yoshiike, Y., Park, J. M., Matsuda, K., Nakao, S., Sun, X., Sato, S., Yamaguchi, H., & Takashima, A. (2001).' Formation of filamentous tau aggregations in transgenic mice expressing V337M human tau'. Neurobiology of disease, 8(6), 1036–1045.

Tepper, K., Biernat, J., Kumar, S., Wegmann, S., Timm, T., Hübschmann, S., Redecke, L., Mandelkow, E. M., Müller, D. J., & Mandelkow, E. (2014). 'Oligomer formation of tau protein hyperphosphorylated in cells'. The Journal of biological chemistry, 289(49), 34389–34407.

Thornton, C., Bright, N. J., Sastre, M., Muckett, P. J., & Carling, D. (2011). 'AMP-activated protein kinase (AMPK) is a tau kinase, activated in response to amyloid beta-peptide exposure'. Biochemical Journal, 434(3), 503-512.

Trojanowski, J. Q., & Lee, V. M. (2005). 'Pathological tau: a loss of normal function or a gain in toxicity?'. Nature neuroscience, 8(9), 1136–1137.

Uéda, K., Masliah, E., Saitoh, T., Bakalis, S. L., Scoble, H., & Kosik, K. S. (1990). 'Alz-50 recognizes a phosphorylated epitope of tau protein'. The Journal of neuroscience: the official journal of the Society for Neuroscience, 10(10), 3295–3304.

Uematsu, M., Nakamura, A., Ebashi, M., Hirokawa, K., Takahashi, R., & Uchihara, T. (2018). 'Brainstem tau pathology in Alzheimer's disease is characterized by increase of three repeat tau and independent of amyloid β'. Acta neuropathologica communications, 6(1), 1.

Vassar, P. S., & Culling, C. F. (1959). 'Fluorescent stains, with special reference to amyloid and connective tissues'. Archives of pathology, 68, 487–498.

# Bibliography


von Bergen, M., Barghorn, S., Biernat, J., Mandelkow, E. M., & Mandelkow, E. (2005). 'Tau aggregation is driven by a transition from random coil to beta sheet structure'. Biochimica et Biophysica Acta, 1739(2-3), 158-166.

von Bergen, M., Barghorn, S., Li, L., Marx, A., Biernat, J., Mandelkow, E. M., & Mandelkow, E. (2001). 'Mutations of tau protein in frontotemporal dementia promote aggregation of paired helical filaments by enhancing local beta-structure'. Journal of Biological Chemistry, 276(51), 48165-48174

von Bergen, M., Friedhoff, P., Biernat, J., Heberle, J., Mandelkow, E. M., & Mandelkow, E. (2000). 'Assembly of tau protein into Alzheimer paired helical filaments depends on a local sequence motif ((306)VQIVYK(311)) forming beta structure'. Proceedings of the National Academy of Sciences of the United States of America, 97(10), 5129–5134.

Wang, Y., & Mandelkow, E. (2016). 'Tau in physiology and pathology'. Nature Reviews Neuroscience 17, 22–35.

Wang, Z. X., Tan, L., & Yu, J. T. (2015). 'Axonal transport defects in Alzheimer's disease'. Molecular Neurobiology, 51(3), 1309-1321.

Weaver, C. L., Espinoza, M., Kress, Y., & Davies, P. (2000). 'Conformational change as one of the earliest alterations of tau in Alzheimer's disease'. Neurobiology of aging, 21(5), 719–727.

Wegmann, S., Jung, Y. J., Chinnathambi, S., Mandelkow, E. M., Mandelkow, E., & Muller, D. J. (2010). 'Human Tau isoforms assemble into ribbon-like fibrils that display polymorphic structure and stability'. The Journal of biological chemistry, 285(35), 27302–27313.

Wegmann, S., Medalsy, I., D., Mandelkow, E., &Müller, D. (2013). 'Quantifying the fuzzy coat of human Tau fibrils'. Proceedings of the National Academy of Sciences.110 (4) E313-E321;

Weingarten, M. D., Lockwood, A. H., Hwo, S. Y., & Kirschner, M. W. (1975). 'A protein factor essential for microtubule assembly'. Proceedings of the National Academy of Sciences of the United States of America, 72(5), 1858–1862.

Wille, H., Drewes, G., Biernat, J., Mandelkow, E. M., & Mandelkow, E. (1992). 'Alzheimer-like paired helical filaments and antiparallel dimers formed from microtubule-associated protein tau in vitro'. The Journal of cell biology, 118(3), 573–584.

Williams DR. (2006) 'Tauopathies: classification and clinical update on neurodegenerative diseases associated with microtubule-associated protein tau'. Internal Medicine. 36(10):652-60.

Wischik, C. M., Novak, M., Edwards, P. C., Klug, A., Tichelaar, W., & Crowther, R. A. (1988). 'Structural characterization of the core of the paired helical filament of Alzheimer disease'. Proceedings of the National Academy of Sciences of the United States of America, 85(13), 4884–4888.

# Bibliography

Wittmann, C. W., Wszolek, M. F., Shulman, J. M., Salvaterra, P. M., Lewis, J., Hutton, M., & Feany, M. B. (2001). 'Tauopathy in Drosophila: neurodegeneration without neurofibrillary tangles'. Science, 293(5530), 711-714.

Wolfe M. S. (2012). 'The role of tau in neurodegenerative diseases and its potential as a therapeutic target'. Scientifica, 2012, 796024.

Wu, T. H., Lu, Y. N., Chuang, C. L., Wu, C. L., Chiang, A. S., Krantz, D. E., & Chang, H. Y. (2013). Loss of vesicular dopamine release precedes tauopathy in degenerative dopaminergic neurons in a Drosophila model expressing human tau'. Acta Neuropathologica Communications, 125(5), 711-725.

Xu, H., Rösler, T. W., Carlsson, T., de Andrade, A., Bruch, J., Höllerhage, M., Oertel, W. H., & Höglinger, G. U. (2014). 'Memory deficits correlate with tau and spine pathology in P301S MAPT transgenic mice'. Neuropathology and applied neurobiology, 40(7), 833–843.

Yamada, K., Holth, J. K., Liao, F., Stewart, F. R., Mahan, T. E., Jiang, H., Cirrito, J. R., Patel, T. K., Hochgräfe, K., Mandelkow, E. M., & Holtzman, D. M. (2014). 'Neuronal activity regulates extracellular tau in vivo'. The Journal of experimental medicine, 211(3), 387–393.

Yamaguchi, H., Ishiguro, K., Uchida, T., Takashima, A., Lemere, C. A., & Imahori, K. (1996). 'Preferential labeling of Alzheimer neurofibrillary tangles with antisera for tau protein kinase (TPK) I/glycogen synthase kinase-3 beta and cyclin-dependent kinase 5, a component of TPK II'. Acta neuropathologica, 92(3), 232–241.

Yiannopoulou, K. G., & Papageorgiou, S. G. (2013). 'Current and future treatments for Alzheimer's disease'. Therapeutic advances in neurological disorders, 6(1), 19–33.

Yoshiyama, Y., Higuchi, M., Zhang, B., Huang, S. M., Iwata, N., Saido, T. C., Maeda, J., Suhara, T., Trojanowski, J. Q., & Lee, V. M. (2007). 'Synapse loss and microglial activation precede tangles in a P301S tauopathy mouse model'. Neuron, 53(3), 337–351.

Zeng, Y., Yang, J., Zhang, B., Gao, M., Su, Z., & Huang, Y. (2021). 'The structure and phase of tau: from monomer to amyloid filament'. Cellular and Molecular Life Sciences, 78(5), 1873-1886.

Zhang, W., Tarutani, A., Newell, K. L., Murzin, A. G., Matsubara, T., Falcon, B., Vidal, R., Garringer, H. J., Shi, Y., Ikeuchi, T., Murayama, S., Ghetti, B., Hasegawa, M., Goedert, M., & Scheres, S. (2020). 'Novel tau filament fold in